Direct conversion and microfluidic chambers as tools to study the *in-vivo* sketch of human sensory neurons

Simona Giorgi

Director de la tesis: Dr. D. Antonio Ferrer Montiel

Codirectora de la tesis: Dra. Dña. Asia Fernández Carvajal

Programa de Doctorado en Biotecnología Sanitaria

Elche, 2023

UNIVERSIDAD MIGUEL HERNÁNDEZ DE ELCHE

Instituto de Investigación, Desarrollo e Innovación en

Biotecnología Sanitaria de Elche (IDiBE)

La presente tesis doctoral titulada “Direct conversion and microfluidic chambers as tools to study the *in-vivo* sketch of human nociceptors” realizada por Dña. Simona Giorgi se presenta en formato por compendio de artículos previamente publicados, cuyas referencias son las indicadas a continuación:

Is TRPA1 Burning Down TRPV1 a Druggable Target for the Treatment of Chronic Pain?

Simona Giorgi,† Magdalena Nikolaeva-Koleva,† David Alarcón-Alarcón, Laura Butrón and Sara González-Rodríguez.
Int J Mol Sci. 2019 Jun; 20(12): 2906.
doi: 10.3390/ijms20122906 (Q1; Impact factor: 6.21)

Compartmentalized primary cultures of dorsal root ganglion neurons to model peripheral pathophysiological conditions.

Simona Giorgi, Angela Lamberti, Laura Butrón, Olivia Gross-Amat, David Alarcón Alarcón, Enrique Rodríguez-Cañas, Asia Fernández-Carvajal, Antonio Ferrer-Montiel.
Mol Pain 2023 Aug 14;17448069231197102.
doi: 10.1177/17448069231197102 (Q1; Impact factor: 3.37)

El **Dr. Antonio Ferrer Montiel**, director, y la **Dra. Asia Fernández Carvajal**, codirectora, y catedráticos de la Universidad Miguel Hernández de Elche de la tesis doctoral titulada "Direct conversion and microfluidic chambers as tools to study the *in-vivo* sketch of human nociceptors"

INFORMAN:

Que Dña. Simona Giorgi ha realizado bajo nuestra supervisión el trabajo titulado **"**Direct conversion and microfluidic chambers as tools to study the *in-vivo* sketch of human nociceptors**"** conforme a los términos y condiciones definidos en su Plan de Investigación y de acuerdo al Código de Buenas Prácticas de la Universidad Miguel Hernández de Elche, cumpliendo los objetivos previstos de forma satisfactoria para su defensa pública como tesis doctoral.

Lo que firmamos para los efectos oportunos, en Elche, a 18 de diciembre de 2023

Director de la tesis

Fdo: Dr. Antonio Ferrer-Montiel

Codirectora de la tesis

Fdo: Dra. Asia Fernández-Carvajal

El **Dr. Gregorio Fernández Ballester**, Catedrático y Coordinador del Programa de Doctorado en Biotecnología Sanitaria del Instituto de Investigación, Desarrollo e Innovación en Biotecnología de Elche (IDiBE) de la Universidad Miguel Hernández de Elche.

Da su conformidad para el depósito y la defensa de la tesis doctoral titulada: “Direct conversion and microfluidic chambers as tools to study the *in-vivo* sketch of human nociceptors”, presentada por Dña. Simona Giorgi.

Y para que así conste a los efectos oportunos, se expide el presente documento

Fdo: Dr Gregorio Fernández Ballester

Coordinador de la CAPD de Biotecnología Sanitaria

Universidad Miguel Hernández

Elche, a 18 de diciembre de 2023

La presente tesis doctoral ha sido financiada por la Comunidad Valenciana a través del Programa Santiago Grisolía, becas para la formación de personal investigador, en centros de investigación de la Comunitat Valenciana con referencia GRISOLIAP/2019/094.

Además, durante este periodo, Dña. Simona Giorgi ha realizado una estancia de investigación de 3 meses en el Instituto de Medicina Traslacional (EOK) en la Semmelweis University en Budapest, Hungría, financiada por BEFPI, Subvenciones para estancias predoctorales fuera de la Comunitat Valenciana con referencia CIBEFP/2021/50.

SUMMARY

INDEX OF ABBREVIATIONS

AF	Adult Human Dermal Fibroblasts Extracted from Skin Punch Biopsies
AITC	Allyl Isothiocyanate
Ascl1	Achaete-Scute Family Bhlh Transcription Factor 1
ATP	Adenosine Triphosphate
BDNF	Brain-Derived Neurotrophic Factor
bHLH	Basic Helix-Loop-Helix
BK	Bradykinin
BMP	Bone Morphogenetic Proteins
BN1/BN2	Brn3A and Ngn1 / Brn3A and Ngn2
Brn2	POU Domain, Class 3, Transcription Factor 2
Brn3a	Brain-Specific Homeobox/POU Domain Protein 3A
cAMP	Cyclic Adenosine Monophosphate
Cav	Voltage-Gated Calcium Channel
CGRP	Calcitonin Gene-Related Peptide
CIPN	Chemotherapy-Induced Peripheral Neuropathy
CMOS	Complementary Metal–Oxide–Semiconductor
CNS	Central Nervous System
Db-cAMP	Dibutyryl Cyclic Adenosine Monophosphate
Did'	1,1'-Dioctadecyl-3,3,3',3'-Tetramethylindodicarbocyanine
DIV	Days In Vitro
DMEM	Dulbecco's Modified Eagle's Medium
DMSO	Dimethyl Sulfoxide
DRG	Dorsal Root Ganglia
EDTA	Ethylenediamine tetraacetic acid
Edu	5-Ethynyl-2′-Deoxyuridine
ENM / LNM	Early / Late Neuronal Media
FESEM	Field Emission Scanning Electron Microscope
FGF	Fibroblasts Growth Factor
Fsp1	Fibroblast-specific protein 1
GDNF	Glial-Derived Neurotrophic Factor
GFP	Green Fluorescent Protein
GSK3β	Glycogen synthase kinase-3 beta
HaCaT	Human Keratinocytes
HBS	HEPES Balanced Solution
HBSS	Hank's Balanced Salt Solution

HDFa/ HDFn	Human Dermal Fibroblasts from Adult/Neonatal Donors
HEK293 LTV	Human Embryonic Kidney 293 Lentiviral Vectors
hESCs	Human Embryonic Stem Cells
HGF	Hepatocyte Growth Factor
IASP	International Association For The Study Of Pain
IB4	Isolectine B4
IM	Induction Media
IMR90	Human Foetal Lung Fibroblasts
iNs	Induced Neurons
iPSCs	Induced Pluripotent Stem Cells
ISL-1/ Islet1	Insulin Gene Enhancer Protein
iSNs	Induced Sensory Neurons
KCl	Potassium Chloride
Klf7	Kruppel-like factor 7
Kv	Voltage-Gated Potassium Channel
LTMRs	Low-Threshold Mechanoreceptors
LTR	Long Terminal Repeat
LTV	Lentiviral Vector
Map2	Microtubule-Associated Protein 2
MEA	Multi-Electrode Array
MEM NEAA	MEM Non-essential Amino Acids
MFC	Microfluidic Chambers
miRNA	Micro RNA
MOI	Multiplicity Of Infection
MTT	3-[4,5-dimethylthiazol-2-yl]-2,5 diphenyl tetrazolium bromide
Myt1l	Myelin Transcription Factor 1-Like Gene
Nav	Voltage-Gated Sodium Channel
NF200	Neurofilament 200
NGF	Nerve Growth Factor
Ngn1/Ngn2	Neurogenin 1/ Neurogenin 2
NGS	Normal Goat Serum
NM	Neural Media
Notch	And Neurogenic Locus Notch Homolog Protein
NSAIDs	Non-Steroidal Anti-Inflammatory Drugs
NT3	Neurotrophin-3
P_2X_3	Purinoceptor X2 subtype 3
PBS	Phosphate buffered saline
PDMS	Polydimethylsiloxane

PEI	Polyethyleneimine
PFA	Paraformaldehyde
PG	Prostaglandin
PKA	Protein Kinase A
PTX	Paclitaxel
REST	Repressor Element 1 Silencing Transcription Factor
RFP	Red Fluorescent Protein
ROIs	Regions Of Interest
RPM	Revolutions Per Minute
RT	Room Temperature
RT-qPCR	Real Time Quantitative Polymerase Chain Reaction
rtTA	Reverse Tetracyclin-Controlled Transactivator
Runx1	RUNX Family Transcription Factor 1
scRNA-seq	Single Cell RNA-Sequencing
shRNA	Short Hairpin RNA
SM	Small Molecules
SP	Substance P
Tau	Tubulin-Associated Unit
TF	Transcription Factor
TG	Trigeminal Ganglia
TGFβ	Transforming Growth Factor-Beta
TH	Tyrosine Hydroxylase
TRE	Tetracycline-Response Element
TrkA/B/C	Tropomyosin Receptor Kinase A/B/C
TRP	Transient Receptor Potential Channel
TRPA1	Transient Receptor Ankyrin 1
TRPM8	Transient Receptor Potential Channel Melastatin 8
TRPV1	Transient Receptor Vanilloid 1
tTA	Tetracyclin-Controlled Transactivator
Tuj1	Class III Beta-Tubulin
VSV-G	Vesicular Stomatitis Virus G Protein
Wnt	Wingless-Related Integration Site
WPRE	Woodchuck Hepatitis Virus Posttranscriptional Regulatory Element

INDEX OF FIGURES AND TABLES

Figures

Tables

ABSTRACT

Sensory neurons are the primary cells responsible for detecting temperature, mechanical forces, pain, pruritus, and many other somatosensations. These cells, primarily located in the dorsal root ganglia (DRGs) or trigeminal ganglia (TG), exhibit a distinctive morphology, with axons extending up to one meter in length in humans. The cellular and molecular features of sensory neurons, both in physiological and pathological states, are commonly studied *in vitro* using rodent models, which examine both the cell body and its extensions in the same environment. However, the limited applicability of animal models to the human somatosensory system and the differences between cell bodies and neurites have emerged as significant challenges in sensory neuron research.

To address these issues, this work aims to develop a human-based model of sensory neurons through the direct conversion of fibroblasts, a process also known as transdifferentiation. Fibroblasts obtained from foetal lungs, neonatal dermis, or adult dermis were transduced to express Brn3a and Ngn1 using lentiviral vectors. Additionally, the cultured cells were subjected to conversion media containing small molecules that either inhibited or induced intracellular pathways crucial for neuronal development. The effectiveness of the conversion protocols was primarily assessed using calcium imaging, to quantify the functionality of putative induced sensory neurons (iSN). The most promising conversion protocols were further characterized with molecular (qPCR, immunocytochemistry) or functional studies (MEA CMOS, patch clamp). As a result, at least one promising conversion protocol was found for every fibroblast type. Foetal lung fibroblasts presented sensory neurons' morphology and some neuronal markers after few days of conversion. However, we believe these protocols need to be refined due to their cytotoxicity. Neonatal dermal fibroblasts conversion was more challenging, however finally the addition of the small molecule DAPT seemed to increase the conversion protocol efficiency. However, the same protocol was proven to be inefficient in adult dermal fibroblasts. Therefore, Ascl1 and Brn2 induction was added to the protocol as well as REST inhibition. The addition of these genetic modifications and changing media composition led to a significant increase in the conversion efficiency and in generating putative induced sensory neurons cultured *in vitro* up to 50 days, which was the end point of our experiment.

Importantly, electrophysiological assays should be performed to confirm that the converted cells are functional neurons.

Moreover, to recreate the *in vivo* architecture of sensory neurons, the culture of mouse DRGs in microfluidic chambers (MFC) was optimized. MFCs enabled the physical separation of cell bodies and neurites, allowing for targeted stimulation of terminals and the recording of activity in the cell body. The optimization of this compartmentalized culture allowed to co-culture sensory nerve endings with keratinocytes, paving the way to co-culturing with other cell types. Furthermore, nerve endings were treated with inflammatory mediators or a chemotherapeutic agent, demonstrating peripheral sensitization through these agents.

This work paves the way to optimizing several conversion protocols and further investigating the already optimized protocol to understand the role of the different components used during the conversion. Moreover, future experiments may be focused on setting up human sensory neurons' compartmentalized culture, which would be a valuable tool for studying human peripheral signalling.

RESUMEN

Las neuronas sensoriales son las primeras células responsables de detectar la temperatura, las fuerzas mecánicas, el dolor, el prurito y muchas otras sensaciones. Estas células, localizadas principalmente en los ganglios de la raíz dorsal (DRG por sus siglas en inglés) o en los ganglios trigéminos (TG por sus siglas en inglés), presentan una morfología peculiar, con axones que se extienden hasta un metro de longitud en humanos. Las características celulares y moleculares de las neuronas sensoriales, tanto en estados fisiológicos como patológicos, se estudian comúnmente utilizando modelos de roedores *in-vitro*, que examinan tanto el cuerpo celular como sus extensiones en el mismo entorno. Sin embargo, la aplicabilidad limitada de los modelos animales al sistema somatosensorial humano y las diferencias entre cuerpos celulares y neuritas presentan desafíos significativos en la investigación de las neuronas sensoriales.

Para abordar estos temas, este trabajo tiene como objetivo desarrollar un modelo basado en neuronas sensoriales humanas a través de la conversión directa de fibroblastos, un proceso también conocido como transdifferenciación. Fibroblastos obtenidos de pulmón fetal, dermis neonatal o dermis adulta fueron infectados con vectores lentivirales para expresar Brn3a y Ngn1. Además, las células cultivadas fueron sometidas a medios de conversión que contenían pequeñas moléculas que inhiben o inducen vías intracelulares cruciales para el desarrollo de la cresta neural. La efectividad de los protocolos de conversión se evaluó principalmente utilizando imagen de calcio, para cuantificar la funcionalidad de las neuronas sensoriales inducidas (iSN por sus siglas en inglés) en respuesta a agonistas típicos de neuronas sensoriales. Además, los protocolos de conversión más prometedores se caracterizaron con estudios moleculares (qPCR, inmunocitoquímica) o funcionales (MEA CMOS, patch clamp). Como resultado, se encontró al menos un protocolo de conversión prometedor para cada tipo de fibroblasto. En cuanto a la conversión de fibroblastos pulmonares fetales, después de pocos días de conversión, estas células ya presentaban morfología de neuronas sensoriales y algunos marcadores neuronales. Sin embargo, creemos que estos protocolos necesitan ser refinados debido a la toxicidad en las células convertidas. La conversión de fibroblastos dérmicos neonatales fue más desafiante, pero finalmente la adición de la pequeña molécula DAPT pareció

aumentar la eficiencia del protocolo de conversión. Sin embargo, el mismo protocolo demostró ser ineficiente en fibroblastos adultos. Por lo tanto, se decidió inducir la expresión de los factores de transcripción Ascl1 y Brn2, así como la inhibición de REST. La adición de estas modificaciones genéticas y el cambio de la composición de los medios de conversión, llevó a un aumento significativo en la eficiencia del protocolo y a la generación de neuronas sensoriales putativas capaces de sobrevivir hasta 50 días, que fue el punto final de los experimentos. Es importante destacar que todos estos protocolos necesitan ensayos electrofisiológicos para ser caracterizados más profundamente, con el fin de demostrar que las células convertidas son neuronas funcionales.

Además, para recrear la morfología que las neuronas sensoriales presentan *in vivo*, se optimizó el cultivo de DRGs de ratón en cámaras microfluídicas (MFC). Los cultivos compartimentalizados permitieron la separación física de cuerpos celulares y neuritas, permitiendo la estimulación dirigida de los terminales y el registro de la actividad en el cuerpo celular. La optimización de este cultivo permitió co-cultivar terminaciones nerviosas sensoriales con queratinocitos, abriendo el camino al co-cultivo con otros tipos celulares. Además, las terminaciones nerviosas fueron tratadas con mediadores inflamatorios o un agente quimioterapéutico, demostrando sensibilización periférica a través de estos agentes.

Este trabajo abre el camino a la optimización de otros protocolos de conversión a través de modificaciones de los protocolos ya optimizados, con el fin de comprender el papel de todos los componentes utilizados durante la conversión. Además, los experimentos futuros pueden centrarse en optimizar el cultivo compartimentalizado de neuronas sensoriales humanas, que sería una herramienta valiosa para estudiar la señalización periférica.

INTRODUCTION

1. INTRODUCTION

1.1. Somatosensory system

Sensation includes the five senses: vision, hearing, touch, taste, and smell; and the somatic perceptions of proprioception, pain, itch, temperature, visceral sensations, and the vestibular sense of balance and head movement. The **sensory information** is neural activity originating from the stimulation of nerve terminals in specific body parts, which is relied on by specific processing centres in the central nervous system (CNS) [1]. The cells capable of detecting distinct classes of sensory modalities are called sensory neurons, whose differential sensitivity is due to the expression of different **receptor proteins** at the peripheral terminal [2]. Depending on the protein expression and thus the function, sensory neurons can be classified into four groups: (1) mechanoreceptors, responsible for touch, hearing, balance, and proprioception; (2) chemoreceptors, that allow smell, taste, and pain; (3) photoreceptors, implicated in vision; (4) thermoreceptors, which perceive temperature [3].

Sensory neurons present a peculiar morphology called **pseudo-unipolar** [1] (**Figure 1**), characterized by one axon that divides into two branches: one directed peripherally and one centrally [4]. Due to this unique structure, pseudo-unipolar neurons are bidirectional, as they can send and receive signals from both ends [5]. In humans, the peripheral process of a lumbar DRG can reach a 1-meter length, having the majority of the cytosol present in the processes and highlighting the importance of studying not only the cell body but also the neurites [6].

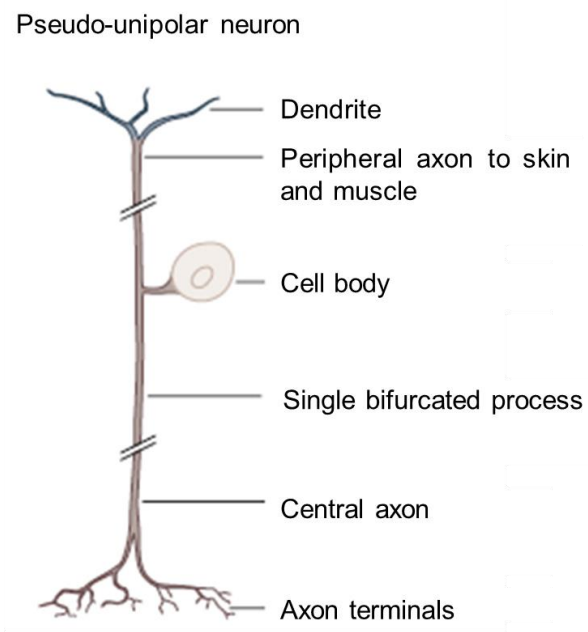

Figure 1 Morphology of a pseudo-unipolar neuron. Adapted from Kandel et al. [1]

As previously introduced, the axon of a somatosensory neuron is comprised of two branches: (1) a **peripheral** specialized ending and (2) a **central** branch forming a synapse with the CNS [7]. The peripheral ending is part of a sense organ or is the sense organ itself, as nociceptors free nerve endings in the skin. Here, **transduction** takes place, which is the process by which the energy of the stimulus is converted into an electrical signal. When a stimulus activates a type of specialized receptor, it allows for an inward cation current (mainly Ca^{2+} and Na^{+}) which partially depolarizes the cell membrane, known as generator potential. If the stimulus has enough strength, the membrane voltage gets over the firing threshold, triggering the opening of voltage-gated channels and calcium-induced calcium release, which will, in turn, trigger action potentials [1][8].

The peripheral terminals are located far from the CNS; therefore, active propagation of the electrical signal is needed for the **transmission** of the information. Trains of action potentials spread via subsequent nerve cells, called first-, second-, and third-order neurons. The cell bodies of first-order neurons are located in the dorsal root (DRGs) or trigeminal ganglia (TGs). These ganglia comprise a mixture of neural and non-neural cells; different reports in rodents account for a presence of neurons in DRGs of 70%-85% [9][10]. Second-order neurons are placed in the spinal cord and third-order neurons are found in the thalamus and

they project to the cerebral cortex [1][3][7]. Throughout the sensory pathway, there are different mechanisms of **modulation**, which are mediated by neurotransmitters and other molecules that decrease or increase the intensity of the noxious signal. Finally, the brain **perceives** the information and integrates signals to mount a response [11] (**Figure 2**).

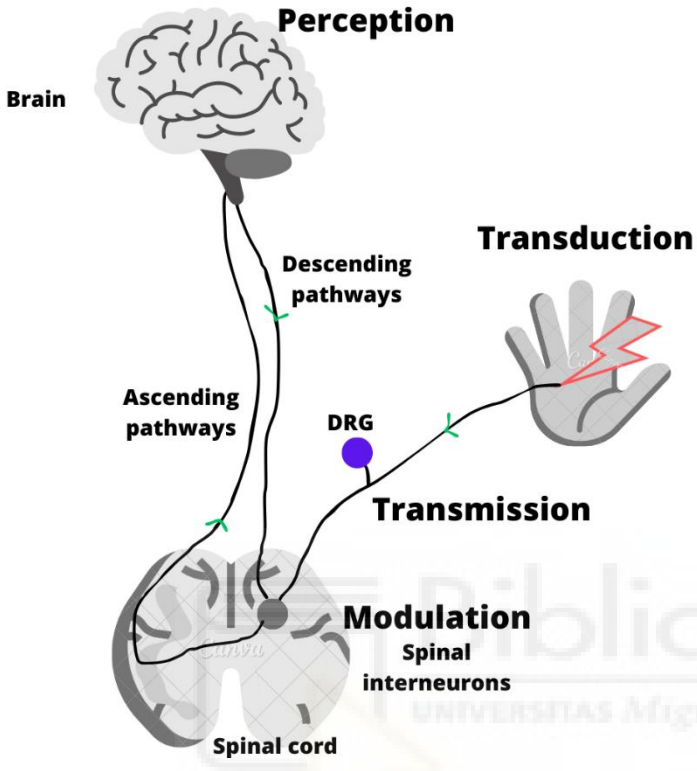

Figure 2 Pain propagation phases: (1) Transduction, (2) Transmission, (3) Modulation, and (4) Perception. Image

created in Canva.

Different sensory modalities are transmitted by peripheral nerve fibres which differ in diameter and electrical conduction velocity [5][1]. The canonical classification distinguishes afferent fibres for being myelinated or not. Among the myelinated, **Aα** and **Aβ** are large and medium diameter neurons, with high conduction velocity. These fibres are mechanoreceptors for touch, proprioception, and other innocuous mechanical stimuli. The high conduction velocity in the mechanical fibres is necessary to allow a fast motor response to the stimulus. Other myelinated fibres are called **Aδ**, which are thinly myelinated small small-diameter neurons. These fibres are thermal receptors, chemoreceptors, and nociceptors mediating localized fast pain, conducting impulses more slowly than other

myelinated fibres. On the other hand, the unmyelinated afferents are small-diameter fibres called **C-fibres**; these neurons convey poorly localized, slow pain. The difference in conduction velocity between fibres, allows the mechanical and innocuous stimuli to be perceived before the noxious ones [1][5]. C-fibre neurons have small cell bodies and can be additionally divided into two subpopulations: (1) **peptidergic** neurons that express neuropeptides such as substance P (SP), calcitonin gene-related peptide (CGRP), and the tropomyosin receptor kinase A (TrkA) which responds to nerve growth factor (NGF); (2) **non-peptidergic** neurons, expressing c-Ret neurotrophin receptor that is targeted by glial-derived neurotrophic factor (GDNF), and a large group of these nociceptors also binds to the isolectine B4 (IB4) in rodents [5]. In contrast, the large diameter neurons are characterized by the expression of the neurofilament NF200 [4][12], however in humans, it seems that NF200 is present in all DRGs sensory neurons co-localized with brain-specific homeobox/POU domain protein 3A (Brn3a) [13]. This fibres classification has been later extended by the introduction of molecular markers that can be correlated with the previous functional classification. For example, scRNA-seq studies have divided DRG neurons into **12 molecularly defined cell types (Figure 3)**. Among these groups, the NF 1-3 are myelinated low-threshold mechanoreceptors (LTMRs) that transmit tactile information and NF4 are proprioceptors that sense the movement and position of the body. Tyrosine hydroxylase (TH) labels unmyelinated C-fibres LTMRs which also encode noxious information. Another type of unmyelinated cells is PEP1 which are peptidergic neurons expressing CGRP and SP. On the contrary, myelinated neurons PEP2 do not express SP, while PEP3 expresses TRPM8, PIEZO2, and probably CGRP. Furthermore, nociceptors are also present in the NP1 subpopulation, which are unmyelinated polymodal nociceptors that respond to noxious mechanical, thermal, and pruritic stimuli. Itch is also sensed by NP2 and NP3, although these neurons are also able to transmit pain-related information as well. TRPM8 cells comprise a different group, defined by their expression of the cold-sensing transient receptor potential (TRP) channel melastatin 8 [10][15][16][17][18][19].

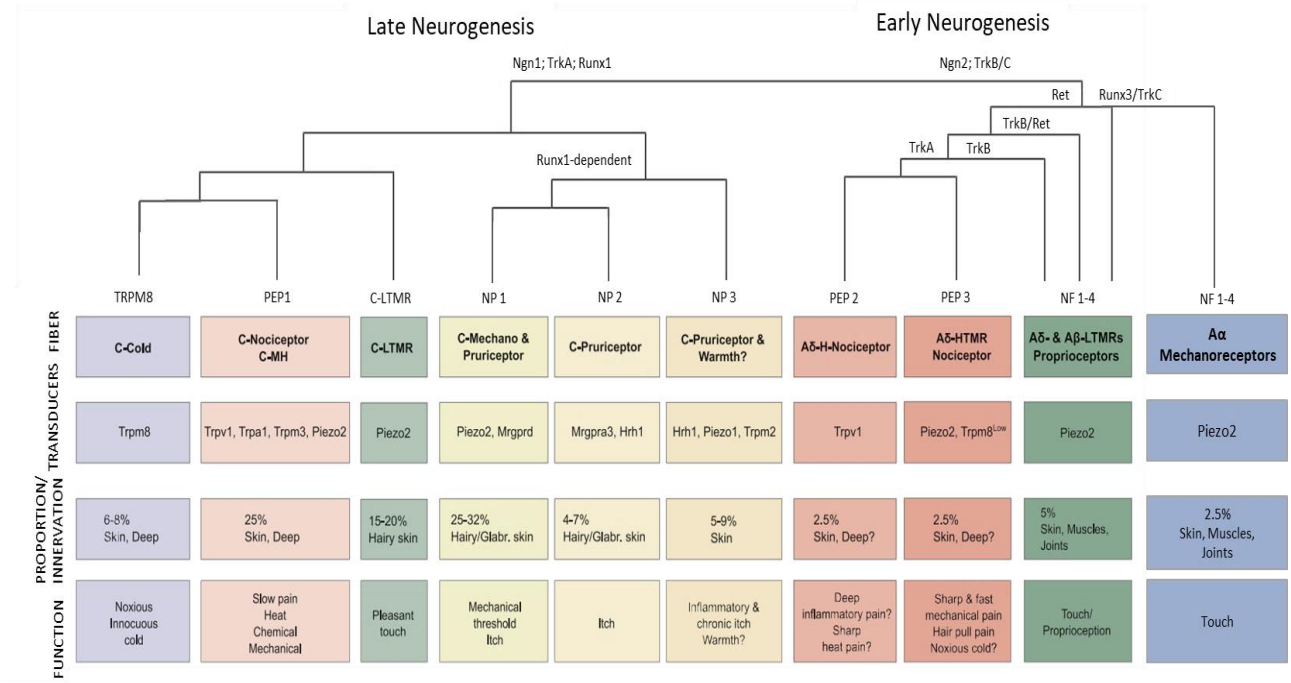

Figure 3 Molecular and functional taxonomy of mouse dorsal root ganglion sensory neuron types based on mouse scRNA-seq data. Legend: M, mechanical; H, heat; HTMR, high-threshold mechanoreceptor; LTMR, low-threshold mechanoreceptor); question mark indicates prediction based on expression. Adapted from Kupari and Ernfors [20]

Although many somatosensory markers have been extensively studied, a globally accepted view of the transcriptional profile of DRG neurons has not been established yet. With the advancement of transcriptomics studies, traditional functional characterization has become more intricate. For instance, these studies have shed light on phenomena such as thinly myelinated fibres expressing CGRP and their capacity to perceive itch [20]. Importantly, the majority of these studies were conducted on rodents' sensory neurons leading to a lack of information about human DRGs or TGs. However, recent studies on **human sensory neurons** highlighted important differences and similarities between species which may be critical in translating data retrieved from rodents to human pathologies. To make some examples, the size of human sensory neurons was estimated in a range between 20 and 100 μm, being larger than rodents', and human sensory neurons do not express IB4, which in rodents DRGs is used as a non-peptidergic marker [5], [21].

1.1.1. Ion channels in sensory neurons

The detection of somatosensory stimuli involves the expression of metabotropic and/or ionotropic receptors, which define the functional properties of the neurons [3]. The cell excitability and sensitivity are regulated by ionotropic channels such as transient receptor potential (TRP), voltage-gated sodium (Nav), calcium (Cav) as well as potassium (Kv) channels [1][13]. **Transient receptor potential channels** (TRPs) are nonselective cation receptor channels similar in structure to voltage-gated channels [1], their activation mainly leads to the influx of Ca^{2+} across the plasma membrane. TRPs are expressed in the cell membrane, where they participate in the homeostasis of Ca^{2+}, $Mg^{+,}$ and Na^{+} among other cations [22], in the membrane of intracellular organelles, and in vesicles in the presynaptic membrane [7]. TRP channels respond to temperature, mechanical stimuli, osmolarity changes, pheromones, taste, and chemicals, such as toxins, venoms, and substances released by injured tissues [23][1]. Among these, **TRPV1** (transient receptor vanilloid 1) is activated by temperatures above 45°C and by the vanilloid capsaicin [1]. This channel contributes to acute thermal nociception and hyperalgesia after tissue injury [15][30]. In humans, the presence of TRPV1 has been confirmed in all-size neurons, in contrast to rodents where the channel marks a population of peptidergic C-fibres, that constitute 30-50% of all somatosensory neurons. A cohort of TRPV1-expressing fibres also expresses TRPA1 (transient receptor ankyrin 1) that can be activated by TRPV1-dependent cytoplasmic calcium increase. Activation of TRPV1-positive fibres promotes peptide-mediated vasodilation and other paracrine actions near the trauma, culminating in the production of a complex mixture of proinflammatory and proalgesic factors, referred to as inflammatory soup, which sensitizes the peripheral terminal [23][14]. Some of these factors can potentiate the channel such as low pH, bradykinin, and nerve growth factor [24]. On the contrary to TRPV1, **TRPM8** responds to cool temperatures below 25°C and it is activated by cooling agents such as menthol or icilin. This channel is expressed in 15% of all sensory neurons, comprising mostly C-fibres, as well as a minor cohort of Aδ fibres [24][23]. A subset of these TRPM8-positive cells may co-express TRPV1 and CGRP, but a major fraction of these neurons is not labelled by other known somatosensory or nociceptive markers, revealing a system where hot and cold information reach the CNS through separated pathways [25]. In contrast to TRPV1, which gives sensitivity only to noxious heat, TRPM8

plays a role in both innocuous and noxious cold sensations *in vivo* [24]. Another cool-activated TRP channel is **TRPA1**, which is sensitive to temperatures below 17°C. Furthermore, this channel is activated by Ca2+ ions and many irritant chemicals such as mustard oil, tetrahydrocannabinol, allicin, acrolein, formaldehyde, cinnamaldehyde, gingerol, and thymol. TRPA1 also participates in thermosensation and mechanosensation. It was initially identified in human foetal lung fibroblasts as a transformation-associated gene product [26]. These three TRP channels were characterized all along this work as a means to identify and classify the putative human sensory neurons generated with conversion protocols. Genetic studies highlighted the importance of TRP channels in development and sensory transduction. Thus, understanding how these channels respond to physiological stimuli and drugs is of clinical and therapeutic importance [24][23][27][28].

Once the stimulus has been transduced into a generator potential, where many different membrane proteins are involved, voltage-gated channels come into play. Notably, **voltage-gated sodium channels** (Nav) are key players in the generation of action potentials in DRG neurons. Out of nine components of the Nav family, Nav 1.7, 1.8, and 1.9 are of particular interest in pain signalling [29]. In humans, the presence of at least one of these three channels was detected in all-size sensory neurons; in contrast to rodents, where these ion channels are typically expressed in small-size neurons. Differences of expression were found between humans and rodents, as Nav 1.8 is more expressed in rodents while Nav 1.7 is more expressed in human DRGs being present in half of human DRG neurons. Interestingly, these channels seem to co-localize with TrkA, the NGF receptor, at different amounts [30][31]. Other important ion channels in sensory neurons' electrophysiological equilibrium are **voltage-gated calcium channels** (Cav), which are pivotal components of sensory neuron function as their activation contributes to the exocytosis of transmitted-filled vesicles at synaptic endings [32]. In recent days, no studies have confirmed the localization of these channels in human DRGs, however, their presence has been confirmed through RT-qPCR. The importance of these channels in pain sensitivity resides in their role after the hyperpolarization of neurons and their ability to be modulated by ATP, as in the case of the P_2X_3 channel, which is expressed in human DRGs [14]. **Potassium channels** are also important in the repolarization after action potentials being involved in the fast membrane potential repolarization, in allowing potassium ions to flow into the cell more easily when the

membrane potential is negative, and in maintaining the resting membrane potential of neurons [33].

1.2. Nociception and pain

Nociception is the process whereby primary afferent nerve fibres of the somatosensory system detect noxious stimuli [24]. According to the International Association for the Study of Pain (IASP), “pain is an unpleasant sensory and emotional experience associated with, or resembling that associated with, actual or potential tissue damage” [34]. This definition takes into account the **subjective** and **emotional** response to pain, highlighting the relevance of the personal experience. Pain is useful to any individual as an alarm to warn the body about the presence of a noxious stimulus so that corrective feedback can be mounted [35], however, painful conditions can lead to a persistent sensitization produced by ongoing inflammatory or neuropathic damage. This persistent and chronic pain can continue even when the initial motive has already been medically addressed and healed [36] [37].

Chronic pain is the principal reason why people look for medical care, affecting more than 40% of the US population [35] and it is a major healthcare problem in Europe, according to the European Pain Federation, being more prevalent in women and older people [38]. The cost of chronic pain in terms of quality of life and suffering is difficult to quantify, however, the economic impact of pain is great due to the effects on workplace absenteeism, reduced levels of productivity, and long-term disability [39]. Many of the treatments available have limiting side effects such as creating addiction, gastrointestinal problems, and difficult compliance to the treatment. Despite its importance, many chronic pain conditions still lack adequate **treatment**, which in many cases require the use of opioids that are known to cause gastrointestinal and respiratory side effects as well as tolerance and reduced efficacy [35][40]. The wrong prescription and use of these antinociceptive drugs led to an increase in opioid use in the USA, which is nowadays translating into a four times increase in fentanyl-induced overdoses in the USA since 1999 [41]. Opiates are efficient pain suppressors but they imply serious side effects. On the other hand, non-steroidal anti-inflammatory drugs (NSAIDs) are much less dangerous but they display limited efficacy outside of specific diseases. NSAIDs are effective in treating inflammatory pain but their use is limited by

gastrointestinal, cardiovascular, and renal side effects [40]. Thus, further knowledge of the pain alterations is crucial for the development of finer non-opioid interventions against mechanisms of pain chronification. In principle, analgesic drugs acting at nociceptor-specific targets have the biological advantage of being specific and selective. Studying the peripheral nervous system and identifying the mechanisms of peripheral sensitization is a promising area for potential analgesic treatments avoiding the CNS, thus limiting off-target adverse effects [26][40]. In addition to adequate treatment, an appropriate multidisciplinary approach is needed, including psychological treatment, physical exercise, nutrition, and dietary supplementation.

Pain can be classified into four different types, depending on which are the physiological and chemical changes occurring. **Nociceptive pain** is a physiological protective sensation related to the perception of noxious stimuli and it occurs in the presence of intense stimuli. This early-warning sensation has a protective role and is essential for maintaining tissue integrity. **Inflammatory pain** is also adaptive and protective, it is the result of the activation of the nociceptive pain pathway and the immune system by mediators released at the site of tissue injury or infection. By increasing the sensitivity after tissue damage, this pain helps in the recovery of the injured body part discouraging physical contact and movement while promoting healing [42]. Pain can also be maladaptive and pathological when it is caused by a dysfunction of the nociceptive system, such as genetic factors or injury to the nervous system. This condition is called **pathological pain**, which can occur after damage to the nervous system (neuropathic pain), but also without damage or inflammation (dysfunctional pain) [35][42]. Lastly, **functional pain** exists, in which chronic pain syndromes occur due to abnormal amplification states in the CNS. In this form of pain, no neurologic or peripheral abnormality is detected. Several common pathological conditions may cause pain such as cancer, inflammatory conditions, fibromyalgia, irritable bowel syndrome, some form of non-cardiac chest pain, and tension-type headache [11].

As mentioned before, the activation threshold of nociceptors can decrease in response to repetitive and intense stimuli, a process called **sensitisation**. In normal conditions, when the tissue lesion or the noxious stimulus disappears, the system returns to the basal state, recovering the normal activation threshold [43]. However, in pathological situations this recovery does not occur, provoking allodynia, a process through which non-painful stimuli

are perceived as noxious; or hyperalgesia, where stimuli that are normally noxious are perceived as more painful or during a longer time [11]. Sensitisation can occur at a central or peripheral level. Both processes are mediated by molecules interacting with receptors or ion channels present in nervous terminals such as extracellular protons, arachidonic acid, serotonin, NGF, prostaglandins (PG), bradykinin (BK), etc...[44]. In turn, nociceptors can release peptides and neurotransmitters that facilitate the production of inflammatory molecules and promote the release of non-neuronal factors producing positive feedback, and giving rise to a process called neurogenic inflammation [45].

1.3. Sensory neurons development

All peripheral nervous tissue originates from the **neural crest**, which is a population of multipotent cells that only exist during the early stages of embryonal development. Immature neuronal tissues receive genetic and environmental cues that induce a hierarchical developmental process, until the formation of the neuronal subtype-specific identities and axonal projections. During the early phase of foetal neuronal development, the signalling pathways wingless-related integration site (Wnt), bone morphogenetic proteins (BMP), fibroblasts growth factor (FGF), and neurogenic locus notch homolog protein (Notch), among others, have a pivotal role in the induction, migration, and conversion of the neural crest cells. In this phase, neural crest cells migrate towards the ventral area of the neural tube where they coalesce into ganglia at regular intervals [15][46][47][48]. During the process of sensory neurons development, the expression of basic helix-loop-helix (bHLH) transcription factors (TFs) **Neurogenin 2** (Ngn2) and **Neurogenin 1** (Ngn1) drives two different waves of neurogenesis. The first wave induces large-size neurons while the second wave induces small-size neurons, both leading to the emergence of a few sensory sub-lineages. After these first two waves of neurogenesis, immature sensory neurons start to express insulin gene enhancer protein (Isl-1 or Islet1) and **brain-specific homeobox/POU domain protein 3A** (Brn3a), which lead to the final specification and suppression of other neural fates [15][49] (**Figure 4**).

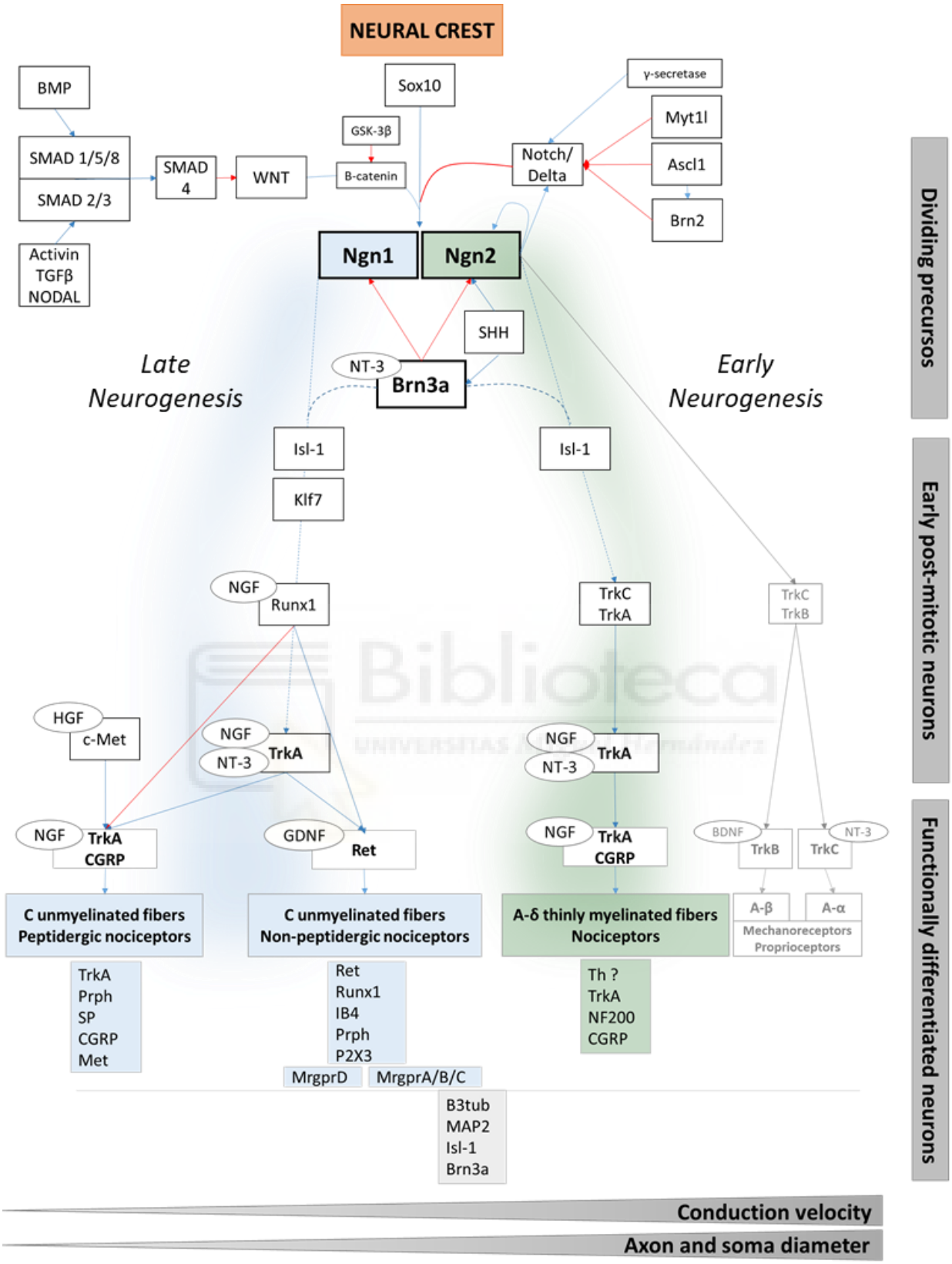

Figure 4 Development of neural crest into mature sensory neurons. Red lines indicate inhibition and blue lines indicate induction. Dashed lines indicate correlation. The image was created using PowerPoint, modified from Marmigère and Carroll [49].

More in detail, during the first neurogenesis wave, mediated by Ngn2, three myelinated populations are generated: (1) early-Ret that expresses GDNF receptor; (2) tropomyosin receptor kinase B/C (TrkB/TrkC) positive cells that are sensitive to brain-derived neurotrophic factor (BDNF) and neurotrophin-3 (NT3); and (3) early-TrkA that expresses NGF receptor. During the second wave of neurogenesis, mediated by Ngn1, unmyelinated late-Trka and late-Ret populations are developed. These populations express both TrkA and RUNX family transcription factor 1 (Runx1) in the early stages, but, later in development, late-TrkA maintain TrkA expression and switch off Runx1 in some cells only. On the other hand, late-Ret will develop to non-peptidergic nociceptors maintaining the expression of Runx1, TrkA, and Met, the hepatocyte growth factor (HGF) receptor. As a result of these changes in the expression signature, neurotrophin receptors become important not only as a way to classify sensory neurons but also for peripheral innervation of the appropriate targets, cell survival, and expression of molecular properties of the different sensory neuron subtypes. For example, large-diameter DRG neurons conveying low-threshold mechanoreception from the skin, express Ret and/or TrkB (in combination, or not, with TrkC); large proprioceptive neurons express TrkC; and small- and medium-diameter neurons, many of which respond to noxious stimuli and mediate pain sensation, express TrkA, Met and/or Ret [49][50][51].

As previously stated, sensory neurons can be classified into **11 different subtypes** based on their molecular signature. However, DRG neurons can also be classified according to their developmental ontogeny (**Figure 3**, **Figure 4**): for example, NF1-4 are generated early, during the first wave of neurogenesis while TH, TRPM8, NP1-3, and PEP1-2 subtypes are developed later. Runx1-persistent neurons, which switch off TrkA and activate the Ret receptor, represent a majority of NP1, TRPM8 neurons, TH neurons, and a small subset of neurons with high levels of TRPV1. On the other hand, neurons that maintain TrkA and switch off Runx1 are PEP1, NP2, and NP3, as well as a small subset of TRPM8 positive neurons. NP2 and NP3 are crucial for itch sensation and their development needs early Runx1 activity before it is switched off. On the contrary, PEP1-2 neurons, which play a pivotal role in nociception, are independent on Runx1 expression [15][17][52].

1.4. Sensory neurons animal models

Pain studies on human subjects are challenging, subjective, and ethically limiting, and thus many preclinical animal models have been developed to research and characterize different types of pain and its symptoms. Pain research is mainly performed on **rodents**, because of the ease of breeding and care, their behavioural complexity, and the possibility of assessing some of the affective components related to pain conditions. Smaller animal models such as *Drosophila sp.* may be more useful in the identification of a molecular target. However, due to the increase of genetically modified rodents, mice and rats are also highly used in investigating the molecular aspects of pain. Furthermore, a large panel of evaluation devices used to characterize pain-like behaviour in animal models have been developed over the years, which in most cases permit to quantify the sensory component of pain. Although rodents have been pivotal in many discoveries of pain mechanisms and molecular targets, the organization of their nervous system remains different from that of humans [53] [54]. The main model for *in vitro* studies of **sensory neurons** relies on dissociated cells from DRGs or TGs. These cells have been widely characterized; however, their use poses ethical issues and their representativity of the human sensory neurons is limited. Furthermore, the number of cells that can be extracted is low, especially from trigeminal ganglia; and neurons have limited survival *in vitro*, therefore high experience is needed to perform reproducible experiments. Human DRGs have also been used in preclinical studies, however, their availability is reduced, and relies on donors, which poses ethical limits. These cells are mainly used to test whether analgesic molecules validated in rodent models can work in human tissue [14][13][55].

While there is no doubt about the necessity of animal models in pain research, they present a high rate of failure in the **translation** of basic science data into effective and commercially available therapies. Many molecules that successfully demonstrated analgesic effects in preclinical studies, fail to produce similar effects when tested in clinical trials. Translation is defined by the National centre for Advancing Translation Science as “the process of turning observations in the laboratory, clinic, and community into interventions that improve the health of individuals and populations from diagnostics and therapeutics to medical procedures and behavioural interventions”. One of the reasons this failure might occur relies

on the genetic and molecular neurochemical differences between humans and animals. However, it could also be due to non-optimal research conditions and not directly related to the failure of the model. Furthermore, the debate is complicated by the lack of published negative data, both from preclinical and clinical trials [17][34][53][54][56]. In light of the failure in translating preclinical to clinical data, the use of human *in-vitro* models will likely facilitate the development of new drugs to treat pain.

1.5. Cell reprogramming

In 1957, Conrad Hal Waddington presented his view of development describing the metaphor of a ball rolling down from the top of a slope towards the bottom of a hill, restricting the developmental options of the cell until a stable state of terminal differentiation. This metaphor led to the understanding that the fate of a cell is decided in the early developmental stages. However, later studies found out that the overexpression of transcription factors or the change in environmental conditions are able to convert embryonic or somatic cells to another cell type, revealing that cell identity can be modified even during latter developmental stages [57] [58]. Cells resembling human sensory neurons have been generated from human embryonic stem cells (hESCs) [59] and **induced pluripotent stem cells** (iPSCs) [60] [61]. In comparison to hDRG neurons, iPSCs induced neurons allow to study rare genetic modifications and generate an almost limitless supply of cells to study. Donor cells are usually obtained from skin biopsies or blood because of the ease of extraction, compared to obtaining hDRG [55]. Skin fibroblasts or blood peripheral blood mononuclear cells (PBMCs) are reprogrammed to pluripotent stem cells that can differentiate into a variety of cell types [62]. The most commonly used protocol to comprehensively generate sensory neurons from iPSC was developed in 2012 by Chambers and colleagues. In this study, human iPSCs were differentiated into a homogenous culture of neurons with a transcriptional and functional profile similar to DRG nociceptors [60]. However, there are also reports of the same protocol generating neurons with gene expression profiles resembling other sensory neuron types. Such differences may be due to minor protocol modifications highlighting the sensitivity of the protocol to small changes in culture media [63][64]. As an alternative to iPSC, as a starting cells type to obtain sensory neurons, two publications in 2015 demonstrated that forced expression of

transcription factors can convert **dermal fibroblasts** to induced sensory neurons (iSNs). One study by Wainger and collaborators [65] used a combination of TFs to generate a pure population of TRPV1+ nociceptors. The second study, conducted by Blanchard, Eade et al., produced a heterogeneous group of neurons that expressed TrkA, TrkB, and TrkC by overexpressing Brn3A and Ngn1 (BN1) or Brn3A and Ngn2 (BN2) in rodent and human fibroblasts [66]. The process of inducing a desired cell fate, by converting somatic cells from one lineage to another, without transitioning through an intermediate pluripotent or multipotent state, has been described as 'transdifferentiation' or 'direct conversion' [54] [55] (**Figure 5**).

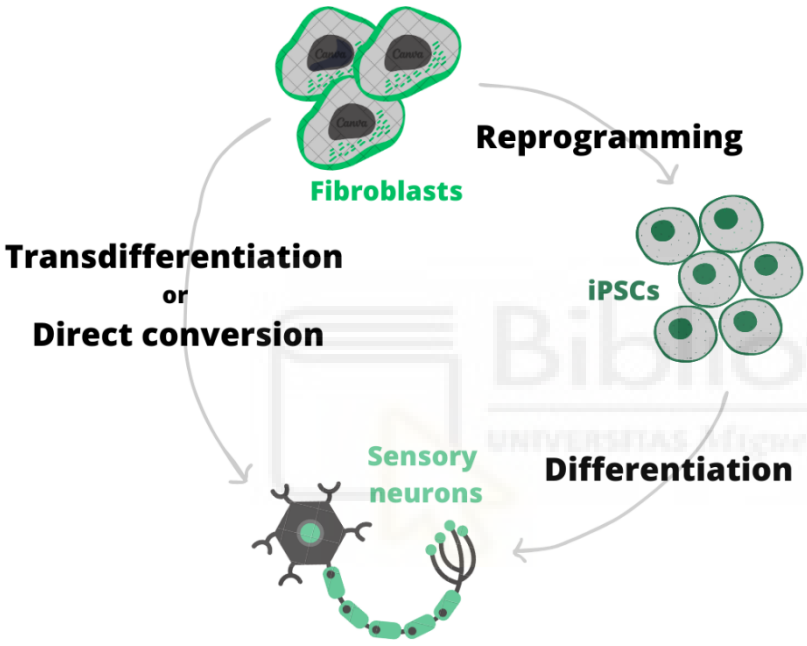

Figure 5 Direct conversion, also known as transdifferentiation, refers to the direct change in cell fate from one cell type to another. In contrast, reprogramming involves an intermediate pluripotent state that is followed by the differentiation to a terminal differentiated cell. The image was created by the author using Canva.

Direct conversion is faster, more efficient, and presents advantages for tissue repair, in comparison to iPSC differentiation. However, the direct conversion efficiency of fibroblasts to iSNs is less than 5% [66][65]. Transdifferentiation does not benefit from the advantages of using a pluripotent intermediate but removes the costly and variability-inducing step of cellular reprogramming. Low conversion efficiency may be a consequence of the starting cell type, as direct conversion of neural crest cells shows substantially increased differentiation efficiency [55][61]. Several additional factors such as

species and age of the donor, passage number, and prolonged culturing of cells before conversion, affect the efficiency of this approach [67][68]. To assess the impact of donors' age in reprogramming, transcriptomes of fibroblast-induced neurons (iNs) and iPSCs were compared, demonstrating that directly reprogrammed iNs retained donor aging signatures, while iPSCs-derived neurons were rejuvenated [67]. Interestingly, in 2017, Drouin-Ouellet, Lau, and colleagues directly converted fibroblasts to a heterogeneous population of neurons by inducing the expression of Ascl1, Brn2, and two short hairpin RNAs (shRNA) inhibiting **repressor element 1 silencing transcription factor** (REST). This protocol presented efficiency between 30 and 60%, whereas the efficiency was calculated as the number of Tubulin-associated unit (Tau) positive cells over the total number of fibroblasts plated. The high conversion efficiency was confirmed using fibroblasts from different donors and did not decrease at high passages, identifying REST as a barrier to human fibroblasts reprogramming [68].

A common challenge to all differentiation protocols is to validate how **representative** induced cells are to their native counterparts. Sensory neuron populations are commonly classified based on their functional response to stimuli and/or their transcriptional profile. However, being rodents' sensory neurons the most characterized system, human differentiated neurons are often compared to markers as defined in rodents. Another issue to be addressed is how mature the iSNs are, since human sensory neurons develop and mature over years, while iSNs are cultured for few weeks or months and are therefore unlikely to represent fully mature neurons [55]. So far, iPSC or fibroblasts-derived iSNs have provided valuable insight into rare genetic pain conditions, such as mutations in $Na_v1.7$ [63][64], the role of PIEZO2 in mechanotransduction [61] and much more. Moreover, iSNs from healthy donors are assumed to be naïve and uninjured sensory neurons, which creates an opportunity to induce pathological conditions or injury *de novo* [55]. While we cannot yet recreate the full range of sub-populations among sensory neurons, there has been recent progress in expanding the list of populations that can be generated (**Table 1**) both through iPSc differentiation and direct conversion.

Table 1 Main sensory neurons differentiation strategies and resultant subtypes. Modified from Chrysostomidou et al. [55]

Afferent subtypes	Functional and molecular main features	Reference
Cold thermoreceptor	TRPM8+, Menthol sensitive, Noxious cooling sensitive	Nickolls et al.[58], Blanchard and Eade et al [59], Wainger et al [60]
Non-peptidergic nociceptor	RET+, Activated by α,β me-ATP	Chambers et al.[57]
Peptidergic nociceptor	TrkA+, CGRP+ and CGRP release, Capsaicin sensitive, Noxious heat sensitive	Blanchard and Eade et al, Wainger et al, Saito-Diaz et al [61], Alshawaf et al [56]
Aδ-LTMR	TrkB+, Activated by osmotic swelling	Alshawaf et al
Pruriceptor	Activated by His, IL-4, IL-31, Bam8-22	Umehara et al [62], Blanchard and Eade et al
Proprioceptor	TrkC+,	Mazzara et al [63]
Aβ-LTMR	TrkB/C+, FAM191A1+, Activated by osmotic swelling	Nickolls et al, Saito-Diaz et al, Alshawaf et al

Another issue to be addressed is that nociception requires sensory neurons to act in concert with **many cell types** and abnormal inter-cell signalling can lead to pathological pain conditions [1]. The possibility of developing *in vitro* systems that allow studying cell–cell interactions is, therefore, attractive. Rodent sensory neurons have been co-cultured with many cell types such as glia, immune cells, peripheral end targets, and second-order neurons [55][69]. Lately, a study was published where authors induced epithelial and neural crest cells within one skin organoid. The tissue presented dermis, epidermis, and functional hair follicles, it was innervated by iSNs and also contained glial cells [70]. Homogeneous cultures reduce experimental variability and offer greater power to characterize cellular phenotypes. However, the ability, to assess the effect of an analgesic candidate on multiple subtypes of sensory neurons in the same culture may generate more translational data. Further work is required to develop protocols where many types of cells co-exist and communicate, but the presence of studies trying to include the many sensory components in one *in-vitro* model is an exciting prospect. For these experiments to be representative, efforts are made to validate consistent *in vitro* protocols.

Previous studies have shown that it is possible to change cell fate by inducing the expression of TFs or non-coding RNAs. This is usually done by the introduction of lentiviral or adenoviral vectors into the target cells. Viral vectors are necessary in this field to induce transgene expression in primary cell lines such as human fibroblasts.

1.5.1. Lentiviral vectors and TetOn system

Lentivirus is a viral genus that is part of the Retroviridae family. Their genome is formed by two molecules of positive mono-catenary RNA. In the production of lentiviral vectors (LTVs), the components necessary for virus production are split across multiple plasmids to increase the safety of lentivirus. The **2nd-generation systems** are comprised of three plasmids.

- the transfer plasmid which contains the gene of interest, the viral long terminal repeats (LTRs), and the psi packaging signal. The transgene sequence is flanked by LTR sequences, typically, it is the sequence between the LTRs that is integrated into the host genome upon viral transduction. For safety reasons, transfer plasmids are all replication incompetent and self-inactivating after integration into the host cell;
- the packaging plasmid which encodes for the regulatory proteins of lentivirus such as Gag, Pol, Rev, and Tat;
- the envelope plasmid that encodes the protein Env, usually pseudotyped with Vesicular Stomatitis Virus G protein (VSV-G) which has wide infectivity.

The development of **3rd generation system** composed of four plasmids increased safety, where packaging is split into two plasmids: one transcribing Rev and one Gag and Pol, while Tat is eliminated. All 2nd generation lentiviral transfer plasmids must be used with a 2nd generation packaging system because transgene expression from the LTR is Tat-dependent. Although safer, 3rd generation LTVs can be more inconvenient to use and result in lower viral titres. In all transfer plasmids used in this work, the Woodchuck Hepatitis Virus Posttranscriptional Regulatory Element (WPRE) is present. This sequence stimulates the expression of transgenes via increased nuclear export and it is used to titrate lentiviral vectors.

To have a tight time-control of the expression of the exogenous genes introduced with lentiviral vectors in the host cells, some of the LTVs used in this work (Brn3a and Ngn1) are

doxycycline-inducible. Doxycycline is a tetracycline-derived antibiotic used to activate or inhibit the expression of genes of interest in Tet systems [71]. Gene regulation in the Tet systems is highly specific and responds fast allowing a tight time regulation of the gene expression. The first Tet system was created by Hillen and Berens in 1994 [72][72] [73]. The authors optimized a Tet-Off system based on the presence of a tetracyclin-controlled transactivator (tTA) which inhibits the expression of the target gene in the presence of doxycycline. In the TetOn system, which was developed later, the presence of doxycycline activates the transcription of reverse tTA (rtTA), which binds to the tetracycline-response element (TRE) that, in turn, activates the transcription of the gene of interest (**Figure 6**) [71].

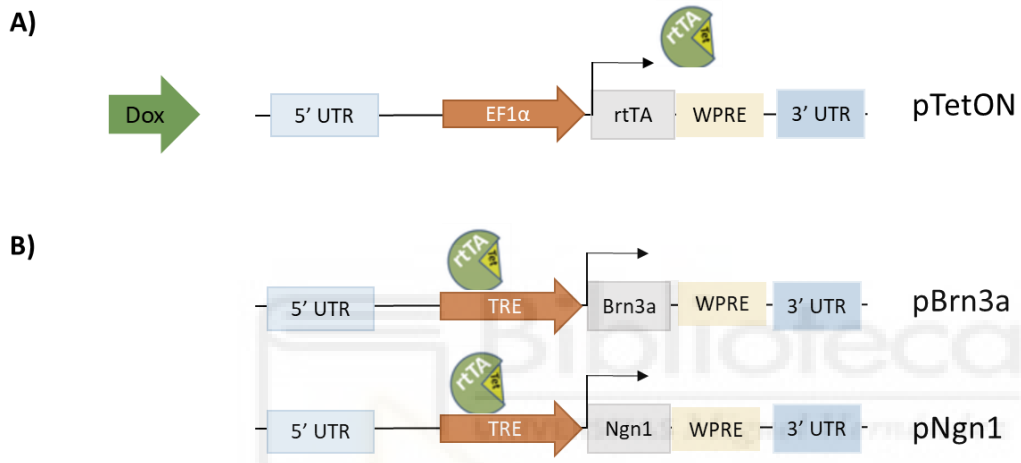

Figure 6 TetOn system: **A.** Transcription of rtTA in response to doxycycline; **B.** Binding of rtTA and TRE and the subsequent transcription of the genes of interest Brn3a and Ngn1. The vectors here represented are oversimplified to focus on the TetOn system mechanism. The image was created by the author using PowerPoint.

1.5.2. Small molecules

In addition to LTVs, another promising approach to direct cell fate is the addition of small molecules in culture, targeting many different intracellular pathways. Small molecules permeate easily inside the cell membrane due to their small size of less than 1 kDa [74]. These molecules have been shown to promote cell reprogramming and generate induced pluripotent stem cells and neural progenitors starting from mouse fibroblasts. Furthermore, small molecules enhance the action of transcription factors in the conversion from mesenchymal cells to neuronal-like cells. Small molecules, including GSK3β inhibitors, cAMP/PKA modulators, adenylyl cyclase activators, TGFβ/BMP inhibitors, or γ-secretase

inhibitors (**Figure 7**), showed efficiency to convert somatic cells into neurons and, for example, synergize with Ngn2 to redefine the transcriptional profile of fibroblasts. Even if the mechanisms underlying neural induction from fibroblasts by chemical cocktails have not been elucidated, direct conversion through small molecules, without introducing exogenous genes, could provide a suitable system for neural induction. Some authors sustain that it is unlikely that small molecules would be sufficient to completely replace the TFs induction because they do not only affect their target but can inhibit others at the same time [75][76][77][78][79]. As a result, there is still a need to identify novel small molecules that can be used in reprogramming.

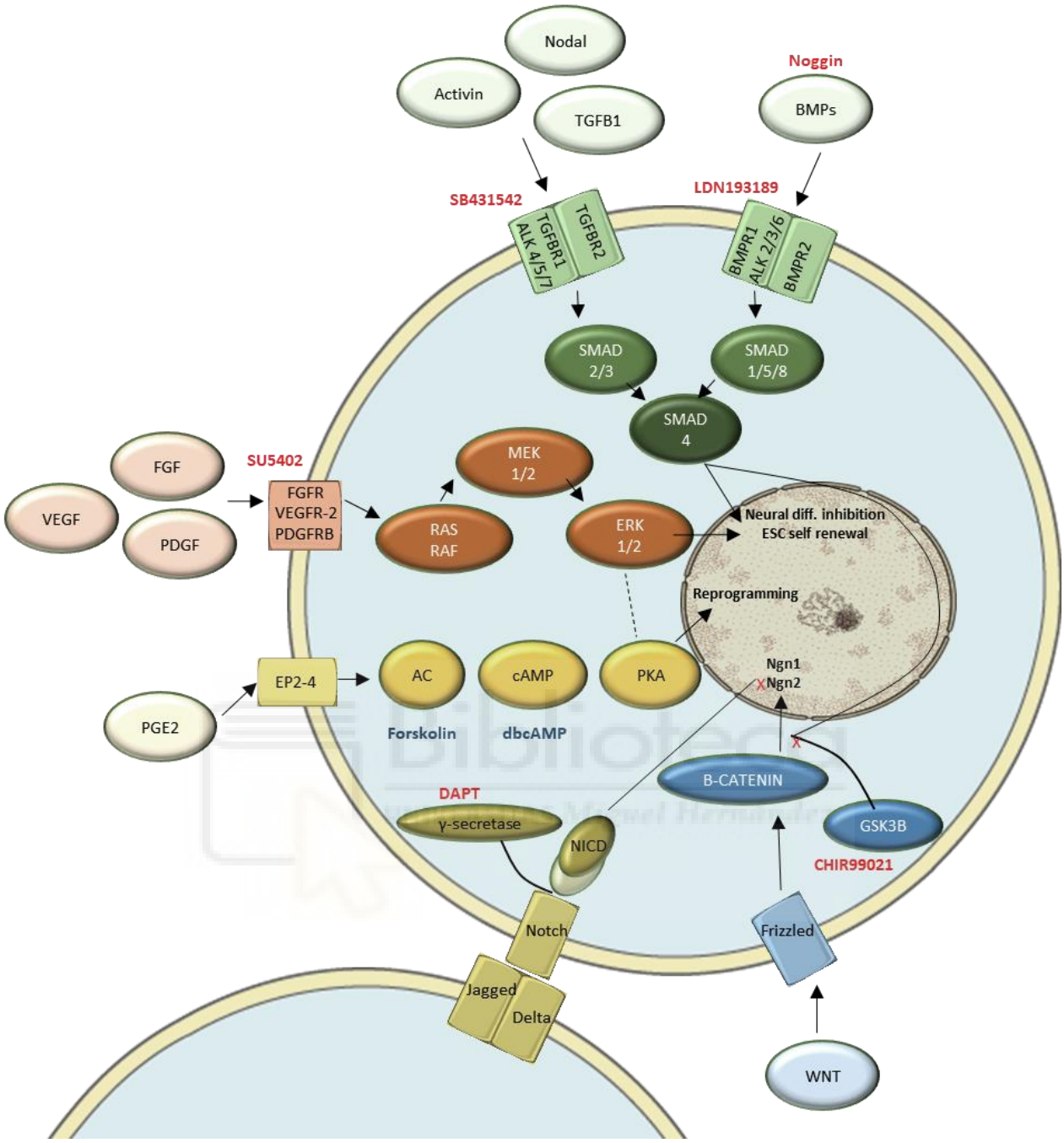

Figure 7 Most commonly cited pathways inhibited or induced through small molecules during cell reprogramming/differentiation. TGFβ (Ser/Thr K) pathway is green, it is involved in self-renewal and differentiation to mesoendodermal lineages. FGF pathway (Tyr K) is represented in orange, the signalling via MEK/ERK allows self-renewal and proliferation of hPSCs. cAMP pathway, in yellow, is involved in reprogramming and differentiation into many subtypes. The Notch/Delta pathway is represented in ochre and it is important in specifying neural subtypes. WNT pathway, in blue, inhibits differentiation to mesoendodermal lineages induces self-renewal of PSCs, and aids in reprogramming. Small molecules are written near their target, in red if they are inhibitors or in blue if they are activators. The image was created using PowerPoint.

1.6. Microfluidic chambers for the study of nerve endings

The peripheral terminals of a sensory neuron are the prime targets of peripheral mediators and stimuli, while the soma and the central terminal are transducers of neuronal excitability [1]. Considering the differences all along a primary sensory neuron and the importance of being able to study each one of its segments, **compartmentalised cultures** have become an emerging scientific topic since 1979, when professor Robert Campenot developed the first compartmentalised cultures to study neurons [80]. The word "**microfluidics**" refers to devices presenting a series of channels and chambers, that range from one to a few hundred μm in size, through which microscopic volumes of fluids can be processed [81]. So far, the peripheral terminal of sensory neurons has been a difficult study subject due to its small size, although it is the main site where painful stimuli activate the cells *in vivo*. In contrast, the soma of the primary afferent neurons is easily accessible for experiments, therefore most *in vitro* sensory neuron data have been obtained studying the cultured cell bodies, assuming that they are reliable and predictable models of their peripheral terminals [82]. As the ability to fabricate tools in the micro- and nanoscale has progressed, it is now possible to study nociceptive terminals at a scale compatible with their size [81]. Compartmentalised culture methods present numerous advantages for studies of nerve fibre, such as (1) cost savings, since they work with micro volumes of media, hormones, and growth factors, that are often expensive, and (2) fine control of the environment around the studied subject, including physical and chemical gradients, which play an important role in driving cell attachment and neurite outgrowth [81]. As shown in **Figure 8**, the microfluidic chambers (MFC) used in this work present four wells, two for the somal compartment and two for the axonal compartment. Nerve endings were attracted through media volume and neurotrophin gradients.

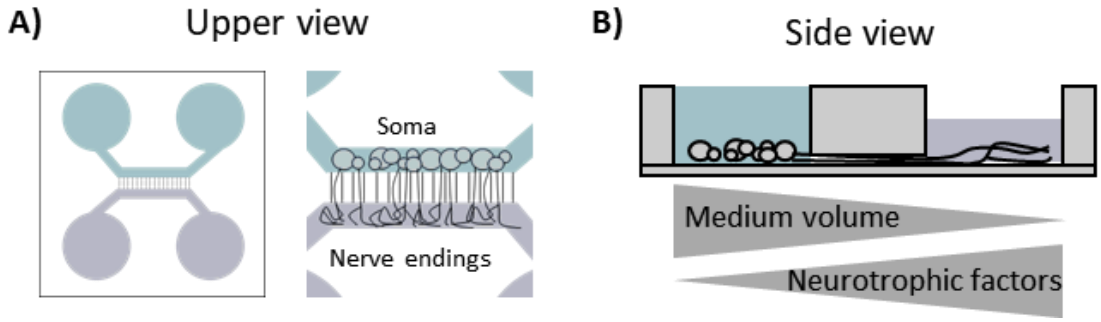

Figure 8 Microfluidic chambers scheme. A. Scheme of upper view of the microfluidic chamber without cells or with cells and developed axons. **B.** Scheme of a side view of a microfluidic chamber with cells. Axons are drawn to grow in the direction of the axonal compartment due to a physical gradient (medium volume) and a chemical gradient (neurotrophic factors concentration). Image from Giorgi et al [83].

The environmental control we have in microfluidic devices helped reveal new insights into cellular physiology and cell behaviour in physio-pathological states. Prior MFC cultures of DRG or TG neurons yielded valuable insights into various aspects of neural function such as axonal regeneration, the peripheral expression and activation of TRP channels, distinct regulatory mechanisms governing sensory neurons across neuronal regions, manipulation of synapses, compound evaluation as well as the establishment of co-cultures involving different cell types, extending to the development of three-dimensional (3D) cultures [69][84][85][86]. While a significant number of these systems operate in a two-dimensional context and therefore do not completely replicate the intricate *in vivo* arrangement of sensory neurons, MFCs offer a distinctive advantage by enabling the study of DRG or TG neurons in a manner that more closely approximates the *in vivo* layout. The multitude of capabilities afforded by MFCs should be taken into account when the aim is to uncover novel insights into neuronal physiology under both healthy and diseased conditions.

OBJECTIVES

2. OBJECTIVES

2.1. General objectives

Sensory neurons are usually studied *in-vitro* through the analysis of rodent cells extracted from DRGs or TGs. These models pose ethical limitations and have low translatability to humans due to species differences and to the environment in which the cells are studied (e.g., soma and neurites undergo the same treatments). To increase the translatability of *in-vitro* studies of sensory neurons, the main objectives of this thesis are to:

1. develop an in-vitro preclinical system of human sensory neurons;
2. develop a compartmentalized culture of rodent sensory neurons.

2.2. Specific objectives

To develop an *in-vitro* preclinical system of **human sensory neurons**, the following specific objectives were carried out:

a. Production and titration of high titer lentiviral vectors (LTVs);
b. Direct conversion of fibroblasts into sensory neurons through forced expression of Brn3a and Ngn1 through LTVs and defined small molecules;
c. Optimization of foetal lung fibroblasts conversion protocols and characterization by molecular and functional techniques;
d. Optimization of neonatal dermal fibroblast conversion protocols and characterization by molecular and functional techniques;
e. Optimization of adult dermal fibroblasts conversion protocols and characterization by molecular and functional techniques.

For the development of a **compartmentalized** culture of sensory neurons:

a. DRGs were cultured in microfluidic chambers;
b. Nerve endings were co-cultured with human fibroblasts as a proof of concept for co-culturing models;
c. Nerve endings were treated with inflammatory compounds or chemotherapeutic agents to test compartmentalized sensitization.

RESULTS

3.RESULTS

3.1. Lentiviral vectors optimization

LTVs are necessary for the transgene expression into primary fibroblasts. Therefore, the first step in this project was to optimize a protocol for LTVs production. LTVs were produced through calcium phosphate or lipofectamine transfection methods by multiple transfection in HEK293 LTV. This process was optimized with GFP LTV, which expresses GFP constitutively. As shown in **Figure 9**, HEK 293 LTV transfected with the calcium phosphate method presented fewer cells expressing GFP compared to the lipofectamine transfection method. Thus, lipofectamine transfection fostered a higher efficiency compared to calcium phosphate. Furthermore, looking at transmitted light photos, the cells transfected with lipofectamine presented lower cell confluence while cells transfected with calcium phosphate displayed normal growth.

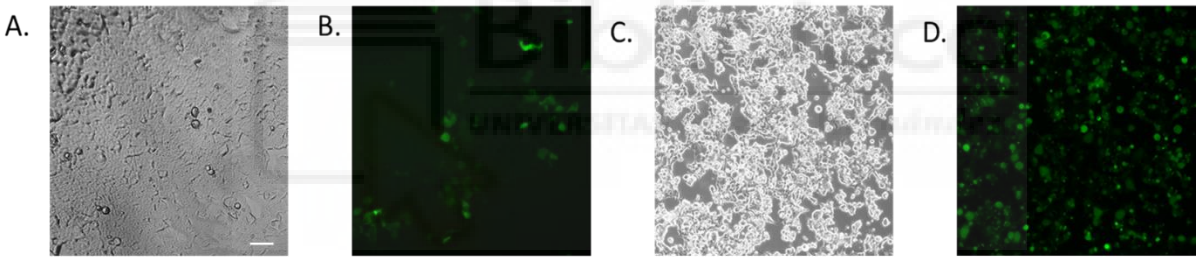

Figure 9 HEK 293 LTV 48 hours after the transfection with calcium phosphate or lipofectamine method to produce eGFP lentiviral vectors. **A., B.** transmitted light and fluorescent light of calcium phosphate method. **C., D.** transmitted light and fluorescent light of lipofectamine method. Scale bar = 100 µm

After the transfection, LTVs were collected, concentrated by ultracentrifugation, and titered by qPCR [87], obtaining titres of 10^{8}-10^{9} IU/mL. High and stable titres allowed to infect a high number of cells using low and stable vector volumes throughout independent experiments.

To demonstrate that the LTVs produced were able to induce GFP expression in human dermal fibroblasts from adult donors (HDFa), these cells were infected with GFP LTV and polybrene 8 µg/mL. The LTVs optimization assays were performed on HDFa since these

cells represent a model of adult dermal fibroblasts, which is our final goal cell type. As shown in **Figure 10**, the infection of HDFa with calcium phosphate lentiviral vectors did not induce GFP expression while the LTVs produced with lipofectamine induced high-intensity GFP expression 36 hours after the infection.

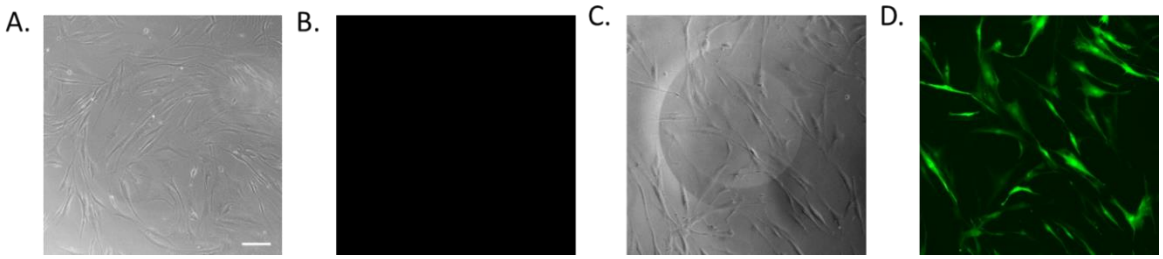

Figure 10 HDFa 36 hours after being infected with GFP LTV **A., B.** HDFa infected with GFP LTV produced with calcium phosphate method **C., D.** HDFa infected with GFP LTV produced with lipofectamine transfection. Scale bar = 100 µm

Furthermore, the infection with GFP LTVs produced with lipofectamine was compared to commercial GFP LTV (Addgene*)* and non-infected cells. As shown in **Figure 11**, GFP LTV produced with lipofectamine seemed to have a slightly faster kinetic in the GFP expression compared to commercial GFP LTV, however, 4 days after the infection, both LTVs induced the same values of fluorescence intensity. Thus, the lipofectamine transfection method was chosen as the best one to produce LTVs, compared to calcium phosphate protocol.

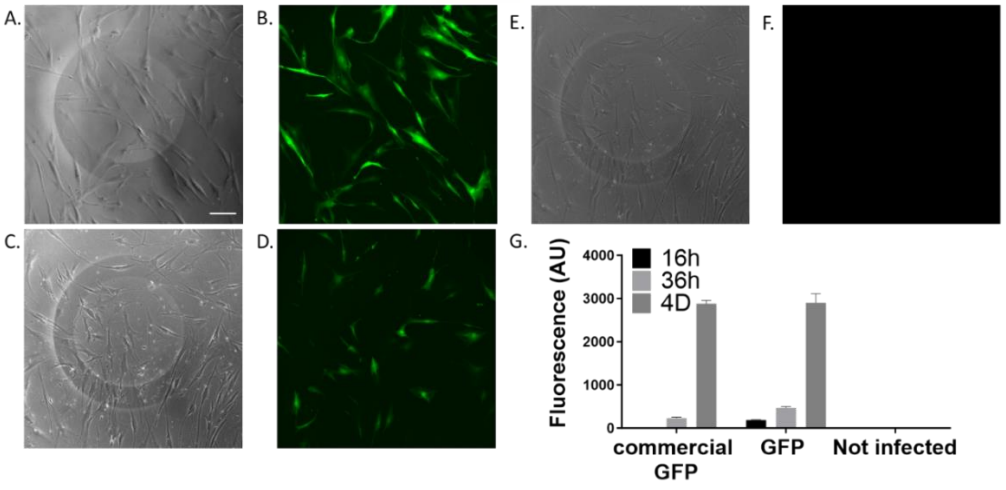

Figure 11 GFP fluorescence intensity of HDFa 36h after infection A., B. HDFa infected with GFP LTV produced with lipofectamine method **C., D.** HDFa infected with commercial GFP LTV **E., F.** HDFa not infected. **G.** Quantification of fluorescence intensity measured 16 hours, 36 hours, or 4 days after the infection. Data represented as mean ± SEM. N=2 independent experiments, n≥30 cells.

When infecting fibroblasts with LTVs, many authors use polybrene, a cationic polymer that increases the infection efficiency. However, this polymer can be toxic to some cell types, therefore toxicity was assessed through the MTT test. HDFa cells were treated with polybrene 8 µg/mL for 6, 24 or 48 hours. MTT results (**Figure 12**) showed that polybrene did not affect cell health, as measured by this test. However, it is to be noted that the MTT assay only demonstrated the presence or absence of metabolic toxicity, while it does not account for other types of cytotoxicity.

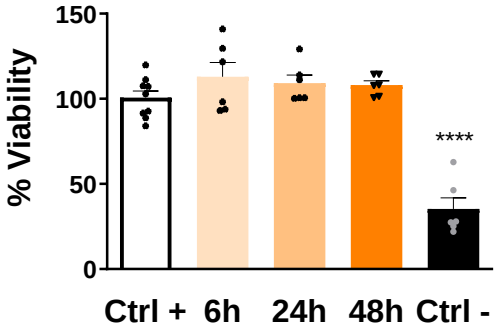

Figure 12 MTT assay on HDFa incubated with polybrene 8 µg/mL for 6, 24 or 48 hours. Positive control cells were not treated; the negative control cells were treated with DMSO 10% for 24 hours. Wells without cells were also present to know the effect of the cell medium on the absorbance measurement. Results are represented as mean ± SEM. Statistical analysis ordinary one-way ANOVA, Tukey's post-hoc test. **** $P \leq 0.0001$. N=2 independent experiments, n=6 wells.

Furthermore, to know if polybrene could increase the infection efficiency, HDFa were infected with GFP LTV in the presence or absence of polybrene. Results in **Figure 13** show that polybrene increased infection efficiency (p=0.0383). Together with the results shown in **Figure 12**, this demonstrated that polybrene does not display metabolic cytotoxicity and it increases the infection efficiency of GFP LTV in HDFa.

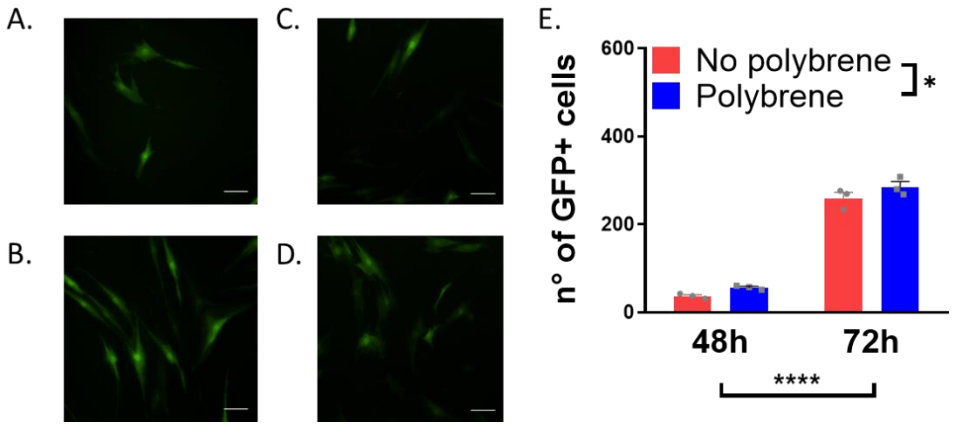

Figure 13 HDFa infected with GFP LTV with or without polybrene. A. GFP positive cells 48h after the infection without polybrene **B.** GFP positive cells 48h after the infection with polybrene **C.** GFP positive cells 72h after the infection without polybrene. **D.** GFP positive cells 72h after the infection with polybrene. **E.** Quantification of the number of GFP-positive cells at 48 or 72 hours with or without polybrene during the infection. Data are represented as mean ± SEM. Statistical analysis two-way ANOVA. * P = 0.0383; **** P ≤ 0.0001. N=3 wells.

Once the GFP expression was assessed in HDFa, we wanted to optimize a doxycycline-inducible LTV system to have a tight time control of the transgene expression. For a doxycycline-dependent LTV to work, it needs to be co-infected with the transactivator rtTA, which is activated by doxycycline and therefore induces transgene expression. For this reason, TetOGFP LTV was produced, which can only express GFP in the presence of rtTA and the antibiotic doxycycline. HDFa were co-infected with TetOGFP and rtTA (rtGFP cells) (**Figure 14**) and 16 hours after the infection doxycycline 1 µg/mL was added to the medium. As a positive control, cells were infected with GFP LTV constitutively expressing the green fluorescent protein (GFP cells). As shown in the fluorescence quantification in **Figure 14**, not infected cells did not express GFP while GFP cells presented high levels of fluorescence. rtGFP cells treated with doxycycline presented increasing GFP expression from day 2 to day 4 after induction, while the cells that were not treated with doxycycline presented a leaking basal level of GFP expression. Notably, GFP cells reached higher levels of GFP expression and presented faster kinetics than rtGFP cells.

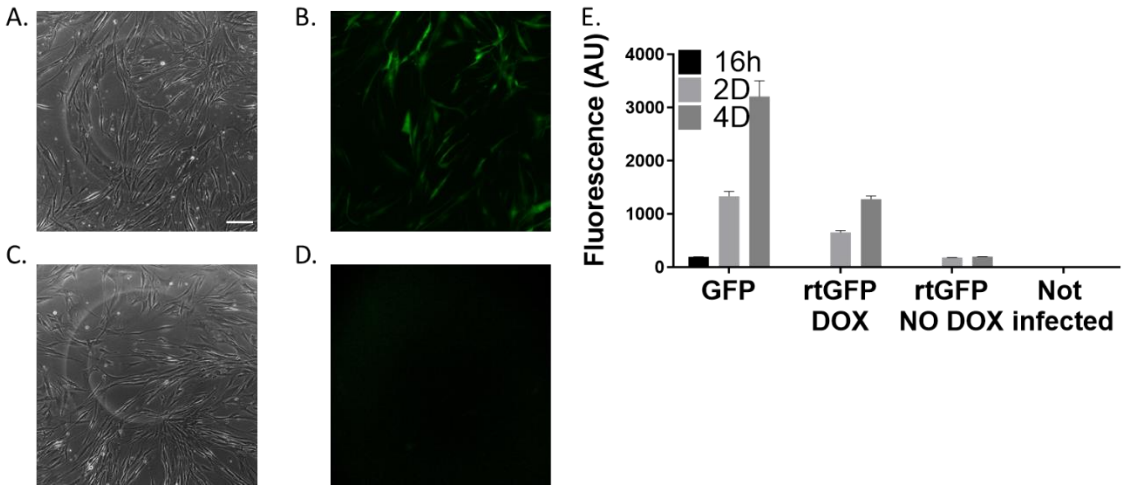

Figure 14 HDFa infected with rtGFP A., B. HDFa infected with rtGFP and treated with doxycycline **C., D.** HDFa infected with rtGFP not treated with doxycycline. Scale bar = 100 µm. **E.** Fluorescence intensity of HDFa 16 hours, 2 days, or 4 days after the infection with GFP, rtGFP induced with doxycycline, not induced with doxycycline, or not infected. Data represented as mean ± SEM. N=2 independent experiments, n≥35 cells.

Brn3a and Ngn1 (BN1) are two pivotal genes during the development from neural crest to mature sensory neurons. To convert fibroblasts to sensory neurons, Blanchard, Eade and collaborators induced BN1 expression through the infection with LTV [66]. To optimize the doxycycline-inducible system to induce BN1 expression in fibroblasts; HDFa were infected with Ngn1, Brn3a, and rtTA and treated with doxycycline. A MOI (multiplicity of infection) of 10 for Brn3a and Ngn1 or MOI 20 for rtTA were chosen according to the literature [88][68][89]. On day 4 of induction with doxycycline, immunocytochemistry was performed targeting Brn3a and Ngn1, and fluorescence intensity was quantified. As shown in **Figure 15**, double-positive cells presented a pseudo-neuronal morphology already at day four, while the same does not occur in cells that only express one transgene. Cells infected and treated with doxycycline presented higher fluorescence intensity compared to non-infected cells ($p \leq 0.0001$) and to cells infected but not treated with doxycycline ($p \leq 0.0001$). Interestingly, the expression intensity of both Brn3a and Ngn1 was higher in cells infected and induced with doxycycline compared to rodent DRGs (Brn3a $p \leq 0.0001$; Ngn1 $p = 0.0002$).

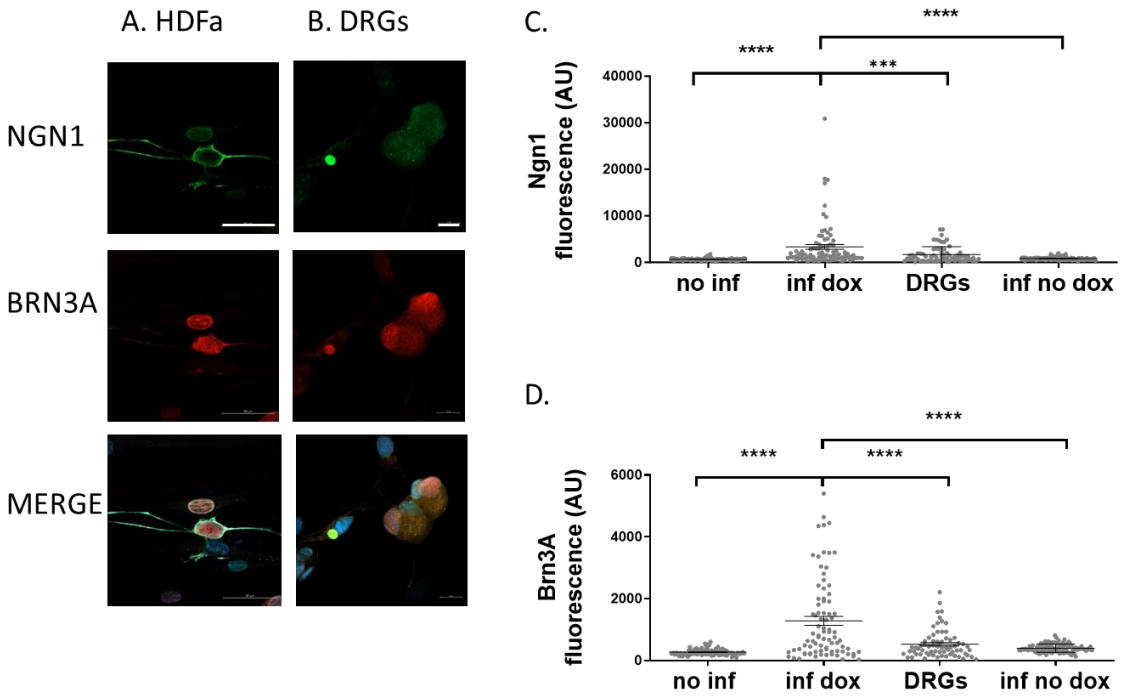

Figure 15 Immunocytochemistry of Ngn1 (green), Brn3a (red), DAPI (blue), and Merge in A. HDFa infected with Brn3a, Ngn1, and rtTA and treated with doxycycline for four days, scale bar 50 µm, **B.** rat DRGs, scale bar 10 µm, scale bar 50 µm. **C** Fluorescence intensity quantification of immunocytochemistry at day 4 labelling Brn3a or **D.** Ngn1 in HDFa not infected, HDFa infected and treated with doxycycline, rat DRGs or HDFa infected but not treated with doxycycline. Data presented as mean ± SEM in box and whiskers. Statistical analysis: ordinary one-way ANOVA with Tukey's post-hoc test. *** P=0.0002; **** P ≤ 0.0001. Every dot is a cell, n≥68 cells.

The same experiment was performed on day 8 and day 14 of induction with doxycycline, to gain more knowledge about the kinetics about the doxycycline-dependent LTVs. During the development and maturation of neural crest to sensory neurons, Ngn1 and Ngn2 induce Brn3a expression, which, in turn, inhibits the expression of neurogenins. As represented in **Figure 16**, the *in vitro* kinetics is consistent with the *in vivo* one. It was indeed observed that after the co-infection of Brn3a and Ngn1, Ngn1's maximal expression was at day 4 (p≤0.0001), while the highest expression of Brn3a was at day 8 (p≤0.0001), later than Ngn1. Interestingly, Brn3a expression could be observed in samples only infected with Ngn1 and rtTA, suggesting that Ngn1 expression *in vitro* can induce Brn3a expression.

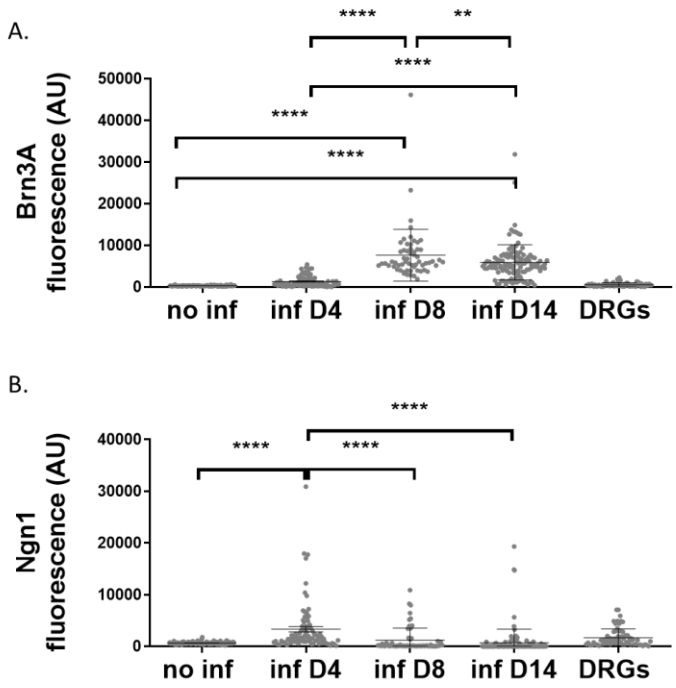

Figure 16 Fluorescence intensity quantification of immunocytochemistry at day 4, 8, or 14 labelling **A.** Brn3a or **B.** Ngn1 in HDFa not infected, HDFa infected and treated with doxycycline, rat DRGs or HDFa infected but not treated with doxycycline. Data presented as mean ± SEM in box and whiskers. Statistical analysis: ordinary one-way ANOVA with Tukey's post-hoc test. ** P=0.0062; **** P ≤ 0.0001. Every dot is a cell, n≥48 cells.

Once assessed that the doxycycline-dependent system was effectively inducing Brn3a and Ngn1 expression *in vitro*, various conversion protocols were performed on different fibroblast cells to find a good model of induced sensory neurons.

In summary, LTV production was optimized and LTVs with constitutive or doxycycline-dependent expression were produced with high titers.

Doxycycline-dependent systems allow a tight time control of the transgene's expression, nevertheless, constitutively GFP expression was faster and more intense compared to doxycycline-dependent ones.

3.2. Direct conversion of foetal lung fibroblasts to sensory neurons

IMR90 is a foetal lung fibroblasts cell line. Conversion protocols were performed on IMR90 to verify the conversion efficiency in young and highly potent cells. Notably, these cells are not the optimal cell type for conversion because they were extracted from lung tissue, which is not easily accessible.

3.2.1. Protocol 1 and Protocol 2

Conversion protocols 1 and 2 consisted of seeding IMR90, infecting the cells with Brn3a, Ngn1, and rtTA, and treating them with an induction medium with small molecules (SM) and neurotrophic factors (**Figure 17**, **Figure 48**, **Figure 49**). Media composition and timing were different between the two protocols. Protocol 1 was designed by modifying Li et al. [90], while Protocol 2 was modified from Qin et al. [91]. After conversion, calcium imaging was performed stimulating the cells with KCl 40 mM, capsaicin 1 µM, menthol 100 µM, and AITC 100 µM. The percentage of response was calculated by normalizing data to Ionomycin (used as a positive control of living cells) or to KCl (positive control for cells able de be depolarized). The response size was also analysed normalising the stimulus peak height to Ionomycin. As shown in **Figure 17**, 7.8% of protocol 1 cells and 8.5% of protocol 2 cells responded to KCl while IMR90 control cells only presented 2.7% of cells responding to KCl. Analysing KCl response size, protocol 2 cells presented significantly higher responses than control cells ($p= 0.0325$), while the same did not occur in protocol 1. TRPs agonists responses were also analysed, and both conversion protocols slightly increased the responses to capsaicin compared to control cells, however the difference was not statistically significant. On the other hand, menthol and AITC percentages of responses in converted cells were as high as in control cells.

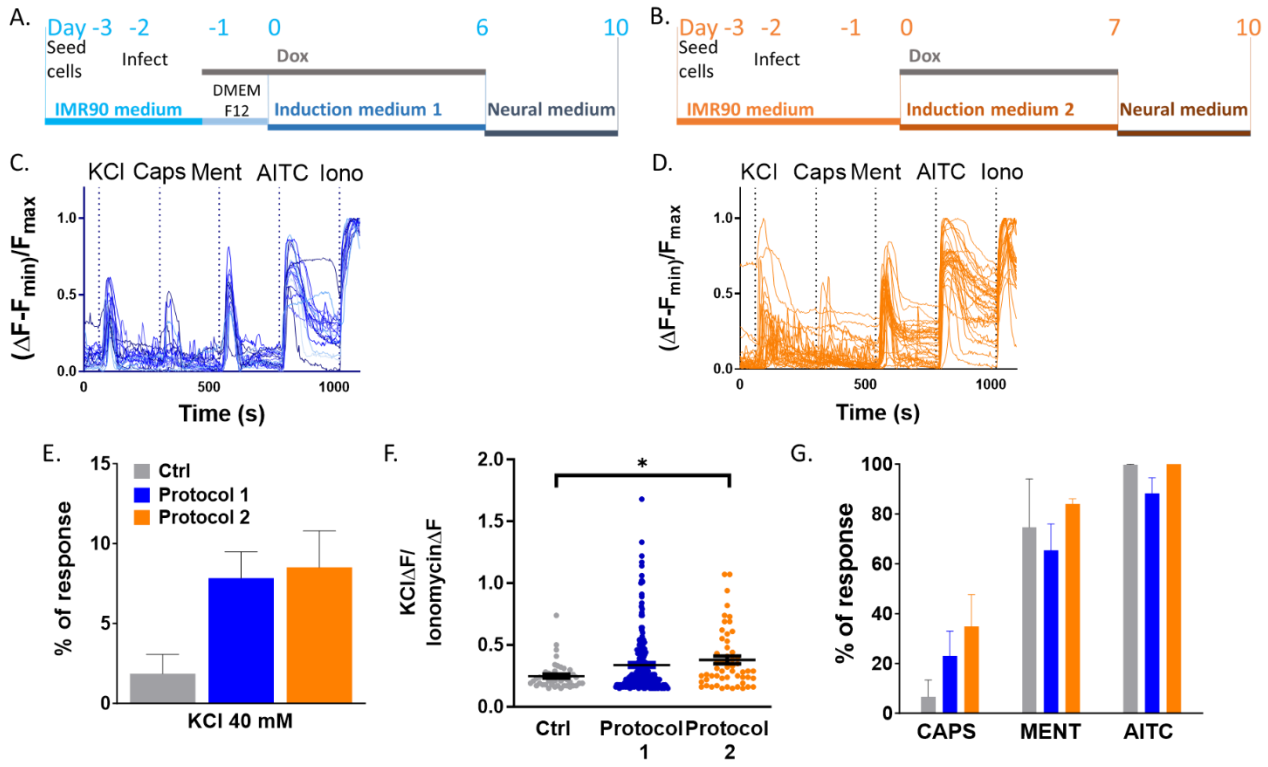

Figure 17 Calcium imaging results of IMR90 converted with protocol 1 or protocol 2 A. Scheme of protocol 1 of conversion from IMR90 to sensory neurons. **B.** Scheme of protocol 2 of conversion from IMR90 to sensory neurons. **C.** Representative traces of cells treated with protocol 1. **D.** Representative traces of cells treated with protocol 2. **E.** Percentage of cells responding to KCl in control cells, cells converted with protocol 1 or with protocol 2. Data presented as mean ±SEM. **F.** KCl response size normalized to Ionomycin response size. Data presented as mean ±SEM in box and whiskers, every dot is a cell. Statistical analysis: ordinary one-way ANOVA with Tukey's post-hoc test. * P=0.0137. **G.** Percentage of cells responding to capsaicin, menthol, or AITC normalized to KCl. Data presented as mean ±SEM. Control N=3, Protocol1 N=4, Protocol2 N=3 independent experiments.

Responses to two or three TRP agonists in the same cell were quantified to have a better understanding of the subtypes of putative iSNs obtained. As shown in **Figure 18**, among KCl responsive cells, in protocol 1 capsaicin and AITC elicited a response in 21,7%, menthol and AITC increased intracellular calcium concentration in 62.5%, 12% of converted cells responded to both menthol and AITC while 11% responded to all three stimuli. In protocol 2, AITC or menthol responses were highly prevalent (100% and 84% respectively), as a result, all menthol and AITC-responsive cells, also responded to capsaicin (34.9%).

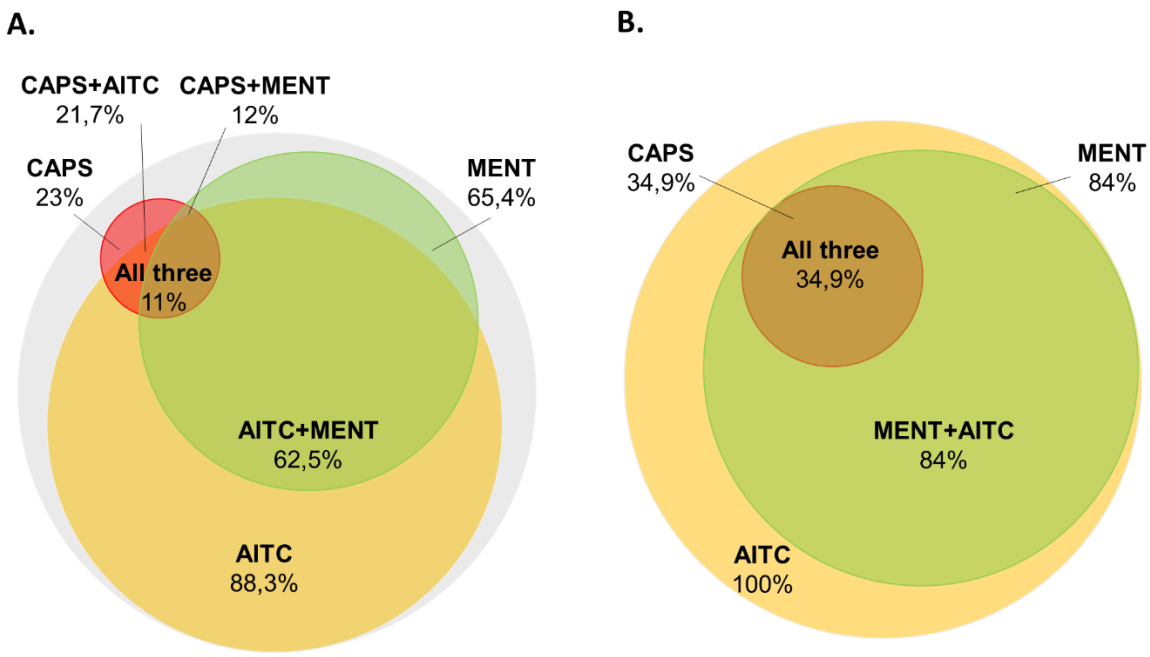

Figure 18 Venn diagram representing the percentage of KCl responders, responding to TRPs agonists in calcium imaging: **A.** results for protocol 1 **B.** results for protocol 2.

In protocol 1, cells' morphology changed rapidly during the first days of conversion from a fibroblast-like morphology to an oval body with long prolongations. However, at the end of the conversion protocol, cells returned to a fibroblast-like morphology. Immunocytochemistry against Tuj1 and Map2, two pan-neuronal markers, TRPV1, TRPM8, TRPA1, and CGRP was performed on day 10 (**Figure 19**). Converted cells expressed Map2 and Tuj1 however, control cells also slightly expressed these neuronal markers. Treated and control cells also expressed TRPA1, TRPV1, and TRPM8 slightly. Interestingly, treated cells expressed CGRP while control cells did not.

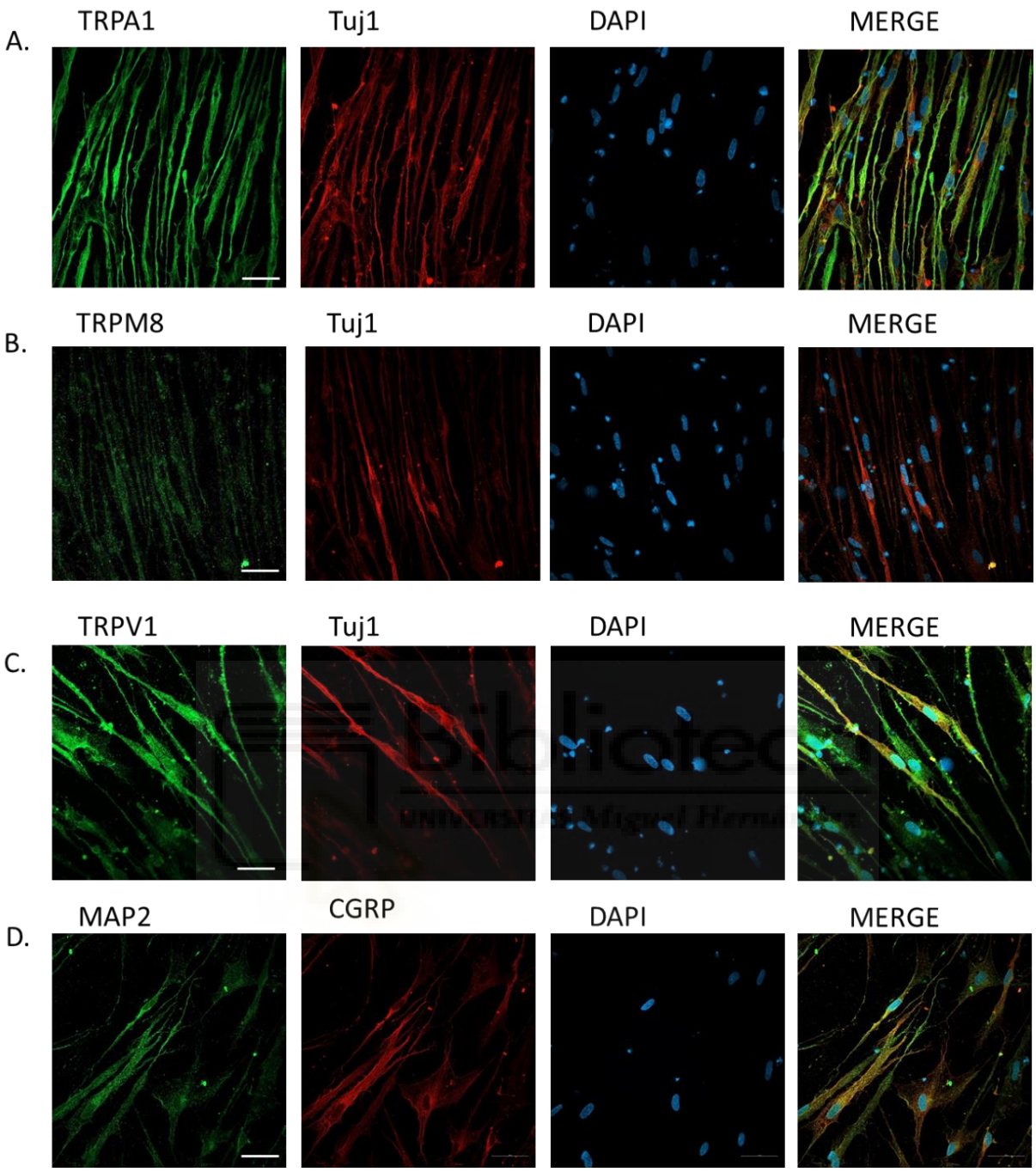

Figure 19 Immunocytochemistry of cells converted with protocol 1. A. TRPA1 (green), Tuj1 (red), DAPI (blue) and merge. **B.** TRPM8 (green), Tuj1 (red), DAPI (blue) and merge. **C.** TRPV1 (green), Tuj1 (red), DAPI (blue) and merge. **D.** MAP2 (green), CGRP (red), DAPI (blue) and merge. Scale bar= 50 µm.

Immunocytochemistry was also performed in protocol 2 converted cells. As shown in **Figure 20**, converted cells had round bodies and prolongations resembling neurites and expressed Tuj1, Map2, Ngn1, and Brn3a revealing the expression of neuronal and sensory neuron

markers. In addition, protocol 2 converted cells expressed TRPV1, TRPM8, TRPA1, Nav 1.8, and CGRP while control cells did not.

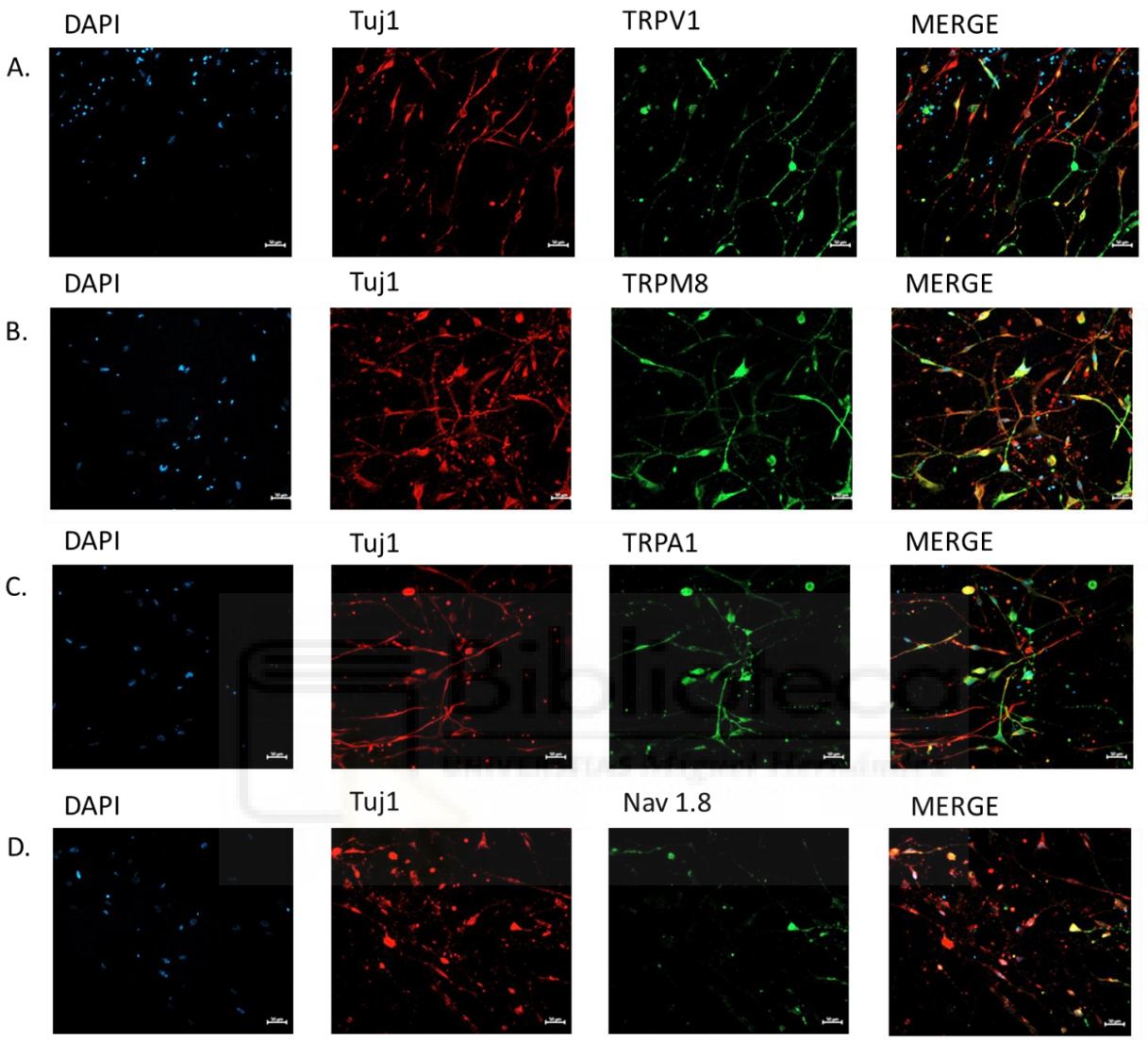

Figure 20 Immunocytochemistry of cells converted with protocol 2. A. DAPI (blue), TRPV1 (green), Tuj 1 (red) or merge of converted cells, **B.** DAPI (blue), TRPM8 (green), Tuj 1 (red) or merge of converted cells, **C.** DAPI (blue), TRPA1 (green), Tuj 1 (red) or merge of converted cells, **D.** DAPI (blue), TRPA1 (green), Nav 1.8 (red) or merge of converted cells. Scale bar = 50μm

To assess if putative iSNs were postmitotic cells, as mature neurons are, the cell cycle block was assessed with Edu Click It assay. As shown in **Figure 21**, in control cells 10% of the cells were loaded with Edu, meaning 10% of IMR90 were replicating. On the other hand, on day three of conversion, protocol 1 cells had their cycle completely blocked ($p<0.0001$

compared to control) while 0,81% of the cells treated with protocol 2 were still replicating (p<0.0001 compared to control).

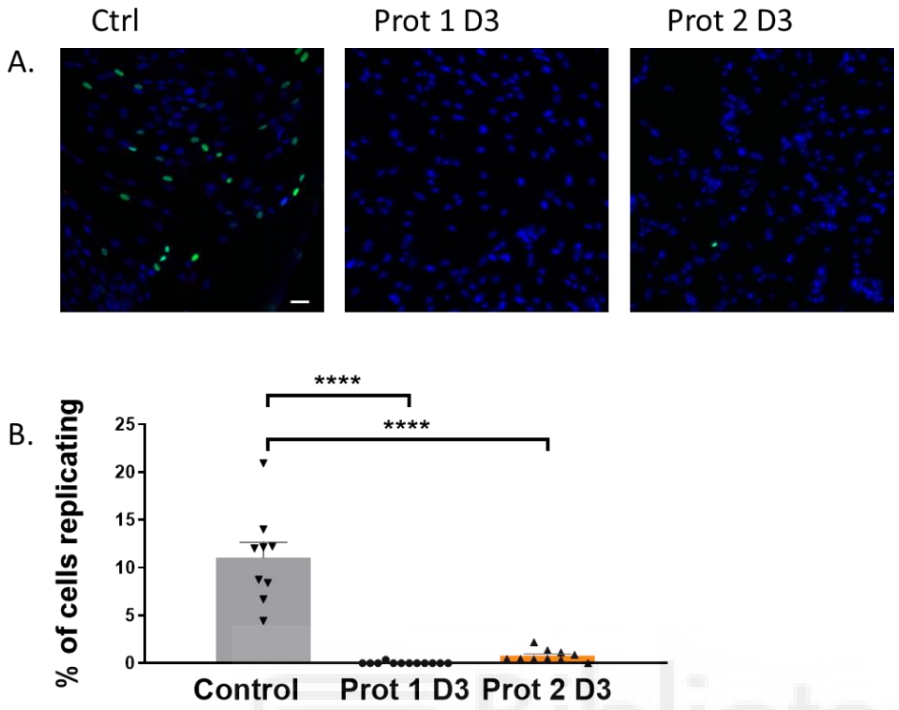

Figure 21 Click-it Edu cell proliferation assay. A. IMR90 labelled with Edu Alexa Fluor 488 (green) and Hoechst 33342 (blue) in control cells, cells converted with protocol 1 at day 3 or cells converted with protocol 2 at day 3. Scale bar = 50 µm **B.** Quantification of Edu labelled cells normalized to the number of Hoechst 33342 positive cells. Statistical analysis ordinary one-way ANOVA, Tukey's post-hoc test. **** P ≤ 0.0001. Data presented as mean ± SEM. N=2 independent experiments, n≥9 fields.

Considering the results from calcium imaging and immunocytochemistry assays, protocol 2 seemed to induce putative iSNs with a morphology that resembled sensory neurons more closely than protocol 1. Therefore, RT-qPCR was performed on protocol 2 measuring mRNA expression of Map2 as a neuronal marker and Brn3a, CGRP, and Isl1 which are markers of sensory neurons or sensory neuron subtypes. Furthermore, Fsp1 mRNA was quantified as a fibroblast marker (**Figure 22**). Due to a lack of human sensory neuron tissue, human brain mRNA was used as a positive control. As a result, converted cells expressed 5 times more Map2 mRNA compared to the control, however, the expression was lower than in human brain (p=0.0102). On the other hand, converted cells expressed high levels of Brn3a, even higher than human brain (p≤0.0001). Interestingly, protocol 2 cells expressed CGRP 5 times more than control cells and 10 times more Isl1 than control cells (which is not expressed in

human brain). Furthermore, there was a slight decrease in the expression of Fsp1 in converted cells and the human brain with respect to control cells.

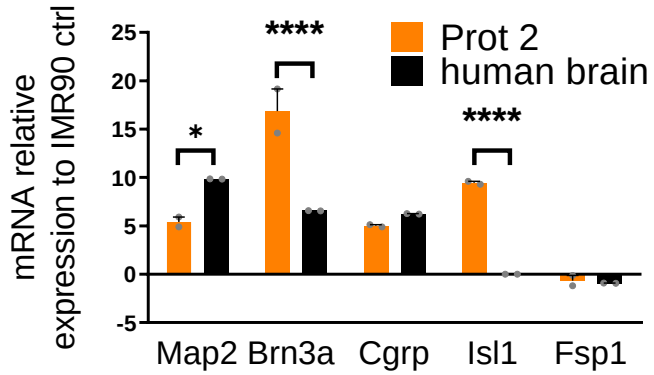

Figure 22 RT-qPCR of cells converted with protocol 2 or human brain. Data presented as mean ±SEM normalized to IMR90 control. Statistical analysis: two-way ANOVA with Tukey's post-hoc test. * P=0.0102; **** P≤ 0.0001. N=2 independent experiments, n=6 wells.

To assess whether protocol 2 converted cells may serve to investigate inflammatory processes, putative iSNs were challenged with acute incubation of an inflammatory soup comprised of ATP 10 µM, histamine 100 µM, serotonin 10 µM, prostaglandin E2 (PGE2) 10 µM and bradykinin 1 µM or their vehicle (H_2O). Calcium imaging was performed by stimulating converted IMR90 with KCl 40 mM, a TRPs agonist (capsaicin 1 µM, menthol 100 µM and AITC 100 µM), inflammatory soup for 4 minutes and another pulse of the same TRPs agonist (**Figure 23**). As a result, there was no difference in the percentage of response between cells stimulated with inflammatory soup or extracellular buffer. However, calculating the difference in the size of the response between the second and first pulse of the TRP agonist, the inflammatory soup seemed to slightly potentiate TRPV1, TRPM8, and TRPA1, however, there was no statistically significant difference.

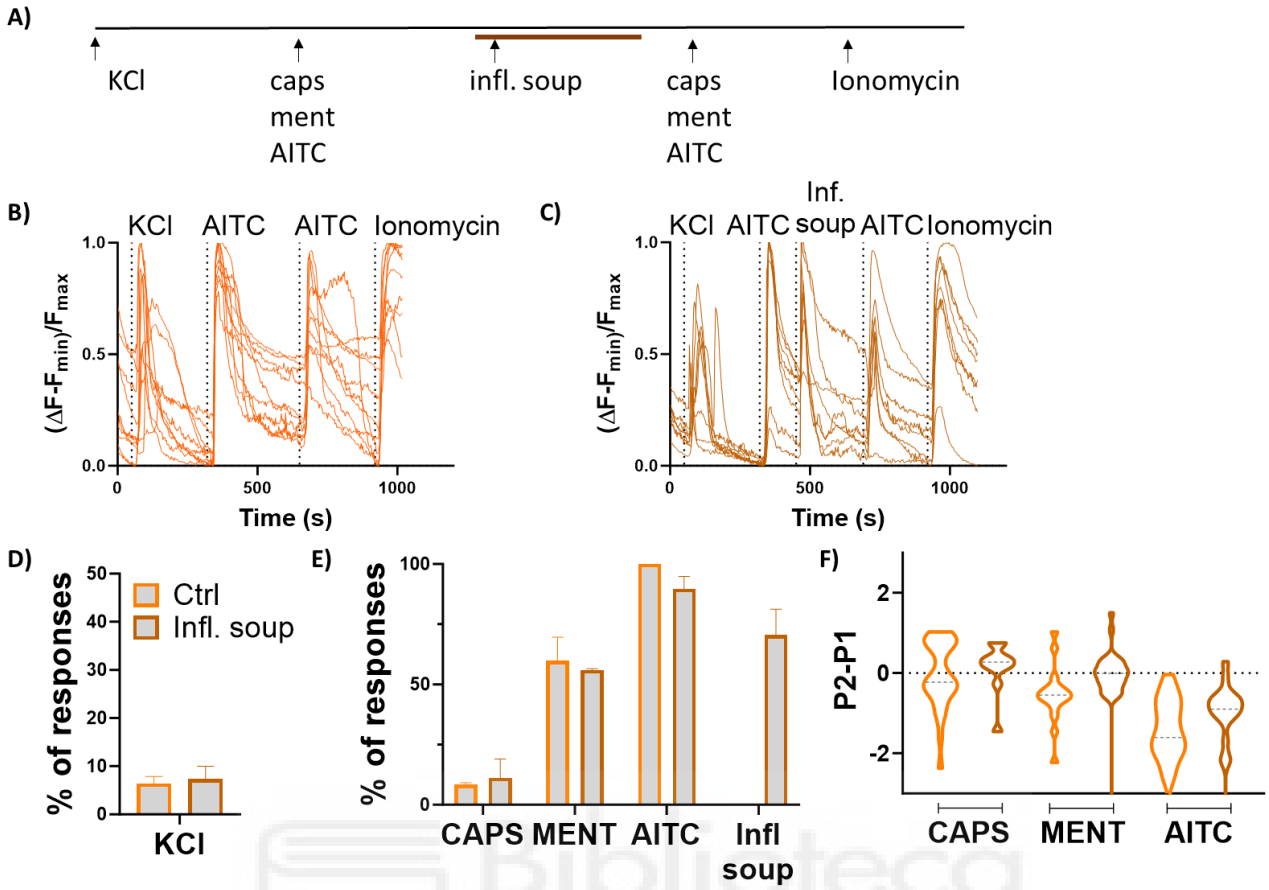

Figure 23 Calcium imaging results of IMR90 converted with protocol 2, challenged with an acute exposition to inflammatory soup A. Scheme of calcium imaging recording **B.** Representative traces of control cells stimulated with AITC. **C.** Representative traces of cells exposed to inflammatory soup for 4 minutes, stimulated with AITC. **D.** Percentage of KCl responders. Data presented as bars, mean ± SEM. **E.** Percentage of KCl responders, responding to TRPs agonists in the second pulse. Data presented as bars, mean ± SEM. **F**. The normalized response size of the second pulse was subtracted from the normalized response size of the first pulse to visualize the potentiation of desensitization. Data are represented as a violin box plot, dashed line at the median. N=2 independent experiments, n=6 coverslips.

Although the calcium imaging results appeared promising, electrophysiology stands as the definitive evidence confirming the conversion of cells into neurons. Patch clamp experiments were conducted on putative iSNs converted with protocol 2. Regrettably, the cell membrane did not exhibit sufficient stability to establish a reliable seal and maintain an open configuration and it was impossible to perform any recording. Therefore, the cells were seeded onto CMOS MEA chips to enable the measurement of extracellular voltage changes in response to capsaicin, menthol, AITC, and KCl. **Figure 24** illustrates the outcomes, revealing that the applied stimuli induced extracellular voltage changes both in mDRGs and

putative iSNs. The frequency of responses in mDRGs closely resembled that of putative iSNs, suggesting that TRP agonists or KCl induce membrane depolarization in converted cells, resulting in electrochemical alterations in the extracellular environment. However, it is crucial to emphasize that mDRGs exhibited a relatively limited number of responsive sensors compared to the benchmarks set by conventional MEA recordings.

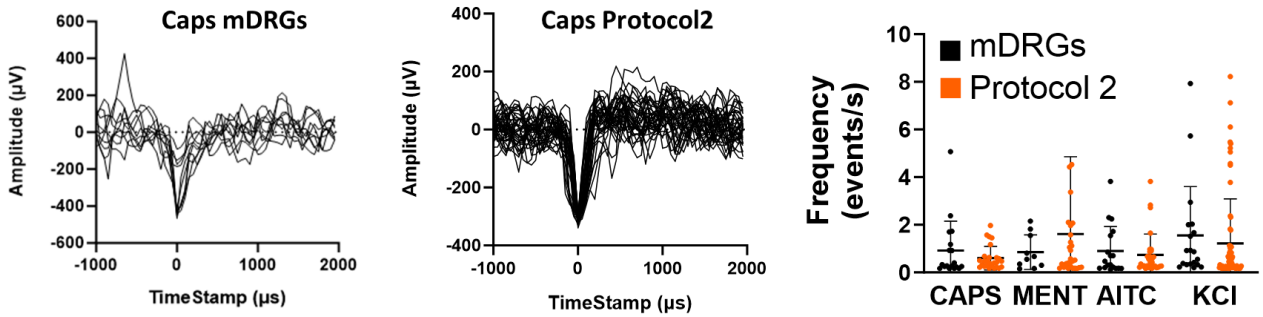

Figure 24 MEA CMOS was performed on mDRGs or IMR90 directly converted with protocol2. **A.** Representative response to capsaicin in mDRGs. **B.** Representative response to capsaicin of IMR90 directly converted with protocol2. **C.** Quantification of events/s. Every dot is a sensor where a response is detected. mDRG N=2 mice; iSNs N=5 independent experiments.

In summary, IMR90 were converted to putative sensory neurons both with protocol 1 and protocol 2, as assessed through calcium imaging and immunocytochemistry. However, protocol 2 seemed to induce cells with a morphology that resembled more closely sensory neurons.

Protocol 2 converted cells could not be recorded by patch clamp due to membrane instability, however, they did present electrophysiological properties similar to mDRGs as measured in MEA CMOS.

3.3. Direct conversion of neonatal dermal fibroblasts to sensory neurons

Considering the age of donors as a notable factor influencing conversion efficiency [67], [68], the establishment of conversion protocols for neonatal dermal fibroblasts (HDFn) preceded the optimization of protocols for adult dermal fibroblasts in this work. Moreover, HDFn exhibited a higher replication index compared to adult dermal fibroblasts, allowing a greater number of conversion protocols to be performed before reaching senescence. This advantageous characteristic proves particularly beneficial during the optimization phases, where a high number of cells is required to facilitate the refinement of protocols.

3.3.1. Blanchard and Eade conversion protocol

In 2015 Blanchard, Eade, and collaborators published an article converting mouse embryonic fibroblasts and human dermal fibroblasts to sensory neurons using lentiviral vectors Brn3a and Ngn1 and a simple cell culture media with N2 supplement (progesterone, insulin, transferrin, putrescine and sodium selenite), FGF and neurotrophic factors [66]. We performed this protocol on human dermal fibroblasts from neonatal donors. Converted cells were characterized through calcium imaging, stimulating the cells with capsaicin, menthol, AITC, and KCl. As shown in **Figure 25**, in our hands only 0.54% of converted cells responded to KCl, compared to 0.3% of KCl responsive cells in control cells. Interestingly, control cells presented more responses to capsaicin, menthol, and AITC compared to treated cells. No KCl-responsive cells responded to any TRP agonist. Therefore, this protocol was discarded.

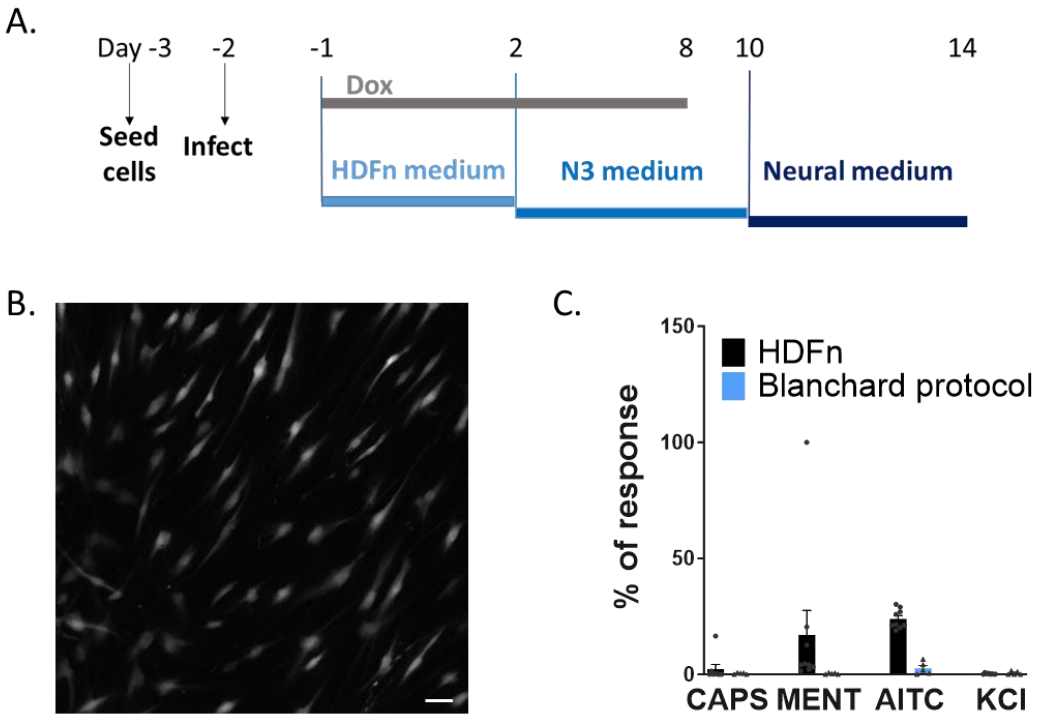

Figure 25 Human dermal fibroblasts from neonatal donors converted with Blanchard and Eade et al. protocol. A. Protocol scheme **B.** Morphology of cells converted at day 14, loaded with Fluo-4. Scale bar= 100 µm. **C.** Percentage of response of control cells or converted cells to capsaicin, menthol, AITC, and KCl normalized to Ionomycin. Data presented as mean ±SEM. N=2 independent experiments, n=9 coverslips for HDFn, n=6 coverslips for Blanchard protocol.

3.3.2. cAMP and DAPT conversion protocol

Media composition was changed adding small molecules to induce or inhibit defined intracellular pathways. Such molecules were SB431542, a TGFβ antagonist; Noggin and LDN193189, which are BMP antagonists; and CHIR99021, a GSK3 antagonist which induces WNT pathway. These molecules were used based on the results published by Ladewig and collaborators [77][67][92], which directly converted human dermal fibroblasts to neurons. Furthermore, cAMP was added to the induction media to activate PKA, which has effectively been demonstrated to mediate neural differentiation [93] and stimulate reprogramming by inducing Ngn2 [66]. cAMP is frequently used in culture media to induce neural crest stem cells into neural lineage, as well as other molecules that raise the intracellular cAMP levels. For example, dibutyryl-cAMP (db-cAMP), inhibits phosphodiesterases, which degradate intracellular cAMP. cAMP conversion protocol

consists of infecting HDFn with Brn3A, Ngn1, and rtTA, treating the cells with induction medium with defined small molecules for 14 days, and with a neural medium which presents neurotrophic factors for 7 days afterwards (**Figure 26**, **Figure 51**). In an attempt to further increase conversion efficiency, we decided to act on the Notch/Delta pathway, which is an important conversion route targeted by several authors, through the small molecule DAPT [60] [94] [65], which is a γ-secretase inhibitor, therefore increasing transition from Sox10 to Ngn1 and Ngn2. For these reasons, DAPT was added to the cAMP induction medium. To assess the effect of cAMP or DAPT conversion protocols, an RT-qPCR against Map2, Brn3A, and Isl1 was performed (**Figure 26**, **Figure 52**), showing no statistically significant differences between conversion protocols in the mRNA expression. However, DAPT slightly increased the expression of MAP2 and cell morphology seemed rounder compared to the cAMP conversion protocol.

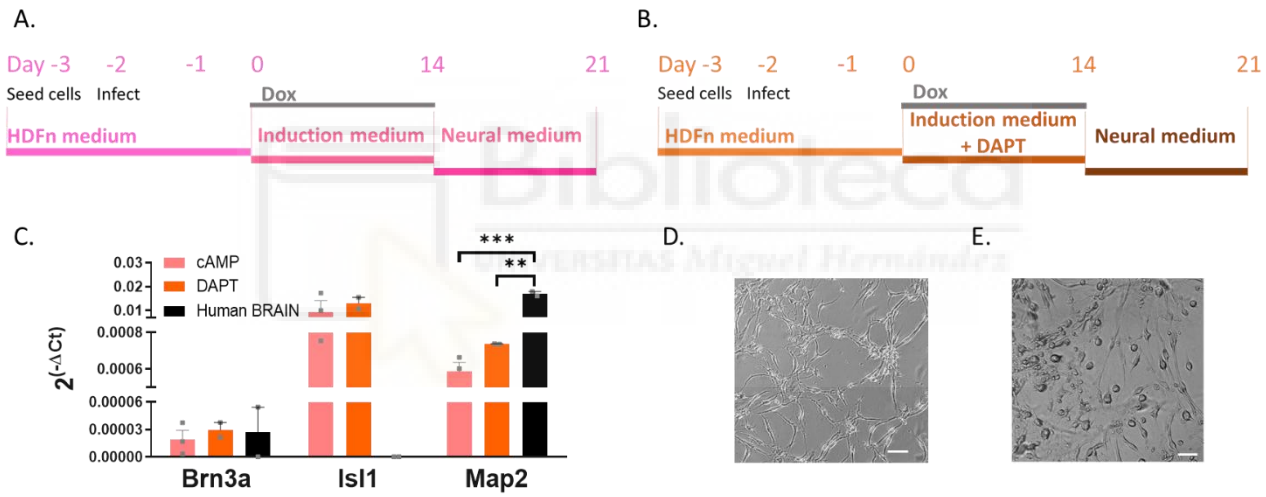

Figure 26 RT-qPCR of HDFn converted with cAMP or DAPT conversion protocol. A. cAMP protocol scheme **B.** DAPT protocol scheme. **C.** RT-qPCR of cells converted with cAMP or DAPT protocol against Brn3a, Isl1, and Map2. Data are presented with mean ± SEM. Statistical analysis: two-way ANOVA with Tukey's post-hoc test. ** P=0.0051; *** P=0.0006. Human brain was used as a positive control, N≥2 independent experiments. **D.** Morphology of cAMP converted cells. **E.** Morphology of DAPT converted cells. Scale bar = 50 µm.

When calcium imaging experiments were performed (**Figure 27**), cAMP-converted cells presented a percentage of response to KCl of 0.66% while the addition of DAPT slightly increased the percentage of responses to KCl up to 3.3%, however, no statistical difference was detected due to high variability in the data sets. Among KCl responsive cells, DAPT-converted cells also responded to capsaicin (2.5%), menthol (16.5%), and AITC (22%)

(AITC response percentage p= 0.0039, DAPT compared to cAMP protocol). KCl response size was also quantified and it seemed that DAPT addition increased it (p=0.0041) presenting a small population of cells that showed KCl responses between 0.5-0.9 ΔF, which was not present in cAMP-converted cells. In addition, the response size to TRPs agonists was measured: menthol response size in DAPT-converted cells seemed smaller than in cAMP-converted cells while AITC did not seem to vary among conversion protocols.

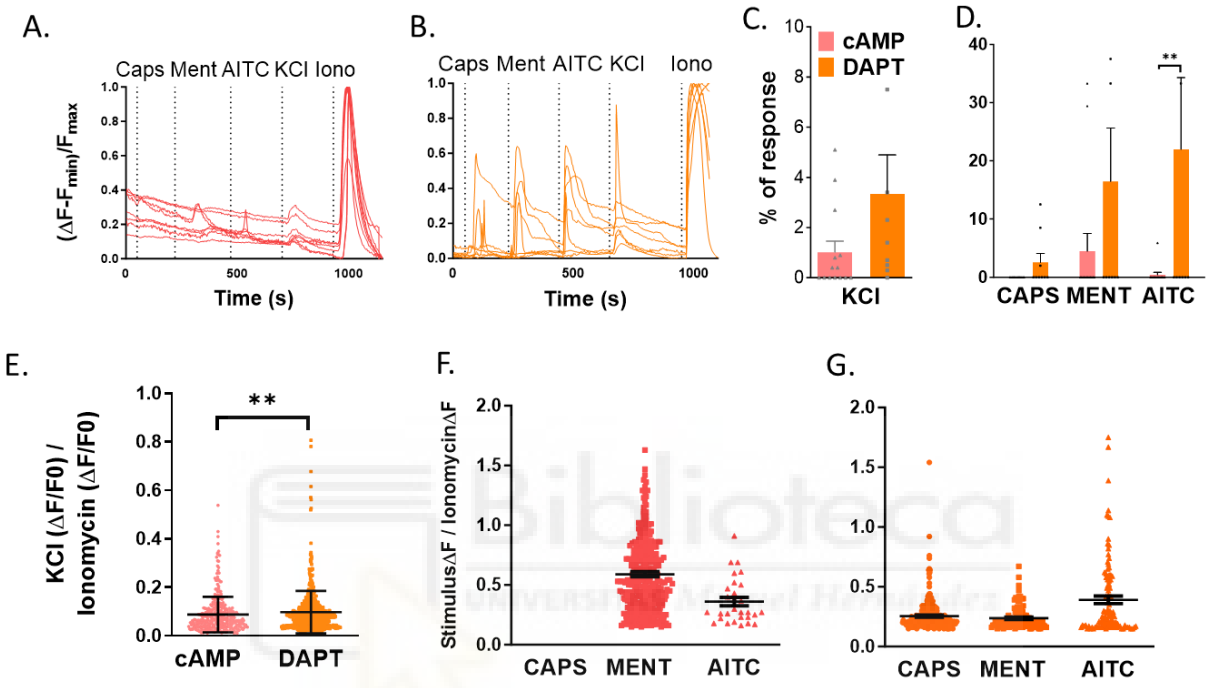

Figure 27 Calcium imaging results of human dermal fibroblasts from neonatal donors treated with cAMP, DAPT, or RA conversion protocol. A. Representative traces of cAMP converted cells. **B.** Representative traces of DAPT-converted cells. **C.** Percentage of responses of cAMP or DAPT converted cells to capsaicin, menthol, AITC, or KCl normalized to Ionomycin. N≥4, data are represented as mean ± SEM. **D.** Percentage of responses of cAMP or DAPT converted cells to capsaicin, menthol, or AITC normalized to KCl. N≥4, data are represented as mean ± SEM. Statistical analysis: two-way ANOVA, Tukey's post-hoc test. ** P=0.0039. **E.** KCl response size of cells converted with cAMP or DAPT conversion protocol. Data are represented as mean ± SEM in box and whiskers, every dot is a cell. Statistical analysis: Mann-Whitney U. ** P=0.0041. **F.** KCl response size of cells converted with cAMP conversion protocol. Data are represented as mean ± SEM in box and whiskers, every dot is a cell. **G.** KCl response size of cells converted with DAPT conversion protocol. Data are represented as mean ± SEM in box and whiskers, every dot is a cell. N≥3 independent experiments, n≥8 coverslips.

Cell size of cAMP and DAPT conversion protocol was also analysed, to further characterize the converted cells. **Figure 28** B and C show the cell area of cells responding or not

responding to KCl. This specific analysis was made to assess if there was a specific size population responding to KCl depending on the conversion protocol. It appears that cAMP had an even cell size distribution among cells that respond to KCl. On the other hand, the DAPT conversion protocol seemed to increase small-size cells responding to KCl.

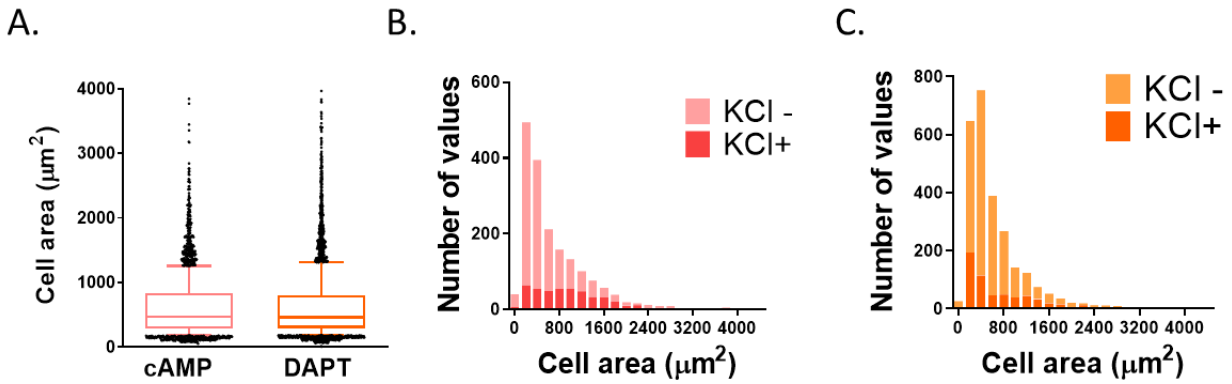

Figure 28 Area of cells converted with cAMP or DAPT conversion protocol A. Cell area of converted cells treated with cAMP or DAPT. Data presented as mean ± SEM. **B.** Histogram of cells responding or not responding to KCl based on cell area of cAMP-converted cells. **C.** Histogram of cells responding or not responding to KCl based on cell area of DAPT converted cells. N≥2415 cells.

Moreover, DAPT-converted cells presented 2.2% of cells that responded both to capsaicin and menthol, 2.3% of cells that responded to both capsaicin and AITC and 1.4% of cells that responded to both menthol and AITC. Interestingly, 0.4% of cells responded to all three TRP agonists (**Figure 29**).

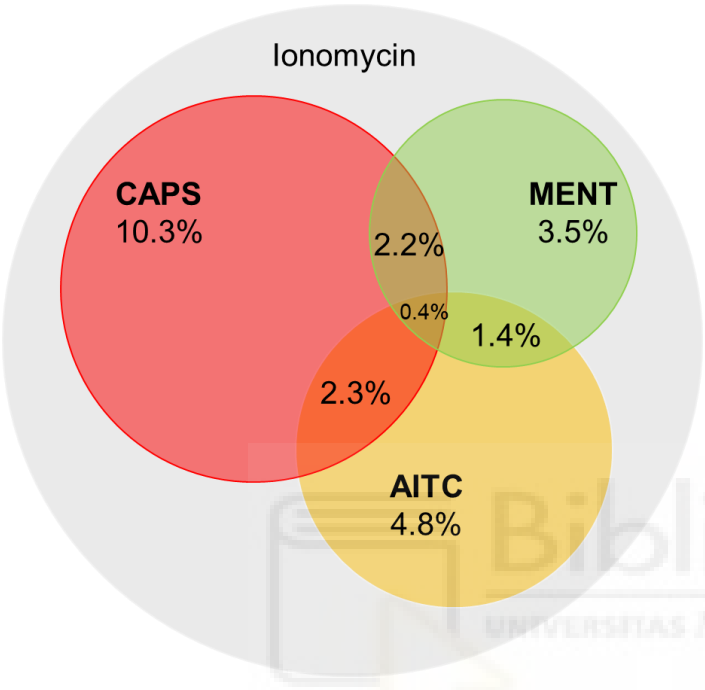

Figure 29 Venn diagram representing DAPT converted cells percentage of response to KCl, capsaicin, menthol, AITC, capsaicin and menthol, capsaicin and AITC, menthol, and AITC or to the three stimuli. N≥3 independent experiments, n≥8 coverslips.

In our hands, Brn3a and Ngn1 induction with N2 conversion media (Blanchard, Eade et al protocol) did not work to convert neonatal dermal fibroblasts to sensory neurons. However, the addition of defined small molecules improved the properties of converted cells. Interestingly, DAPT was crucial to obtain KCl-responsive putative neurons which also responded to capsaicin, menthol, or AITC.

3.4. Direct conversion of adult dermal fibroblasts to sensory neurons

After having acquired more experience with dermal fibroblasts cell culture and with conversion protocols, human adult derma fibroblasts (HDFa) were converted. Blanchard and Eade conversion protocol was performed as a baseline protocol, even if it was discarded in HDFn due to its low conversion efficiency. Afterwards, DAPT and other conversion protocols were performed to optimize a robust, reproducible and high-efficiency conversion protocol.

3.4.1. Blanchard and Eade conversion protocol

Blanchard and Eade conversion protocol in HDFa (**Figure 30**) generated cells with mainly elongated morphology and few cells which presented prolongations. The cells were analysed by calcium imaging and many assays resulted in no responses to KCl, leading to 1.34 % of cells responding to KCl and high variability in the data. Among KCl-responsive cells, there were no responses to TRPs agonists.

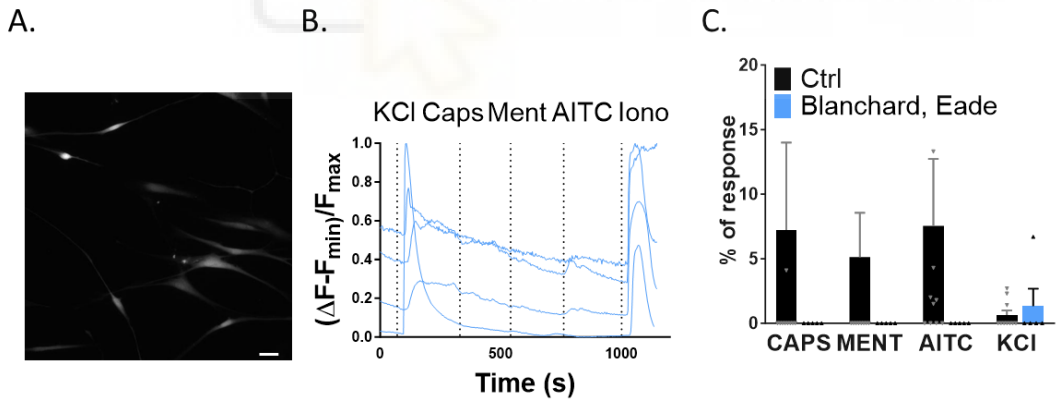

Figure 30 Human dermal fibroblasts from adult donors converted with Blanchard and Eade at al. protocol. A. Protocol scheme **B.** Morphology of cells converted at day 14, loaded with Fluo-4. Scale bar =20 µm **C.** Representative traces of converted cells. **D.** Percentage of response of control cells or converted cells normalized to Ionomycin. Data presented as mean ± SEM. N≥2 independent experiments, n≥5 coverslips.

3.4.2. DAPT conversion protocol

DAPT conversion protocol was performed on HDFa as it was performed on HDFn, on which results were positive (**Figure 27**, **Figure 52**). DAPT-converted HDFa (**Figure 31**) presented 2.55% of cells responding to KCl. Among these cells, there was high variability and many experiments did not present cells that responded to both KCl and TRP agonists. Furthermore, the responses to KCl or TRP stimuli did not present a high response size.

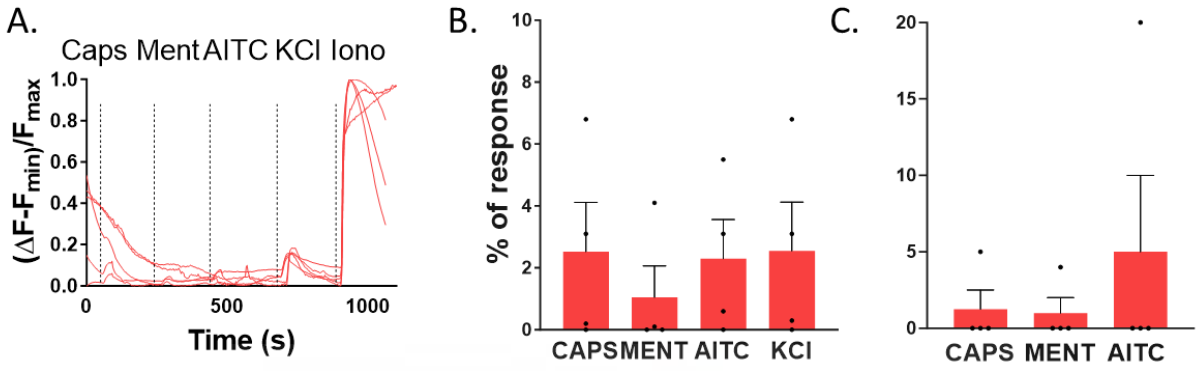

Figure 31 Human dermal fibroblasts from adult donors converted with DAPT conversion protocol. A. Representative traces of DAPT converted cells **B.** Percentage of the response of converted cells to capsaicin, menthol, AITC and KCl normalized to Ionomycin. **C.** Percentage of response of converted cells to capsaicin, menthol or AITC normalized to KCl. Data presented as mean ± SEM. N=2 independent experiments, n=4 coverslips.

Therefore, this protocol which gave promising results on HDFn, was discarded on HDFa; confirming that the age of the donor is an important feature that may affect conversion efficiency.

3.4.3. Cycle arrest conversion protocol

DAPT conversion protocol was modified into the cycle arrest conversion protocol (**Figure 32**, **Figure 53**) in which the cell cycle was blocked in G1 through the small molecule PD 0325901, a cell-permeable inhibitor of the MEK/ERK pathway that inhibits the activation and downstream signalling of MEK. Cells were infected with Brn3a, Ngn1 and rtTA as for the previous experiments and then treated with an induction medium with small molecules or with vehicle (0.03 % DMSO). Converted cells (inf SM) presented 1.5% of responses to KCl while the treatment with vehicle (inf veh) presented less putative neurons. Furthermore,

12.5% of KCl-responsive cells responded to capsaicin or menthol while 13.2 % responded to AITC. However, the variability was high and in most experiments no KCl-responsive cells responded to TRPs agonists,. Furthermore, the morphology of converted cells was round, with few neurites and very low confluence, indicating high cell death during the conversion protocol.

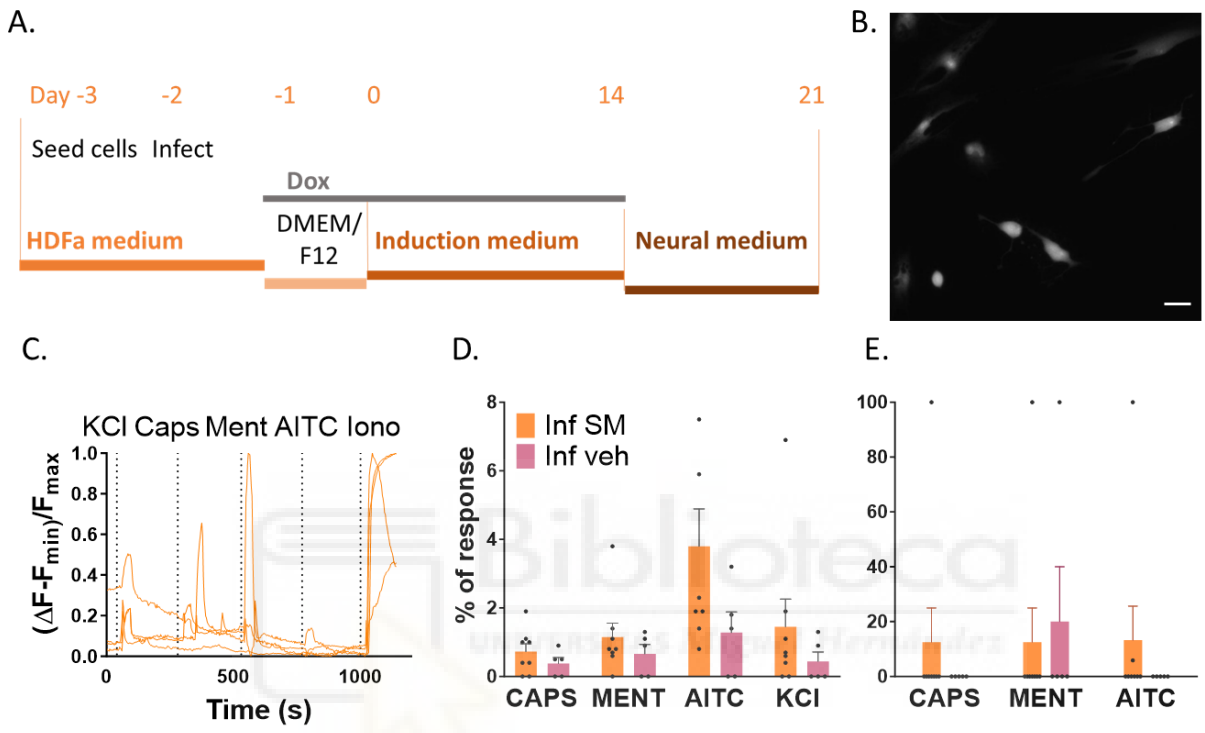

Figure 32 Human dermal fibroblasts from adult donors converted with cycle arrest protocol. A. Cycle arrest protocol scheme. **B.** Morphology of converted cells, loaded with Fluo-4. Scale bar = 20 µm **C.** Representative traces of converted cells **D.** Percentage of response of converted cells to capsaicin, menthol, AITC and KCl normalized to Ionomycin. N=4, data presented as mean ± SEM. **E.** Percentage of response of converted cells to capsaicin, menthol or AITC normalized to KCl. Data presented as mean ± SEM. N=2 independent experiments, n≥5 coverslips.

Human dermal fibroblasts from adult donors presented lower conversion efficiency than HDFn. The modification of the conversion protocol blocking the cell cycle did not generate putative induced sensory neurons. These results prove that the age of the donor is a crucial factor for conversion efficiency.

3.4.4. Drouin-Ouellet and Lau protocol

Due to the failure of previous conversion protocols performed on human dermal fibroblasts from adult donors, a new conversion strategy was pursued. In 2017 Drouin-Ouellet, Lau and collaborators [68] published a work where they directly converted human dermal fibroblasts from adult donors to a mixed population of neurons. Fibroblasts were infected with the LTV 3410, which expresses Ascl1 and Brn2 and inhibits REST through two short hairpin RNA, and treated with conversion media reach in small molecules (**Figure 54**). During an internship at the Institute of Translational Medicine of Semmelweis University, this protocol was applied to human dermal fibroblasts extracted from skin biopsies and several modifications were applied to increase the number of sensory neurons. The cells were then characterized by immunocytochemistry labelling Tau, a marker for mature adult neurons, and Nav 1.8, an ion channel typically expressed in functional sensory neurons, and used as a sensory neurons' marker [65].

As shown in **Table 2**, two rounds of experiments with 12 different conversion protocols were performed with various combinations of lentiviral vectors and conversion media. Protocols 1.1, 1.2, 1.5, 2.1 and 2.2 were performed using early (ENM) and late conversion media (LNM) described by Drouin-Ouellet and Lau et al. [68]. In protocol 2.3 the same media were used, with the addition of NGF 10 ng/mL and DAPT 5 µM, which have pivotal roles in sensory neurons conversion and maturation [60][65]. In protocols 1.3, 1.4, 1.6, 1.7, 2.4 and 2.5 cycle arrest conversion protocol conversion media (IM and NM) (**Figure 53**). Protocol 2.5 was a further modification of the cycle arrest conversion protocol: PD0325901 was withdrawn and cAMP was changed to dbcAMP. Furthermore, different LTVs were used: in protocols 1.5-1.7 doxycycline-inducible lentiviral vectors which encoded for Brn3A, Ngn1 and rtTA were used. However, in previous assays it was observed that doxycycline had a harsh effect on cells and increased cell mortality, therefore a BN1 all-in-one LTV was designed to express Brn3a, Ngn1 and RFP (red fluorescent protein) without the need for rtTA and doxycycline. BN1 all-in-one LTV was used alone in protocols 1.2, 1.3. The 3410 vector was used in protocols 1.1 and 2.1. Furthermore, 3410 and BN1 LTVs were used together in protocols 1.4, 2.2-2.5. Importantly, LTVs used in all these protocols were produced by PEI transfection; a different method than the ones described at page 45. Methodological details about LTVs production are described at page 113.

Table 2 Summary of protocols, lentiviral vectors and MOI used and conversion media applied.

Protocol	Lentiviral vectors	MOI	Media
1.1	3410	20	ENM+LNM
1.2	BN1	20	ENM+LNM
1.3	BN1	20	IM+NM
1.4	3410+BN1	10+10	IM+NM
1.5	Brn3A+Ngn1+rtTA	10+10+10	ENM+LNM
1.6	Brn3A+Ngn1+rtTA	10+10+10	IM+NM
1.7	Brn3A+Ngn1+rtTA+3410	5+5+5+5	IM+NM
2.1	3410	20	ENM+LNM
2.2	3410+BN1	10+10	ENM+LNM
2.3	3410+BN1	10+10	ENM+LNM + NGF + DAPT
2.4	3410+BN1	10+10	IM+NM
2.5	3410+BN1	10+10	IM+NM – PD – cAMP

As shown in **Figure 33**, the protocol published by Drouin-Ouellet, Lau and collaborators (protocol 1.1 and 2.1) generates Tau-positive cells and Tau+Nav1.8 double-positive cells. Converted cells have neuronal morphology, with a round body and prolongations. The same protocol was performed changing 3410 LTV to BN1 (protocol 1.2, **Figure 34**); this protocol also generated some round cells with prolongations which were positive to Tau and Nav1.8 positive cells. However, many cells with fibroblast-like morphology were present.

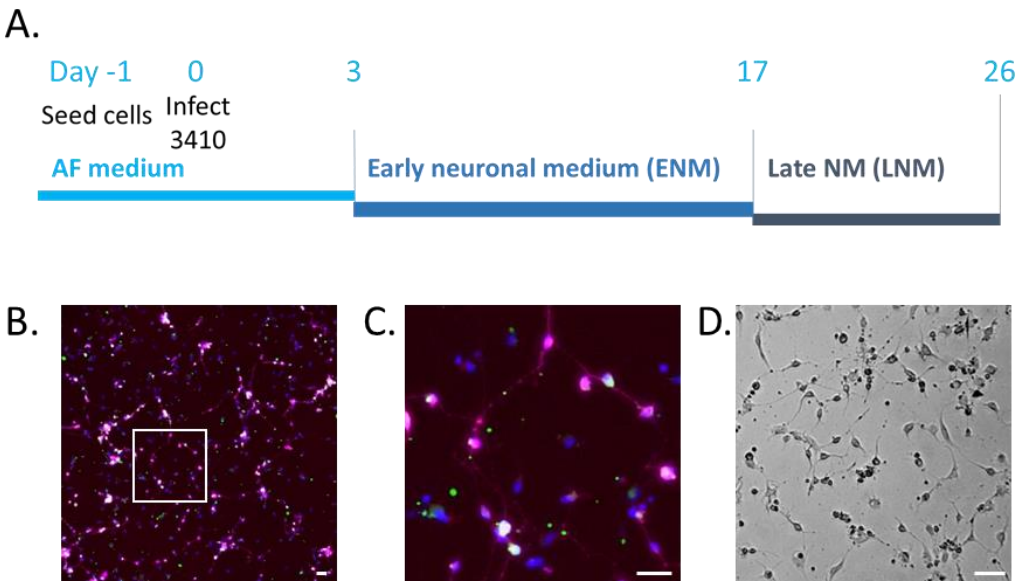

Figure 33 Protocol 1.1 and 2.1 A Protocol scheme. **B-C.** Fluorescence microscopy images of cells converted with protocol 1.1 or 2.1 at different magnifications. Tau (magenta), Nav 1.8 (green), DAPI (blue). **D.** Transmitted light image of cells converted with protocol 1. Scale bar = 50 µm

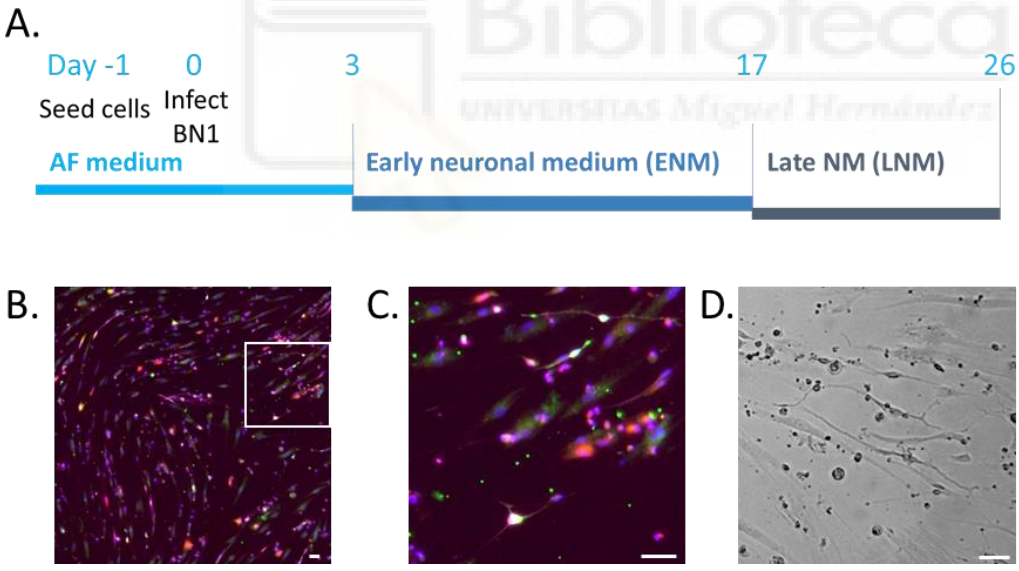

Figure 34 Protocol 1.2 A Protocol scheme. **B-C.** Fluorescence microscopy images of cells converted with protocol 1.2 at different magnifications. Tau (magenta), Nav 1.8 (green), BN1 (red) DAPI (blue). **D.** Transmitted light image of cells converted with protocol 1. Scale bar = 50 µm

The cells converted with cycle arrest conversion media and BN1 all-in-one LTV did not have neuronal morphology and presented very low labelling for Tau and Nav 1.8, while the combination of BN1 with 3410 with cycle arrest conversion media led to an intermediate morphology between neurons and fibroblast-like shape. Doxycycline inducible LTVs (Brn3a, Ngn1 and rtTA) seemed to decrease the cell confluence, probably due to toxicity and cell death during the conversion protocol, converted cells had fibroblast-like morphology and did not label for Tau or Nav 1.8. Considering the results obtained on HDFa and even with these modifications in the protocol, cycle arrest conversion media and doxycycline-inducible LTVs were discarded.

In a second round of experiments, the Drouin-Ouellet and Lau protocol (protocol 1.1) was repeated as an internal control (protocol 2.1). It was then modified with the addition of BN1 LTV (protocol 2.2) and further modified by adding DAPT and NGF in the early conversion media (protocol 2.3, **Figure 35**). These protocols generated neuronal-shaped cells which labelled positively for both Tau and Nav 1.8.

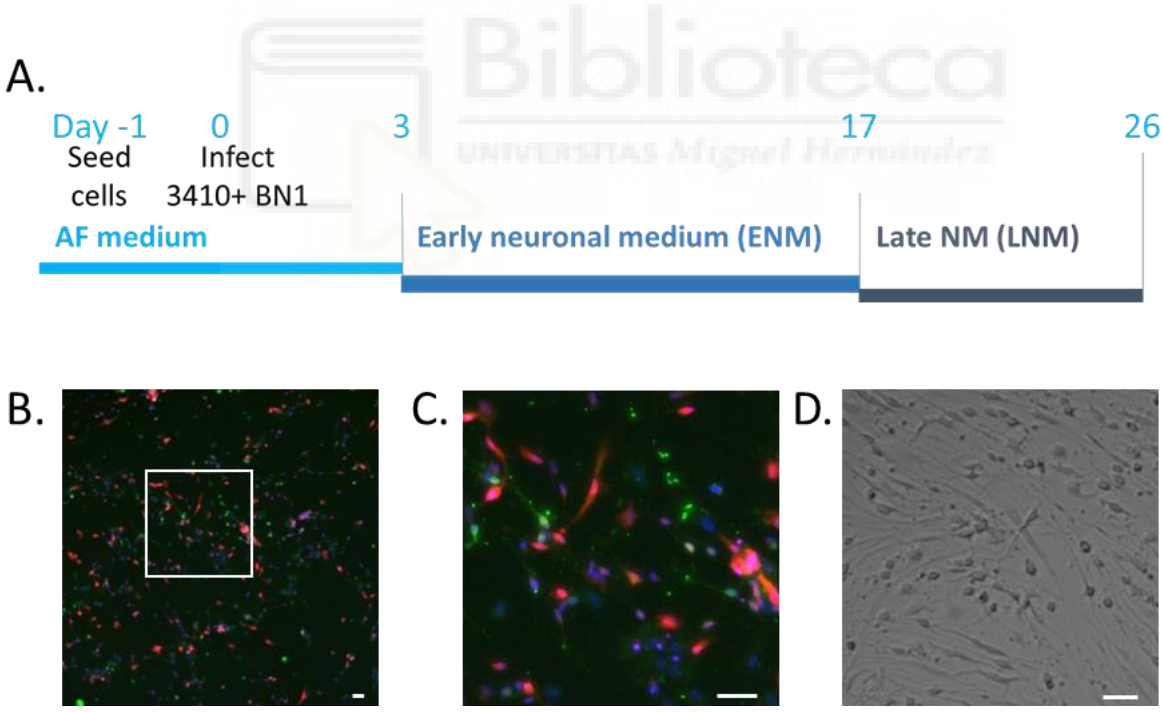

Figure 35 Protocol 2.3 A Protocol scheme. **B-C.** Fluorescence microscopy images of cells converted with protocol 2.3 at different magnifications. Tau (magenta), Nav 1.8 (green), DAPI (blue). **D.** Transmitted light image of cells converted with protocol 1. Scale bar = 50 µm

The percentage of Tau or Tau+Nav1.8 double-positive cells was quantified and normalized to the number of nuclei, labelled with DAPI (**Figure 36**). The Drouin-Ouellet and Lau protocol presented 15% of neurons and 3% of putative sensory neurons. Notably, protocols 1.1 and 2.2 (which are two independent experiments of the same conversion protocols) presented statistically significant differences ($p=0.0024$) highlighting experimental high variability. However, every protocol was compared to its internal control, i.e., protocols from the first round of experiments were compared to protocol 1.1 while protocols performed in the second round of experiments were compared to protocol 2.1.

Protocols 1.2-1.7 presented between 0.3% and 1% of Tau-positive cells and around 0.2% of Tau+Nav 1.8 double-positive cells. Protocols 2.2 and 2.3 presented a higher number of neurons compared to protocol 2.1 ($p\leq0.0001$), up to 36.2% and 32.8% respectively, while protocols 2.4 and 2.5 presented ~1% of Tau positive cells, therefore cycle arrest conversion protocol could not induce the conversion of human dermal fibroblasts to sensory neurons, both with 3410 or BN1 transduction. Interestingly, protocols 2.2 and 2.3 presented a higher percentage of Tau+Nav1.8 double-positive cells compared to the Drouin-Ouellet protocol, leading to 9.9% and 13.2% or putative sensory neurons respectively ($p= 0.0170$ between protocol 2.2 and 2.3). In conclusion, protocol 2.3, which implies 3410 and BN1 co-infection, the Drouin-Ouellet and Lau conversion media, DAPT and NGF, seems to induce the highest percentage of sensory neurons and a high amount of Tau positive cells.

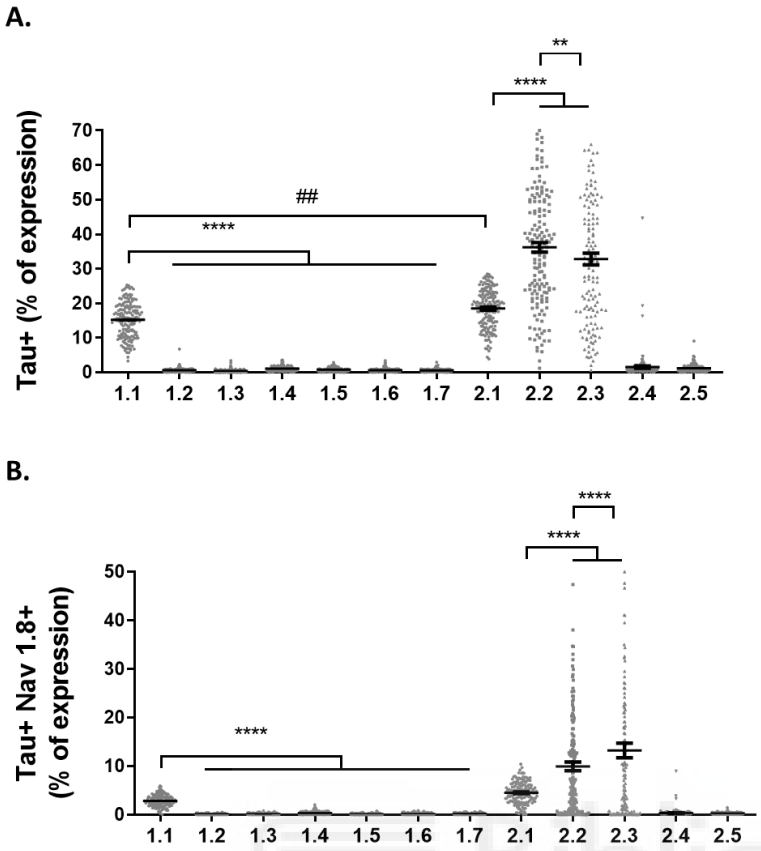

Figure 36 Quantification of Tau or Tau+Nav1.8 double-positive cells in protocols 2.1 to 2.5. A. Percentage of expression of Tau-positive cells normalized to nuclei. Statistical analysis Kruskal Wallis, Dunn's post-hoc test. ** P= 0.0170; ## P= 0.0024; **** P≤0.0001. **B.** Percentage of expression of Tau and Nav1.8 positive cells normalized to nuclei. Statistical analysis Kruskal Wallis, Dunn's post-hoc test. **** P≤0.0001. N≥160 fields.

The induction of Ascl1, Brn2, Brn3a and Ngn1 together with the inhibition of REST and culture media with defined small molecules, converts adult dermal fibroblasts to putative sensory neurons, which present neuronal-like morphology and express Tau and Nav 1.8. As expected, adding NGF and DAPT increased the amount of putative sensory neurons.

The most efficient conversion protocol (protocol 2.3) was then performed on human dermal fibroblasts from age-paired adult male (AF2201) and female (AF2101) donors. Calcium imaging was performed on day 27 or day 50 of conversion. On day 27, both female and male converted fibroblasts responded to KCl exhibiting 5.27% and 3.24% of putative neurons respectively, significantly higher values than what was detected in control fibroblasts. Among these, fibroblasts from female donor presented capsaicin (2.57%), menthol (5%) and AITC (20.3%) responses. Similarly, male putative neurons responded to capsaicin (20%), menthol (12.2%) and AITC (14.3%) (**Figure 37**). No statistically significant difference was observed between male and female donors induced sensory neurons, nor in the percentage of response nor the size of the response. The co-response to two or all TRPs agonists was also analysed and it was found that 0.22% (female) or 0.16% (male) of converted cells responded to KCl, menthol and AITC. Response size was similar between stimuli and donors, in a range between 0.2 to 2 ΔF.

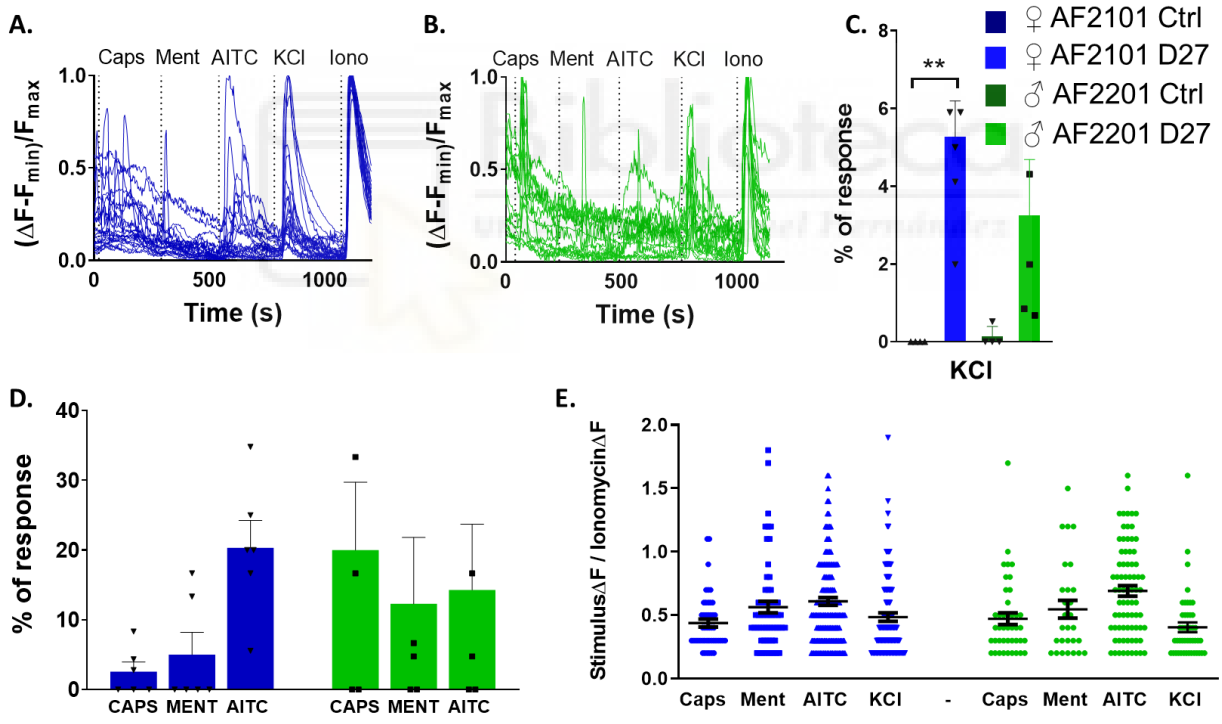

Figure 37 Calcium imaging results of converted adult dermal fibroblasts 2101 (Female donor) or 2201 (Male donor), day 27 of conversion. A. Representative calcium imaging traces of converted AF2101 **B.** Representative calcium imaging traces of converted AF2201 **C.** Quantification of the percentage of responses, normalized to Ionomycin. Statistical analysis One-way ANOVA, Tukey's post-hoc test ** P= 0.0074. **D.** Quantification of percentage of responses, normalized to KCl. **E.** Quantification of the size of the responses normalized to Ionomycin. N=2 independent experiments, n≥4 coverslips.

The same assay was performed on day 50 of conversion (**Figure 38**), revealing a similar percentage of response to KCl (3.8% female, 5.8% male) in comparison to converted cells analysed at D27. Interestingly, putative neurons capsaicin responses were increased up to 24.3% in female and decreased to 10.4% in male converted cells. As for menthol, responses in female donor's converted cells were absent while 7.9% of male converted cells responded to both menthol and KCl. AITC responses in putative neurons were decreased in comparison to cells analysed at D27 of conversion, down to 6.6% in female and 3.4% in male fibroblasts. These evidences reveal donor-to-donor differences in iNs maturation. Regarding response size, no statistically significant differences were found between stimuli or donors.

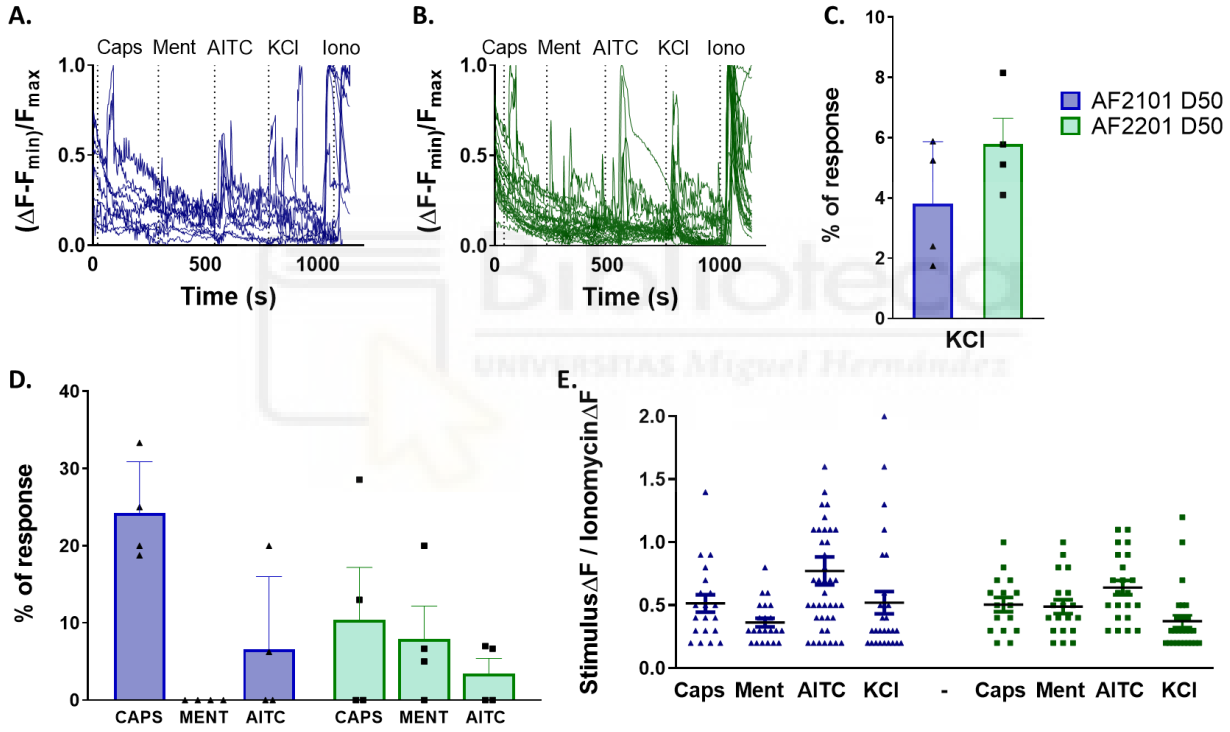

Figure 38 Calcium imaging results of converted adult dermal fibroblasts 2101 (Female donor) or 2201 (Male donor), day 50 of conversion. A. Representative calcium imaging traces of converted AF2101 **B.** Representative calcium imaging traces of converted AF2201 **C.** Quantification of the percentage of responses, normalized to Ionomycin. **D.** Quantification of percentage of responses, normalized to KCl. **E.** Quantification of the size of the responses normalized to Ionomycin. N=2 independent experiments, n=4 coverslips.

The analysis of cell area provided significant insights, as shown in **Figure 39**, the cell area of female control fibroblasts was significantly larger compared to converted cells on both day 27 and day 50 ($p \leq 0.0001$). This suggests distinct cellular morphology in female control

fibroblasts, characterized by larger cell sizes. There was a statistically significant difference in cell area between control fibroblasts from male and female donors (p=0.0002). This difference may underscore donor-related variations in fibroblast morphology. Regarding female converted cells, the cell area of KCl responsive cells on day 27 of conversion was approximately 380.2 µm² ± 25.26, which increased to around 420.1 µm² ± 28.05 by day 50 of conversion. Male converted cells KCl responsive cells exhibited similar cell area values, with approximately 383.5 µm² ± 45.65 on day 27 and around 424.5 µm² ± 30.79 on day 50 of conversion. Considering that the estimated size range of human sensory neurons falls between 300 and 8000 µm² [14], it is evident that the putative neurons generated using this protocol occupy the lower end of this size spectrum.

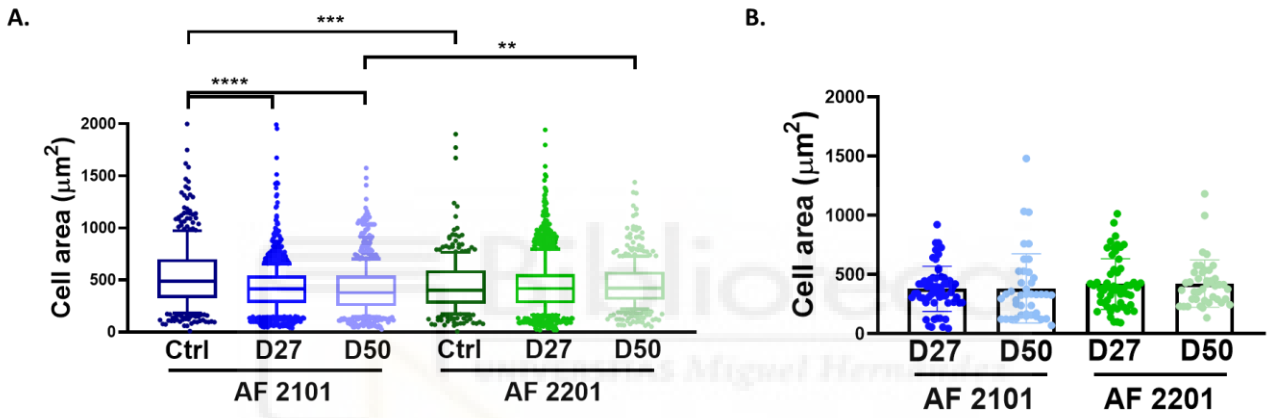

Figure 39 Cell area (µm²) A. Control adult dermal fibroblasts 2101 (Female donor) or 2201 (Male donor), converted cells on day 27 or converted cells on day 50 of conversion. Data represented as 10-90 percentile; every dot is a cell. Statistical analysis: Kruskal-Wallis, Dunn's post-hoc test ** P= 0.0024, *** P=0.0002, **** P≤0.0001. N=2, n≥326 to 1198 cells**. B.** KCl responsive cells. Converted adult dermal fibroblasts 2101 (Female donor) or 2201 (Male donor) on day 27 or converted cells on day 50 of conversion. N=2, n≥41 cells. Data represented as a scatter plot with bar, mean±SEM.

The molecular features of the converted cells were assessed, including the analysis of mRNA expression levels for various neuronal markers and markers associated with specific neuronal subpopulations. The goal was to understand the extent to which the converted cells resembled human neurons and how they differed from control fibroblast cells. As shown in **Figure 40**, converted cells displayed high similarity to the human brain while fibroblast control cells displayed a different pattern of expression. In detail, the expression of Map2, a marker associated with mature neurons, was found to be high in human brain tissue and moderately high in the converted cells. In contrast, its expression was lower in control fibroblast cells. This suggests that the converted cells displayed a

neuronal-like expression pattern compared to fibroblast controls. Interestingly, Brn3a expression was notably high on day 27 of conversion but decreased by day 50. Mature sensory neurons do express Brn3a, so maintaining its high expression in the later stages of conversion might be a consideration for improving the model. As expected, Cgrp, a marker associated with peptidergic sensory neurons, showed medium to high expression in both converted cells and human brain tissue, but low expression in control fibroblasts. On the contrary, Fsp1, a fibroblast marker, was highly expressed in control fibroblasts but had lower expression in converted cells and human brain tissue. Notably, converted cells from female donors showed higher Fsp1 expression than male converted fibroblasts. Moreover, Runx1 and TrkA expression was evaluated to determine the composition of sensory subpopulations within the converted cells. While TrkA is associated with mature C-peptidergic sensory neurons, Runx1 is expressed in mature non-peptidergic cells. However, during early developmental stages, both genes can be co-expressed, guiding subpopulation fate. The co-expression of Runx1 and TrkA in the converted cells suggests that they may represent a mixture of subpopulations. Further insights into whether this co-expression occurs at the single-cell level or at a population level could be gained through single-cell RT-qPCR. Overall, these findings provide valuable insights into the molecular characteristics of the converted cells, their resemblance to sensory neurons, and the potential presence of distinct subpopulations within the culture.

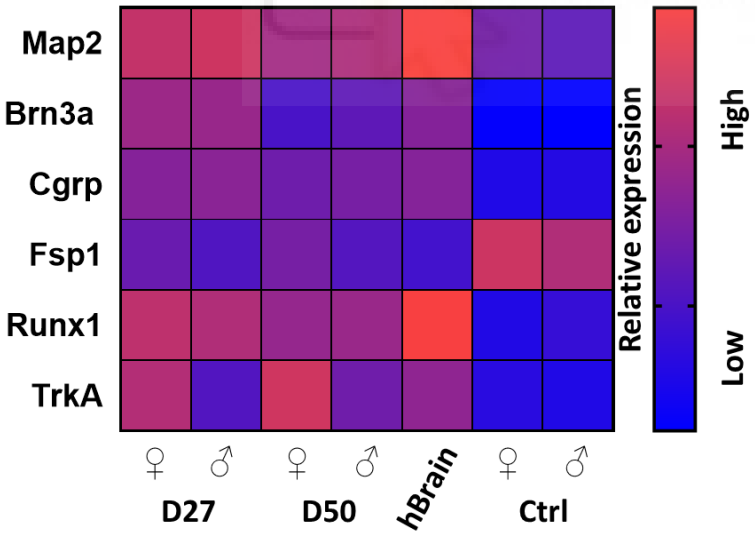

Figure 40 RTqPCR results of converted adult dermal fibroblasts 2101 (Female donor) or 2201 (Male donor), converted fibroblasts on day 27 or 50 of conversion. Heatmap represents Log10 $2^{-\Delta Ct}$ as a relative expression, normalized to βactin. Blue-coloured squares indicate low expression, and red-coloured squares represent high relative expression. N=2 independent experiments.

In addition to molecular assessments, immunocytochemistry was employed to label various markers, including Tau as a neuronal marker, TRPV1, TRPA1, TRPM8, and Nav 1.8 (**Figure 41**). The expression of Tau, TRPs, and Nav 1.8 was detected in both donors at both day 27 and day 50 of conversion. Tau and Nav 1.8 co-expression was quantified as a measure of conversion efficiency. The results indicate variability in the maturation of iSNs from different donors. In detail, female iSNs on day 27 of conversion presented 11% of Tau-Nav 1.8 positive cells while male iSNs presented 6.3% of putative sensory neurons. On day 50 of conversion, female iSNs Tau-Nav 1.8 co-expression decreased to 7.5% while male's iSNs increased to 10.8%. These findings align with previous results from calcium imaging, highlighting differences in how iSNs from different donors mature.

Regarding morphology, the culture displayed a mixture of round, oval, and elongated cells, each with short to medium-sized neurites. Some cells exhibited a bipolar morphology with two prolongations on opposite sides, while others displayed multiple neurites, resembling astrocytes or central neurons more than sensory ones. To conduct a comprehensive analysis correlating morphology with marker expression, high-throughput immunocytochemistry and software-based analysis should be employed. This approach would enable a more systematic exploration of the relationship between cell morphology and marker expression.

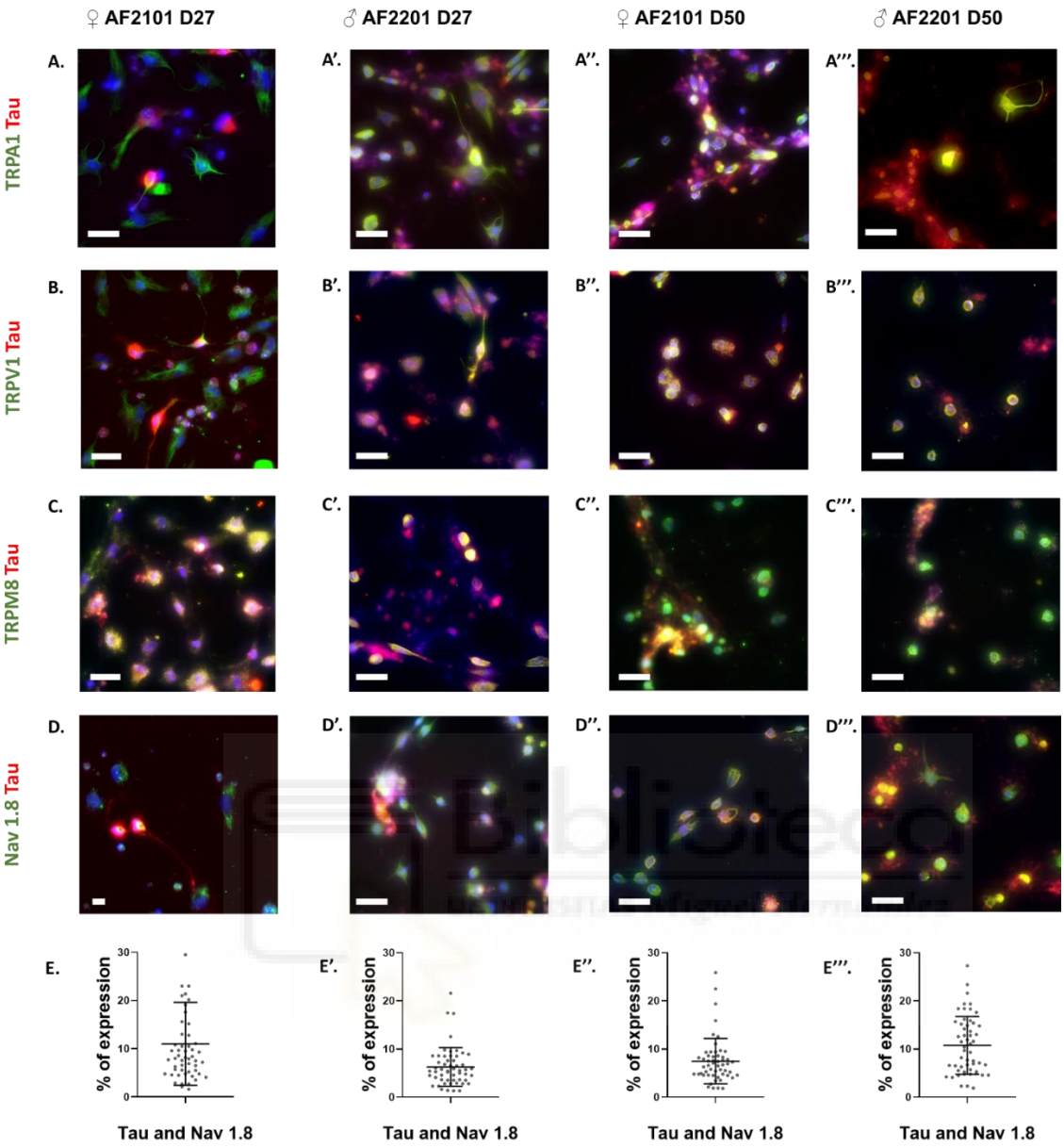

Figure 41 Immunocytochemistry of converted adult fibroblasts 2101 (Female) or 2201 (Male), analysed on day 27 or 50. Tau is labelled in red while **(A)** TRPA1, **(B)** TRPV1, **(C)** TRPM8 and **(D)** Nav 1.8 are labelled in green. N=2 independent experiments, n=54 fields. **E.** represents the quantification of the percentage of expression of Tau and Nav 1.8 normalized to the number of DAPI-positive cells. Scale bar = 50 µm.

Protocol 2.3 efficiently converted human dermal fibroblasts into putative sensory neurons from both male and female donors. Converted cells exhibited sensory neuron features on both day 27 and day 50 of conversion, including calcium imaging responses to TRP agonists and KCl, as well as the expression of mRNA and typical sensory neuron markers.

3.5. Mouse DRGs culture in microfluidic chambers

Having obtained putative sensory neurons from human fibroblasts, it is crucial to refine *in vitro* techniques to mirror their *in vivo* behaviour accurately. Given the peculiar morphology of sensory neurons, compartmentalized culture emerges as a tool for separating DRG or TG soma and neurites [69] [83]. In preparation for the compartmentalized culture of human sensory neurons, we optimized the compartmentalized culture of rodent DRGs, thereby acquiring essential proficiency for future experiments.

3.5.1. DRGs compartmentalized culture and co-culture

Rodent DRGs neurons were seeded in microfluidic chambers at high concentrations to have a consistent axonal outgrowth in the following days (**Figure 42**). During 6 days in-vitro (DIV) a physical and a chemical gradient were established between the 2 compartments to allow the growth of the axons from the somal compartment to the axonal one. To label the neurons that developed prolongations, the far-red retrograde tracer DID' (Invitrogen) was loaded in the axonal compartment. At DIV 6, 53 ± 14% of cells were loaded with Did' (n cells= 482). Calcium imaging was then performed by stimulating the neurites with capsaicin (100 nM), menthol (100 µM) and AITC (100 µM) to activate TRPV1, TRPM8 and TRPA1 respectively. The increase of intracellular calcium was measured in the somal compartment and only on the cells that had prolongations in the axonal compartment, as determined by DiD' staining. After TRPs activation, axons were stimulated with KCl 40 mM. Stimulation of the nerve endings by the different stimuli resulted in calcium increase in the soma quantified in 12.1% for capsaicin, 9.8% for menthol, 7.9% for AITC and 53.6% for axonal KCl. DRGs from male and female mice were used, however, differences among sexes were not observed in the percentage nor the amplitude of the responses.

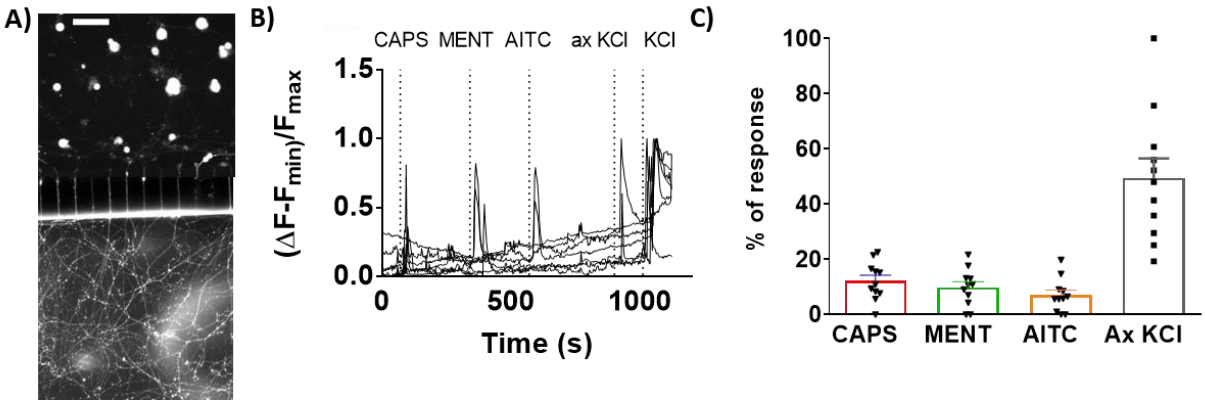

Figure 42 Mouse DRG neurons cultured in microfluidic chambers A. DRGs cultured in microfluidic chambers at DIV 6 loaded with Did'. Scale bar= 100 µm. **B.** Representative traces of calcium imaging performed stimulating the axonal compartment and recording the activity in the soma. **C.** Quantification of the percentage of response to capsaicin, menthol, AITC or axonal KCl normalized to KCl in the soma. Data are represented as bars, mean ÷ SEM. Every dot is a coverslip. N=4 animals, 2 males and 2 females; n≥2 coverslips per animal; total number of neurons=747.

Microfluidic chambers can be employed to study the effect of different cell types on neuronal functionality. To do so, DRG neurites were co-cultured with human keratinocytes. This model could prove useful to reproduce the *in vivo* layout, where keratinocytes are in contact with sensory neurons' endings in the skin. As assessed through electron microscopy, neurites and keratinocytes were in physical contact (**Figure 43**). Calcium imaging was performed as described previously, leading to activation in 27.4% of cells for capsaicin, 31.5% for menthol, 24.4% for AITC and 70.2% for KCl. It is to be noted that the percentage of responses in DRGs co-cultured with keratinocytes increased significantly with respect to the responses recorded in DRGs microfluidic culture (p-value≤0.0001)

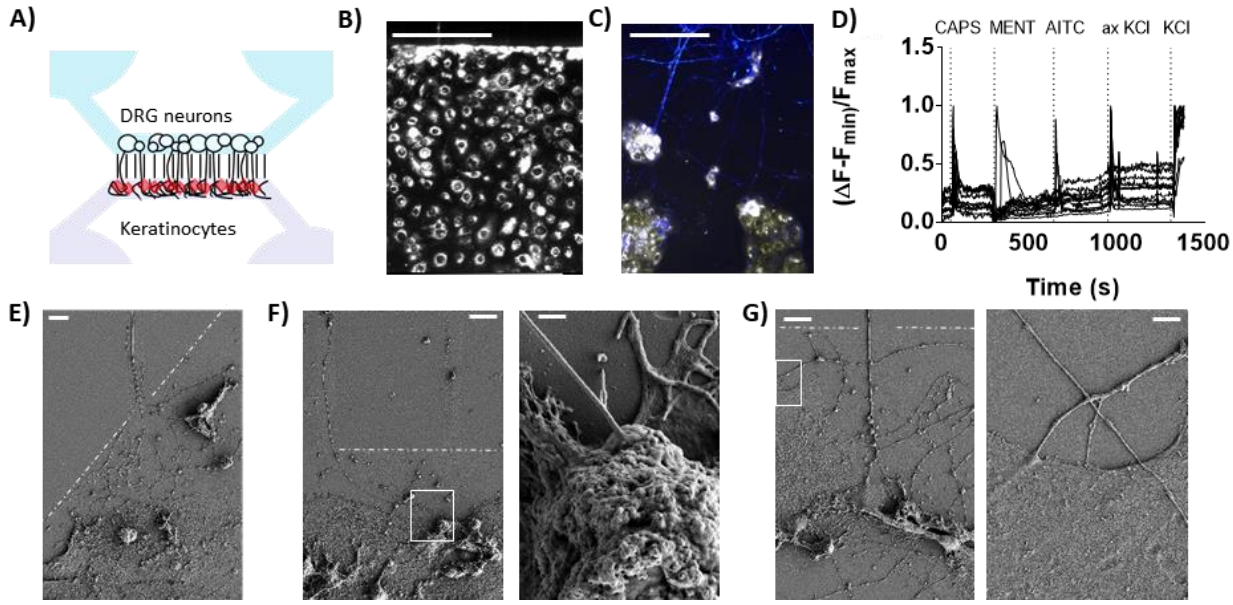

Figure 43 Nerve endings of DRG neurons in co-culture with keratinocytes A. Scheme of upper view of the microfluidic chamber with neurons and keratinocytes **B.** Picture of the axonal side with keratinocytes fully confluent at DIV 6, when calcium imaging was performed. **C.** Pictures of the axonal side with axons (blue) labelled with Fluo-4 and keratinocytes (white) labelled with Did'. Scale bar= 100 µm. **D.** Representative traces of neurons responding to capsaicin, menthol, AITC or axonal KCl. **E-G.** Scanning electron microscope pictures of axons interacting with keratinocytes, the dashed line indicates the end of the microchannels. From left to right, scale bar= 100 µm, 10 µm; 500 nm; 10 µm; 2 µm.

3.5.2. Peripheral sensitization through inflammatory mediators and chemotherapeutic agent

Microfluidic chambers also allow to set up models of localized treatment, therefore two models of peripheral sensitization were optimized and assayed through calcium imaging. To evaluate how the inflammatory mediators released in the periphery terminals affect the soma, at DIV 5, the nerve endings were treated with inflammatory soup or their vehicle (dH_2O) for 24h. At DIV 6 or DIV 8 calcium activity in the soma was recorded in response to stimuli (100 nM capsaicin, 100 µM menthol, 100 µM AITC or 40 mM KCl) applied to the soma (**Figure 44**). Due to the high variability in the datasets, a tendency to sensitization was visible but no statistically significant differences were detected. At DIV 8, the percentage of responses to capsaicin, menthol, AITC and KCl seemed to return to basal level (treated DIV 6 vs. treated DIV 8 p=0.0286), or even to lower percentages than control cells at DIV 6. After the treatment (DIV 6) the size of the responses to capsaicin and AITC increased (p=0.0026

capsaicin, p=0.0214 AITC). Interestingly, KCl response size in control cells at DIV 8 had a smaller response size compared to control at DIV 6 (p≤0.0001), maybe due to cells aging *in vitro* and consequent loss of excitability.

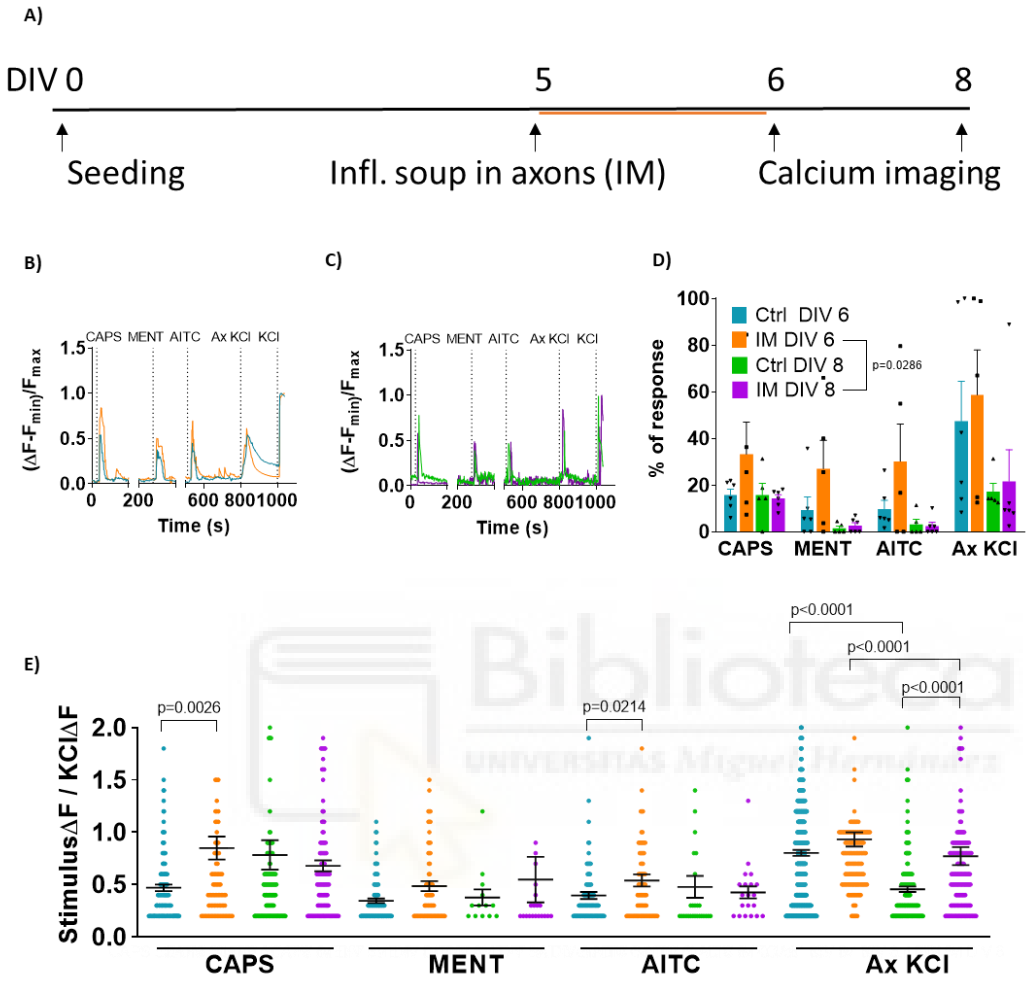

Figure 44 Effect of inflammatory soup on mDRGs cultured in microfluidic chambers A. Scheme of culture and treatment along the days in vitro **B.** Representative traces of responses to capsaicin, menthol, AITC or axonal KCl of control cells at DIV 6 (blue) or treated cells at DIV 6 (orange) **C.** Representative traces of responses to capsaicin, menthol, AITC or axonal KCl of control cells at DIV 8 (green) or treated cells at DIV 8 (purple) **D.** Quantification of the percentage of response to capsaicin, menthol, AITC or axonal KCl normalized to KCl. Axons were treated with bradykinin 1 µM, PGE-2 10 µM, histamine 10 µM, serotonin 10 µM and ATP 15 µM or their vehicles at DIV 5 and recorded at DIV 6 or DIV8. Data are represented as bars, mean ± SEM. Statistical analysis two-tailed Mann-Whitney U. **E.** Quantification of the size of the response normalized to KCl. Data are represented as a scatter dot plot, mean ± SEM, every dot represents a cell. Statistical analysis two-tailed Mann-Whitney U. N=6 animals, 3 males and 3 females; n≥3 coverslips per animal; total number of neurons=3018

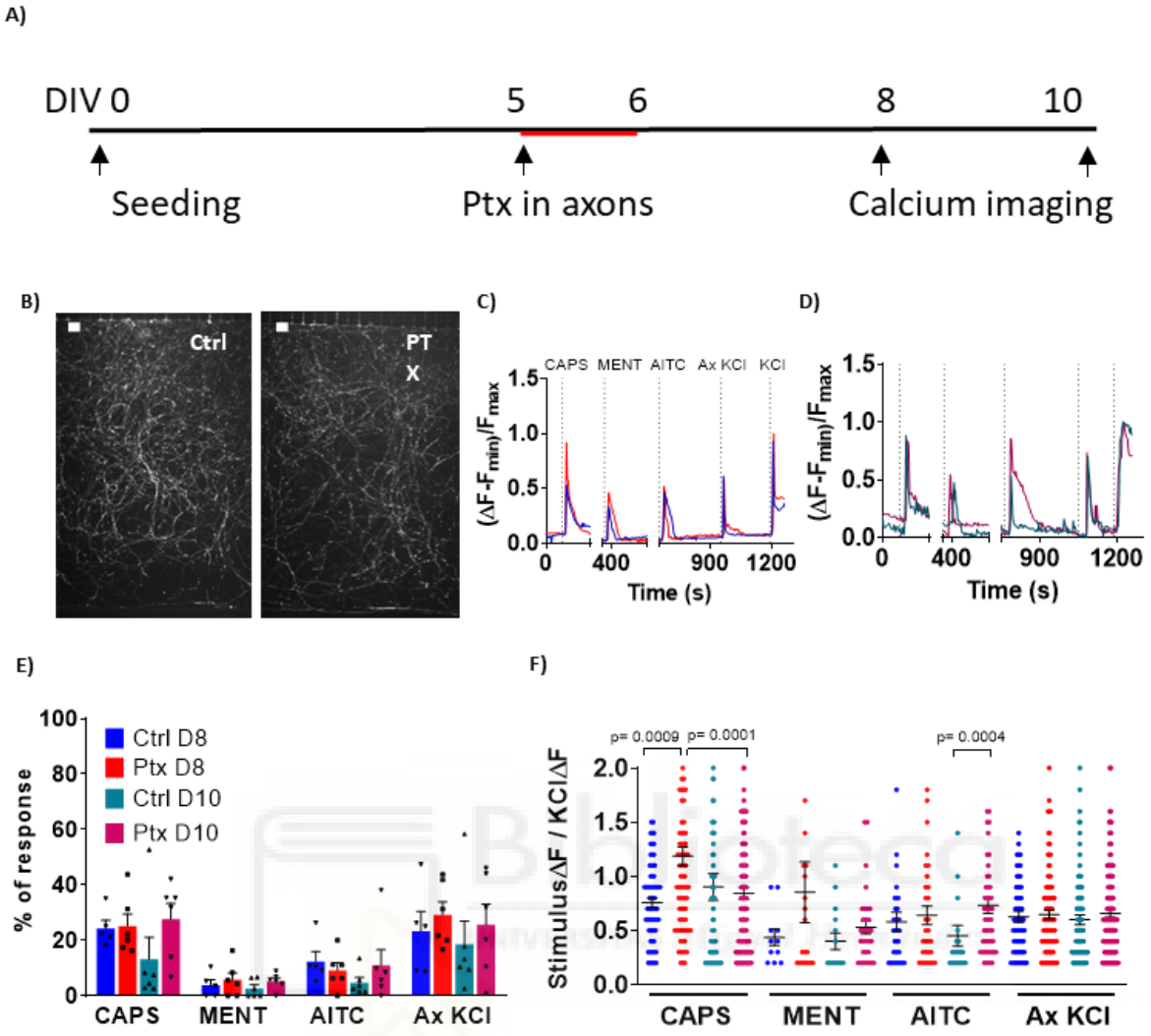

Figure 45 Effect of paclitaxel 1µM on mDRGs cultured in microfluidic chambers A. Scheme of culture and treatment along the days in vitro **B.** Pictures of axonal compartments of DRGs neurons treated with DMSO 0.04% or with paclitaxel 1 µM. Scale bar= 100 µm. **C.** Representative traces of responses to capsaicin, menthol, AITC or axonal KCl of control (blue) or treated cells (red) at DIV 8 **D.** Representative traces of responses to capsaicin, menthol, AITC or axonal KCl of control (light green) or treated cells (pink) at DIV 10 **E.** Quantification of the percentage of response to capsaicin, menthol, AITC or axonal KCl normalized to KCl. Data are represented as bars, mean ± SEM. **F.** Quantification of the size of the response normalized to KCl. Data are represented as a scatter dot plot, mean ± SEM, every dot represents a cell. Statistical analysis two-tailed Mann-Whitney U. N=5 animals, 3 males and 2 females; n≥2 coverslips per animal; total number of neurons=1638.

Moreover, a second peripheral sensitization model was set up using microfluidic chambers. A common chronic pain condition is chemotherapy-induced peripheral neuropathy (CIPN) and previous studies in our lab showed that paclitaxel altered the expression and gating of TRPV1 and TRPM8 implying their contribution to cold hypersensitivity in CIPN [95]. To investigate the impact of paclitaxel (Ptx) on the peripheral endings, at DIV 6 we treated axons with 1 µM PTX or its vehicle (DMSO 0.04%) for 24h, at DIV 7 the treatment was removed and assays

were performed at DIV 8. Calcium influx in response to stimuli was recorded at DIV 8 and DIV 10 by applying 100 nM capsaicin, 100 µM menthol, 100 µM AITC or 40 mM KCl to the axonal compartment (

Figure 45). There were no differences in the percentage of response between control and treated cells at DIV 8 or DIV 10. However, a significant increase in the size of the response to capsaicin (p=0.0009) was detected and, interestingly, an increase in the percentage of the response to AITC was seen in treated cells at DIV 10 compared to control cells at DIV 10 (p=0.004).

In addition to calcium imaging conducted on rodent DRG neurons, we extended our investigations to cultured TG neurons within microfluidic chambers. Furthermore, DRGs cultured in MFC was coupled with differential soma and neurite analysis through RT-qPCR. Further enhancing our study, we integrated MEA technology with the compartmentalized culture of DRGs, facilitating the distinct assessment of electrophysiological features in nerve endings and soma. However, the low density of electrodes in conventional MEA chips led to low rate of detected responses. Our comprehensive efforts are summarized in a recently published article [83].

As a means to obtain expertise in neuronal compartmentalized cultures, rodent DRGs were cultured in microfluidic chambers. This facilitated the exposure of neurites to various factors, including co-culture with other cell types and sensitizing agents like inflammatory mediators or chemotherapeutic compounds.

In light of our findings on direct conversion of human fibroblasts into sensory neurons, the microfluidic chambers DRG culture holds promise for applying compartmentalized cultures to human induced sensory neurons.

DISCUSSION

4. DISCUSSION

Somatosensory neurons are the first cells to detect innocuous and noxious stimuli, acting as the gateway to all the sensations perceived by our body. *In vitro* studies of somatosensory neurons are typically conducted through the analysis of dissected rodent DRGs or TGs. These models have enabled the discovery of numerous molecular and functional mechanisms in sensory transduction, including those related to ion channels; modulation by inflammatory mediators, chemotherapy compounds, hormones and neuropeptides; RNA and protein expression; drug development and even the classification of different sensory fibres [10][96][95][97]. However, the differences between human and rodent sensory neurons, which contributes the a high failure rate in clinical trials, made evident the need for human sensory neuron models which may improve translational research and the development of personalized pain treatments.

4.1. Transcription factors induction

LTVs are fundamental tools in the context of fibroblasts-to-neurons conversion due to their ability to efficiently integrate genetic material into the host cell's genome and mediate long-term gene expression. These features position LTVs as valuable instruments for manipulating gene expression across diverse cell types. [91]. In fibroblasts-to-neurons conversion, LTVs can be engineered to express key transcription factors involved in neuronal development and cell differentiation. These transcription factors can directly convert fibroblasts into neurons, bypassing the need for intermediate pluripotent states and reducing the risk of tumorigenesis associated with other reprogramming methods.

In this work, LTVs optimization with GFP or TetOGFP was crucial to ensure high levels of transgene expression in the target cells. LTVs were initially produced with the calcium phosphate or lipofectamine method, the latter resulting in highly efficient transfection and stronger expression of the transgene in the target cells. Subsequently, LTVs were produced through PEI transfection, which is cheaper than the lipofectamine method and produces high titer LTVs. The efficiency of transgene expression of PEI-produced LTVs was not assessed through GFP expression, as it was done in prior transfection approaches. However, the

successful expression of red fluorescent protein (RFP) within the target cells attested to the functional efficacy of these LTVs.

The most used LTVs employed in this work encoded Brn3a and Ngn1, pivotal transcription factors in sensory neuron development, and were inducible by doxycycline [14][62]. Tet-On system needed co-infection with three LTVs within the same cell and led to cellular toxicity due to high MOIs and the presence of doxycycline in the medium. To surmount these limitations, a constitutive BN1 all-in-one vector was designed, co-expressing Brn3a, Ngn1, and RFP in one vector, without the reliance on doxycycline induction. Employing this LTV resulted in heightened cell viability, albeit quantification was not conducted. A visual comparison between the conversion protocol using doxycycline-inducible vectors and the all-in-one LTVs was the sole measure. Moreover, the inclusion of RFP as part of the expressed genes in this LTV offered a rapid means of confirming gene expression within the target cells.

Throughout this work, different types of fibroblasts and small molecules were employed, while transgene expression of Brn3a and Ngn1 was always present in the different conversion protocols, due to their pivotal role in sensory neurons' development. These transgenes were successfully used in 2015 by Blanchard, Eade and collaborators to directly convert mouse embryonic or human adult fibroblasts to sensory neurons [66] and have been considered as pivotal specification transgenes for the sensory neurons subtype since then [98]. Interestingly, the same year Wainger and collaborators published that, out of 12 transcription factors expressed in human adult fibroblasts, removing Brn3a decreased Trpv1 expression. The same authors identified Ascl1, Myt1l and Klf7 as pivotal transcription factors in the Trpv1 lineage [65]. Ascl1, together with Ngn1, is the most common transcription factor used in fibroblasts to neurons conversion protocols [99]. One of its many functions, together with Myt1l, is to inhibit the Notch/Delta pathway, which is the same role as the small molecule DAPT [60], that in this work was fundamental to increase the efficiency of sensory neurons conversion protocols. Furthermore, out of the many conversion protocols presented in this work, Ascl1 was intentionally induced through LTVs in the Drouin-Ouellet and Lau [68] protocol and all its modifications presented in this work, including protocol 2.3 which proved to be the more effective protocol in inducing sensory neurons from human adult dermal fibroblasts. Lastly, Klf7 is a pivotal transcription factor in sensory neuron development, which

works in concert with Brn3a in maintaining TrkA expression in the embryonic stage [100]. Out of the three pivotal TFs identified by Wainger and collaborators, Klf7 was not induced in this work neither through LTVs nor small molecules. However, the molecular role of many small molecules is not known, therefore it may be interesting to analyse the transcriptomic changes of fibroblasts during the conversion protocol. Interestingly, more dropout experiments conducted by Wainger and collaborators, showed that Brn2 exclusion also increased the number of Trpv1 positive neurons. Brn2 is expressed in the 3410 LTV, used in the Drouin-Ouellet protocol. Investigating different transcription factors and their role in the conversion protocols presented in this work could be of interest in future experiments.

While certain researchers achieved fibroblast-to-neuron conversion solely through small molecules, yielding simpler, more cost-effective, and flexible protocols, the outcomes often comprised a heterogeneous mixture of neuron subtypes or even unknown phenotypes. In contrast, exogenous transcription factor expression via LTVs played an important role in specifying distinct neuronal subtypes [91]. Additionally, LTVs can serve as a means for introducing precise genetic modifications or mutations into the genomes of reprogrammed neurons, facilitating controlled and reproducible exploration of disease mechanisms and potential therapeutic strategies which could be interesting in further applications [92][93][94].

4.2. Calcium imaging as main characterizing technique

In this work, many conversion protocols were performed to convert fibroblasts from different tissues and donors into sensory neurons. Fibroblasts have consistently been chosen as the starting cell type for these protocols due to their accessibility, ease of culture, lack of intermediate cell states, faster conversion times, and reduced risk of tumorigenesis compared to iPSc. Additionally, it has been demonstrated that directly converted cells maintain donors' epigenetic marks, aging, and mosaicism [98][99], allowing for personalized medicine studies and the production of mixed populations of neurons. Throughout this work, different types of fibroblasts and small molecules were applied, with the goal of developing a robust and efficient protocol of conversion from fibroblasts to sensory neurons.

Calcium imaging was chosen as the primary method for characterizing converted sensory neurons due to its high sensitivity compared to high throughput assays, as well as its ability

to image multiple cells simultaneously allowing the evaluation of functional properties. **Table 3** provides a summary of calcium imaging results obtained from all the conversion protocols performed, as a means to easily compare the different conversion protocols. Moreover, since TRP channels are calcium-permeable ion channels and markers for different sensory neuron populations [10], [15], calcium imaging assays were centred on measuring TRP channels responses to agonists as well as cell responses to KCl, as a depolarizing stimulus. As a drawback to this technique, calcium imaging alone does not provide information about the electrophysiological properties of the cells under study. Therefore, it is necessary to further functionally characterize the converted cells using electrophysiological techniques such as patch clamp or MEA.

Performing conversion protocols involving LTVs and small molecules is highly demanding both in terms of time, money and effort. Therefore, not all the conversion protocols were thoroughly characterized with many techniques. In every conversion protocol, calcium imaging was used as a screening technique to decide if further analysis, both molecular and functional, was appropriate. We believe this method allowed us to discard those protocols which were not developing functional putative sensory neurons. However, this method also has drawbacks, such as (1) the lack of deep molecular characterization of the converted cells, leading to a lesser knowledge of the output caused by the changes applied to every protocol; and (2) the difficulty in comparing different conversion protocols, other than with calcium imaging results.

Table 3 Summary of direct conversion protocols and calcium imaging results as percentage of response to KCl, KCl and capsaicin, KCl and menthol or KCl and AITC.

		Mean percentage of response			
Human fibroblasts origin (gender)	**Protocol**	**KCl+**	**KCl+ caps +**	**KCl+ ment +**	**KCl+ AITC +**
Foetal lung (female)	1	7.8	23.0	65.4	88.3
	2	8.5	34.9	84.0	100
Neonatal dermal (male)	Blanchard, Eade et al.	0.5	0	0	0
	cAMP	0.7	2.3	4.5	0.4
	DAPT	3.3	2.5	16.5	22
Adult dermal (female)	Blanchard, Eade et al	1.3	0	0	0
	DAPT	2.5	1.3	1	5
	Cycle Arrest	1.5	12.5	12.5	13.2
Adult dermal skin biopsy (female; male)	2.3 (day27)	5.3; 3.3	2.6; 20	5; 12.3	20.3; 14.3
	2.3 (day50)	3.8; 5.8	24.3; 10.4	0; 7.9	6.6; 3.4

4.3. Direct conversion of foetal lung fibroblasts to sensory neurons

The foetal lung fibroblasts used in this work were an immortalized cell line (IMR90) and therefore did not behave as primary fibroblasts in terms of maximum number of passages, required medium, and morphology. Nevertheless, they proved to be a feasible model for induced sensory neurons as both protocol 1 and 2 provided a high percentage of putative neurons (KCl responsive cells) that responded to capsaicin, menthol, or AITC. It is interesting to note that even after undergoing the conversion protocol, the percentage of cells responding to AITC remained as high as in non-converted cells. This might suggest that TRPA1, which is highly expressed in human foetal fibroblasts, may not be downregulated during the conversion process, indicating that the resulting cells may not be fully converted to sensory neurons. Interestingly, some cells responded to all three TRPs agonists. Co-response to menthol and AITC could be explained by menthol activating TRPA1 [101]. The co-response to capsaicin and menthol is more surprising; however, some authors found TRPM8 and TRPV1 mRNA co-expressed in the same neuronal population [102] and functional studies hypothesised that TRPV1 and TRPM8 may be co-expressed in trigeminal ganglia or oocytes [103][104]. Nevertheless, to our knowledge, a population of sensory neurons which expresses TRPV1, TRPM8 and TRPA1 was not described in humans nor in any other species, therefore IMR90 derived iSNs would not fully recapitulate human sensory neurons.

Regarding morphological analysis, protocol 2 more closely resembled sensory neurons phenotype, while protocol 1 presented an elongated morphology. However, as protocol 2 resulted in a high mortality rate, it may not be suitable for the development of *in vitro* chronic models. Nevertheless, due to the high quantity of IMR90 available, this conversion protocol could be used in high throughput screening for testing compounds active on TRPs channels in a cellular context that is closer to sensory neurons, compared to a stable cell line expressing an exogenous ion channel. In the future, modifications to protocol 2 may be implemented to reduce cell mortality and prolong the conversion protocol using the BN1 all-in-one lentiviral vector instead of using doxycycline-inducible LTVs expressing Brn3A and Ngn1 separately. The use of BN1 LTV would increase the transduction efficiency and reduce

toxicity, probably leading to higher maturation of iSNs. Further future experiments may focus on measuring CGRP secretion through ELISA and may investigate the molecular aspects of cell cycle block in protocol 2. While the cell cycle was actively blocked in protocol 1 and not in protocol 2, statistically significant blockage of the cell cycle was still observed in protocol 2, suggesting that the conversion protocol 2 itself induced cell cycle blockage.

As for protocol 2 alone, TRPV1, TRPM8 and TRPA1 in converted cells seemed to be slightly sensitized after exposure to inflammatory mediators, however statistical significance was not present between control and treated cells. The sensitization tendency is in line with TRPs sensitization induced by inflammatory mediators and neurotrophic factors in rodents DRGs [22][105]. Probably, the inflammatory mediators composition or time of application has to be optimized yet, but this type of experiments may open new possibilities for using this system in inflammatory pain research and compounds screening in a model resembling human sensory neurons. Furthermore, protocol 2 converted cells displayed electrical activity as measured in MEA CMOS experiments, however it was impossible to perform patch clamp due to cell membrane damage. As measured by MTT assay on adult dermal fibroblasts, polybrene does not display cytotoxicity. However, MTT assay only assesses cell metabolic activity. Considering cell membrane health of protocol 2 converted cells, further assessment should be done in the effect of polybrene on cell membrane state. In conclusion, the overall cell health in both protocol 1 and protocol 2 may be improved by slight modifications such as using all-in-one LTVs, avoid using doxycycline and polybrene, and perform half media changes.

4.4. Direct conversion of dermal neonatal fibroblasts to sensory neurons

The results obtained from IMR90 conversion pave the way for the development of a high throughput method to obtain an *in vitro* model of human sensory neurons. However, IMR90 are immortalized cells obtained from foetal lungs, therefore they are not easily obtainable from patients or healthy volunteers. For this reason, further conversion protocols were performed in dermal fibroblasts. Since young fibroblasts display higher conversion efficiency than adult ones [68], the first conversion protocol on dermal fibroblasts was performed with

cells from neonatal donors. In our hands, the Blanchard and Eade protocol [66] did not show KCl responses in converted cells. The reason for this contrast to published data may reside in differences in the starting cells, since Blanchard and Eade 2012 presented limited data on human dermal fibroblasts, while mainly focusing on mouse embryonic fibroblasts. In an attempt to develop an efficient protocol, we modified the protocol published by Ladewig and collaborators [77], which directly converts adult dermal fibroblasts to neurons. Such modification comprised the addition of the small molecule DAPT, which inhibits the Notch/Delta pathway. DAPT proved to be a crucial addition, as the percentage of KCl responses increased almost five times compared to the cAMP protocol. Interestingly, Notch/Delta inhibition may also be obtained by the induction of Ascl1 and Mytl1, which are often induced in conversion protocols. In future experiments it could be interesting to investigate the effect of DAPT and Notch/Delta inhibition, to further increase our understanding of small molecules in conversion protocol which is sometimes limited. Similarly, to what was observed in foetal lung fibroblasts converted cells, there were small populations of KCl responsive cells which responded to both capsaicin and menthol and both capsaicin and AITC. According to Usoskin et al. [10] TRPV1 and TRPA1 are co-expressed in two subpopulations of non peptidergic, unmyelinated sensory neurons, in rodents. In addition, we also observed that 1,4% of cells responded to both menthol and AITC, which were also described in rat primary afferent neurons, however in lower percentage [102]. Furthermore, a small population responded to all three TRPs agonists which, to our knowledge, was never described before, therefore this feature may not recapitulate human sensory neurons phenotype.

4.5. Direct conversion of human dermal adult fibroblasts to sensory neurons

Previous studies showed that adult dermal fibroblasts conversion has lower efficiencies than fibroblasts from younger donors [68]. Nevertheless, since the main objective of this work is to develop a human sensory neurons model which could apply to a variety of fibroblasts from different tissues and donors, we wanted the model to work in fibroblasts extracted from donors of all ages. Therefore, dermal biopsies were extracted from healthy donors and a protocol to extract fibroblasts from human donors was optimized.

Blanchard and Eade protocol in our hands was not successful, while DAPT protocol presented slightly higher percentages of response however the efficiency was not satisfactory to have a robust and reproducible model of human sensory neurons. Furthermore, both protocols induced high cells mortality having a low number of converted cells at the end point and making the maturation of converting cells not possible. In an attempt to increase conversion efficiency, DAPT protocol was modified blocking the cell cycle in G1, which induces cells to exit the cell cycle to the G0 phase [88], which in previous studies increased conversion from human fibroblasts to dopaminergic neurons [106]. Contrary to our expectations, the cell cycle block protocol demonstrated lower efficiency than DAPT protocol. In conclusion, in our hands adult fibroblasts conversion protocols result in lower efficiency than young fibroblasts, confirming results published from other authors [68] [107].

To optimize a reproducible and efficient conversion protocol in adult dermal fibroblasts from skin biopsies, human dermal fibroblasts extracted from dermal biopsies were subjected to various modifications of the cell cycle arrest protocol or Drouin-Ouellet and Lau protocol. As previously published, Drouin-Ouellet and Lau protocol efficiently converted adult dermal fibroblasts to cells with neuronal morphology and positive to Tau. Modifications applied to specify these cells to sensory neurons, involved the combination of LTVs 3410 and BN1. These LTVs combined induced expression of Ascl1, Brn2, REST shRNA, Brn3a and Ngn1 in transduced cells. Ascl1 and Brn2 are among the most commonly used TF in fibroblasts-to-neurons conversion. Their selection is based on their pivotal roles in neural development and their effectiveness in promoting the conversion [98], [99]. However, as demonstrated by Drouin-Ouellet and Lau, these TFs alone may not be sufficient for efficiently converting adult dermal fibroblasts into neurons. REST inhibition through shRNA has been shown to be essential, which was a finding also confirmed by Church and colleagues, who induced REST inhibition through the induction of miRNA 9/9* and miRNA 124 [89]. Adding BN1 LTV to Drouin-Ouellet and Lau protocol increased the percentage of both neurons and sensory neurons. The fact that adding Ngn1 induction increased not only sensory neurons but also Tau+ cells is in line with results from other authors, reviewed by Traxler and colleagues [98]. However, inducing BN1 expression without 3410 did not generate neurons or sensory neurons, demonstrating that Ascl1, Brn2, and REST inhibition are pivotal for adult dermal fibroblasts conversion into neurons. A further modification to the original Drouin-Ouellet and

Lau protocol was the addition of NGF and DAPT to conversion media. Nerve growth factor is a widely used neurotrophic factor in rodents DRGs culture, allowing their survival and maturation after dissection. It has been also widely used in fibroblasts to sensory neurons conversion protocols because of its pivotal role in sensory neurons fate specification during the embryonic development and maturation [1]. DAPT is also widely used in sensory neurons generation from iPSCs [60] and in our experience it increased conversion efficiency in neonatal and adult dermal fibroblasts. As expected, the addition of NGF and DAPT to the early neuronal media increased the percentage of sensory neurons in comparison to a conversion protocol where these molecules where not present. Interestingly, the inclusion of NGF and DAPT led to an increase in the percentage of sensory neurons, but it resulted in a decrease in the percentage of overall neurons. It was not explored whether this was due to a higher mortality rate or perhaps a competitive mechanism that prevented a high proportion of both neurons and sensory neurons simultaneously. Nevertheless, despite the reduction in the percentage of neurons, protocol 2.3 was selected as the preferred choice because of its sensory neurons yield.

The outcomes of protocol 2.3 offer valuable insights into the potential and complexities of this method. Notably, the results obtained from calcium imaging assays and the molecular characterization, both at mRNA and protein level, exhibited considerable variability among donors and between endpoints. These variations strongly suggest the presence of donor-specific factors and maturation-related dynamics influencing the functional properties of the induced sensory neurons. To gain a deeper and more comprehensive understanding of the maturation processes of converted cells, further assays are needed involving fibroblasts from a diverse pool of donors, comprising various ages and genders. Transcriptomic and proteomic analyses will be instrumental in uncovering donor-specific factors contributing to the induction of neuronal cells.

These findings contribute to our understanding of the potential and challenges associated with the conversion of fibroblasts into sensory neurons, opening avenues for future research in the field of sensory neuron biology and disease modelling.

4.6. Mouse DRGs culture in microfluidic chambers

Microfluidic chambers were used in this work to provide a tool to compartmentalize rodent DRGs soma and neurites. Once the model of compartmentalized culture was optimized, our findings substantiated that compartmentalized sensory neurons in microfluidic chambers are suitable models to investigate the interaction of the sensory endings with dermal cells, as well as to study the mechanisms involved in their peripheral sensitization either by pro-inflammatory or neuropathic drugs.

Compartmentalized culture presents numerous advantages, such as being able to expose axons to a different fluid and cellular environment than cell bodies, which is useful for studies of trophic and pharmacological regulation. Specifically, in the case of nociceptors, it is of vital importance to separate the soma from the nerve endings because of their peculiar anatomy *in-vivo*. Whereas only the peripheral terminal of the nociceptor will respond to environmental stimuli, both the peripheral and central terminals can be targeted by endogenous molecules. MFCs present a multitude of applications that have the potential to yield novel insights into neuronal physiology and pathology. These applications encompass diverse areas, including the subcellular localization of molecules, vesicle trafficking, *in situ* translation, and the localization of transduction proteins. Furthermore, MFCs offer the opportunity to investigate interactions between neurons and other cell types, enabling co-culturing nerve endings with fibroblasts, keratinocytes, endothelial cells, glial cells, and more. This approach facilitates a more comprehensive exploration of sensory transduction, signal conduction and integration, neuropeptide secretion, as well as mechanisms underlying neuronal sensitization and chronic conditions. Intriguingly, MFC design holds the potential to replicate the *in vivo* spatial arrangement of cells, for example the addition of microchannels with controlled and constant fluidic conditions could potentially mimic aspects of the blood or lymphatic vascular systems. The capability to design and construct customized MFCs confers a remarkable degree of flexibility, enabling the pursuit of diverse research objectives.

While the compartmentalized culture of DRGs and TG presents numerous advantages, certain uncertainties remain. As an example, it is unclear whether the neurites under investigation are of peripheral, central, or combined origin. The dissection process of

sensory neurons removes existing neurites, which subsequently regrow over the course of days in culture. As a consequence, it is plausible that the neurites present in the culture might regrow as naive neurites. To address this, future investigations may use a MFC with three distinct compartments. Such a design could facilitate the optimization of protocols tailored to attract peripheral and central axons separately. This approach may shed light on the specific properties and behaviours of these neurite populations, enhancing our understanding of peripheral neurons.

These models hold great promise for the future of sensory neurons and pain investigation and open to the possibility of culturing induced sensory neurons derived from human cells. In fact, culturing rodent sensory neurons in MFC presents challenges in standardization due to limited cell numbers and a reliance on user experience. Furthermore, using iSNs would reduce the use of animals and limit problems of unreliability and low translatability of animal experimentation. Culturing iSNs in microfluidic chambers would increase the representativity of this model, increasing its similarity to the *in-vivo* morphology of human sensory neurons.

CONCLUSIONS

5. CONCLUSIONS

5.1. Transdifferentiation or direct conversion

1. In the context of fibroblasts direct conversion, constitutive all-in-one LTVs are preferable compared to doxycycline-dependent systems, because they present higher transgene expression, require lower MOIs and seem to induce lower cell mortality.
2. The conversion of fibroblasts to putative sensory neurons can be achieved through a variety of methods, each with their own advantages and limitations. Each model is adequate for the study of certain aspects of sensory neurons.
3. Direct conversion of lung foetal fibroblasts into putative sensory neurons is feasible both with protocol 1 and 2. Protocol 2 seems to have higher conversion efficiency than protocol 1 however it induced high cytotoxicity.
4. In our hands, Blanchard, Eade and collaborators conversion protocol did not induce sensory neurons from neonatal or adult human dermal fibroblasts.
5. The addition of DAPT to conversion media improved cells morphology and it increased the performance of converted cells as measured by calcium imaging, in neonatal and adult human dermal fibroblasts.
6. Cell cycle block through small molecules and/or serum withdrawal does not seem to increase the conversion efficiency both in human lung foetal fibroblasts and in human dermal adult fibroblasts.
7. Drouin-Ouellet, Lau and collaborators conversion protocol successfully induced neurons and sensory neurons from human adult dermal fibroblasts. In adult dermal fibroblasts, Ascl1 and Brn2 induction, and REST inhibition, combined with defined conversion media, are crucial for conversion of fibroblasts to neurons. Inducing Brn3a and Ngn1 expression, and adding NGF and DAPT, increases the amount of putative sensory neurons generated. Brn3a and Ngn1 induction alone does not generate Tau positive cells.
8. Converted adult dermal fibroblasts displayed functionality typical of sensory neurons up to 50 days *in vitro*.

9. Conversion efficiency is highly dependent on fibroblasts type, tissue of origin, donor's age, fibroblasts and reagents batch etc.

5.2. Microfluidic chambers

1. Microfluidic chambers are feasible tools to perform compartmentalized culture of rodent DRGs.
2. Calcium imaging can be performed stimulating neurites and recording activity in the cell soma.
3. Neurites can be co-cultured with human keratinocytes, with slight modifications to the culture media. In this system, neurites are in physical contact with keratinocytes.
4. Microfluidic chambers allow to expose neurites to inflammatory mediators or chemotherapeutic agents. These substances sensitize neurites to different extent and the sensitization can be observed in the soma.

6. CONCLUSIONES

6.1. Transdiferenciación o conversión directa

1. En el contexto de la conversion directa de fibroblastos, los LTV de expression constitutiva son de preferir a los sistemas dependientes de doxiciclina, porque presentan expresión del transgén mayor, necesitan MOIs menores y parecen inducir menos mortalidad celular.
2. La conversion de fibroblastos a neuronas sensoriales putativas puede ser obtenida a través de varios métodos, cada uno con sus ventajas y limitaciones. Cada modelo podrá considerarse para estudiar ciertos aspectos de las neuronas sensoriales u otros.
3. La conversión directa de fibroblastos pulmonares fetales en neuronas sensoriales putativas es posible tanto con el protocolo 1 como con el 2. El protocolo 2 parece tener una mayor eficiencia de conversión que el protocolo 1, sin embargo, indujo una alta citotoxicidad.
4. En nuestras manos, el protocolo de conversión de Blanchard, Eade y colaboradores no indujo neuronas sensoriales a partir de fibroblastos dérmicos humanos neonatales o adultos.
5. La adición de DAPT al medio de conversión mejoró la morfología celular y aumentó el rendimiento de las células convertidas, medido mediante imágenes de calcio, en fibroblastos dérmicos humanos neonatales y adultos.
6. El bloqueo del ciclo celular a través de moléculas pequeñas y/o la retirada de suero no parece aumentar la eficiencia de conversión tanto en fibroblastos pulmonares fetales humanos como en fibroblastos dérmicos adultos humanos.
7. El protocolo de conversión de Drouin-Ouellet, Lau y colaboradores indujo con éxito neuronas y neuronas sensoriales a partir de fibroblastos dérmicos humanos adultos. En los fibroblastos dérmicos adultos, la inducción de Ascl1 y Brn2, y la inhibición de REST, combinadas con un medio de conversión, son cruciales para la conversión de fibroblastos a neuronas. La inducción de la expresión de Brn3a y Ngn1, y la adición de NGF y DAPT, aumentan la cantidad de neuronas sensoriales putativas

generadas. La inducción de Brn3a y Ngn1 por sí sola no genera células positivas para Tau.

8. Los fibroblastos dérmicos adultos convertidos mostraron funcionalidad típica de neuronas sensoriales hasta 50 días *in vitro*.
9. La eficiencia de conversión depende en gran medida del tipo de fibroblastos, el tejido de origen, la edad del donante, los lotes de fibroblastos y reactivos, etc.

6.2. Cámaras microfluídicas

1. Las cámaras microfluídicas son buenas herramientas para realizar cultivos compartimentados de ganglios de raíz dorsal de roedores.
2. La imagen de calcio se puede realizar estimulando neuritas y registrando la actividad en el soma celular.
3. Las neuritas se pueden co-cultivar con queratinocitos humanos, con ligeras modificaciones en el medio de cultivo. En este sistema, las neuritas están en contacto físico con los queratinocitos.
4. Las cámaras microfluídicas permiten exponer las neuritas a mediadores inflamatorios o agentes quimioterapéuticos. Estas sustancias sensibilizan las neuritas en diferentes grados y la sensibilización se puede observar en el soma.

MATERIALS AND METHODS

7. MATERIALS AND METHODS

7.1. Plasmids

Transfer plasmids for TetO Ngn1 (Addgene #62222) and TetO Brn3a (Addgene #62221) were deposited by the Kristin Baldwin laboratory [66] on the Addgene repository. As shown in **Figure 46**, transfer plasmids present a region between the LTRs, which will integrate in the host genome and will be transcribed in response to doxycycline.

The TetO promoter needs a transactivator (rtTA) to induce the doxycycline-dependent transcription of the genes of interest. The plasmid was deposited by Ron Weiss laboratory (plv_hEF1_rtTA Addgene #61472) [108].

Packaging and envelope plasmids are detailed below:

- pCMV delta R.2 (Addgene #12263): packaging plasmid carrying the genes GAG, POL, TAT and REV; this plasmid was a gift from Didier Trono laboratory;
- pCMV-VSV-G (Addgene #8454): envelope plasmid, is an empty backbone that, used in combination with the packaging plasmid, allows to produce LTVs. Deposited by Bob Weinberg laboratory [109].

In addition, pLenti CMV GFP Hygro (Addgene # 17446) [111] and FUW TetO eGFP (Addgene # 84041) [112] were used to optimize the transfection in HEK293 LTV and the infection in human fibroblasts. These plasmids are lentiviral transfer plasmid that expresses eGFP in mammalian cells under the control of a constitutive promoter or a doxycycline inducible promoter.

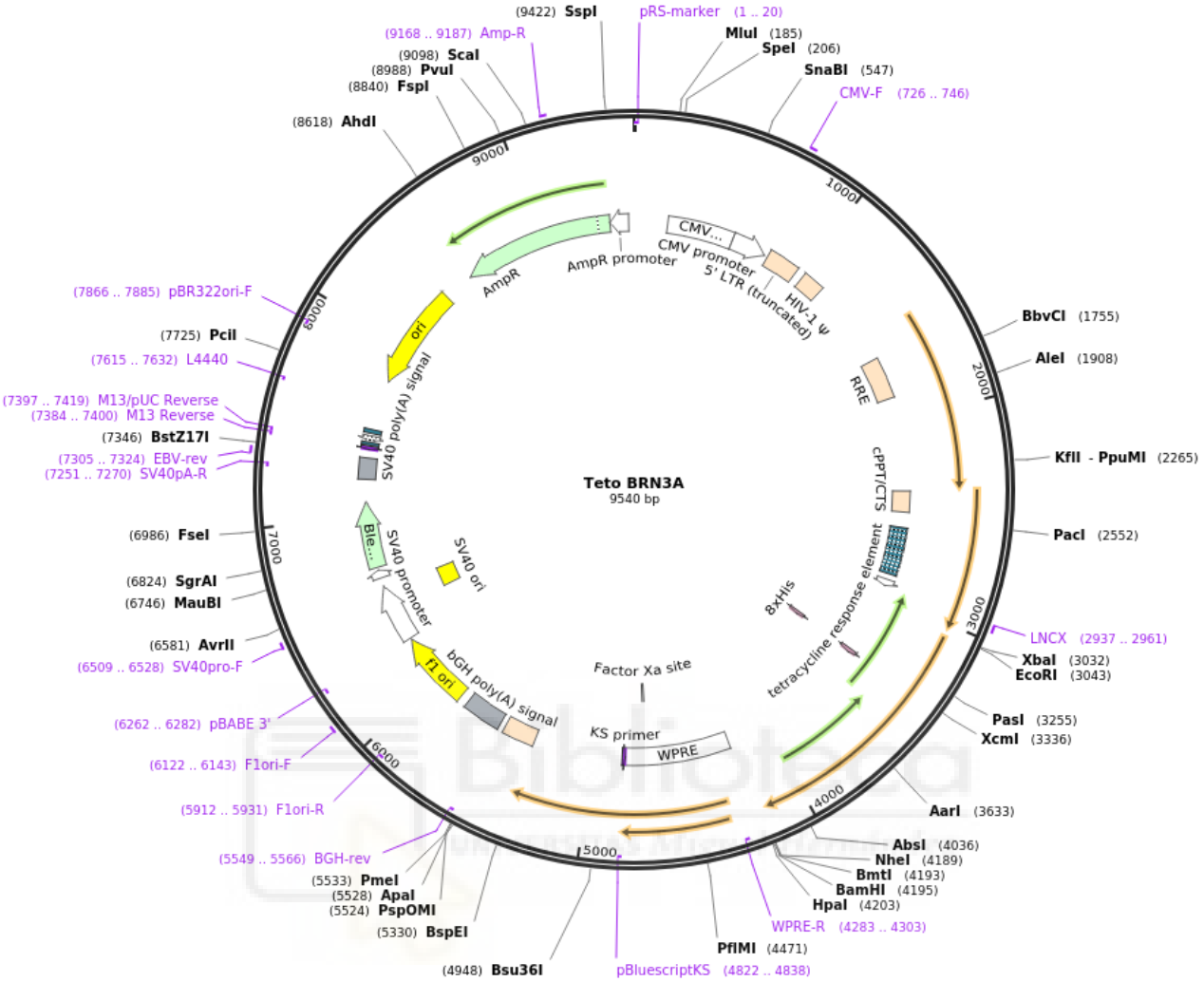

Figure 46 TetOBrn3a plasmid structure. TetONgn1 and TetONgn2 share the same structure and sequence, save the gene of interest sequence.

For the production of LTVs 3410 and BN1, 3rd generation packaging system was used, using the following plasmids:

- BN1 transfer plasmid which encodes for Brn3a, Ngn1 and RFP, all separated by a 2A self-cleaving peptides, which induce ribosomal skipping. The genes of interest are under the control of the constitutive promoter EF1α.This plasmid was self-designed and cloned by Vector Builder.
- 3410 transfer plasmid which encodes for Ascl1, Brn2 and two different shRNA for REST [68].
- 3043 (pMD2G): VSV-G encoding envelope plasmid.

- 3044 (pMDLg_pRRE): GAG, POL and RRE encoding packaging plasmid.
- 3045 (pRSV_REV): REV packaging plasmid. These plasmids were a gift from Karolina Pircs' laboratory.

Upon arrival, transformed bacterial strain were grown in LB Agar medium supplemented with ampicillin 100 µg/mL at 37°C for 24h. On the following day, one bacterial colony was chosen and grown in LB medium supplemented with ampicillin at 37°C shaking overnight. After 16-24h, the DNA was extracted using E.Z.N.A. Plasmid Midi Kit (Omega Bio-Tek). Plasmids were stored at -20°C for up to 6 months.

7.2. Lentiviral vectors production

HEK 293LTV cell line was used to produce all lentiviral vectors however different transfection protocols were performed. For the production of GFP LTV, TetO GFP LTV, TetO Brn3a LTV, TetO Ngn1 LTV and rtTA LTV; $1x10^6$ cells were seeded in a 100 mm diameter petri dish and transfected when cells reached 70% confluence and were spread evenly onto the plate. Transfection was performed using the calcium phosphate [113][114] or lipofectamine method.

For calcium phosphate method, 16 µg of lentiviral transfer vector DNA were combined with 16 µg of dR8.2 packaging and 4 µg of VSV-G envelope plasmid DNA. The precipitate was formed by adding 86 µL 2.5M $CaCl_2$ (Sigma) reaching a final volume of 700 µL with DEPC-H_2O (Ambion), afterwards 700 µL of 2X HBS (HEPES 50 mM, $Na_2HPO_4 \cdot 2H_2O$ 1,5 mM, NaCl 280 mM, KCl 10 mM, Sucrose 12 mM, pH=7.2) (Sigma) was added to the DNA mix dropwise while vortexing. The solution was then vortexed and incubated at room temperature (RT) for 30 min and then added to the cells, that were incubated at 37°C 5% CO_2 overnight.

For lipofectamine transfection, 37,5 µL of Lipofectamine 3000 (Invitrogen) was added to 500 µL of DMEM GlutaMAX (Gibco) and 1% Penicillin/ Streptomycin (Gibco). In another eppendorf, 500 µL of medium was mixed with plasmid DNA (7 µg of lentiviral transfer vector DNA, 5,5 µg of dR8.2 packaging and 2,5 µg of VSV-G envelope) and 30 µL of P3000. DNA solution was added to lipofectamine solution and incubated for 15 minutes at RT.

Afterwards, the transfection mix was added dropwise to the cells and incubated at 37°C 5% CO_2 overnight.

After the transfection, viruses were collected at 24, 48 and 72 hours. The medium containing the viruses was then filtered with a 0,45 µm filter to eliminate cell debris and stored at -80°C or immediately concentrated. The concentration was performed by ultracentrifugation at 38000 RPM (Beckman 45Ti rotor) at 4 °C for 2h, using a sucrose cushion (Sucrose 20%, NaCl 100mM, HEPES 20 mM, EDTA 1mM) (Sigma) to purify the viruses from cell medium and cell debris. The pellets were then resuspended in D-PBS (Sigma) and working aliquots were stored at -80°C up until one year [115][87].

On the other hand, 3410 and BN1 LTV were produced using PEI transfection method. HEK 293 LTV were seeded in T175 flasks and transfected with 21 µg of transfer plasmid, 5.5 µg of 3043 envelope plasmid, 7.5 µg of 3044 packaging plasmid and 3.9 µg of 3045 packaging plasmid. LTVs were collected 45h after the transfection, concentrated through ultracentrifugation at 35000 RPM (Beckman 45Ti rotor) at 4 °C for 1.5h. The pellets were resuspended and stored as described previously.

7.3. Lentiviral vectors titration

HEK 293 LTV were infected with serial dilutions of lentiviral vectors 1:1000, 1:10.000 and 1:100.000. Four days after infection, cells were collected and genomic DNA was extracted using Nucleo Spin Tissue Genomic DNA (Machery Nagel) to perform quantitative PCR targeting the viral gene WPRE. TaqMan probe and primers sequences are described in **Table 4**.

Table 4 WPRE TaqMan probe and primers.

Probe	Forward primer	Reverse Primer
FAM-TGCTGACGCAACCCCCACTGGT-TAMRA	CCGTTGTCAGGCAACGTG	AGCTGACAGGTGGTGGCAAT

qPCR was performed as in Kutner et al [87] with some variations. TaqMan RNaseP control reagent (Applied Biosystems) was used to target RNaseP as endogenous gene. TaqMan

qPCR was performed using QuantStudio 3 thermocycler (Applied Biosystems), with the following protocol: 50°C for 2 min, 95°C for 10 min, 95°C for 15s, 60 °C for 1min for 35 cycles. Standard curves for WPRE and RNaseP were prepared, using plasmid and human genomic DNA respectively, to calculate the viral and genomic copies present in the samples. Viral vector copy numbers in HEK 293 LTV were normalized to human RNaseP gene copies and presented as proviral copies per genome equivalent. Integration units per mL (IU/ml) were calculated according to the following formula:

$$IU/mL = (C\ x\ N\ x\ D\ x\ 1{,}000)/V$$

Equation 1 titration qPCR analysis equation: C is proviral copies per genome, N is the number of cells at time of transduction, D is the dilution of vector preparation, V is the volume of diluted vector added in each well for transduction [115].

7.4. Cell culture

HEK 293LTV (Cell Biolabs Inc.) is specifically designed to produce high lentiviral titers throughout a transfection [116]. Cells were cultured in DMEM GlutaMAX high glucose + 1% Penicillin/Streptomycin + 10% FBS + 0,1 mM MEM NEAA (Gibco) and passaged with 0,05% Trypsin – EDTA 1X (Gibco) when 80 % confluent. For one-week maintenance, 70 µL of an 80% T25 flask were seeded onto a new T25.

Foetal lung fibroblasts from female donor (IMR90) were cultured in MEM (ATCC) + 10% FBS + 1%P/S (Gibco) and passaged with 0,05% Trypsin – EDTA 1X (Gibco) when 80 % confluency was reached.

Human dermal fibroblasts form neonatal donors (HDFn) (Gibco) are human dermal fibroblasts isolated from neonatal foreskin. The cells were cultured in Medium 106 + LSGS supplement + 1% Penicillin/Streptomycin (Gibco) and passaged, when 70% confluence was reached, with 0,025% Trypsin – EDTA 1X, neutralized with Trypsin Neutralizer Solution (Gibco). For one-week maintenance, 62.500 cells were seeded in a T25 flask [117].

Human dermal fibroblasts form adult donors (HDFa) (Gibco) culture and passaging were performed as for HDFn. For one-week maintenance, 125.000 cells were seeded in a T25 flask [118]. The cells purchased and used in this work where obtained from a 22 years old

female donors. The cell growth rate of primary fibroblasts changed due to cell passage and treatment. Furthermore, the older the donor, the sooner cells seemed to reach senescence and stop their growth at much younger passages (i.e., passage 5 for HDFa and passage 8 for HDFn).

HaCaT were maintained in Dulbecco's modified Eagle's medium (DMEM) GlutaMAX (Gibco) with 10% foetal bovine serum (Gibco), 1% penicillin/streptomycin (10000 U/mL, Gibco) and 1% L-glutamine (200mM, Gibco) at 37℃ with 5% CO_2. Cells were serially passaged at 70-90% confluence.

All cells were regularly tested for mycoplasma.

7.5. Extraction of fibroblasts from skin biopsies

Adult human dermal fibroblasts (AF) were extracted from 3mm skin punch biopsies from adult donors and cultured in DMEM GlutaMAX + 1% Penicillin/Streptomycin (Gibco) + 10% FBS (Gibco). Briefly, epidermis was cut and separated, dermis was then cut in 12 pieces and put in gelatine-coated 6 well plate. After 3-4 days, fibroblasts started to migrate and replicate (**Figure 47**). Once confluent, the cells were trypsinized with 0,05% Trypsin – EDTA (Gibco) and passaged in T175 flasks. When 80 % confluency was reached cells were passaged or frozen. Cells were regularly tested for mycoplasma.

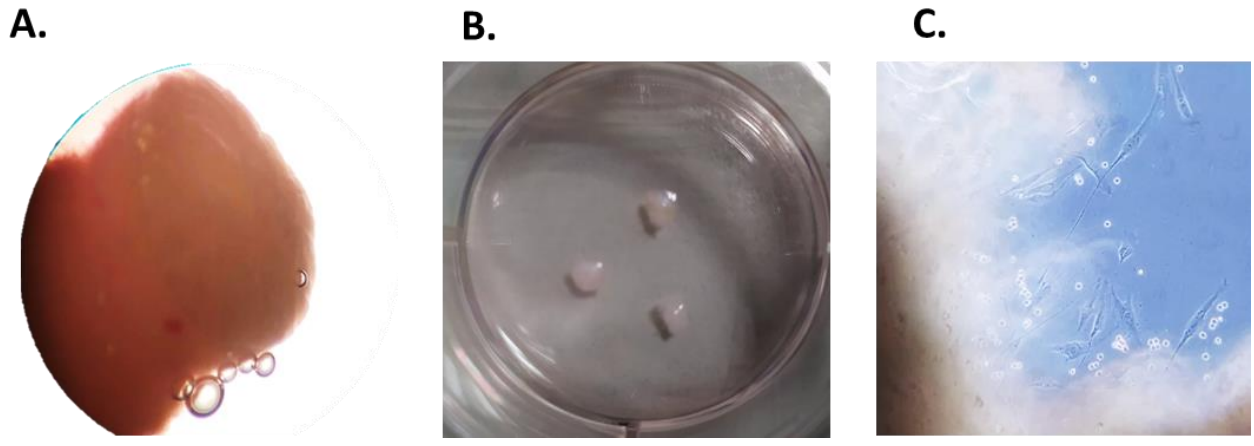

Figure 47 Fibroblasts extraction from a skin punch biopsy. A. Skin punch biopsy seen through a stereoscopic microscope. Epidermis and dermis are visible. **B**. Biopsy pieces in a 6well plate **C**. Fibroblasts emerging from a skin biopsy.

7.6. Fibroblasts infection

For conversion protocols, IMR90 were seeded at 15.000 cells/ cm^2, HDFn were seeded at 12.500 cells/cm^2, while human dermal fibroblasts from adult donors (HDFa and AF) were seeded at 25.000 cells/ cm^2. 24h post seeding, IMR90 were infected with lentiviral vectors Brn3a (MOI 20), Ngn1 (MOI 20) and rtTA (MOI 40), HDFn or HDFa were infected with lentiviral vectors Brn3a (MOI 10), Ngn1 (MOI 10) and rtTA (MOI 20) while AF were infected with 3410 (MOI 10) and BN1 (MOI 10). MOI (Multiplicity of infection) is the quantity of lentiviral vector per cell. Depending on the LTV titer and the MOI established, the volume of LTV to be added is calculated using the equation below:

$$\mu L\ virus/well = \frac{(\frac{cells}{well})\ x\ MOI}{TU/\mu L}$$

Equation 2 The volume of virus to be added per well was calculated by multiplying the number of cells seeded per well for the MOI desired. This value is then divided by the lentiviral particle titre expressed in transfection unit per mL (TU/mL).

Lentiviral vectors were added to the cells in basal media with or without polybrene (Hexadimethrine bromide, Sigma) 8 µg/mL and were incubated with the cells for 16-72 hours depending on the conversion protocol in a humidified incubator at 37°C and 5% CO_2. Polybrene was not used in AF infection.

7.7. MTT test

HDFa were seeded in 96 wells plate at 25.000 cells/ cm^2. 24h afterwards, cells were treated with polybrene 8 µg/mL or 4 µg/mL for 6h, 24h and 48h. Negative control cells were treated with 10% DMSO for 24h. Three wells per condition were left without cells, to have a blank control. After the treatment, diphenyltetrazolium bromide (MTT) (Sigma) was added to the cells to reach a final concentration of 0,25 mg/mL. Cells were incubated 2.5 h at 37°C and 5% CO_2 and then treated with 100% DMSO for 10 minutes. The plate was analysed with POLARstar (Omega) Plate Reader at 570 nm and data were then normalized to untreated cells.

7.8. Foetal lung fibroblasts (IMR90) conversion protocols

IMR90 were seeded onto glass coverslips or plastic multiwell plates treated with poly-l-lysine (Sigma) 8.3 µg/mL and laminin (Cultrex) 20 µg/mL. The conversion protocol 1 was modified from Li et al. [90], adding PD0325901 and substituting Purmorphamine and TGFβ3, that are used to obtain dopaminergic neurons, with DAPT y SU5402, to generate sensory neurons (**Figure 48**). PD0325901 is a selective, blocks cell cycle in G1 due to its effect on MEK/ERK, increasing the number of cells that enter G0 [119][88]. Cells were infected withLTVs Brn3a and Ngn1 MOI 20 and rtTA MOI 40.

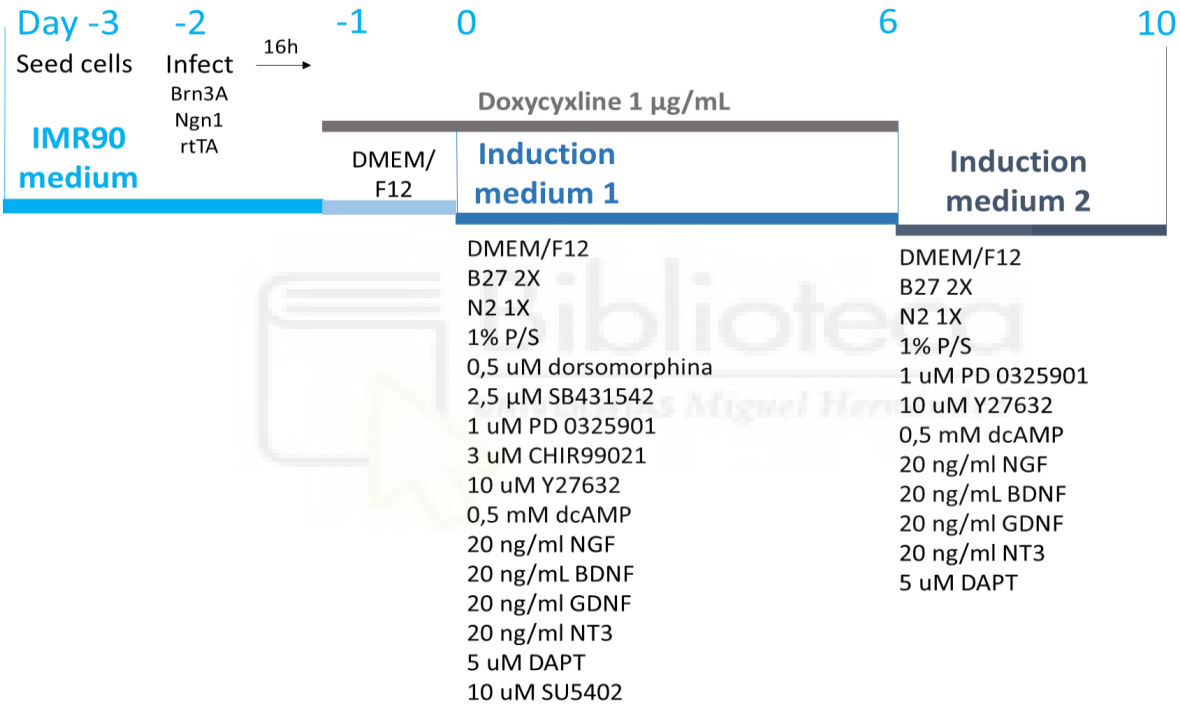

Figure 48 Experimental design of the conversion protocol 1, modified from Li et al.

24h after the infection, lentiviral vectors were withdrawn and the cells were incubated for 24h at 37°C with DMEM/F12 media without serum, to block the cell cycle. The following day, cells were treated with induction medium prepared as follows: DMEM/F12, B27 1X, N2 1X, NEAA 1X, P/S 1 % (all from Gibco), LDN193189 0,5 µM (Stemgent), SB431542 2,5 µM (Sigma), PD0325901 1 µM (Sigma), CHIR99021 3 µM (Tocris), Y27632 10 µM (Sigma), dcAMP 0,5 mM (Sigma), NGF 20 ng/ml (Peprotech), GDNF 20 ng/ml (Peprotech), BDNF 20 ng/ml (Peprotech), NT3 20 ng/ml (Peprotech), Doxycycline 1 µg/ml (Sigma), DAPT 5 µM

(Tocris) and SU5402 10 µM (Sigma). At day 6, media composition was changed withdrawing LDN193189, SB431542, CHIR99021, Doxycycline and SU5402. Control cells were recorded in calcium imaging 3 days after seeding and were cultured with basal maintenance medium. The medium was changed every 2 days.

Conversion protocol 2 was modified from Qin et al [91] (**Figure 49**), modifications with respect to the published article were applied to enrich the neuronal population in sensory neurons. As a difference to protocol 1, in protocol 2 the cell cycle was not actively blocked with serum withdrawal or with PD 0325901. Furthermore, different small molecules are used such as bFGF (Gibco), Forskolin (Sigma), SHH (PeproTech) and Valproic acid (Sigma). Doxycycline was left in culture for 7 days and media was changed every other day.

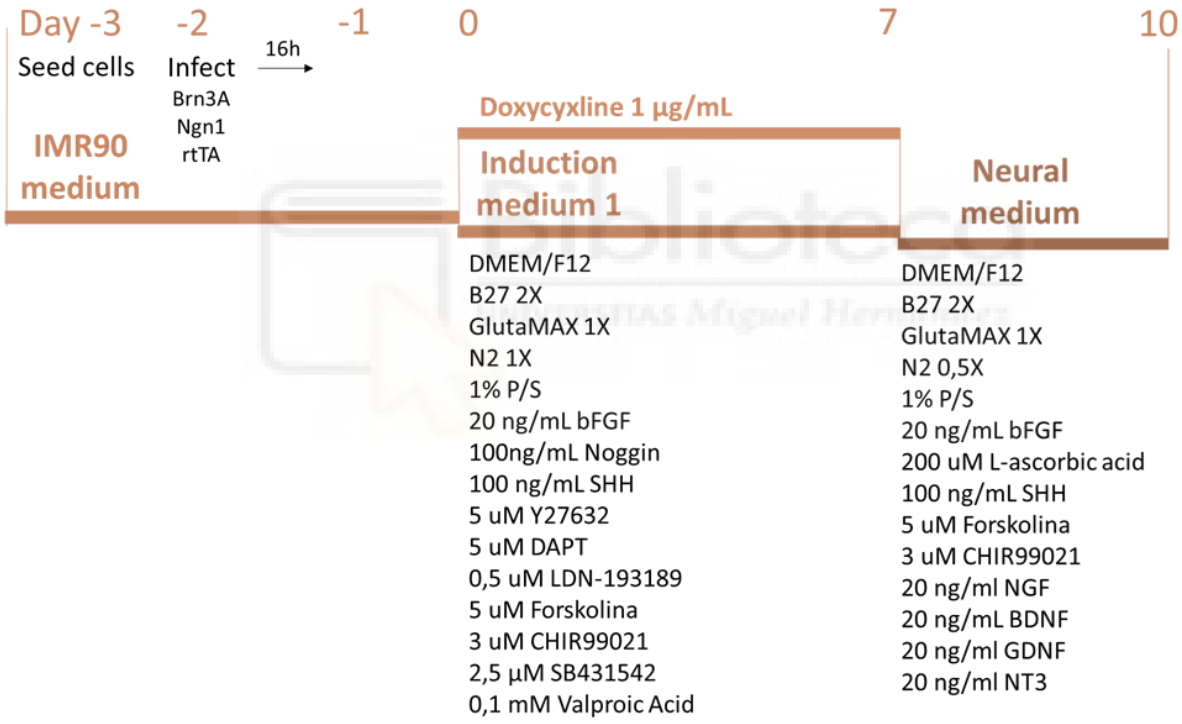

Figure 49 Experimental design of the conversion protocol 2, modified from Qin et al.

7.9. Human dermal fibroblasts from neonatal donors conversion protocols

HDFn (Gibco) were seeded onto glass coverslips or plastic multiwell plates treated with poly-l-lysine (Sigma) 8.3 µg/mL and laminin (Cultrex) 20 µg/mL. Blanchard and Eade conversion protocol was applied to HDFn (**Figure 50**) by infecting them LTVs Brn3a, Ngn1 (MOI 10) and rtTA (MOI 20) and then treating them with a simple induction medium with N2 supplement (comprised of progesterone, insulin, transferrin, putrescine and sodium selenite) (Gibco), FGF (Gibco) and neurotrophic factors (PeproTech).

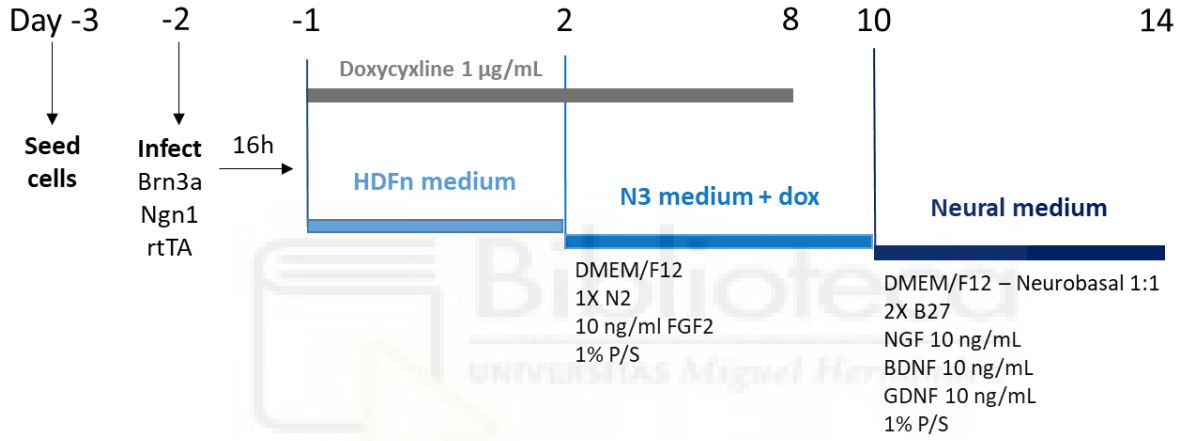

Figure 50 Experimental design of the Blanchard, Eade et al. conversion protocol.

Afterwards, the cAMP conversion protocol, that was modified from Ladewig and colleagues [77], was performed (**Figure 51**). In this protocol, induction medium containing small molecules was added to the cells. At day 14 of conversion, doxycycline and small molecules where withdrawn and neural medium with dcAMP and neurotrophic factors was added. Cells were maintained with neural medium for 7 days [66].

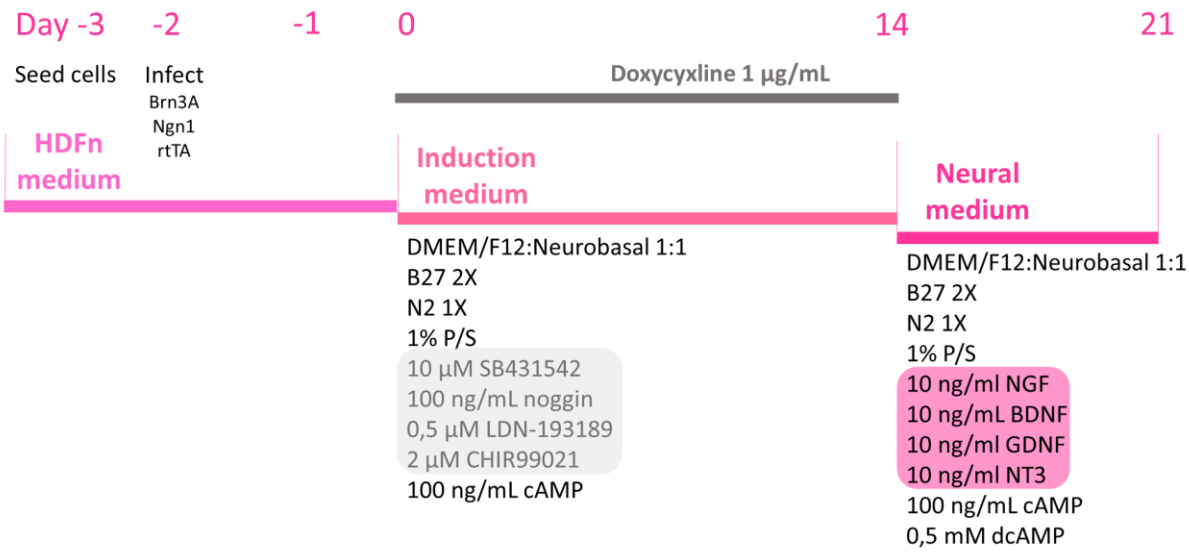

Figure 51 Experimental design of the cAMP conversion protocol, modified from Ladewig et al [77].

The conversion protocol detailed previously was modified adding the small molecule DAPT 5 µM (Tocris) (**Figure 52**), which inhibits the γ-secretase in the Notch-Delta pathway. In both cAMP and DAPT conversion protocol, media were changed every other day.

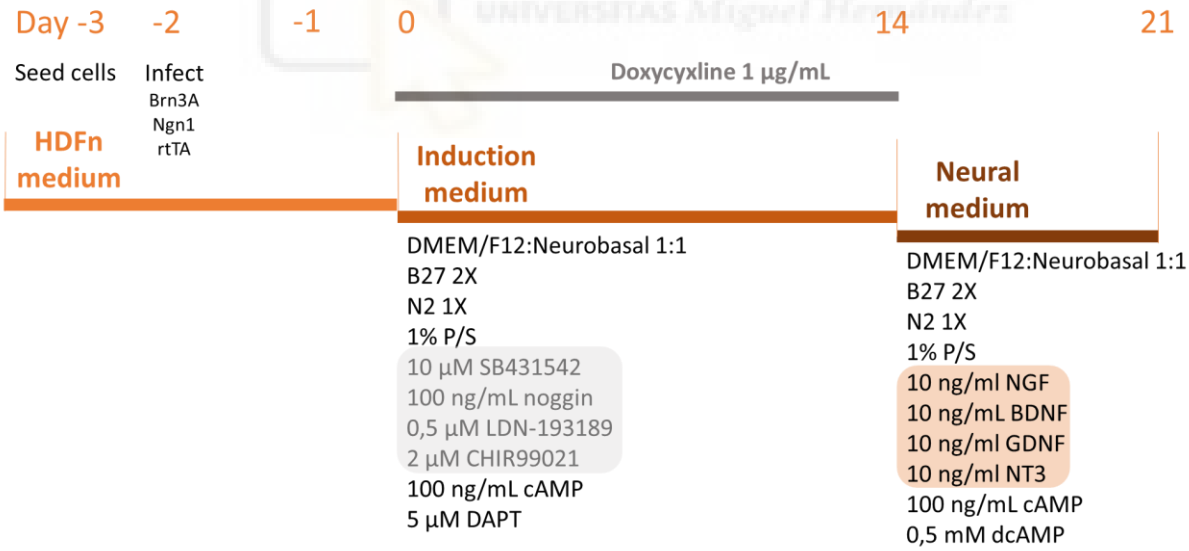

Figure 52 Experimental design of the DAPT conversion protocol.

7.10. Human dermal fibroblasts from adult donors conversion protocols

HDFa (Gibco) were seeded onto glass coverslips or plastic multiwell plates treated with poly-l-lysine (Sigma) 8.3 µg/mL and laminin (Cultrex) 20 µg/mL. HDFa were treated with Blanchard, Eade and collaborators conversion protocol (**Figure 50**) and DAPT protocol (**Figure 52**), as described for HDFn. DAPT conversion protocol was further modified to block cell cycle (**Figure 53**). The cell cycle arrest was achieved by withdrawing the serum from cell culture through a 24 h incubation with DMEM/F12. Furthermore, the small molecule PD0325901 (Tocris) 1 µM was added to the induction medium.

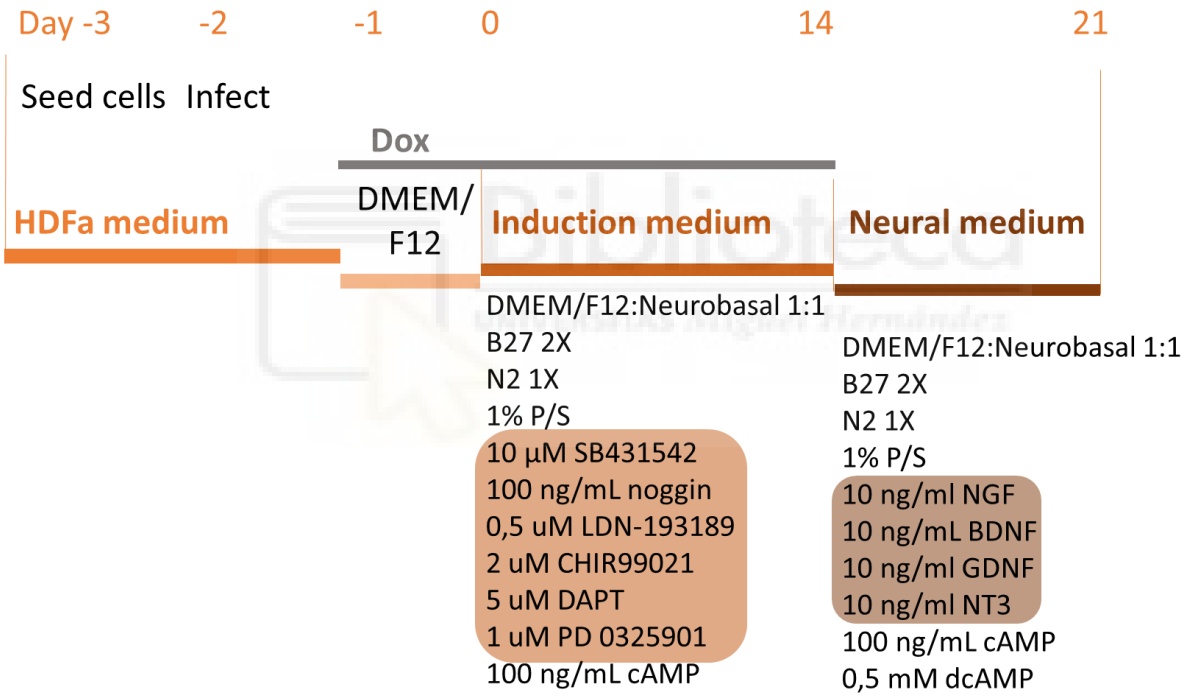

Figure 53 Experimental design of the cycle arrest conversion protocol.

For Drouin-Ouellet and Lau protocol and its modifications (**Table 2**) nunc 24 wells plate or 6 well plate with Thermanox plastic coverslips (ThermoFisher) were treated with poly-ornithine 15 µg/mL (Sigma) overnight at 37°C, laminin 111 (BioLamina) 5 µg/mL 3 hours at 37°C and fibronectin (ThermoFisher) 5 µg/mL overnight at 37°C. Adult fibroblasts extracted from skin biopsies (AF) were seeded and 24h after seeding the cells were infected with LTVs

Ngn1, Brn3a, rtTA, BN1 and/or 3410. MOIs are detailed in **Table 2**. For protocol 2.3, which was the most successful in generating putative sensory neurons (**Figure 54**), early and late conversion media described by Drouin-Ouellet et al. were modified with the addition of NGF (PeproTech) and DAPT (Sigma). Media were changed every other day. Cells were maintained in culture up to day 50 of conversion.

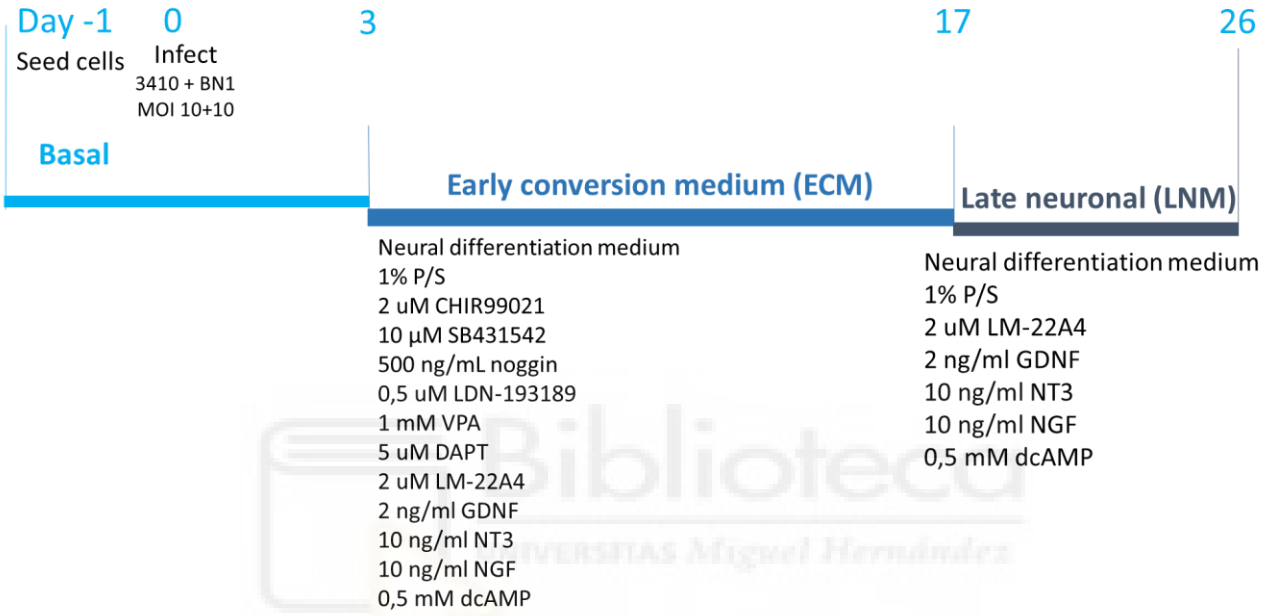

Figure 54 Experimental design of the AF conversion protocol.

7.11. RT-qPCR

At the end point of the conversion protocol, cells were collected with 0,025% Trypsin – EDTA 1X and centrifuged at 13.000 RPM for 5 minutes at 4°C. Supernatant was discarded and the cell pellet was stored at -80°C or RNA was immediately extracted with RNeasy Mini Kit (Qiagen). mRNA was then retrotranscribed with First strand cDNA Synthesis Kit (ThermoFisher) to cDNA. Quantitative PCR was performed using PowerUp SYBR Green Master Mix (Applied Biosystems) and primers for neuronal markers, sensory neuron markers or TRP channels (**Table 5**).

Table 5 Primers used for RT-qPCR, gene function and sequence.

Gene	Marker	Primer forward	Primer reverse
Map2	mature sensory neuron	GGGCCTTTTCTTTGAAATCTAGTTT	CAAATGTGGCTCTCTGAAGAACA
Brn3a	neural progenitor	CGTACCACACGATGAACAGC	CGTACCACACGATGAACAGC
Cgrp	peptidergic sensory neurons	AGACATCCAGCAAGCAACA	CCAGCCAAGAAAATAATAC
Isl1	neural progenitor	TGGACATTACTCCCTCTTACAG	CCCGTACAACCTGATATAATCTC
Fsp1	fibroblasts	GTGTCCACCTTCCACAAAT	ACTTCATTGTCCTCGTTGCT
Runx1	C-non peptidergic sensory neurons	CACGCACGAATTTTCAG	GTGGTCCTATTTAAGCCAGC
TrkA	C-peptidergic sensory neurons	CAGGACTTCCAGCGTGAGG	GCAGCTTGGCATCAGGTC
B Actin	endogenous control	CTGGAACGGTGAAGGTGACA	AAGGGACTTCCTGTAACAATGCA

$\Delta\Delta Ct$ SYBR Green PCR was performed using QuantStudio 3 thermocycler (Applied Biosystems), with the following protocol: 50°C 2', 95°C 2', 95°C 15s, 60°C 1' for 40 cycles. Data were normalized to β-Actin and represented as relative expression $2^{(-\Delta Ct)}$ using the following equation:

$$2^{(-\text{ mean Ct } \beta\text{actin} - \text{mean Ct gene of interest})}$$

Equation 3 RT-qPCR analysis equation

As a positive control, human brain tissue was utilized due to the suboptimal quality of preliminary experiments conducted using commercial human DRGs. While it is acknowledged that human brain tissue may not serve as the ideal reference tissue for the specific conversion protocols employed in this study, it nevertheless provides insights into the expression patterns characteristic of neuronal tissue.

7.12. Immunocytochemistry

At the endpoint of conversion protocols, cells were washed with D-PBS (Sigma) and fixed with PFA (Sigma) 4% for 20 minutes at RT. Cells were then permeabilized with Triton 100-X (Sigma) 0,1% v/v for 5 minutes at RT while shaking. Blocking with normal goat serum (NGS) (Sigma) 5% in D-PBS was performed incubating the cells 1h at RT shaking. Finally, the primary antibody was added at the appropriate concentration (**Table 6**) and incubated overnight at 4°C shaking.

Table 6 Primary antibodies used in this work with details about company, reference and concentration.

Antibody	Supplier	Reference	Concentration
Ms Brn3a	Millipore	MAB1585	1:200
Rb Ngn1	Abcam	66498	1:500
Rb β3 Tubulin (TUJ1)	Covance	MMS-435P	1:1000
Rb TRPA1	Alomone	ACC-037	1:200
Rb TRPM8	Alomone	ACC-049	1:200
Rb TRPV1	Alomone	ACC-030	1:200
Rb MAP2	Proteintech	17480-1-AP	1:250
Ms CGRP	Abcam	AB81887	1:250
Ms Tau	ThermoFisher	MN1000	1:500
Rb Nav 1.8	Alomone	ASC-016	1:500

The following day, the primary antibody was washed with D-PBS and the secondary antibody was added for 1 hour at RT while shaking, protected from light. Afterwards DAPI

(Sigma) 1,5:10000 was added and incubated 5 minutes at RT while shaking, protected from light. If cells were seeded onto coverslips, 4 µL Mowiol (Calbiochem) were added onto a glass slide and the coverslips were mounted on it to fix the fluorescence. The coverslips were then sealed with varnish and stored at 4°C. Fluorescence images were taken with confocal microscope LSM900 with Airyscan 2 (Zeiss) or with IN Cell Analyzer 6000 (GE Healthcare). Quantification was performed by Fiji ImageJ.

7.13. Cell proliferation assay

Click-iT Edu Cell Proliferation Kit for Imaging (Invitrogen, C10337) was performed. In this assay the modified thymidine analogue Edu (5-ethynyl-2'-deoxyuridine) is incorporated into DNA during active DNA synthesis and fluorescently labelled with Alexa Fluor 488. Edu 10 µM was incubated for 16h, afterwards the cells were fixed with 4% PFA for 20 minutes at RT and then permeabilized with 0,5% Triton X-100 for 20 minutes. The reaction cocktail was then added to the cells (Click-iT reaction buffer, CuSO4, Alexa Fluor azide and Reaction buffer additive) and left incubating for 30 minutes at RT protected by the light. Last, nuclei were stained with Hoechst 33342 (1:2000) for 30 minutes and cells were then imaged using INCell Analyzer 6000 cell imaging system (GE Healthcare, Little Chalfont, UK). The number of nuclei and the number of cells positive to Edu were then quantified with ImageJ.

7.14. Calcium imaging

On the day of the experiments, cells were loaded with Fluo-4 AM 5µM (Molecular Probes, Invitrogen) and pluronic acid 0.02% p/v (Molecular Probes, Invitrogen) in 1 mL of Hank's Balanced Salt Solution (HBSS), consisting of NaCl 140 mM, HEPES 10 mM, KCl 4 mM, $CaCl_2$ 1.8 mM, $MgCl_2$ 1 mM (Sigma), D-glucose 5 mM (VWR|BDH Prolabo Chemicals), pH 7,4. After 1-hour incubation at 37°C and 20 minutes wash with HBSS, coverslips were mounted onto a RC-25 chamber (Harvard Apparatus) and were continuously perfused with HBSS at RT. Regions of interest (ROIs) of individual cells were drawn and used to monitor the fluorescence variation through a 10x air objective (Axiovert 200 inverted microscope, Carl Zeiss) with an ORCA Flash LT camera (Hamamatsu Photonics). Images were processed with HC Image package software (Hamamatsu Photonics). Fluo-4-AM was excited at 500 nm with an exposure time of 300 ms and emitted fluorescence was filtered at

535 nm (Lambda-10-2-filter wheel, Sutter Instruments). Data were acquired each 3 seconds. HBSS and stimuli were applied by a perfusion system; the stimuli used were capsaicin 1 µM, menthol 100 µM, AITC 100 µM, KCl 40 mM and Ionomycin 10 µM. Analysis was performed on Excel to quantify the percentage of responses normalized to Ionomycin or KCl, the size of the responses normalized to Ionomycin and the area of cells. The percentage of responses was quantified by applying **Equation 4** and **Equation 5**, if the value obtained was bigger than 0, it indicated that a response to stimulus had occurred. The number of responses was then normalized to Ionomycin or KCl responses, to obtain the percentage of response.

$$\Delta F = [MAX(\Delta F\ stimulus\ application + 90\ s) - MEAN(\Delta F\ before\ stimulus\ application)$$

Equation 4 The variation of fluorescence (ΔF) between the highest fluorescence intensity (MAX) and the fluorescence intensity variation of the baseline (MEAN).

$$\Delta F - noise = \Delta F - [DESVEST(\Delta F\ before\ stimulus\ application)\ x\ 10]$$

Equation 5 Ten times the standard deviation (DESVEST) of the basal line was subtracted to ΔF to validate the response.

The size of the responses was quantified applying **Equation 6**, where the response of the stimulus was normalized to the size of Ionomycin response.

$$Stimulus\ response\ size = \frac{\Delta F\ stimulus}{\Delta F\ Ionomycin}$$

Equation 6 ΔF of each stimulus was divided by ΔF of Ionomycin to calculate the response size relative to the biggest calcium increase in the same cell.

7.15. CMOS Microelectrode Array (MEA) measurements

IMR90 were seeded onto poly-d-lysine 100 µg/mL (Sigma) and laminin 20 µg/mL (Cultrex) treated MEA CMOS 16/32 chips (Multichannel Systems GmbH). Extracellular recordings on converted IMR90 were performed using CMOS MEA 5000 and CMOS MEA Control Software (Multichannel Systems GmbH). Stimuli were applied with a perfusion system (2 mL/min); the stimuli used were capsaicin 1 µM, menthol 100 µM, AITC 100 µM and KCl 40

mM. Between each stimulus cells were washed with HBSS for 4.5 minutes. Data were filtered through a 200 Hz highpass butterworth filter. Spike explorer settings were set on absolute, to detect both positive and negative extracellular voltage variations. Data from active sensors were obtained and the frequency was calculated dividing the number of events by the seconds of recording.

7.16. Chronic DRGs culture in microfluidic chambers

DRGs were extracted from adult mice with 15-20 week-of age (strain: CD57BL/6J). Animals were group housed in a 12-12 light-dark cycle, where the lights were turned on at 8 hours and turned off at 20 hours. Food and water were available ad libitum. Experimental procedures were performed on male and female mice. All procedures were approved by the Institutional Animal and Ethical Committee of the Miguel Hernández University of Elche, following the guidelines of the Economic European Community, the National Institutes of Health, and the Committee for Research and Ethical Issues of the International Association for the Study of Pain. DRGs cells were seeded in microfluidic chambers using Millipore devices AXIS™ Axon Investigation System – Tissue Culture Ready in the design AX150, a PDMS device with 4 microwells of 8 mm diameter each, 2 microchannels of 1,5 mm length that are interconnected by approximately 120 microgrooves each 150 µm long [120]. Clean and sterile microfluidic devices were mounted onto clean and sterile 24x60 mm coverslips treated with poly-L-lysine (0,5 mg/mL, Sigma). Microfluidic devices were filled with laminin (20 µg/ml, Sigma) until the seeding of DRGs cells, when 5µL of cell suspension ~4 x106 cells/mL were loaded into the somal compartment. 30-45 minutes after seeding, complete medium containing murine NGF (mNGF 25s 100 ng/mL, Promega) and human GDNF (hGDNF 100ng/mL, PeproTech) was added to the four wells (**Table 7**). 200µL of medium were added to each well of the somal compartment and 100µL to each well of the axonal compartment, to facilitate axonal growth. Medium was changed at day 1, 3 and 5, decreasing mNGF and hGDNF concentration in the somal compartment (**Table 7**) and adding the anti-mitotics uridine and 5-fluoro-2'-deoxyuridine (Sigma) to prevent glial proliferation.

Table 7 Medium composition during the days in vitro (DIV). NGF and GDNF concentration in somal compartment decrease from 100ng/mL at DIV 1 to 25 ng/mL at DIV 3 to establish a neurotrophic gradient to help axonal growth.

Day	SOMAL COMPARTMENT		AXONAL COMPARTMENT	
0	Neurobasal A (Gibco)		Neurobasal A (Gibco)	
	GlutaMAX (Gibco)	1%	GlutaMAX (Gibco)	1%
	B27 Supplement (Gibco)	2%	B27 Supplement (Gibco)	2%
	Penicillin-Streptomycin (10000 U/mL, Gibco)	1%	Penicillin-Streptomycin (10000 U/mL, Gibco)	1%
	mNGF 25 s (Promega)	100 ng/mL	mNGF 25 s (Promega)	100 ng/mL
	hGDNF (PeproTech)	100 ng/mL	hGDNF (PeproTech)	100 ng/mL
1	Neurobasal A (Gibco)		Neurobasal A (Gibco)	
	GlutaMAX (Gibco)	1%	GlutaMAX (Gibco)	1%
	B27 Supplement (Gibco)	2%	B27 Supplement (Gibco)	2%
	Penicillin-Streptomycin (10000 U/mL, Gibco)	1%	Penicillin-Streptomycin (10000 U/mL, Gibco)	1%
	mNGF 25 s (Promega)	50 ng/mL	mNGF 25 s (Promega)	100 ng/mL
	hGDNF (PeproTech)	50 ng/mL	hGDNF (PeproTech)	100 ng/mL
	Uridine (Sigma)	17,5 µg/mL	Uridine (Sigma)	17,5 µg/mL
	5-fluoro-2'-deoxyuridine (Sigma)	7,5 µg/mL	5-fluoro-2'-deoxyuridine (Sigma)	7,5 µg/mL
3, 5	Neurobasal A (Gibco)		Neurobasal A (Gibco)	
	GlutaMAX (Gibco)	1%	GlutaMAX (Gibco)	1%
	B27 Supplement (Gibco)	2%	B27 Supplement (Gibco)	2%
	Penicillin-Streptomycin (10000 U/mL, Gibco)	1%	Penicillin-Streptomycin (10000 U/mL, Gibco)	1%
	mNGF 25 s (Promega)	25 ng/mL	mNGF 25 s (Promega)	100 ng/mL
	hGDNF (PeproTech)	25 ng/mL	hGDNF (PeproTech)	100 ng/mL
	Uridine (Sigma)	17,5 µg/mL	Uridine (Sigma)	17,5 µg/mL
	5-fluoro-2'-deoxyuridine (Sigma)	7,5 µg/mL	5-fluoro-2'-deoxyuridine (Sigma)	7,5 µg/mL

7.17. Calcium imaging in microfluidic chambers

Calcium imaging in microfluidic chambers was performed as described in paragraph 7.14. The perfusion system velocity was changed to have much slower influx (0.2-0.4 mL/min) and waste in order to limit shear forces. In order to identify the cells whose axons crossed to the axonal compartment, at day 5 the axonal compartment was loaded with the fluorescent tracer 1,1'-Dioctadecyl-3,3,3',3'-Tetramethylindodicarbocyanine (DiD' 1:200, Invitrogen) and incubated overnight. At day 6, the somal compartment was loaded with Fluo-4. Regions of interest were drawn onto the DiD' picture and Fluo-4 fluorescence values where then measured over time. Stimuli (capsaicin 100 nM, menthol 100 µM, AITC 100 µM, KCl 40 mM) were added to the axonal compartment and calcium concentration was measured in the soma. Data were analysed as described in the paragraph 7.14.

7.18. Mouse DRGs and keratinocytes co-culture

To co-culture HaCaT with DRGs, at DIV1 of DRGs culture, the keratinocytes were trypsinized and counted with a Neubauer chamber. After drying up the lower microchannel with a vacuum pump, HaCaT were seeded at 40.000 cell/mL to obtain a 90-100% confluence at DIV 6, when calcium imaging assays were performed. 30 minutes after seeding, medium was added to the axonal wells. The medium for keratinocytes-axons co-culture was HaCaT maintaining medium supplemented with mNGF 25s (100ng/mL, Promega) and hGDNF (100 ng/mL, PeproTech), to create a neurotrophic gradient between compartments to allow axonal outgrowth. The medium was changed every two days.

7.19. FESEM in microfluidic chambers

At DIV 6 of co-culture of mDRGs and keratinocytes, the cells were fixed with 2.5% glutaraldehyde (EMS) for 45 minutes maintaining fluidic isolation between soma and keratinocytes. Afterwards, cells were washed with dH_2O and dehydrated with serial washes of ethanol [121]. Liquid was removed, microfluidic chambers were carefully detached and dried at RT for at least 24h. The slides were coated with a chromium layer under vacuum and the cells were analysed by the SIGMA 300 VP (Zeiss) field emission scanning electron microscope (FESEM).

7.20. Statistical Analyses

Statistical analyses were carried out with GraphPad Prism v 8.0.1. Normal distribution was tested with Shapiro-Wilk or D'Agostino & Pearson omnibus normality tests. Afterwards, when data presented a normal distribution, parametric t-test was performed for one-to-one comparison or one-way or two-way ANOVA with Tukey's post-hoc test was applied for multiple comparison. In case datasets did not present normal distribution, Mann Whitney U or Kruskal Wallis with Dunn's post-hoc test was applied for one-to-one comparison or multiple comparison respectively. Figures present asterisks: $p > 0.05$ is represented as *; $P \leq 0.05$ is represented as **; $P \leq 0.01$ is represented as ***; $P \leq 0.001$ is represented as ****. Exact P-values are presented in figures' legends.

REFERENCES

[1] Eric R. Kandel; James H. Schwartz; Thomas M. Jessell; Steven A. Siegelbaum; A.J.Hudspeth, *Principles of Neural Science - Fifth edition*. McGRAW-HILL, 2013.

[2] A. Marzvanyan and A. F. Alhawaj, “Physiology, Sensory Receptors,” *StatPearls*, Aug. 2021, Accessed: Feb. 15, 2022. [Online]. Available: https://www.ncbi.nlm.nih.gov/books/NBK539861/

[3] D. Purves *et al.*, *Neuroscience*, Third edit. Sinauer Associates, Inc, Sunderland, MA, USA, 2004. doi: 10.1016/B978-0-12-801238-3.62132-3.

[4] P. Rand Swenson, DC, MD, “Review of clinical and functional neuroscience.” [Online]. Available: https://www.dartmouth.edu/~rswenson/NeuroSci/chapter_3.html

[5] A. I. Basbaum, D. M. Bautista, G. Scherrer, and D. Julius, “Cellular and Molecular Mechanisms of Pain,” *Cell*, vol. 139, no. 2, pp. 267–284, 2009, doi: 10.1016/j.cell.2009.09.028.

[6] M. Devor, “Unexplained peculiarities of the dorsal root ganglion,” *Pain*, vol. Suppl 6, no. SUPPL.1, 1999, doi: 10.1016/S0304-3959(99)00135-9.

[7] L. Kruger, A. R. Light, and F. E. Schweizer, “Axonal terminals of sensory neurons and their morphological diversity,” *J Neurocytol*, vol. 32, no. 3, pp. 205–16, 2003.

[8] C. Belmonte and F. Viana, “Transduction and Encoding of Noxious Stimuli,” *Encyclopedia of Pain*, pp. 2515–2528, Nov. 2007, doi: 10.1007/978-3-540-29805-2_4561.

[9] D. M. Lopes, F. Denk, and S. B. McMahon, “The molecular fingerprint of dorsal root and trigeminal ganglion neurons,” *Front Mol Neurosci*, vol. 10, no. September, pp. 1–11, 2017, doi: 10.3389/fnmol.2017.00304.

[10] D. Usoskin *et al.*, “Unbiased classification of sensory neuron types by large-scale single-cell RNA sequencing,” *Nat Neurosci*, vol. 18, no. 1, pp. 145–153, 2015, doi: 10.1038/nn.3881.

[11] C. J. Woolf, A. C. of Physicians, and A. P. Society, “Pain: moving from symptom control toward mechanism-specific pharmacologic management,” *Ann Intern Med*, vol. 140, no. 6, pp. 441–51, 2004.

[12] L. Li *et al.*, “The functional organization of cutaneous low-threshold mechanosensory neurons,” *Cell*, vol. 147, no. 7, pp. 1615–1627, 2011, doi: 10.1016/j.cell.2011.11.027.

[13] C. Rostock, K. Schrenk-Siemens, J. Pohle, and J. Siemens, “Human vs. Mouse Nociceptors - Similarities and Differences,” *Neuroscience*, vol. 387, pp. 13–27, Sep. 2018, doi: 10.1016/J.NEUROSCIENCE.2017.11.047.

[14] F. Lallemend and P. Ernfors, “Molecular interactions underlying the specification of sensory neurons,” *Trends Neurosci*, vol. 35, no. 6, pp. 373–381, 2012, doi: 10.1016/j.tins.2012.03.006.

[15] C. L. Li *et al.*, “Somatosensory neuron types identified by high-coverage single-cell RNA-sequencing and functional heterogeneity,” *Cell Res*, vol. 26, no. 1, pp. 83–102, 2016, doi: 10.1038/cr.2015.149.

[16] Q. Ma, “A functional subdivision within the somatosensory system and its implications for pain research,” *Neuron*, vol. 110, pp. 1–21, 2022, doi: 10.1016/j.neuron.2021.12.015.

[17] N. Sharma, K. Flaherty, K. Lezgiyeva, D. E. Wagner, A. M. Klein, and D. D. Ginty, “The emergence of transcriptional identity in somatosensory neurons,” *Nature*, vol. 577, no. 7790, pp. 392–398, 2020, doi: 10.1038/s41586-019-1900-1.

[18] J. Kupari *et al.*, “Single cell transcriptomics of primate sensory neurons identifies cell types associated with chronic pain,” *Nat Commun*, vol. 12, no. 1, Dec. 2021, doi: 10.1038/s41467-021-21725-z.

[19] J. Kupari and P. Ernfors, “Molecular taxonomy of nociceptors and pruriceptors,” *Pain*, vol. 164, no. 6, pp. 1245–1257, Jun. 2023, doi: 10.1097/j.pain.0000000000002831.

[20] D. Tavares-Ferreira *et al.*, “Spatial transcriptomics of dorsal root ganglia identifies molecular signatures of human nociceptors,” 2022. [Online]. Available: https://www.science.org

[21] R. V. Haberberger, C. Barry, N. Dominguez, and D. Matusica, “Human dorsal root ganglia,” *Front Cell Neurosci*, vol. 13, no. June, pp. 1–17, 2019, doi: 10.3389/fncel.2019.00271.

[22] I. Jardín *et al.*, “TRPs in pain sensation,” *Front Physiol*, vol. 8, no. JUN, pp. 1–10, 2017, doi: 10.3389/fphys.2017.00392.

[23] D. E. Clapham, “TRP channels as cellular sensors,” *Nature*, vol. 426, no. 6966, pp. 517–524, 2003, doi: 10.1038/nature02196.

[24] D. Julius, *TRP Channels and Pain*. 2013. doi: 10.1146/annurev-cellbio-101011-155833.

[25] R. Paricio-Montesinos *et al.*, “Sensory Coding of Warm Perception,” *Neuron*, vol. 106, pp. 830–841, 2020.

[26] S. Giorgi, M. Nikolaeva-Koleva, D. Alarcón-Alarcón, L. Butrón, and S. González-Rodríguez, “Is TRPA1 Burning Down TRPV1 as Druggable Target for the Treatment of Chronic Pain?,” *Int J Mol Sci*, vol. 20, no. 12, p. 2906, Jun. 2019, doi: 10.3390/ijms20122906.

[27] E. A. Lumpkin and M. J. Caterina, “Mechanisms of sensory transduction in the skin,” *Nature*, vol. 445, no. 7130, pp. 858–865, 2007, doi: 10.1038/nature05662.

[28] D. Cabañero, E. Villalba-Riquelme, G. Fernández-Ballester, A. Fernández-Carvajal, and A. Ferrer-Montiel, “ThermoTRP channels in pain sexual dimorphism: new insights for drug intervention,” *Pharmacology and Therapeutics*, vol. 240. Elsevier Inc., Dec. 01, 2022. doi: 10.1016/j.pharmthera.2022.108297.

[29] E. E. Benarroch, “Ion channels in nociceptors,” *Clinical Implications of Neuroscience Research*, vol. 84, no. 11, pp. 1153–1164, 2015, doi: 10.1212/WNL.0000000000001382.

[30] Y. Li *et al.*, “DRG Voltage-Gated Sodium Channel 1.7 Is Upregulated in Paclitaxel-Induced Neuropathy in Rats and in Humans with Neuropathic Pain,” *J Neurosci*, vol. 38, no. 5, pp. 1124–1136, Jan. 2018, doi: 10.1523/JNEUROSCI.0899-17.2017.

[31] K. Coward *et al.*, “Immunolocalization of SNS/PN3 and NaN/SNS2 sodium channels in human pain states,” *Pain*, vol. 85, no. 1–2, pp. 41–50, Mar. 2000, doi: 10.1016/S0304-3959(99)00251-1.

[32] J. F. Park and Z. D. Luo, “Calcium channel functions in pain processing,” *Channels*, vol. 4, no. 6, p. 510, 2010, doi: 10.4161/CHAN.4.6.12869.

[33] P. Ávalos Prado, A. A. Chassot, A. Landra-Willm, and G. Sandoz, “Regulation of two-pore-domain potassium TREK channels and their involvement in pain perception and migraine,” *Neurosci Lett*, vol. 773, p. 136494, Mar. 2022, doi: 10.1016/J.NEULET.2022.136494.

[34] S. N. Raja *et al.*, “The Revised IASP definition of pain: concepts, challenges, and compromises,” *Pain*, vol. 161, no. 9, pp. 1976–1982, 2020, doi: 10.1097/j.pain.0000000000001939.The.

[35] A. S. Yekkirala, D. P. Roberson, B. P. Bean, and C. J. Woolf, “Breaking barriers to novel analgesic drug development,” *Nat Rev Drug Discov*, vol. 16, no. 8, pp. 545–564, 2017, doi: 10.1038/nrd.2017.87.

[36] R. Yasaei, E. Peterson, and A. Saadabadi, “Chronic Pain Syndrome,” *StatPearls*, Aug. 2021, Accessed: Feb. 16, 2022. [Online]. Available: https://www.ncbi.nlm.nih.gov/books/NBK470523/

[37] S. P. Cohen, L. Vase, and W. M. Hooten, “Chronic pain: an update on burden, best practices, and new advances,” *The Lancet*, vol. 397, no. 10289, pp. 2082–2097, May 2021, doi: 10.1016/S0140-6736(21)00393-7.

[38] O. Van Hecke, N. Torrance, and B. H. Smith, “Chronic pain epidemiology and its clinical relevance,” *Br J Anaesth*, vol. 111, no. 1, pp. 13–18, 2013, doi: 10.1093/bja/aet123.

[39] C. J. Phillips, “The Cost and Burden of Chronic Pain,” *Rev Pain*, vol. 3, no. 1, pp. 2–5, 2009, doi: 10.1177/204946370900300102.

[40] M. Alsaloum and S. G. Waxman, “iPSCs and DRGs: stepping stones to new pain therapies,” *Trends Mol Med*, vol. 28, no. 2, pp. 110–122, Feb. 2022, doi: 10.1016/J.MOLMED.2021.11.005.

[41] “Understanding the Opioid Overdose Epidemic | CDC’s Response to the Opioid Overdose Epidemic | CDC.” Accessed: Feb. 28, 2022. [Online]. Available: https://www.cdc.gov/opioids/basics/epidemic.html

[42] C. J. Woolf, “What is this thing called pain?,” *J Clin Invest*, vol. 120, no. 1, pp. 3742–3744, 2010, doi: 10.1172/JCI45178.3742.

[43] E. S. J. Smith and G. R. Lewin, “Nociceptors: a phylogenetic view.,” *J Comp Physiol A Neuroethol Sens Neural Behav Physiol*, vol. 195, no. 12, pp. 1089–1106, 2009, doi: 10.1007/s00359-009-0482-z.

[44] J. Scholz and C. J. Woolf, “Can we conquer pain?,” *Nat Neurosci*, vol. 5, no. 11s, pp. 1062–1067, 2002, doi: 10.1038/nn942.

[45] J. D. Richardson and M. R. Vasko, “Cellular mechanisms of neurogenic inflammation,” *Journal of Pharmacology and Experimental Therapeutics*, vol. 302, no. 3, pp. 839–845, 2002, doi: 10.1124/jpet.102.032797.

[46] A. I. Nascimento, F. M. Mar, and M. M. Sousa, “The intriguing nature of dorsal root ganglion neurons: Linking structure with polarity and function,” *Prog Neurobiol*, vol. 168, pp. 86–103, Sep. 2018, doi: 10.1016/J.PNEUROBIO.2018.05.002.

[47] M. S. Prasad, R. M. Charney, and M. I. García-Castro, “Specification and formation of the neural crest: Perspectives on lineage segregation,” *Genesis*, vol. 57, no. 1, p. e23276, Jan. 2019, doi: 10.1002/DVG.23276.

[48] P. Pla and A. H. Monsoro-Burq, “The neural border: Induction, specification and maturation of the territory that generates neural crest cells,” *Dev Biol*, vol. 444 Suppl 1, pp. S36–S46, Dec. 2018, doi: 10.1016/J.YDBIO.2018.05.018.

[49] F. Marmigère and P. Carroll, “Neurotrophin signalling and transcription programmes interactions in the development of somatosensory neurons,” *Handb Exp Pharmacol*, vol. 220, pp. 329–353, 2014, doi: 10.1007/978-3-642-45106-5_13/FIGURES/2.

[50] P. Bernd, “The Role of Neurotrophins During Early Development,” *Gene Expr*, vol. 14, no. 4, p. 241, 2008, doi: 10.3727/105221608786883799.

[51] E. J. Huang and L. F. Reichardt, “Neurotrophins: Roles in Neuronal Development and Function *”, doi: 10.1146/annurev.neuro.24.1.677.

[52] J. Hjerling-Leffler, M. AlQatari, P. Ernfors, and M. Koltzenburg, “Emergence of Functional Sensory Subtypes as Defined by Transient Receptor Potential Channel Expression,” *Journal of Neuroscience*, vol. 27, no. 10, pp. 2435–2443, 2007, doi: 10.1523/JNEUROSCI.5614-06.2007.

[53] C. Abboud *et al.*, “Animal models of pain: Diversity and benefits,” *J Neurosci Methods*, vol. 348, no. May 2020, 2021, doi: 10.1016/j.jneumeth.2020.108997.

[54] J. S. Mogil, “Animal models of pain: Progress and challenges,” *Nat Rev Neurosci*, vol. 10, no. 4, pp. 283–294, 2009, doi: 10.1038/nrn2606.

[55] L. Chrysostomidou, A. H. Cooper, and G. A. Weir, “Cellular models of pain: New technologies and their potential to progress preclinical research,” *Neurobiology of Pain*, vol. 10, no. March, p. 100063, 2021, doi: 10.1016/j.ynpai.2021.100063.

[56] K. Nakao, “Translational science: Newly emerging science in biology and medicine — Lessons from translational research on the natriuretic peptide family and leptin —,” *Proceedings of the Japan Academy, Series B*, vol. 95, no. 9, pp. 538–567, Nov. 2019, doi: 10.2183/PJAB.95.037.

[57] M. H. Sieweke, “Waddington’s valleys and captain cook’s islands,” *Cell Stem Cell*, vol. 16, no. 1, pp. 7–8, 2015, doi: 10.1016/j.stem.2014.12.009.

[58] H. Wang, “Direct cell reprogramming: approaches, mechanisms and progress,” *Nat Rev Mol Cell Biol*, vol. 0123456789, doi: 10.1038/s41580-021-00335-z.

[59] A. J. Alshawaf *et al.*, “Phenotypic and Functional Characterization of Peripheral Sensory Neurons derived from Human Embryonic Stem Cells,” no. December 2017, pp. 1–12, 2018, doi: 10.1038/s41598-017-19093-0.

[60] S. M. Chambers *et al.*, “Combined small-molecule inhibition accelerates developmental timing and converts human pluripotent stem cells into nociceptors,” *Nat Biotechnol*, vol. 30, no. 7, pp. 715–720, 2012, doi: 10.1038/nbt.2249.

[61] A. R. Nickolls *et al.*, “Transcriptional Programming of Human Mechanosensory Neuron Subtypes from Pluripotent Stem Cells Resource Transcriptional Programming of Human Mechanosensory Neuron Subtypes from Pluripotent Stem Cells,” pp. 932–946, 2020, doi: 10.1016/j.celrep.2019.12.062.

[62] K. Takahashi and S. Yamanaka, “Induction of pluripotent stem cells from mouse embryonic and adult fibroblast cultures by defined factors,” *Cell*, vol. 126, no. 4, pp. 663–676, Aug. 2006, doi: 10.1016/J.CELL.2006.07.024.

[63] L. A. McDermott *et al.*, “Defining the Functional Role of Na V 1.7 in Human Nociception,” *Neuron*, vol. 101, no. 5, pp. 905-919.e8, 2019, doi: 10.1016/j.neuron.2019.01.047.

[64] J. E. Meents *et al.*, “The role of Nav1.7 in human nociceptors: Insights from human induced pluripotent stem cell-derived sensory neurons of erythromelalgia patients,” *Pain*, vol. 160, no. 6, pp. 1327–1341, 2019, doi: 10.1097/j.pain.0000000000001511.

[65] B. J. Wainger *et al.*, “Modeling pain in vitro using nociceptor neurons reprogrammed from fibroblasts,” *Nat Neurosci*, vol. 344, no. 6188, pp. 1173–1178, 2015, doi: 10.1126/science.1249098.Sleep.

[66] J. W. Blanchard *et al.*, “Selective conversion of fibroblasts into peripheral sensory neurons,” *Nat Neurosci*, vol. 18, no. 1, pp. 25–35, 2015, doi: 10.1038/nn.3887.Selective.

[67] J. Mertens *et al.*, “Directly Reprogrammed Human Neurons Retain Aging-Associated Transcriptomic Signatures and Reveal Age-Related Nucleocytoplasmic Defects,” *Cell Stem Cell*, vol. 17, no. 6, pp. 705–718, 2015, doi: 10.1016/j.stem.2015.09.001.

[68] J. Drouin-Ouellet *et al.*, “REST suppression mediates neural conversion of adult human fibroblasts via microRNA-dependent and -independent pathways,” *EMBO Mol Med*, vol. 9, no. 8, pp. 1117–1131, 2017, doi: 10.15252/emmm.201607471.

[69] C. Tsantoulas, C. Farmer, P. Machado, K. Baba, S. B. McMahon, and R. Raouf, “Probing functional properties of nociceptive axons using a microfluidic culture system,” *PLoS One*, vol. 8, no. 11, pp. 1–17, 2013, doi: 10.1371/journal.pone.0080722.

[70] J. Lee *et al.*, “Hair-bearing human skin generated entirely from pluripotent stem cells,” *Nature*, vol. 582, p. 399, 2020, doi: 10.1038/s41586-020-2352-3.

[71] Clontech, “Tet-On Advanced Inducible Gene Expression System - User Manual,” 2008.

[72] W. Hillen and C. Berens, “Mechanisms underlying expression of TN10 encoded tetracycline resistance,” *Annu Rev Microbiol*, vol. 48, pp. 345–69, 1994.

[73] M. Gossen, S. Freundlieb, G. Bender, G. Muller, W. Hillen, and H. Bujardt, “Transcriptional Activation by Tetracyclines in Mammalian Cells,” *Science (1979)*, vol. 268, no. June, pp. 1766–1770, 1995.

[74] M. Chhabra, “Biological therapeutic modalities,” *Translational Biotechnology: A Journey from Laboratory to Clinics*, pp. 137–164, Jan. 2021, doi: 10.1016/B978-0-12-821972-0.00015-0.

[75] N. Rujanapun *et al.*, “Small molecules re-establish neural cell fate of human fibroblasts via autophagy activation,” *In Vitro Cell Dev Biol Anim*, vol. 55, no. 8, pp. 622–632, Sep. 2019, doi: 10.1007/S11626-019-00381-0/FIGURES/5.

[76] D. K. Smith, J. Yang, M. L. Liu, and C. L. Zhang, “Small Molecules Modulate Chromatin Accessibility to Promote NEUROG2-Mediated Fibroblast-to-Neuron Reprogramming,” *Stem Cell Reports*, vol. 7, no. 5, pp. 955–969, 2016, doi: 10.1016/j.stemcr.2016.09.013.

[77] J. Ladewig *et al.*, “Small molecules enable highly efficient neuronal conversion of human fibroblasts,” *Nat Methods*, vol. 9, no. 6, pp. 575–578, 2012, doi: 10.1038/nmeth.1972.

[78] Y. Takayama *et al.*, “Brief exposure to small molecules allows induction of mouse embryonic fibroblasts into neural crest-like precursors,” *FEBS Lett*, vol. 591, no. 4, pp. 590–602, Feb. 2017, doi: 10.1002/1873-3468.12572.

[79] J. K. Ichida *et al.*, “A small-molecule inhibitor of tgf-Beta signaling replaces sox2 in reprogramming by inducing nanog,” *Cell Stem Cell*, vol. 5, no. 5, pp. 491–503, Nov. 2009, doi: 10.1016/J.STEM.2009.09.012.

[80] S. Fedoroff and A. Richardson, “Protocols for Neural Cell Culture,” *Protocols for Neural Cell Culture*, 2001, doi: 10.1385/1592592074.

[81] P. G. Gross, E. P. Kartalov, A. Scherer, and L. P. Weiner, “Applications of microfluidics for neuronal studies,” *J Neurol Sci*, vol. 252, no. 2, pp. 135–143, 2007, doi: 10.1016/j.jns.2006.11.009.

[82] G. Pethö and P. W. Reeh, “Sensory and signaling mechanisms of bradykinin, eicosanoids, platelet-activating factor, and nitric oxide in peripheral nociceptors,” *Physiol Rev*, vol. 92, no. 4, pp. 1699–1775, 2012, doi: 10.1152/physrev.00048.2010.

[83] Simona Giorgi *et al.*, “Compartmentalized primary cultures of dorsal root ganglion neurons to model peripheral pathophysiological conditions,” *Mol Pain*, Aug. 2023.

[84] A. J. Clark *et al.*, “Functional imaging in microfluidic chambers reveals sensory neuron sensitivity is differentially regulated between neuronal regions,” *Pain*, vol. 159, no. 7, pp. 1413–1425, Jul. 2018, doi: 10.1097/j.pain.0000000000001145.

[85] G. Jocher, S. H. Mannschatz, M. Offterdinger, and R. Schweigreiter, “Microfluidics of small-population neurons allows for a precise quantification of the peripheral axonal growth state,” *Front Cell Neurosci*, vol. 12, Jun. 2018, doi: 10.3389/fncel.2018.00166.

[86] N. R. Wevers *et al.*, “High-throughput compound evaluation on 3D networks of neurons and glia in a microfluidic platform,” *Sci Rep*, vol. 6, Dec. 2016, doi: 10.1038/srep38856.

[87] R. H. Kutner, X. Y. Zhang, and J. Reiser, “Production, concentration and titration of pseudotyped HIV-1-based lentiviral vectors,” *Nat Protoc*, vol. 4, no. 4, pp. 495–505, 2009, doi: 10.1038/nprot.2009.22.

[88] H. Jiang *et al.*, “Cell cycle and p53 gate the direct conversion of human fibroblasts to dopaminergic neurons,” *Nat Commun*, vol. 6, pp. 1–14, 2015, doi: 10.1038/ncomms10100.

[89] V. A. Church, K. Cates, L. Capano, S. Aryal, W. K. Kim, and A. S. Yoo, “Generation of Human Neurons by microRNA-Mediated Direct Conversion of Dermal Fibroblasts,” *Nuclear Reprogramming: Methods and Protocols*, vol. 2239, pp. 77–100, 2021, doi: 10.1007/978-1-0716-1084-8.

[90] H. Li, H. Jiang, X. Yin, J. E. Bard, B. Zhang, and J. Feng, “Attenuation of PRRX2 and HEY2 enables efficient conversion of adult human skin fibroblasts to neurons,” *Biochem Biophys Res Commun*, vol. 516, no. 3, pp. 765–769, 2019, doi: 10.1016/j.bbrc.2019.06.089.

[91] H. Qin, A. D. Zhao, M. L. Sun, K. Ma, and X. B. Fu, “Direct conversion of human fibroblasts into dopaminergic neuron-like cells using small molecules and protein factors,” *Mil Med Res*, vol. 7, no. 1, pp. 1–12, 2020, doi: 10.1186/s40779-020-00284-2.

[92] J. Herdy *et al.*, “Chemical modulation of transcriptionally enriched signaling pathways to optimize the conversion of fibroblasts into neurons,” *Elife*, vol. 8:e41356, pp. 1–21, 2019.

[93] V. Neirinckx, C. Coste, B. Rogister, and S. Wislet-, “Neural Fate of Mesenchymal Stem Cells and Neural Crest Stem Cells: Which Ways to Get Neurons for Cell Therapy Purpose?,” *Trends in Cell Signaling Pathways in Neuronal Fate Decision*, no. May, 2013, doi: 10.5772/53260.

[94] R. Wilson, A. A. Ahmmed, A. Poll, M. Sakaue, A. Laude, and M. Sieber-Blum, “Human peptidergic nociceptive sensory neurons generated from human epidermal neural crest stem cells (hEPI-NCSC),” *PLoS One*, vol. 13, no. 6, pp. 1–18, 2018, doi: 10.1371/journal.pone.0199996.

[95] E. Villalba-Riquelme, R. de la Torre-Martínez, A. Fernández-Carvajal, and A. Ferrer-Montiel, “Paclitaxel in vitro reversibly sensitizes the excitability of IB4(-) and IB4(+) sensory neurons from male and female rats,” *Br J Pharmacol*, vol. 179, no. 14, pp. 3693–3710, Jul. 2022, doi: 10.1111/BPH.15809.

[96] A. Dhaka *et al.*, “TRPV1 senses both acidic and basic pH,” vol. 29, no. 1, pp. 153–158, 2009, doi: 10.1523/JNEUROSCI.4901-08.2009.TRPV1.

[97] D. Alarcón-Alarcón *et al.*, “TRPM8 contributes to sex dimorphism by promoting recovery of normal sensitivity in a mouse model of chronic migraine,” *Nat Commun*, vol. 13, no. 1, Dec. 2022, doi: 10.1038/S41467-022-33835-3.

[98] L. Traxler, F. Edenhofer, and J. Mertens, “Next-generation disease modeling with direct conversion: a new path to old neurons,” *FEBS Lett*, vol. 593, no. 23, p. 3316, Dec. 2019, doi: 10.1002/1873-3468.13678.

[99] J. Mertens, M. C. Marchetto, C. Bardy, and F. H. Gage, “Evaluating cell reprogramming, differentiation and conversion technologies in neuroscience,” *Nat Rev Neurosci*, vol. 17, no. 7, pp. 424–437, Jul. 2016, doi: 10.1038/NRN.2016.46.

[100] Y. Mao, Y. Chen, and Z. Zhang, “Molecular function of Krüppel-like factor 7 in biology,” *Acta Biochim Biophys Sin (Shanghai)*, vol. 55, no. 5, pp. 713–725, May 2022, doi: 10.3724/ABBS.2023061.

[101] Y. Karashima *et al.*, “Bimodal action of menthol on the transient receptor potential channel TRPA1,” *Journal of Neuroscience*, vol. 27, no. 37, pp. 9874–9884, 2007, doi: 10.1523/JNEUROSCI.2221-07.2007.

[102] K. Kobayashi *et al.*, “Distinct expression of TRPM8, TRPA1, and TRPV1 mRNAs in rat primary afferent neurons with Aδ/C-fibers and colocalization with Trk receptors,”

Journal of Comparative Neurology, vol. 493, no. 4, pp. 596–606, 2005, doi: 10.1002/cne.20794.

[103] F. Viana, E. De la Peña, and C. Belmonte, “Specificity of cold thermotransduction is determined by differential ionic channel expression,” *Nat Neurosci*, vol. 5, no. 3, pp. 254–260, 2002, doi: 10.1038/nn809.

[104] D. D. McKemy, W. M. Neuhausser, and D. Julius, “Identification of a cold receptor reveals a general role for TRP channels in thermosensation,” *Nature*, vol. 416, no. 6876, pp. 52–58, 2002, doi: 10.1038/nature719.

[105] I. Devesa *et al.*, “αCGRP is essential for algesic exocytotic mobilization of TRPV1 channels in peptidergic nociceptors,” *Proc Natl Acad Sci U S A*, vol. 111, no. 51, pp. 18345–18350, Dec. 2014, doi: 10.1073/PNAS.1420252111/SUPPL_FILE/PNAS.1420252111.SAPP.PDF.

[106] S. I. Ohnuma and W. A. Harris, “Neurogenesis and the cell cycle,” *Neuron*, vol. 40, no. 2, pp. 199–208, 2003, doi: 10.1016/S0896-6273(03)00632-9.

[107] M. Birtele *et al.*, “Dual modulation of neuron-specific microRNAs and the REST complex promotes functional maturation of human adult induced neurons,” *FEBS Lett*, vol. 593, no. 23, pp. 3370–3380, 2019, doi: 10.1002/1873-3468.13612.

[108] V. Busskamp *et al.*, “Rapid neurogenesis through transcriptional activation in human stem cells,” *Mol Syst Biol*, vol. 10, no. 11, p. 760, 2014, doi: 10.15252/msb.20145508.

[109] S. A. Stewart *et al.*, “Lentivirus-delivered stable gene silencing by RNAi in primary cells,” *Rna*, vol. 9, no. 4, pp. 493–501, 2003, doi: 10.1261/rna.2192803.

[110] R. K. Akkina, R. M. Walton, M. L. Chen, Q. X. Li, V. Planelles, and I. S. Chen, “High-efficiency gene transfer into CD34+ cells with a human immunodeficiency virus type 1-based retroviral vector pseudotyped with vesicular stomatitis virus envelope glycoprotein G.,” *J Virol*, vol. 70, no. 4, pp. 2581–2585, 1996, doi: 10.1128/jvi.70.4.2581-2585.1996.

[111] E. Campeau *et al.*, “A versatile viral system for expression and depletion of proteins in mammalian cells,” *PLoS One*, vol. 4, no. 8, Aug. 2009, doi: 10.1371/JOURNAL.PONE.0006529.

[112] T. Panciera *et al.*, “Induction of Expandable Tissue-Specific Stem/Progenitor Cells through Transient Expression of YAP/TAZ,” *Cell Stem Cell*, vol. 19, no. 6, pp. 725–737, 2016, doi: 10.1016/j.stem.2016.08.009.

[113] G. Tiscornia, O. Singer, and I. M. Verma, “Production and purification of lentiviral vectors,” *Nat Protoc*, vol. 1, no. 1, pp. 241–245, 2006, doi: 10.1038/nprot.2006.37.

[114] N. Baumlin-Schmid, M. Salathe, and N. L. Fregien, “Optimal lentivirus production and cell culture conditions necessary to successfully transduce primary human bronchial epithelial cells,” *Journal of Visualized Experiments*, vol. 2016, no. 113, pp. 1–7, 2016, doi: 10.3791/54176.

[115] G. Lizée, J. L. Aerts, M. I. Gonzales, N. Chinnasamy, R. A. Morgan, and S. L. Topalian, “Real-time quantitative reverse transcriptase-polymerase chain reaction as a method for determining lentiviral vector titers and measuring transgene expression,” *Hum Gene Ther*, vol. 14, no. 6, pp. 497–507, 2003, doi: 10.1089/104303403764539387.

[116] ATCC, “293T Product Sheet,” pp. 1–2, 1994.

[117] GIBCO, “Human Dermal Fibroblasts, neonatal (HDFn) Product description,” no. C, pp. 0–3, 2019.

[118] GIBCO, “HDFa manual,” no. C, pp. 3–5, 2009.

[119] L. Ciuffreda *et al.*, “Growth-inhibitory and antiangiogenic activity of the MEK inhibitor PD0325901 in malignant melanoma with or without BRAF mutations,” *Neoplasia*, vol. 11, no. 8, pp. 720–731, 2009, doi: 10.1593/neo.09398.

[120] F. Catalog and N. Ax, “AXIS ™ : AX on I nvestigation S ystem,” vol. 1, no. 800.

[121] Domínguez-Bajo A *et al.*, “Nanostructured gold electrodes promote neural maturation and network connectivity. ,” *Biomaterials*, vol. 1, no. 279, 2021.

ACKNOWLEDGEMENTS

Seven years ago, while attending a summer school in Bologna, I had the idea of doing my final master project abroad but never imagined I would have done a phD in Spain. After all this work, my deepest gratitude goes to professors Antonio Ferrer Montiel and Asia Fernández Carvajal for having me in their lab. Their support, coupled with the freedom they granted me, though challenging at times, taught me invaluable lessons about research independence. Thank you for the confidence you had in me, for your professionality and for understanding and respecting the choices I made. I'm thankful to professor Gregorio Fernandez Ballester, whose kindness and guidance were pivotal in the final stages of this work. A heartfelt thank you goes out to professor Karolina Pircs and my Budapest "family" for their warm welcome, introducing me to different research approaches, and helping me when I was thinking of giving up.

Doing a phD is a rollercoaster and I could not have done it without the support of my colleagues, friends and family. Laura, thank you for being a firm point in the bad and good moments. You listened to my doubts, shared my struggles and moments of laughter and tears in the *despacho*, it meant the world to me. Thank you for all time, the coffees, the beers and the MEA plates. Angela, you have been such a good colleague and friend, supportive and always cheerful. I hope I've helped make you feel at home, as you have for me. Having a person who knows where to find a proper pizza is invaluable. And to both of you *mucho ánimo, hay luz al final del túnel.* Maggie, I still remember when we went out when I arrived here, it was all new to me but you made me feel that I was not alone. Thank you for that, for everything you taught me, for always listening and for cooking a moussaka that I still remember to this day. Alicia, it's been a while now but I cannot forget the laughter and the *tía sabes que me ha pasado hoy?* when you came to do polarstar by my bench. There have been some bad moments but you always found the strength to learn new things and keep working. Jose, I could not thank you enough for all the emotional and technical support. Knowing that you where there, ready to solve problems, was always helpful, thank you so much. Olivia, your laughter was a source of joy, even when I heard it from another room. Thank you for the board games, I wish you all the best for the future. Vero, thank you for the trust and the coffee breaks, we will definitely keep working together. Thank you Eva for the

help with the patch clamp and I hope you will find good options for your future, close or far away, wherever you like. Jorge, even if it doesn't seem so, the end is near and you can do it. Thank you for the mini talks when we were "neighbours". And least but not last, thank you to David Cabañero or David postdoc, you were always available to help me, even just to organize my thoughts when I was very confused.

Additionally, I would like to thank those who moved on from the lab, like Cloti, who was a wonderful guide and is now a wonderful confidante. Alberto, thank you for opening your home and Garcia's doors to me. To Gema, Sara, Maite, Jan Albert, Cristina, Carol, Antonio Zafra. To all the degree and master students who passed by the lab, we were learning together and it is great to see how we have all grown up now.

David, you have been and still are a great teacher. We learned, grew up and changed together and I am very proud of us for overcoming two phDs together. It was hard sometimes, and it was difficult to love me, but it was also strengthening and, comes what may, thank you for our past and for our future.

Finally, I switch to Italian to express gratitude to my family and friends. Elena, nonostante la distanza ti ho sempre sentita vicina anche quando volermi bene era difficile. Grazie per essere sempre stata orgogliosa di me, anche quando non lo ero io stessa. Mamma, Babbo, grazie per avermi lasciata libera di fare le mie scelte, e di cambiare di paese per qualche mese, poi per qualche anno, e poi chissà. Vi voglio bene e voglio che sappiate che siete sempre con me. Grazie a Fabrizio, per essere una roccia e per aver imparato a parlare in una lingua inventata. E per concludere GRAZIE ai miei amici. So che sapete che nonostante la distanza vi voglio bene come quando avevamo 15 anni, anzi forse di più. Fede, la prima ad essere venuta e trovarmi a Elche, anche quando non potevo camminare. Eli, che forse sei cambiato anche più di me in questi anni e per questo capisci lo struggle. Benni, grazie per i gossip e non smettere mai di farmi da mangiare, grazieeee. Ili, grazie per la dolcezza, la comprensione e per non farmi mai mai mai sentire giudicata.

Lastly, I extend my gratitude to all those not explicitly mentioned here. I am very grateful for all the experiences that I was able to live in these last years, both the tough and the good ones.

ANNEX I

Is TRPA1 Burning Down TRPV1 as Druggable Target for the Treatment of Chronic Pain?

Simona Giorgi[1, †], Magdalena Nikolaeva-Koleva[1, 2, †], David Alarcón-Alarcón[1], Laura Butrón[1] and Sara González-Rodríguez[1, *]

[1] Instituto de Investigación, Desarrollo e Innovación en Biotecnología Sanitaria de Elche (IDiBE), Avda de la Universidad s/n, Universidad Miguel Hernández, 03202 Elche, Spain.

[2] AntalGenics, SL. Ed. Quorum III, Parque Científico Universidad Miguel Hernández, Avda de la Universidad s/n, 03202 Elche, Spain.

* Correspondence: saragonzalezrodriguez@gmail.com

† These authors contributed equally to this work.

International Journal of Molecular Sciences 2019, 20, 2906; doi:10.3390/ijms20122906

(Q1, impact factor 6.208)

International Journal of
Molecular Sciences

MDPI

Review

Is TRPA1 *Burning Down* TRPV1 as Druggable Target for the Treatment of Chronic Pain?

Simona Giorgi [1,†], Magdalena Nikolaeva-Koleva [1,2,†], David Alarcón-Alarcón [1], Laura Butrón [1] and Sara González-Rodríguez [1,*]

[1] Instituto de Investigación, Desarrollo e Innovación en Biotecnología Sanitaria de Elche (IDiBE), Avda de la Univesidad s/n, Universidad Miguel Hernández, 03202 Elche, Spain; sgiorgi@umh.es (S.G.); mnikolaeva@umh.es (M.N.-K.); david.alarcon.alarcon.91@gmail.com (D.A.-A.); lbutron@umh.es (L.B.)
[2] AntalGenics, SL. Ed. Quorum III, Parque Científico Universidad Miguel Hernández, Avda de la Universidad s/n, 03202 Elche, Spain
* Correspondence: saragonzalezrodriguez@gmail.com
† These authors contributed equally to this work.

Received: 24 May 2019; Accepted: 13 June 2019; Published: 14 June 2019

Abstract: Over the last decades, a great array of molecular mediators have been identified as potential targets for the treatment of chronic pain. Among these mediators, transient receptor potential (TRP) channel superfamily members have been thoroughly studied. Namely, the nonselective cationic channel, transient receptor potential ankyrin subtype 1 (TRPA1), has been described as a chemical nocisensor involved in noxious cold and mechanical sensation and as rivalling TRPV1, which traditionally has been considered as the most important TRP channel involved in nociceptive transduction. However, few TRPA1-related drugs have succeeded in clinical trials. In the present review, we attempt to discuss the latest data on the topic and future directions for pharmacological intervention.

Keywords: TRPA1; pain; inflammation; neuropathy; molecular modulation

1. Introduction

The International Association for the Study of Pain (IASP) defines pain as "an unpleasant sensory and emotional experience associated with actual or potential tissue damage, or described in terms of such damage". This sensory response is necessary for survival since it warns us about potential injuries; however, what are the consequences if this response fails or becomes chronic? Sometimes the pathways that should be only activated in presence of harmful stimuli lose their physiological function and lead to the development of chronic painful pathologies. This kind of disorders have an important societal impact in health and in economic terms, affecting 740 million people in Europe where ~20% of the population suffers from chronic pain [1]. As a consequence, this prevalence results in a large number of medical consultations, becoming an important economic investment [2]. In addition, these pathologies cause absenteeism from work, being responsible for 500 million sick days in Europe and costing €240 billion per year [1]. Chronic pain is the main reason why people leave their employments prematurely [3]. Furthermore, the long-term consumption of current available treatments such as NSAIDs (non-steroidal anti-inflammatory drugs) or opioids induces detrimental side effects limiting their use. Accordingly, understanding how pain pathways work is still an overriding goal in order to discover new molecular targets as well as to improve already available pharmacological treatments.

Somatosensations such as touch, proprioception, nociception, or thermosensation are detected by the somatosensory system where primary sensory neurons are responsible for receiving the aforementioned stimuli. In terms of pain, sensory neurons can be divided into two main types:

nociceptive and non-nociceptive. The latter detects stimuli in a continuous range of intensity, while the nociceptive sensory neurons show a higher activation threshold being able to detect potentially harmful stimuli. The process by which primary sensory neurons detect and transmit nociceptive information is denominated nociception and the neurons responsible for this action are nociceptors [4,5].

Nociceptors soma is located either in trigeminal (TG) or dorsal root ganglia (DRG); nerve fibres depart from these ganglia that connect to somatic, visceral, and trigeminal regions as well as to the spinal cord and brain transmitting the nociceptive signals between peripheral (PNS) and central (CNS) nervous system [5]. The most widely used classification of nociceptors is based on the axon type displayed: (i) Aβ fibres that, with high conduction, detect innocuous stimuli; (ii) Aδ fibres that, with lower conduction velocities, detect mechanical and thermal stimuli and are responsible for acute pain sensation; and (iii) C fibres that are activated by chemical, mechanical, and thermal stimuli [4,6].

Pain propagation is usually described in four phases: transduction, transmission, modulation, and perception. Briefly, peripheral nerve fibres, which innervate skin, muscles, and viscera detect and translate stimuli into action potentials that travel along the axon, which penetrates into the dorsal horn of the spinal cord. This nociceptive information eventually reaches supra-spinal areas in the brain where is integrated [7].

In pathological conditions, these pathways might be altered and nociceptors undergo a sensitisation process. In such case, their activation threshold decreases, leading to an increase in sensitivity and excitability of the nerve fibres. During healthy conditions, when the stimulus ceases, the nociceptive system reaches again its basal state, recovering its activation threshold, which takes no place in pathological conditions. This process can occur both peripherally and centrally [8,9].

Nociceptors express a broad range of ion channels and/or receptors that have to be considered in order to understand the molecular pathways they take part in. Among these mediators, TRP channels are one of the most prominent family studied in the field of pain [10], and since TRPA1 seems to play a key role in nociception, it will be discussed in the present review.

2. TRP Channels Family

The TRP channels superfamily was initially described by the discovery of the *Drosophila*–TRP channels in genetically altered photoreceptors. This mutation showed transient voltage responses to the light stimuli; thus, it was denominated transient receptor potential [11,12]. These ion channels form a family of evolutionarily conserved ligand-gated ion channels that act as sensors of physical and chemical stimuli. Unlike other channels, this family possesses a wide range of activators (chemical compounds, temperature, mechanical stimuli, osmolarity, lipids, light, oxidative species, and pH), and their regulation (transcription, alternative splicing, glycosylation, and phosphorylation) is linked to an extensive tissue distribution and thus to different biological roles [13]. They are nonselective cationic channels that permeate mainly calcium but also potassium and sodium. The influx of calcium to the cell triggers several actions such as cellular proliferation, cell death, gene transcription, and the release of neurotransmitters.

To date, there have been several TRP channels described that are present in mammals as six families: TRPC, TRPM, TRPV, TRPA, TRPP, and TRPML based on amino acid homologies (IUPHAR), being TRPV1-4, TRPA1, and TRPM8 the most prominent expressed in nociceptors and the most extensively studied [13]. Additionally, TRPV1, TRPA1, and TRPM3 conform an important thermoregulatory system in sensory neurons [14].

2.1. TRPV1 Channel

In the description of the nociceptive transmission, TRPV1 was the first TRP cloned channel in 1997 and it is a cationic channel that displays high calcium permeability [15]. TRPV1 is found in both peripheral and central terminals of nociceptors in the DRG, TG, nodose ganglion (NG), geniculate ganglion (GG), and jugular ganglion [16–19]. TRPV1 also modulates pain transmission at the first sensory synapse [19,20]. This channel acts as a polymodal sensor since it can be activated by noxious

heat (≥43 °C), low pH (<6.5), and some other exogenous or endogenous compounds (camphor, allicin, toxins, anandamide) besides the well-known agonist, capsaicin.

It is estimated that approximately 35–50% of all DRG or TG neurons are TRPV1 positive [21], being a large population of unmyelinated C-fibres and a small population of thinly myelinated Aδ fibres. TRPV1 expression is usually accompanied by the expression of some other pain mediators such as Substance P (SP) or Calcitonin Gene-Related Peptide (CGRP).

Regarding pain involvement, it has been described that the administration of some of the aforementioned chemicals evokes pain-related behaviours, and they are mediated by TRPV1 as TRPV1-deficient mice showed. These animals displayed a full loss of behavioural responses to capsaicin and reduction in heat responses. Intriguingly, some studies also showed that TRPV1 null mice display normal sensitivity to acute noxious heat [22,23]. However, normal responses to mechanical stimuli were observed. In vitro data revealed that calcium influx or electrophysiological responses to capsaicin are abolished in these animals that might suggest that other mediators could participate in the sensation of noxious heat when TRPV1 is not expressed [24,25].

2.2. TRPA1 Channel

Originally denominated ANKTM1 (ankyrin-like with transmembrane domains protein 1) but currently called transient receptor potential ankyrin 1 (TRPA1), this receptor has been conserved in different species during evolution. It was initially identified in human foetal lung fibroblasts as a transformation-associated gene product [26]. It is a non-selective cationic channel and it is expressed in the PNS and CNS. TRPA1 is clearly linked to pain due to its expression in nociceptive structures [7,10,27–29]. It is generally co-expressed with TRPV1 in nociceptors and also acts as a polymodal sensor as it might be activated by several chemical, thermal (≤18 °C), mechanical, and osmotic stimuli [30].

Since different stimuli can activate TRPA1, each mode of activation indicates a different role for this channel in a different pain pathway. Thus, in chemosensation, TRPA1 can be activated by a plethora of molecules which are able to evoke a stinging sensation [31,32]. An important group of TRPA1 activators are reactive oxygen species (ROS) that together with ultraviolet light can stimulate TRPA1 [33,34]. Indeed, higher levels of ROS are usually found during inflammation [35]. Likewise, TRPA1 is a thermosensor as it has been shown that cold can elicit TRPA1 currents in in-vitro systems [36]. However, this stimulation is minimal compared to chemical agonist-induced currents, which means that cooling enhances TRPA1 currents in presence of TRPA1 agonists [37]. Furthermore, cold induces the release of ROS or calcium, which in turn activates the TRPA1 channel [35]. Finally, TRPA1 also participates in mechanosensation but it is not intrinsically mechanosensitive as shown in null mice after high pressure stimuli application [38].

From a structural point of view, understanding TRPA1 function and regulation is tightly linked to unveiling the structural mechanisms responsible for them. Recently, the three-dimensional atomic structure of the full-length human TRPA1 channel has been determined with ~4 Å resolution [39] (PDB Code: 3J9P). As the rest of the TRP superfamily [40], TRPA1 forms a homotetramer. Each monomer has an intracellular N-terminal ankyrin repeats domain and a C-terminal coiled-coil domain. The N-terminus is followed by a linker domain and a Pre-S1 helix. Four transmembrane helixes come after (S1–S4), a S4–S5 linker, S5, and S6. Between these last, the pore helix 1 and 2 are found. Finally, the TRP-like domain connects with a β-sheet that ends into the C-terminus. The oligomer structure reveals channel organisation, pore architecture, and key regulatory interactions and establishes a base for structure-based design of analgesic, anti-inflammatory, and anaesthetic agents (Figure 1, Table 1).

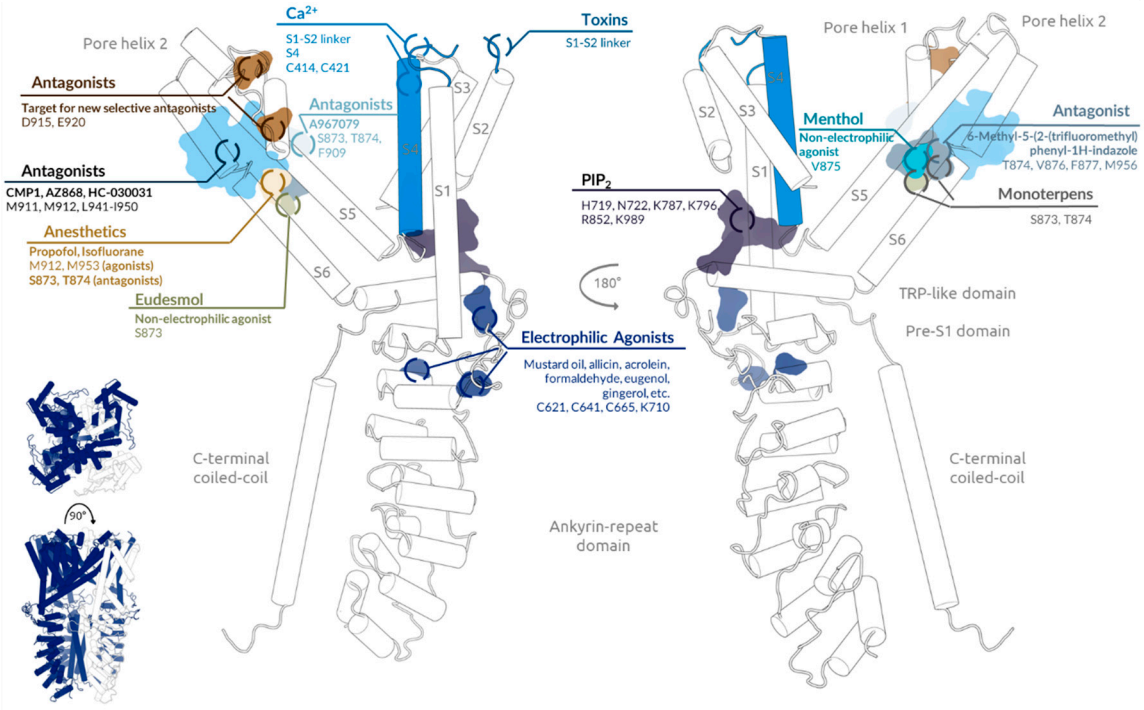

Figure 1. Main TRPA1 chemical modulators binding sites. General view of human transient receptor potential ankyrin subtype 1 (TRPA1) structure is shown in the inset. Detailed view of one subunit (white) is shown on the right. Main chemical modulators' binding sites are highlighted on the structure. Labels tag key residues for each site, give an example of, and/or classify each substance.

Many irritant chemicals are potent electrophiles that activate the channel through covalent modification of cysteine (C621, C641, C665) or lysine (K710) residues on its N-terminus [41,42], specifically the Pre-S1 region. These agonists include mustard oil, tetrahydrocannabinol, allicin, acrolein, formaldehyde, N-methylmaleimide [43–45], cinnamaldehyde [46], eugenol, gingerol, and thymol [47]. TRPA1 is also activated by Ca^{2+} ions [48,49] binding to residues C414 and C421 in the ankyrin-repeat domain [50]. Nonetheless, recently it has been suggested that Ca^{2+} could also bind to negatively charged amino acids in the S1–S2 linker [51], a region that is also involved in a tarantula toxin binding [52], but also to residues in the S4 segment [53]. Menthol is an exception given that it activates the channel by binding to residues from the S5–S6 transmembrane domain especially to V875 [54] like other non-electrophilic agonists such as eudesmol (S873) [55] and protons [56]. 6-Methyl-5-(2-(trifluoromethyl)phenyl)-1H-indazole has been identified as an inhibitor that acts directly on the predicted menthol binding-site located on the outer-side of the pore domain binding to residues T874, V876, F877, and M956 [57]. Several studies point out the pore domain as a druggable binding site of TRPA1. Some antagonists such as CMP1 [58], AZ868 [59], and HC-030031 [60] bind to residues M911 and M912 from the inner mouth of the selectivity filter and/or a group of residues in S6 from I940 to I950 [61]. It has been determined that the antagonist A-967079 [62] binds to a discrete site different from the one of HC-030031 formed by residues S873, T874, and F909 [39]. The inhibitory effects of monoterpens also require S873, T874 [63]. Some general anaesthetics like propofol and isofluorane share this binding pocket but they also interact with M912 and M953 required for their agonistic effects [64]. It is also suggested that the region of the selectivity filter (D915) along with the residue E920 located on the outer mouth of the pore which attracts cations to the pore could conform a binding site for TRPA1 selective antagonists in terms of highly charged molecules [65]. Another notable structural regulatory region is the one beneath the lower segment of the S1–S4 sensor domain capable of binding to phosphoinositides and regulating channel gating. It has been determined that the negatively charged inositol triphosphate head group of PIP_2 contacts residues H719, N722, K787, K796, R852, and K989 [66].

Table 1. Summary of action sites of the different TRPA1 modulators.

Effect	Region	Residues	Example Substances	References
Electrophilic agonists	Pre-S1 region	C621, C641, C655, K710	Mustard oil, tetrahydrocannabinol, allicin, acrolein, formaldehyde, *N*-methylmaleimide, cinnamaldehyde, eugenol, gingerol, thymol	[41–47]
Modulators	Ankyrin-repeat domain	C414	Ca^{2+} ions	[48–51,53]
	S4			
	S1–S4	Negatively charged residues	Tarantula toxin	[52]
Modulator	S5–S6	V875	Menthol	[54]
Nonelectrophilic agonists		S873	Eudesmol	[55]
			Protons	[56]
Antagonists	S5–S6	T874, V876, F877, M956	6-Methyl-5-(2-(trifluoromethyl)phenyl)-1H-indazole	[57]
	Selectivity filter	M911, M912	CMP1, AZ868, HC-030031	[58–61]
	S6	I940–I950		
	S5	S873, T874	F909	A-967079	[39,62]
			Monoterpens	[63]
Anaesthetics			M912 M953	Propofol, isofluorane	[64]
Modulator	S1–S4	H719, N722, K787, K796, R852, K989	Phosphoinositides	[66]

The pore phenomenon where TRPA1 [67,68], like other TRPs, is found on its dilated state is of great interest because it could stand for a novel way for delivering hydrophilic or low-permeability compounds, lower drug doses required for therapeutic effect, thus decreasing the risks of side effects [69] like in the case of capsaicin-gabapentin application on TRPV1 [70]. Moreover, during the dilation process, new potentially therapeutic binding sites could be revealed [71].

As pain signalling relies on sensitization of nociception-related TRPs, another noteworthy strategy to control pain relies on the inhibition of only sensitized TRP channels [72]. Between all factors involved in sensitization, the development of agents that specifically inhibit post-translational changes such as phosphorylation or glycosylation or blocking the translocation process of the channel from the cytoplasm to the cell membrane [73–75] appear as a more realistic intervention and reduce possible undesirable side effects. However, the exact molecular basis for this process for TRPA1, in which PKA and PLC seem to be involved [37,76], is still unclear.

3. TRPA1 in Inflammatory Pain

3.1. The Double Face of TRPA1 in Gastrointestinal Pain Models

TRPA1 channel has a pivotal role in mechanosensation and nociception within the viscera [77]. It is highly expressed in human and rat enterochromaffin cells which store serotonin and can be stimulated by TRPA1 agonists [78,79]. Interestingly, serotonin participated in the pathogenesis of post-infectious irritable bowel syndrome and modulated visceral nociception, being the levels of serotonin in patients higher than in healthy controls [80], suggesting that TRPA1 is an interesting target in the treatment of this syndrome.

TRPA1 has also been investigated in inflamed colon models, where nerve growth factor (NGF) and glial derived neurotrophic factor (GDNF) are increased potentiating expression and functionality

of TRPA1 and TRPV1 in skin, muscle, and colon [81]. TRPV1 and TRPA1 concert has been further investigated in acute colitis and visceral hypersensitivity model, where the blockade of both channels reduced visceromotor responses when compared to a single channel inhibition. Consistently, colitis symptoms might be alleviated by intrathecal administration of TRPA1 antisense oligodeoxynucleotide or by pharmacological inhibition of TRPA1 [82–84]. Similarly, colitis in mice was attenuated by capsazepine due to a desensitisation of TRPA1 [85] or to the reduction of neuropeptides release such as SP and CGRP [86].

On the contrary, selective TRPA1 agonists relieved colitis and abdominal pain in murine models [87,88]. This effect is still unclear, however, the inhibition of TRPA1 did not improve in a different model of colitis in mice [89], highlighting the importance of the experimental model when studying the TRPA1 channel role in irritable bowel syndrome. Additionally, a protective role for TRPA1 has been postulated in intestinal mucositis and in fibrotic inflammatory disorders such as Chron's disease [90,91].

3.2. TRPA1 Is Involved in Joint and Muscle Pain

In human chondrocytes, TRPA1 is functionally expressed during osteoarthritis (OA) and it participated in mechanical hypersensitivity and inflammation in OA animals, and its expression was increased after treatment with inflammatory factors [92,93]. Complete Freund's adjuvant (CFA) or monosodium iodoacetate (MIA) models showed that the blockage of TRPA1 relieved some of the painful symptoms [94–96].

TRPs are also involved and upregulated in rheumatoid arthritis (RA) [97] where the preincubation of synovial fibroblasts with TNF upregulated and sensitized TRPA1, reducing cell viability by inducing necrosis [98]. In human and murine synovial fibroblasts, the activation of TRPV1 and TRPA1 by endocannabinoids downregulated proinflammatory cytokines, and the treatment with endocannabinoids alleviated collagen-induced arthritis in mice [99].

Gout is another joint disease in which monosodium urate (MSU) crystals deposit intra-articularly and cause painful arthritis [100]. In mice, painful symptoms of intra-articularly injected MSU crystals might be relieved when TRPA1 is inhibited by antagonists or genetically ablated [101]. The joint could also be affected by yeast *Candida osteomyelitis* that induces pain and bone destruction, in which TRPV1 and TRPA1 deficiency caused osteoinflammation and diminished CGRP production [102].

Intramuscular injections of TRPA1 agonists aroused nocifensive responses and mechanical hyperalgesia in muscle afferents [103], and in a model of masseter inflammation, TRPA1 mRNA expression was found to be increased in the TG [104,105]. Inhibition of both TRPA1 and TRPV1 in masseter muscle decreased spontaneous pain but did not alleviate bite-evoked pain [106]. Consistently, in orofacial pain models, intramuscular injection of AP18, a selective TRPA1 antagonist, blocked the progress of acute mechanical hypersensitivity and persistent muscle pain [103]. Additionally, in a model of skin and deep tissue incision, TRPA1 pharmacological blockade reduced spontaneous guarding pain behaviour. Interestingly, oxidative TRPA1 agonists (ROS and H_2O_2) were increased in incised skin and muscle [107]. Finally, it has been more recently hypothesised that TRPA1 may be beneficial in delaying the progression of Duchenne's muscular dystrophy as tetrahydrocannabidivarin showed improving myotube formation through the activation of TRPA1 [108].

3.3. TRPA1 and TRPV1 Cooperate in Skin Pathologies

In mouse models of pruritus and psoriasis, genetic ablation of TRPA1 abrogated scratching and improved skin lesions, demonstrating that the channel controls itch transduction to the central nervous system and pathophysiological alterations in the skin [109,110]. TRPV1 role in skin diseases has also been investigated, showing that both channels are involved in IL-31 induced itch; indeed, TRPV1 or TRPA1 pharmacological antagonism and ROS scavengers decreased itch in mice [111,112].

In allergic contact dermatitis (ACD) models, it is not clear yet whether TRPA1 and/or TRPV1 are implicated in the pathophysiology. Genetic ablation or pharmacological blockage of TRPA1, but not

TRPV1, decreased ACD typical symptoms and histamine independent scratching behaviour [113]. Notably, oxidative stress-induced itch is mediated by TRPA1 and is TRPV1-independent, while chloroquine and BAM8-22 induced TRPA1-dependent scratching behaviour that is histamine-independent [114,115]. Interestingly, chloroquine activated the itch-related G-protein-coupled receptor MrgprA3 to trigger histamine-independent itch, and TRPA1 has been found to signal downstream of MrgprA3 [115]. Another hypothesis about the interaction between TRPA1 and TRPV1 in ACD has been recently published demonstrating that both channels are required for the development of ACD but only TRPV1 protected from skin inflammation [116].

Expression of TRPA1 in dermal sensory nerves during atopic dermatitis (AD) was markedly elevated in injured skin biopsies from AD patients when compared to healthy controls. Thus, TRPA1 is not only necessary as a sensor for pruritogens but is also essential in maintaining skin inflammation [109,113,117].

3.4. TRPA1 Is a Sentinel for External Threats in the Airways and Urinary Tract

TRPA1 is expressed in the airways where it functions as a nocisensor for external threats [118]. Indeed, stimulation of C-fibres in the airways caused the release of inflammatory neuropeptides (CGRP and SP) that induce neurogenic inflammation. Extended and prolonged inflammation can lead to cough, asthma, and chronic obstructive pulmonary disease (COPD) and, interestingly, TRPA1 expression has been demonstrated in immune cells involved in the inflammatory response in asthma and COPD [119,120]. Unfortunately, to date, TRPA1 role has not been investigated in experimental models of COPD.

Several inflammatory compounds such as nitric oxide, protons, and ozone activated human TRPA1 heterologously through an oxidative mechanism [121,122], highlighting the importance of oxidative stress and TRPA1 in inflammatory conditions. Consistently, exposition to cigarette smoke may increment extracellular ROS, which activate TRPA1 inducing an increase of intracellular ROS and activation of pro-inflammatory signalling [123].

Another respiratory clinical condition is allergic rhinitis. In-vitro, periodic applications of antihistamine azelastine hydrochloride and/or corticosteroid fluticasone propionate desensitized sensory neurons expressing TRPA1 and TRPV1 [124]. The two channels have also shown a synergistic effect in rat vagal pulmonary sensory neurons and in the apnoeic response to application of AITC or capsaicin [125,126]. Moreover, TRPV1, TRPA1, and TRPM8 agonists produced nasal pain and smart in healthy volunteers and capsaicin and mustard oil also caused rhinorrhea [127]. TRPA1 is also expressed in deep airways, specifically in the epithelium facing the bronchial lumina of cystic fibrosis patients where inhibition of the channel led to a decrease of various proinflammatory cytokines [128].

TRPA1-expressing C-fibres comprise 50% of all bladder-innervating sensory neurons and mostly express CGRP, SP, and TRPV1 [129]. The expression of TRPA1 mRNA and protein in both mucosa and DRGs is increased in cyclophosphamide-induced cystitis and can be decreased by treatment with TRPA1 antagonists [130–132]. Similarly, spinal cord injury also affected the bladder and the urinary system upregulating TRPA1 protein and mRNA in the periphery but not in the central nervous system [133]. In addition, it has been shown that after intravesical lipopolysaccharide-administration, TRPA1 is implicated in bladder mechanosensory and nociceptive hypersensitivity that also present inflammation, while it was not involved in physiological bladder function [134], suggesting that the channel plays a role in detecting urinary pathogens. Moreover, it has been demonstrated that ROS are involved in urinary bladder disorders, and in a H_2O_2-induced cystitis model, TRPA1 contributed to acute bladder hyperactivity but did not seem to play a pivotal role in the pathological development of chronic cystitis [135]. Another frequently used bladder hypersensitivity model that consists on formalin injection increases TRPA1 expression in the bladder mucosa together with NGF and P_2X_2 receptors [136]. Formalin is, indeed, a standard substance that causes pain and its effects seem to be usually mediated by TRPA1 [137,138]

3.5. TRPA1 Senses Oxidation in the Cardiovascular System

TRP channels are widely expressed in the cardiovascular system with TRPA1 expressed in smooth muscle and endothelial cells of different species [139], making this channel important in the regulation of vascular tone and in the development of atherosclerotic disease accompanied of angina and leg pain [117]. In atherosclerosis, TRPA1 may be an important regulator because of its activation by oxidized low-density lipoproteins, confirming the channel as a sensor of oxidative stress [140,141]. The blockage of the receptor could counteract inflammatory pain in cardiovascular system [142]. Furthermore, TRPA1 is increased in heart after doxorubicin treatment and in human and mouse hypertrophic hearts, where blocking the channel improved these pathological conditions [143,144].

3.6. TRPA1 Role in Eye Diseases

TRP channels are found in the eye being TRPV1 the most characterised TRP in this organ because of its role in maintaining homeostasis [145]. TRPV1, TRPA1, and TRPM8 channels appeared to be important in UV corneal sensitisation [146] while TRPV1 and TRPA1 inhibition after alkali burn decreased corneal fibrosis inflammation and opacification [147,148]. TRPA1 was also important for the sensitisation of ocular-responsive trigeminal brainstem neurons in a model for tear-deficient dry eye [149], but further studies are necessary to assess the role of this channel in different eye pathological conditions.

4. TRPA1 in Neuropathic Pain

4.1. TRPA1 Is Essential for Nerve Injury and Chemotherapy-Induced Neuropathic Pain

Many neuropathic pain models induced by nerve injury are characterised by mechanical and cold hypersensitivity [150,151], suggesting a relevant role for TRPA1 [92,152] as it is a key transducing channel in mechanical/cold-sensing nociceptors [38,153]. Indeed, TRPA1 blockers or genetic ablation decreased nociceptive changes observed in animal models of neuropathic pain [60,154–156]. Another standard model of neuropathic pain is the one induced by the administration of chemotherapy drugs that may produce, as side effects, intense cold and mechanical hyperalgesia and/or allodynia, limiting administration to patients [157,158]. Similar to nerve injury models, the blockage of TRPA1 counteracted pain in several models of chemotherapy-induced neuropathic pain [159,160]. Oxaliplatin is often used to establish experimental neuropathic pain, through TRPA1 [161,162] but not TRPV1 sensitisation [163]. It has been shown that aluminium accumulates in DRGs of patients treated with oxaliplatin, increasing cold but not heat hypersensitivity, suggesting not TRPV1 but TRPA1 activation instead [164,165].

4.2. TRPA1 Is Upregulated in Neuropathic Pain

Nerve lesion and chemotherapy models of neuropathic pain showed that TRPA1 mRNA and protein are upregulated in peripheral and central terminals of nociceptors and in central sensory pathways [154,166–168]. Importantly, TRPA1 upregulation can be accompanied by an increased expression of TRPV1, α-CGRP, SP and pro-inflammatory cytokines release in dorsal root and trigeminal ganglia, cervical spinal cord, and medulla in mice [154,166]. The importance of TRPA1 upregulation has been assessed by studies which showed that blocking TRPA1 upregulation ameliorated pain, for example, microRNA 449a improved neuropathic painful symptoms by decreasing TRPA1 expression in mice [169]. Notably, it has been reported that some models of neuropathic pain undergo upregulation of TRPA1 but not TRPV1. These last studies are characterized by an increase in mechanical and cold, but not heat, sensitivity [164,170]. An important physiological role of TRPA1 is to promote α-CGRP and SP exocytosis as elicitors of vasodilation and neuro-inflammation [171], as seen in a trigeminal neuropathy in which blocking TRPA1 showed decreased levels of α-CGRP, SP, and even TRPV1 gene expression [154].

4.3. TRPA1 Modulation in Neuropathic Pain Shares Convergent Signalling Pathways in Different Models of Neuropathic Pain

Recent studies have enlightened some of the mechanisms underlying TRPA1 gene regulation in neuropathic pain. Acrolein is an endogenous aldehyde produced in some nerve lesion models [172,173]. It is known to produce TRPA1-dependent calcium currents in DRG cultures [156], and it upregulated TRPA1 expression in central and peripheral endings of nociceptors [170]. Furthermore, exogenous acrolein, as the one present in tobacco smoke, exacerbated pain in a mouse model of sciatic nerve injury [174]. Oxidative stress produced by nerve lesion may increase acrolein production. Both oxidative stress and acrolein upregulated TRPA1 and could be responsible for the post-traumatic hyperalgesia as pain could be decreased by acrolein scavengers and TRPA1 blockers [172,175]. Regulatory mechanisms of TRPA1 expression in nerve lesion models include p38 MAPK [165,176], ERK, and JNK signalling pathways, [171,177] while PKA and Mass Related G-protein-coupled receptor D upregulate TRPA1 functionality and are essential to establish pain in chronic constriction injury models [178]. Accordingly, in models of neuropathic pain generated by chemotherapeutic agents such as docetaxel, bortezomib, and oxaliplatin, TRPA1 expression is also increased through MAPK signalling [160,179]. Furthermore, TNF-α, released by mast cells, activates p38-MAPK and downstream JNK through TrkA, highlighting the importance of immune system in TRPA1 sensitisation process [180]. In chemotherapy-induced pain models, proteinase activated receptor 2 (PAR2) is another TRPA1 modulator as injection of a PAR2 blocker decreased protein expression of TRPA1 [181], SP, and α-CGRP release [182] and attenuated PKCε and PKA [183]. Additionally, a functional coupling between PAR2 and TRPV1 seems to exist [173]. Finally, in paclitaxel-induced neuropathic pain, TNF-α secreted by glial satellite cells increased TRPA1 and TRPV4 in small size nociceptors [184]. All the mechanisms described above increased TRPA1 expression and consequently α-CGRP and SP secretion, leading to a lower activation threshold of the nociceptors and neurogenic inflammation [185].

4.4. Oxidative Stress Is a Major Integrator of TRPA1 Regulation in Neuropathic Pain

Oxidative (ROS) and nitrogen reactive species (RNS) are key factors in the development of neuropathic pain [166,186]. Trevisan et al. described that pain symptoms in a mouse model of nerve injury could be reverted by deleting TRPA1 or blocking TRPA1 receptor. Interestingly, the authors could also reduce pain by injection of an antioxidant (alfa-lipoic acid) or apocynin (a NOX inhibitor), demonstrating that oxidative stress plays a key role in neuropathic pain through TRPA1 action [186]. In accordance, in a saphenous nerve constriction model, TRPA1 and D-amino acid oxidase mRNA were found to be increased in DRGs [166]. Oxidative stress is also necessary in chemotherapy-induced neuropathic pain models. In fact, paclitaxel-induced pain could be abolished by knocking out or blocking both TRPA1 and TRPV4 or by the application of the reducing agent glutathione [164], which also decreased α-CGRP and SP secretion [187]. Furthermore, oxaliplatin-induced cold sensitivity is produced by an increased responsiveness of TRPA1 to ROS. This mechanism is generated by prolyl hydroxylases inhibition [188] whose action on TRPA1 prolynes decreased the channel sensitivity to ROS [34]. Oxaliplatin also acts on cysteine oxidation, which regulated the channel opening confirming that oxidative stress is a pivotal TRPA1 regulator [189]. In the same line, bortezomib-induced neuropathy is characterized by cold, mechanical allodynia and hypersensitivity to a TRPA1 agonist; this effect could be blocked by TRPA1 antagonist HC-03003 or the antioxidant α-lipoic acid [190]. Finally, a recent study found that microRNA 155 mediates TRPA1 upregulation produced by ROS in an oxaliplatin-induced neuropathic pain model [191]. Activation of TRPA1 by oxidative stress has also been seen in other cell types besides primary sensory neurons. In-vivo experiments showed that injection of TRPA1 antagonists or antioxidants in the central nucleus of the amygdala blocked pain produced in the spare nerve injury model in rats [192]. In this regard, TRPA1 expressed in Schwann cells have been described to generate a gradient of oxidative stress, which maintains macrophage-nociceptor communication in mechanical allodynia [193]. In fact, release of H_2O_2 and other oxidative stress by-products by macrophage and monocyte has been reported to activate TRPA1 in pain models [167].

Previously mentioned evidence points to ROS-mediated activation of TRPA1 being a major trigger in neuropathic pain; thus antioxidant molecules are being proposed as candidates to treat painful symptoms in neuropathic pain [162,191], such as a blocker of semicarbazide-sensitive amine oxidase (SSAO), TRPA1, and TRPV1 [194].

5. TRPA1 in Clinical Trials

To our knowledge, TRPA1 has been implicated in chronic cough [195] and a gain-of-function point mutation has been linked to familial episodic pain syndrome [53]. To date, three TRPA1 antagonists have reached clinical trials for the treatment of pain conditions: GRC1753 (Glenmark) for chronic pain; CB-625 (Cubist Pharmaceuticals Inc.) for acute surgical pain [195,196]; and ODM-108, a highly potent TRPA1 antagonist developed by Orion Pharma to treat neuropathic pain. This drug reached phase 1, but the study failed due to complex pharmacodynamic properties [197]. Finally, acidosis activated human TRPA1 in pathologies such as myocardial infarction or peripheral vascular occlusive disease [198], but it still has to be proven that targeting TRPA1 could alleviate acidosis evoked-pain in clinical trials [199].

6. Conclusions

In summary, although TRPV1 has always been the prime TRP channel targeted to develop new drugs to treat pain, accumulating evidences now identify TRPA1 as a potential crucial player in mediating and modulating pain conditions due to its expression in numerous tissues and its key involvement in pivotal signalling pathways. TRPA1 has been demonstrated to cooperate with TRPV1 in the establishment and maintenance of pain and also to be important on its own as a nocisensor of a plethora of molecules. Furthermore, sensitisation of TRPA1 by endogenous mediators and metabolites of oxidative stress position this channel under the spotlight in the study of plenty of diseases, not only in the field of pain. As a consequence, pharmacological inhibition of TRPA1 seems to be an interesting strategy for treating some painful diseases. Further investigation is needed to unveil all the pharmacological potential TRPA1 may have.

Author Contributions: S.G., M.N.-K., L.B., D.A.-A. wrote the manuscript. S.G.-R. conceived the idea and wrote the manuscript. All authors reviewed and agreed the manuscript.

Funding: S.G. is funded by PAR-2019-Universidad Miguel Hernández. M.N.-K. is a recipient of an Industrial Doctorate Fellowship from MINECO (DI-16-08303). L.B. is a Personal Técnico de Apoyo recipient from MICINN (PTA2017-14381-I). D.A.-A. is a recipient of a Researcher Personal Formation Doctorate Fellowship from MINECO (SAF2015-66275-C2-1-R). S.G.-R. is funded by SAF2015-66275-C2-1-R from MICINN.

Acknowledgments: We would like to thank Dr. Ferrer-Montiel, Dr. Fernández-Ballester, and Dr. Fernández-Carvajal for their suggestions, support, and amendments to the manuscript.

Conflicts of Interest: The authors declare no conflict of interest. The funders had no role in the design of the study; in the collection, analyses, or interpretation of data; in the writing of the manuscript, or in the decision to publish the results.

References

1. Eccleston, C.; Wells, C.; Morlion, B. *European Pain Management*; Oxford University Press: Oxford, UK, 2018.
2. Gureje, O.; Simon, G.E.; Von Korff, M. A cross-national study of the course of persistent pain in primary care. *Pain* **2001**, *92*, 195–200. [CrossRef]
3. Saastamoinen, P.; Laaksonen, M.; Kääriä, S.M.; Lallukka, T.; Leino-Arjas, P.; Rahkonen, O.; Lahelma, E. Pain and disability retirement: a prospective cohort study. *Pain* **2012**, *153*, 526–531. [CrossRef] [PubMed]
4. Dubin, A.E.; Patapoutian, A. Nociceptors: The sensors of the pain pathway. *J. Clin. Investig.* **2010**, *120*, 3760–3772. [CrossRef] [PubMed]
5. Julius, D.; Basbaum, A.I. Molecular mechanisms of nociception. *Nature* **2001**, *413*, 203–210. [CrossRef] [PubMed]
6. Belmonte, C.; Viana, F. Molecular and cellular limits to somatosensory specificity. *Mol. Pain* **2008**, *4*, 14. [CrossRef] [PubMed]

7. Woolf, C.J. Pain: Moving from symptom control toward mechanism-specific pharmacologic management. *Ann. Intern. Med.* **2004**, *140*, 441–451. [CrossRef] [PubMed]
8. Chaban, V.V. Peripheral sensitization of sensory neurons. *Ethn. Dis.* **2011**, *20*, S1-3-6.
9. Basbaum, A.I.; Bautista, D.M.; Scherrer, G.; Julius, D. Cellular and Molecular Mechanisms of Pain. *Cell* **2009**, *139*, 267–284. [CrossRef] [PubMed]
10. Ferrer-Montiel, A.; Fernández-Carvajal, A.; Planells-Cases, R.; Fernández-Ballester, G.; González-Ros, J.M.; Messeguer, A.; González-Muñiz, R. Advances in modulating thermosensory TRP channels. *Expert Opin. Ther. Pat.* **2012**, *22*, 999–1017. [CrossRef] [PubMed]
11. Minke, B. Drosophila mutant with a transducer defect. *Biophys. Struct. Mech.* **1977**, *3*, 59–64. [CrossRef]
12. Montell, C.; Jones, K.; Hafen, E.; Rubin, G. Rescue of the Drosophila phototransduction mutation trp by germline transformation. *Science* **1985**, *230*, 1040–1043. [CrossRef] [PubMed]
13. Levine, J.D.; Alessandri-Haber, N. TRP channels: targets for the relief of pain. *Biochim. Biophys. Acta* **2007**, *1772*, 989–1003. [CrossRef] [PubMed]
14. Vandewauw, I.; De Clercq, K.; Mulier, M.; Held, K.; Pinto, S.; Van Ranst, N.; Segal, A.; Voet, T.; Vennekens, R.; Zimmermann, K.; et al. A TRP channel trio mediates acute noxious heat sensing. *Nature* **2018**, *555*, 662–666. [CrossRef] [PubMed]
15. Caterina, M.J.; Schumacher, M.A.; Tominaga, M.; Rosen, T.A.; Levine, J.D.; Julius, D. The capsaicin receptor: a heat-activated ion channel in the pain pathway. *Nature* **1997**, *389*, 816–824. [CrossRef] [PubMed]
16. Yamamoto, Y.; Sato, Y.; Taniguchi, K. Distribution of TRPV1- and TRPV2- immunoreactive afferent nerve endings in rat trachea. *J. Anat.* **2007**, *211*, 775–783. [CrossRef] [PubMed]
17. Tatsumi, E.; Katsura, H.; Kobayashi, K.; Yamanaka, H.; Tsuzuki, K.; Noguchi, K.; Sakagami, M. Changes in transient receptor potential channels in the rat geniculate ganglion after chorda tympani nerve injury. *Neuroreport* **2015**, *26*, 856–861. [CrossRef] [PubMed]
18. Jeffry, J.A.; Yu, S.Q.; Sikand, P.; Parihar, A.; Evans, M.S.; Premkumar, L.S. Selective targeting of TRPV1 expressing sensory nerve terminals in the spinal cord for long lasting analgesia. *PLoS ONE* **2009**, *4*, e7021. [CrossRef] [PubMed]
19. Sikand, P.; Premkumar, L.S. Potentiation of glutamatergic synaptic transmission by protein kinase C-mediated sensitization of TRPV1 at the first sensory synapse. *J. Physiol.* **2007**, *581*, 631–647. [CrossRef]
20. Kobayashi, K.; Fukuoka, T.; Obata, K.; Yamanaka, H.; Dai, Y.; Tokunaga, A.; Noguchi, K. Distinct expression of TRPM8, TRPA1, and TRPV1 mRNAs in rat primary afferent neurons with adelta/c fibers and colocalization with trk receptors. *J. Comp. Neurol.* **2005**, *493*, 596–606. [CrossRef]
21. Woodbury, C.J.; Zwick, M.; Wang, S.; Lawson, J.J.; Caterina, M.J.; Koltzenburg, M.; Albers, K.M.; Koerber, H.R.; Davis, B.M. Nociceptors lacking TRPV1 and TRPV2 have normal heat responses. *J. Neurosci.* **2004**, *24*, 6410–6415. [CrossRef]
22. Davis, J.B.; Gray, J.; Gunthorpe, M.J.; Hatcher, J.P.; Davey, P.T.; Overend, P.; Harries, M.H.; Latcham, J.; Clapham, C.; Atkinson, K.; et al. Vanilloid receptor-1 is essential for inflammatory thermal hyperalgesia. *Nature* **2000**, *405*, 183–187. [CrossRef] [PubMed]
23. Caterina, M.J.; Leffler, A.; Malmberg, A.B.; Martin, W.J.; Trafton, J.; Petersen-Zeitz, K.R.; Koltzenburg, M.; Basbaum, A.I.; Julius, D. Impaired nociception and pain sensation in mice lacking the capsaicin receptor. *Science* **2000**, *288*, 306–313. [CrossRef] [PubMed]
24. Bolcskei, K.; Helyes, Z.; Szabo, A.; Sandor, K.; Elekes, K.; Nemeth, J.; Almasi, R.; Pinter, E.; Petho, G.; Szolcsanyi, J. Investigation of the role of TRPV1 receptors in acute and chronic nociceptive processes using gene-deficient mice. *Pain* **2005**, *117*, 368–376. [CrossRef] [PubMed]
25. Jaquemar, D.; Schenker, T.; Trueb, B. An ankyrin-like protein with transmembrane domains is specifically lost after oncogenic transformation of human fibroblasts. *J. Biol. Chem.* **1999**, *274*, 7325–7333. [CrossRef] [PubMed]
26. Story, G.M.; Peier, A.M.; Reeve, A.J.; Eid, S.R.; Mosbacher, J.; Hricik, T.R.; Earley, T.J.; Hergarden, A.C.; Andersson, D.A.; Hwang, S.W.; et al. ANKTM1, a TRP-like channel expressed in nociceptive neurons, is activated by cold temperatures. *Cell* **2003**, *112*, 819–829. [CrossRef]
27. Nagata, K.; Duggan, A.; Kumar, G.; Garcia-Anoveros, J. Nociceptor and hair cell transducer properties of TRPA1, a channel for pain and hearing. *J. Neurosci.* **2005**, *25*, 4052–4061. [CrossRef] [PubMed]
28. Smith, M.P.; Beacham, D.; Ensor, E.; Koltzenburg, M. Cold-sensitive, menthol insensitive neurons in the murine sympathetic nervous system. *Neuroreport* **2004**, *15*, 1399–1403. [CrossRef] [PubMed]

29. Katsura, H.; Obata, K.; Mizushima, T.; Yamanaka, H.; Kobayashi, K.; Dai, Y.; Fukuoka, T.; Tokunaga, A.; Sakagami, M.; Noguchi, K. Antisense knock down of TRPA1, but not TRPM8, alleviates cold hyperalgesia after spinal nerve ligation in rats. *Exp. Neurol.* **2006**, *200*, 112–123. [CrossRef] [PubMed]
30. Zhang, X.F.; Chen, J.; Faltynek, C.R.; Moreland, R.B.; Neelands, T.R. Transient receptor potential A1 mediates an osmotically activated ion channel. *Eur. J. Neurosci.* **2008**, *27*, 605–611. [CrossRef]
31. Bautista, D.M.; Movahed, P.; Hinman, A.; Axelsson, H.E.; Sterner, O.; Högestätt, E.D.; Julius, D.; Jordt, S.E.; Zygmunt, P.M. Pungent products from garlic activate the sensory ion channel TRPA. *Proc. Natl. Acad. Sci. USA* **2005**, *102*, 12248–12252. [CrossRef]
32. Macpherson, L.J.; Geierstanger, B.H.; Viswanath, V.; Bandell, M.; Eid, S.R.; Hwang, S.; Patapoutian, A. The pungency of garlic: activation of TRPA1 and TRPV1 in response to allicin. *Curr. Biol.* **2005**, *15*, 929–934. [CrossRef] [PubMed]
33. Babes, A.; Sauer, S.K.; Moparthi, L.; Kichko, T.I.; Neacsu, C.; Namer, B.; Filipovic, M.; Zygmunt, P.M.; Reeh, P.W.; Fischer, M.J. Photosensitization in porphyrias and photodynamic therapy involves TRPA1 and TRPV. *J. Neurosci.* **2016**, *36*, 5264–5278. [CrossRef] [PubMed]
34. Miyake, T.; Nakamura, S.; Zhao, M.; So, K.; Inoue, K.; Numata, T.; Takahashi, N.; Shirakawa, H.; Mori, Y.; Nakagawa, T.; et al. Cold sensitivity of TRPA1 is unveiled by the prolyl hydroxylation blockade-induced sensitization to ROS. *Nat. Commun.* **2016**, *7*, 12840. [CrossRef] [PubMed]
35. Bessac, B.F.; Sivula, M.; von Hehn, C.A.; Escalera, J.; Cohn, L.; Jordt, S.E. TRPA1 is a major oxidant sensor in murine airway sensory neurons. *J. Clin. Investig.* **2008**, *118*, 1899–1910. [CrossRef] [PubMed]
36. del Camino, D.; Murphy, S.; Heiry, M.; Barrett, L.B.; Earley, T.J.; Cook, C.A.; Petrus, M.J.; Zhao, M.; D'Amours, M.; Deering, N.; et al. TRPA1 contributes to cold hypersensitivity. *J. Neurosci.* **2010**, *30*, 15165–15174. [CrossRef]
37. Wang, Y.Y.; Chang, R.B.; Waters, H.N.; McKemy, D.D.; Liman, E.R. The nociceptor ion cannel TRPA1 is potentiated and inactivated by permeating calcium ions. *J. Biol. Chem.* **2008**, *283*, 32691–32703. [CrossRef]
38. Kwan, K.Y.; Allchorne, A.J.; Vollrath, M.A.; Christensen, A.P.; Zhang, D.S.; Woolf, C.J.; Corey, D.P. TRPA1 contributes to cold, mechanical, and chemical nociception but is not essential for hair-cell transduction. *Neuron* **2006**, *50*, 277–289. [CrossRef]
39. Paulsen, C.E.; Armache, J.P.; Gao, Y.; Cheng, Y.; Julius, D. Structure of the TRPA1 ion channel suggests regulatory mechanisms. *Nature* **2015**, *520*, 511–517. [CrossRef]
40. Ferrer-Montiel, A.; García-Martínez, C.; Morenilla-Palao, C.; García-Sanz, N.; Fernández-Carvajal, A.; Fernández-Ballester, G.; Planells-Cases, R. Molecular architecture of the vanilloid receptor. Insights for drug design. *Eur. J. Biochem.* **2004**, *271*, 1820–1826. [CrossRef]
41. Macpherson, L.J.; Dubin, A.E.; Evans, M.J.; Marr, F.; Schultz, P.G.; Cravatt, B.F.; Patapoutian, A. Noxious compounds activate TRPA1 ion channels through covalent modification of cysteines. *Nature* **2007**, *445*, 541–545. [CrossRef]
42. Hinman, A.; Chuang, H.H.; Bautista, D.M.; Julius, D. TRP channel activation by reversible covalent modification. *Proc. Natl. Acad. Sci. USA* **2006**, *103*, 19564–19568. [CrossRef] [PubMed]
43. Jordt, S.E.; Bautista, D.M.; Chuang, H.H.; McKemy, D.D.; Zygmunt, P.M.; Högestätt, E.D.; Meng, I.D.; Julius, D. Mustard oils and cannabinoids excite sensory nerve fibres through the TRP channel ANKTM. *Nature* **2004**, *427*, 260–265. [CrossRef] [PubMed]
44. Bautista, D.M.; Jordt, S.E.; Nikai, T.; Tsuruda, P.R.; Read, A.J.; Poblete, J.; Yamoah, E.N.; Basbaum, A.I.; Julius, D. TRPA1 mediates the inflammatory actions of environmental irritants and proalgesic agents. *Cell* **2006**, *124*, 1269–1282. [CrossRef] [PubMed]
45. Bandell, M.; Story, G.M.; Hwang, S.W.; Viswanath, V.; Eid, S.R.; Petrus, M.J.; Earley, T.J.; Patapoutian, A. Noxious cold ion channel TRPA1 is activated by pungent compounds and bradykinin. *Neuron* **2004**, *41*, 849–857. [CrossRef]
46. Mendes, S.J.F.; Sousa, F.I.A.B.; Pereira, D.M.S.; Ferro, T.A.F.; Pereira, I.C.P.; Silva, B.L.R.; Pinheiro, A.J.M.C.R.; Mouchrek, A.Q.S.; Monteiro-Neto, V.; Costa, S.K.P.; et al. Cinnamaldehyde modulates LPS-induced systemic inflammatory response syndrome through TRPA1-dependent and independent mechanisms. *Int. Immunopharmacol.* **2016**, *34*, 60–70. [CrossRef] [PubMed]
47. Xu, H.; Delling, M.; Jun, J.C.; Clapham, D.E. Oregano, thyme and clove-derived flavors and skin sensitizers activate specific TRP channels. *Nat. Neurosci.* **2006**, *9*, 628–635. [CrossRef] [PubMed]

48. Cavanaugh, E.J.; Simkin, D.; Kim, D. Activation of transient receptor potential A1 channels by mustard oil, tetrahydrocannabinol and Ca^{2+} reveals different functional channel states. *Neuroscience* **2008**, *154*, 1467–1476. [CrossRef] [PubMed]
49. Zurborg, S.; Yurgionas, B.; Jira, J.A.; Caspani, O.; Heppenstall, P.A. Direct activation of the ion channel TRPA1 by Ca^{2+}. *Nat. Neurosci.* **2007**, *10*, 277–279. [CrossRef] [PubMed]
50. Takahashi, N.; Mizuno, Y.; Kozai, D.; Yamamoto, S.; Kiyonaka, S.; Shibata, T.; Uchida, K.; Mori, Y. Molecular characterization of TRPA1 channel activation by cysteine-reactive inflammatory mediators. *Channels* **2008**, *2*, 287–298. [CrossRef]
51. Marsakova, L.; Barvik, I.; Zima, V.; Zimova, L.; Vlachova, V. The First Extracellular Linker Is Important for Several Aspects of the Gating Mechanism of Human TRPA1 Channel. *Front. Mol. Neurosci.* **2017**, *10*, 16. [CrossRef]
52. Gui, J.; Liu, B.; Cao, G.; Lipchik, A.M.; Perez, M.; Dekan, Z.; Mobli, M.; Daly, N.L.; Alewood, P.F.; Parker, L.L.; et al. A tarantula-venom peptide antagonizes the TRPA1 nociceptor ion channel by binding to the S1–S4 gating domain. *Curr. Biol.* **2014**, *24*, 473–483. [CrossRef] [PubMed]
53. Kremeyer, B.; Lopera, F.; Cox, J.J.; Momin, A.; Rugiero, F.; Marsh, S.; Woods, C.G.; Jones, N.G.; Paterson, K.J.; Fricker, F.R.; et al. A gain-of-function mutation in TRPA1 causes familial episodic pain syndrome. *Neuron* **2010**, *66*, 671–680. [CrossRef] [PubMed]
54. Xiao, B.; Dubin, A.E.; Bursulaya, B.; Viswanath, V.; Jegla, T.J.; Patapoutian, A. Identification of transmembrane domain 5 as a critical molecular determinant of menthol sensitivity in mammalian TRPA1 channels. *J. Neurosci.* **2008**, *28*, 9640–9651. [CrossRef] [PubMed]
55. Ohara, K.; Fukuda, T.; Okada, H.; Kitao, S.; Ishida, Y.; Kato, K.; Takahashi, C.; Katayama, M.; Uchida, K.; Tominaga, M. Identification of significant amino acids in multiple transmembrane domains of human transient receptor potential ankyrin 1 (TRPA1) for activation by eudesmol, an oxygenized sesquiterpene in hop essential oil. *J. Biol. Chem.* **2015**, *290*, 3161–3171. [CrossRef] [PubMed]
56. de la Roche, J.; Eberhardt, M.J.; Klinger, A.B.; Stanslowsky, N.; Wegner, F.; Koppert, W.; Reeh, P.W.; Lampert, A.; Fischer, M.J.; Leffler, A. The molecular basis for species-specific activation of human TRPA1 protein by protons involves poorly conserved residues within transmembrane domains 5 and 6. *J. Biol. Chem.* **2013**, *288*, 20280–20292. [CrossRef] [PubMed]
57. Moldenhauer, H.; Latorre, R.; Grandl, J. The pore-domain of TRPA1 mediates the inhibitory effect of the antagonist 6-methyl-5-(2-(trifluoromethyl)phenyl)-1H-indazole. *PLoS ONE* **2014**, *9*, e106776. [CrossRef]
58. Chen, J.; Zhang, X.F.; Kort, M.E.; Huth, J.R.; Sun, C.; Miesbauer, L.J.; Cassar, S.C.; Neelands, T.; Scott, V.E.; Moreland, R.B.; et al. Molecular determinants of species-specific activation or blockade of TRPA1 channels. *J. Neurosci.* **2008**, *28*, 5063–5071. [CrossRef]
59. Vallin, K.S.; Sterky, K.J.; Nyman, E.; Bernström, J.; From, R.; Linde, C.; Minidis, A.B.; Nolting, A.; Närhi, K.; Santangelo, E.M.; et al. N-1-Alkyl-2-oxo-2-aryl amides as novel antagonists of the TRPA1 receptor. *Bioorg. Med. Chem. Lett.* **2012**, *22*, 5485–5492. [CrossRef]
60. Eid, S.R.; Crown, E.D.; Moore, E.L.; Liang, H.A.; Choong, K.C.; Dima, S.; Henze, D.A.; Kane, S.A.; Urban, M. O HC-030031, a TRPA1 selective antagonist, attenuates inflammatory- and neuropathy-induced mechanical hypersensitivity. *Mol. Pain* **2008**, *4*, 48. [CrossRef]
61. Klement, G.; Eisele, L.; Malinowsky, D.; Nolting, A.; Svensson, M.; Terp, G.; Weigelt, D.; Dabrowski, M. Characterization of a ligand binding site in the human transient receptor potential ankyrin 1 pore. *Biophys. J.* **2013**, *104*, 798–806. [CrossRef]
62. Chen, J.; Joshi, S.K.; DiDomenico, S.; Perner, R.J.; Mikusa, J.P.; Gauvin, D.M.; Segreti, J.A.; Han, P.; Zhang, X.F.; Niforatos, W.; et al. Selective blockade of TRPA1 channel attenuates pathological pain without altering noxious cold sensation or body temperature regulation. *Pain* **2011**, *152*, 1165–1172. [CrossRef] [PubMed]
63. Takaishi, M.; Uchida, K.; Fujita, F.; Tominaga, M. Inhibitory effects of monoterpenes on human TRPA1 and the structural basis of their activity. *J. Physiol. Sci.* **2014**, *64*, 47–57. [CrossRef] [PubMed]
64. Ton, H.T.; Phan, T.X.; Abramyan, A.M.; Shi, L.; Ahern, G.P. Identification of a putative binding site critical for general anesthetic activation of TRPA. *Proc. Natl. Acad. Sci. USA* **2017**, *114*, 3762–3767. [CrossRef] [PubMed]
65. Christensen, A.P.; Akyuz, N.; Corey, D.P. The Outer Pore and Selectivity Filter of TRPA. *PLoS ONE* **2016**, *11*, e0166167. [CrossRef]
66. Zimova, L.; Sinica, V.; Kadkova, A.; Vyklicka, L.; Zima, V.; Barvik, I.; Vlachova, V. Intracellular cavity of sensor domain controls allosteric gating of TRPA1 channel. *Sci. Signal.* **2018**, *11*, eaan8621. [CrossRef]

67. Banke, T.G.; Chaplan, S.R.; Wickenden, A.D. Dynamic changes in the TRPA1 selectivity filter lead to progressive but reversible pore dilation. *Am. J. Physiol. Cell Physiol.* **2010**, *298*, C1457–C1468. [CrossRef]
68. Chen, J.; Kim, D.; Bianchi, B.R.; Cavanaugh, E.J.; Faltynek, C.R.; Kym, P.R.; Reilly, R.M. Pore dilation occurs in TRPA1 but not in TRPM8 channels. *Mol. Pain* **2009**, *5*, 3. [CrossRef]
69. Ferreira, L.G.; Faria, R.X. TRPing on the pore phenomenon: what do we know about transient receptor potential ion channel-related pore dilation up to now? *J. Bioenerg. Biomembr.* **2016**, *48*, 1–12. [CrossRef]
70. Biggs, J.E.; Stemkowski, P.L.; Knaus, E.E.; Chowdhury, M.A.; Ballanyi, K.; Smith, P.A. Suppression of network activity in dorsal horn by gabapentin permeation of TRPV1 channels: implications for drug access to cytoplasmic targets. *Neurosci. Lett.* **2015**, *584*, 397–402. [CrossRef]
71. Banke, T.G. The dilated TRPA1 channel pore state is blocked by amiloride and analogues. *Brain Res.* **2011**, *1381*, 21–30. [CrossRef]
72. Sousa-Valente, J.; Andreou, A.P.; Urban, L.; Nagy, I. Transient receptor potential ion channels in primary sensory neurons as targets for novel analgesics. *Br. J. Pharmacol.* **2014**, *171*, 2508–2527. [CrossRef] [PubMed]
73. Patapoutian, A.; Tate, S.; Woolf, C.J. Transient receptor potential channels: targeting pain at the source. *Nat. Rev. Drug. Discov.* **2009**, *8*, 55–69. [CrossRef] [PubMed]
74. Vay, L.; Gu, C.; McNaughton, P.A. The thermos-TRP ion channel family: properties and therapeutic implications. *Br. J. Pharmacol.* **2012**, *165*, 787–801. [CrossRef] [PubMed]
75. Holtzer, P. Transient receptor potential (TRP) channels as drug targets for diseases of the digestive system. *Pharmacol. Ther.* **2011**, *131*, 142–170. [CrossRef] [PubMed]
76. Schmidt, M.; Dubin, A.E.; Petrus, M.J.; Earley, T.J.; Patapoutian, A. Nociceptive signals induce trafficking of TRPA1 to the plasma membrane. *Neuron* **2009**, *64*, 498–509. [CrossRef] [PubMed]
77. Brierly, S.M.; Hughes, P.A.; Page, A.J.; Kwan, K.Y.; Martin, C.M.; O'Donnell, T.A.; Cooper, N.J.; Harrington, A.M.; Adam, B.; Liebregts, T.; et al. The Ion Channel TRPA1 Is Required for Normal Mechanosensation and Is Modulated by Algesic Stimuli. *Gastroenterology* **2009**, *137*, 2084–2095. [CrossRef]
78. Nozawa, K.; Kawabata-shoda, E.; Doihara, H.; Kojima, R.; Okada, H.; Mochizuki, S.; Sano, Y.; Inamura, K.; Matsushime, H.; Koizumi, T.; et al. TRPA1 regulates gastrointestinal motility through serotonin release from enterochromaffin cells. *Proc. Natl. Acad. Sci. USA* **2009**, *106*, 3408–3413. [CrossRef]
79. Zielińska, M.; Jarmuz, A.; Wasilewski, A.; Sałaga, M.; Fichna, J. Role of transient receptor potential channels in intestinal inflammation and visceral pain: Novel targets in inflammatory bowel diseases. *Inflamm. Bowel. Dis.* **2015**, *21*, 419–427. [CrossRef]
80. Feng, C.; Yan, X.; Chen, X.; Wang, E.; Liu, Q.; Zhang, L.; Chen, J.; Fang, J.Y.; Chen, S. Vagal anandamide signaling via cannabinoid receptor 1 contributes to luminal 5-HT modulation of visceral nociception in rats. *Pain* **2014**, *155*, 1591–1604. [CrossRef]
81. Malin, S.; Molliver, D.; Christianson, J.A.; Schwartz, E.S.; Cornuet, P.; Albers, K.M.; Davis, B.M. TRPV1 and TRPA1 Function and Modulation are Target Tissue- Dependent. *J. Neurosci.* **2011**, *31*, 10516–10528. [CrossRef]
82. Shen, S.; Al-thumairy, H.W.; Hashmi, F.; Qiao, L. Regulation of transient receptor potential cation channel subfamily V1 protein synthesis by the phosphoinositide 3- kinase/Akt pathway in colonic hypersensitivity. *Exp. Neurol.* **2017**, *295*, 104–115. [CrossRef] [PubMed]
83. Kogure, Y.; Wang, S.; Tanaka, K.I.; Hao, Y.; Yamamoto, S.; Nishiyama, N.; Noguchi, K.; Dai, Y. Elevated H_2O_2 levels in trinitrobenzene sulfate-induced colitis rats contributes to visceral hyperalgesia through interaction with the transient receptor potential ankyrin 1 cation channel. *J. Gastroenterol. Hepatol.* **2016**, *31*, 1147–1153. [CrossRef] [PubMed]
84. Yang, J.; Li, Y.; Zuo, X.; Zhen, Y.; Yu, Y.; Gao, L. Transient receptor potential ankyrin-1 participates in visceral hyperalgesia following experimental colitis. *Neurosci. Lett.* **2008**, *440*, 237–241. [CrossRef] [PubMed]
85. Kistner, K.; Siklosi, N.; Babes, A.; Khalil, M.; Selescu, T.; Zimmermann, K.; Wirtz, S.; Becker, C.; Neurath, M.F.; Reeh, P.W.; et al. Systemic desensitization through TRPA1 channels by capsazepine and mustard oil—A novel strategy against inflammation and pain. *Sci. Rep.* **2016**, *30*, e28621. [CrossRef] [PubMed]
86. Engel, M.A.; Leffler, A.; Niedermirtl, F.; Babes, A.; Tribbensee, S.M.M.; Khalil, M.; Siklosi, N.; Nau, C.; Ivanović-Burmazović, I.; Neuhuber, W.L.; et al. TRPA1 and Substance P Mediate Colitis in Mice. *Gastroenterology* **2011**, *141*, 1346–1358. [CrossRef] [PubMed]
87. Romano, B.; Borrelli, F.; Fasolino, I.; Capasso, R.; Piscitelli, F.; Ii, F.; Domenico, V. The cannabinoid TRPA1 agonist cannabichromene inhibits nitric oxide production in macrophages and ameliorates murine colitis. *Br. J. Pharmacol.* **2013**, *169*, 213–229. [CrossRef] [PubMed]

88. Kojima, R.; Nozawa, K.; Doihara, H.; Keto, Y.; Kaku, H. Effects of novel TRPA1 receptor agonist ASP7663 in models of drug-induced constipation and visceral pain. *Eur. J. Pharmacol.* **2014**, *723*, 288–293. [CrossRef] [PubMed]
89. Mitrovic, M.; Shahbazian, A.; Bock, E.; Pabst, M.A.; Holzer, P. Chemo-nociceptive signalling from the colon is enhanced by mild colitis and blocked by inhibition of transient receptor potential ankyrin 1 channels. *Br. J. Pharmacol.* **2010**, *1*, 1430–1442. [CrossRef] [PubMed]
90. Alvarenga, E.M.; Souza, L.K.M.; Araújo, T.S.L.; Nogueira, K.M.; Sousa, F.B.M.; Araújo, A.R.; Martins, C.; Pacífico, D.M.; de C Brito, G.A.; Souza, E.P.; et al. Carvacrol reduces irinotecan-induced intestinal mucositis through inhibition of inflammation and oxidative damage via TRPA1 receptor activation. *Chem. Biol. Interact.* **2016**, *260*, 129–140. [CrossRef] [PubMed]
91. Kurahara, L.H.; Hiraishi, K.; Hu, Y.; Koga, K.; Onitsuka, M.; Doi, M.; Aoyagi, K.; Takedatsu, H.; Kojima, D.; Fujihara, Y.; et al. Activation of Myofibroblast TRPA1 by Steroids and Pirfenidone Ameliorates Fibrosis in Experimental Crohn's Disease. *Cell. Mol. Gastroenterol. Hepatol.* **2018**, *5*, 299–318. [CrossRef] [PubMed]
92. Koivisto, A.; Jalava, N.; Bratty, R.; Pertovaara, A. TRPA1 antagonists for pain relief. *Pharmaceuticals* **2018**, *11*, 117. [CrossRef] [PubMed]
93. Nummenmaa, E.; Hämäläinen, M.; Moilanen, L.J.; Paukkeri, E.L.; Nieminen, R.M.; Moilanen, T.; Vuolteenaho, K.; Moilanen, E. Transient receptor potential ankyrin 1 (TRPA1) is functionally expressed in primary human osteoarthritic chondrocytes. *Arthritis Res. Ther.* **2016**, *18*, e185. [CrossRef] [PubMed]
94. Horváth, Á.; Tékus, V.; Boros, M.; Pozsgai, G.; Botz, B.; Borbély, É.; Szolcsányi, J.; Pintér, E.; Helyes, Z. Transient receptor potential ankyrin 1 (TRPA1) receptor is involved in chronic arthritis: In vivo study using TRPA1-deficient mice. *Arthritis Res. Ther.* **2016**, *18*, e6. [CrossRef] [PubMed]
95. Moilanen, L.J.; Hämäläinen, M.; Nummenmaa, E.; Ilmarinen, P.; Vuolteenaho, K.; Nieminen, R.M.; Lehtimäki, L.; Moilanen, E. Monosodium iodoacetate-induced inflammation and joint pain are reduced in TRPA1 deficient mice - potential role of TRPA1 in osteoarthritis. *Osteoarthr. Cartil.* **2015**, *23*, 2017–2026. [CrossRef] [PubMed]
96. Fernandes, E.S.; Russell, F.A.; Spina, D.; McDougall, J.J.; Graepel, R.; Gentry, C.; Staniland, A.A.; Mountford, D.M.; Keeble, J.E.; Malcangio, M.; et al. A distinct role for transient receptor potential ankyrin 1, in addition to transient receptor potential vanilloid 1, in tumor necrosis factorα-induced inflammatory hyperalgesia and Freund's complete adjuvant-induced monarthritis. *Arthritis Rheum.* **2011**, *63*, 819–829. [CrossRef]
97. Pereira, L.M.S.; Lima-Júnior, R.C.P.; Bem, A.X.C.; Teixeira, C.G.; Grassi, L.S.; Medeiros, R.P.; Marques-Neto, R.D.; Callado, R.B.; Aragão, K.S.; Wong, D.V.; et al. Blockade of TRPA1 with HC-030031 attenuates visceral nociception by a mechanism independent of inflammatory resident cells, nitric oxide and the opioid system. *Eur. J. Pain* **2013**, *17*, 223–233. [CrossRef]
98. Lowin, T.; Bleck, J.; Schneider, M.; Pongratz, G. Selective killing of proinflammatory synovial fibroblasts via activation of transient receptor potential ankyrin (TRPA1). *Biochem. Pharmacol.* **2018**, *154*, 293–302. [CrossRef]
99. Lowin, T.; Apitz, M.; Anders, S.; Straub, R.H. Anti-inflammatory effects of N-acylethanolamines in rheumatoid arthritis synovial cells are mediated by TRPV1 and TRPA1 in a COX-2 dependent manner. *Arthritis Res. Ther.* **2015**, *17*, e321. [CrossRef]
100. Dalbeth, N.; Merriman, T.R.; Stamp, L.K. Gout. *Lancet* **2016**, *388*, 2039–2052. [CrossRef]
101. Moilanen, L.J.; Hämäläinen, M.; Lehtimäki, L.; Nieminen, R.M.; Moilanen, E. Urate crystal induced inflammation and joint pain are reduced in transient receptor potential ankyrin 1 deficient mice - Potential role for transient receptor potential ankyrin1 in gout. *PLoS ONE* **2015**, *10*, e0117770. [CrossRef]
102. Maruyama, K.; Takayama, Y.; Kondo, T.; Ishibashi, K.; Sahoo, B.R.; Kanemaru, H.; Kumagai, Y.; Martino, M.M.; Tanaka, H.; Ohno, N.; et al. Nociceptors Boost the Resolution of Fungal Osteoinflammation via the TRP Channel-CGRP-Jdp2 Axis. *Cell Rep.* **2017**, *19*, 2730–2742. [CrossRef] [PubMed]
103. Asgar, J.; Zhang, Y.; Saloman, J.L.; Wang, S.; Chung, M.K.; Ro, J.Y. The role of TRPA1 in muscle pain and mechanical hypersensitivity under inflammatory conditions in rats. *Neuroscience* **2015**, *310*, 206–215. [CrossRef] [PubMed]
104. Chung, M.K.; Park, J.; Asgar, J.; Ro, J.Y. Transcriptome analysis of trigeminal ganglia following masseter muscle inflammation in rats. *Mol. Pain* **2016**, *4*, e1744806916668526. [CrossRef] [PubMed]
105. Diogenes, A.; Akopian, A.N.; Hargreaves, K.M. NGF Up-regulates TRPA1: Implications for orofacial pain. *J. Dent. Res.* **2007**, *86*, 550–555. [CrossRef] [PubMed]

106. Wang, S.; Brigoli, B.; Lim, J.; Karley, A.; Chung, M.K. Roles of TRPV1 and TRPA1 in Spontaneous Pain from Inflamed Masseter Muscle. *Neuroscience* **2018**, *384*, 290–299. [CrossRef] [PubMed]
107. Sugiyama, D.; Kang, S.; Brennan, T.J. Muscle reactive oxygen species (ROS) contribute to post-incisional guarding via the TRPA1 receptor. *PLoS ONE* **2017**, *12*, e0170410. [CrossRef] [PubMed]
108. Iannotti, F.A.; Pagano, E.; Moriello, A.S.; Alvino, F.G.; Sorrentino, N.C.; D'Orsi, L.; Gazzerro, E.; Capasso, R.; De Leonibus, E.; De Petrocellis, L.; et al. Effects of non-euphoric plant cannabinoids on muscle quality and performance of dystrophic mdx mice. *Br. J. Pharmacol.* **2019**, *176*, 1568–1584. [CrossRef] [PubMed]
109. Wilson, S.R.; Nelson, A.M.; Batia, L.; Morita, T.; Estandian, D.; Owens, D.M.; Lumpkin, E.A.; Bautista, D.M. The Ion Channel TRPA1 Is Required for Chronic Itch. *J. Neurosci.* **2013**, *33*, 9283–9294. [CrossRef] [PubMed]
110. Kodji, X.; Arkless, K.L.; Kee, Z.; Cleary, S.J.; Aubdool, A.A.; Evans, E.; Caton, P.; Pitchford, S.C.; Brain, S.D. Sensory nerves mediate spontaneous behaviors in addition to inflammation in a murine model of psoriasis. *FASEB J.* **2019**, *33*, 1578–1594. [CrossRef]
111. Fernandes, E.S.; Vong, C.T.; Quek, S.; Cheong, J.; Awal, S.; Gentry, C.; Aubdool, A.A.; Liang, L.; Bodkin, J.V.; Bevan, S.; et al. Superoxide generation and leukocyte accumulation: Key elements in the mediation of leukotriene B4-induced itch by transient receptor potential ankyrin 1 and transient receptor potential vanilloid 1. *FASEB J.* **2013**, *27*, 1664–1673. [CrossRef] [PubMed]
112. Cevikbas, F.; Wang, X.; Akiyama, T.; Kempkes, C.; Savinko, T.; Antal, A.; Kukova, G.; Buhl, T.; Ikoma, A.; Buddenkotte, J.; et al. sensory neuron-expressed IL-31 receptor mediates T helper cell-dependent itch: Involvement of TRPV1 and TRPA. *J. Allergy Clin. Immunol.* **2014**, *133*, 448–460. [CrossRef] [PubMed]
113. Liu, B.; Escalera, J.; Balakrishna, S.; Fan, L.; Caceres, A.I.; Robinson, E.; Sui, A.; McKay, M.C.; McAlexander, M.A.; Herrick, C.A.; et al. TRPA1 controls inflammation and pruritogen responses in allergic contact dermatitis. *FASEB J.* **2013**, *27*, 3549–3563. [CrossRef] [PubMed]
114. Liu, T.; Ru-Rong, J. Oxidative stress induces itch via activation of transient receptor potential subtype ankyrin 1 in mice. *Neurosci. Bull.* **2012**, *28*, 145–154. [CrossRef] [PubMed]
115. Wilson, S.R.; Gerhold, K.A.; Bifolck-Fisher, A.; Liu, Q.; Patel, K.N.; Dong, X.; Bautista, D.M. TRPA1 is required for histamine-independent, Mas-related G protein-coupled receptor-mediated itch. *Nat. Neurosci.* **2011**, *14*, 595–602. [CrossRef] [PubMed]
116. Feng, J.; Yang, P.; Mack, M.R.; Dryn, D.; Luo, J.; Gong, X.; Liu, S.; Oetjen, L.K.; Zholos, A.V.; Mei, Z.; et al. Sensory TRP channels contribute differentially to skin inflammation and persistent itch. *Nat. Commun.* **2017**, *8*, e980. [CrossRef] [PubMed]
117. Oh, M.H.; Oh, S.Y.; Lu, J.; Lou, H.; Myers, A.C.; Zhu, Z.; Zheng, T. TRPA1-Dependent Pruritus in IL-13-Induced Chronic Atopic Dermatitis. *J. Immunol.* **2013**, *191*, 5371–5382. [CrossRef] [PubMed]
118. Moore, C.; Gupta, R.; Jordt, S.E.; Chen, Y.; Liedtke, W.B. Regulation of Pain and Itch by TRP Channels. *Neurosci. Bull.* **2018**, *34*, 120–142. [CrossRef] [PubMed]
119. Conklin, D.J. Acute cardiopulmonary toxicity of inhaled aldehydes: role of TRPA. *Ann. N. Y. Acad. Sci.* **2016**, *1374*, 59–67. [CrossRef] [PubMed]
120. Page, C.P.; Barnes, P.J. Pharmacology and Therapeutics of Asthma and COPD. In *Handbook of Experimental Pharmacology*; Springer International Publishing: Cham, Switzerland, 2017; Volume 237.
121. Zholos, A.; McGarvey, L.; Ennis, M. *TRP Channels as Therapeutic Targets: From Basic Science to Clinical Use*; Elsevier Inc.: London, UK, 2015.
122. Taylor-Clark, T.E.; Undem, B.J. Ozone activates airway nerves via the selective stimulation of TRPA1 ion channels. *J. Physiol.* **2010**, *588*, 423–433. [CrossRef] [PubMed]
123. Lin, A.H.; Liu, M.H.; Ko, H.K.; Perng, D.W.; Lee, T.S.; Kou, Y.R. Lung Epithelial TRPA1 Transduces the Extracellular ROS into Transcriptional Regulation of Lung Inflammation Induced by Cigarette Smoke: The Role of Influxed Ca^{2+}. *Mediat. Inflamm.* **2015**, *2015*, e148367. [CrossRef] [PubMed]
124. Kortekaas Krohn, I.; Callebaut, I.; Alpizar, Y.A.; Steelant, B.; Van Gerven, L.; Skov, P.S.; Kasran, A.; Talavera, K.; Wouters, M.M.; Ceuppens, J.L.; et al. MP29-02 reduces nasal hyperreactivity and nasal mediators in patients with house dust mite-allergic rhinitis. *Allergy* **2018**, *73*, 1084–1093. [CrossRef] [PubMed]
125. Hsu, C.C.; Lee, L.Y. Role of calcium ions in the positive interaction between TRPA1 and TRPV1 channels in bronchopulmonary sensory neurons. *J. Appl. Physiol.* **2015**, *118*, 1533–1543. [CrossRef] [PubMed]
126. Lin, Y.J.; Lin, R.L.; Ruan, T.; Khosravi, M.; Lee, L.Y. A synergistic effect of simultaneous TRPA1 and TRPV1 activations on vagal pulmonary C-fiber afferents. *J. Appl. Physiol.* **2015**, *118*, 273–281. [CrossRef] [PubMed]

127. Alenmyr, L.; Herrmann, A.; Högestätt, E.D.; Greiff, L.; Zygmunt, P.M. TRPV1 and TRPA1 stimulation induces MUC5B secretion in the human nasal airway in vivo. *Clin. Physiol. Funct. Imaging* **2011**, *31*, 435–444. [CrossRef] [PubMed]
128. Prandini, P.; De Logu, F.; Fusi, C.; Provezza, L.; Nassini, R.; Montagner, G.; Materazzi, S.; Munari, S.; Gilioli, E.; Bezzerri, V.; et al. Transient receptor potential ankyrin 1 channels modulate inflammatory response in respiratory cells from patients with cystic fibrosis. *Am. J. Respir. Cell Mol. Biol.* **2016**, *55*, 645–656. [CrossRef] [PubMed]
129. Streng, T.; Axelsson, H.E.; Hedlund, P.; Andersson, D.A.; Jordt, S.E.; Bevan, S.; Andersson, K.E.; Högestätt, E.D.; Zygmunt, P.M. Distribution and Function of the Hydrogen Sulfide-Sensitive TRPA1 Ion Channel in Rat Urinary Bladder. *Eur. Urol.* **2008**, *53*, 391–399. [CrossRef] [PubMed]
130. Silva, R.B.M.; Sperotto, N.D.M.; Andrade, E.L.; Pereira, T.C.B.; Leite, C.E.; De Souza, A.H.; Bogo, M.R.; Morrone, F.B.; Gomez, M.V.; Campos, M.M. Spinal blockage of P/Q-or N-type voltage-gated calcium channels modulates functional and symptomatic changes related to haemorrhagic cystitis in mice. *Br. J. Pharmacol.* **2015**, *172*, 924–939. [CrossRef] [PubMed]
131. Chen, Z.; Du, S.; Kong, C.; Zhang, Z.; Mokhtar, A.D. Intrathecal administration of TRPA1 antagonists attenuate cyclophosphamide-induced cystitis in rats with hyper-reflexia micturition. *BMC Urol.* **2016**, *16*, e33. [CrossRef] [PubMed]
132. Meotti, F.C.; Forner, S.; Lima-Garcia, J.F.; Viana, A.F.; Calixto, J.B. Antagonism of the transient receptor potential ankyrin 1 (TRPA1) attenuates hyperalgesia and urinary bladder overactivity in cyclophosphamide-induced haemorrhagic cystitis. *Chem. Biol. Interact.* **2013**, *203*, 440–447. [CrossRef] [PubMed]
133. Andrade, E.L.; Forner, S.; Bento, A.F.; Ferraz, D.; Leite, P.; Dias, M.A.; Leal, P.C.; Koepp, J.; Calixto, J.B. TRPA1 receptor modulation attenuates bladder overactivity induced by spinal cord injury. *Am. J. Physiol. Renal. Physiol.* **2011**, *300*, 1223–1234. [CrossRef] [PubMed]
134. Kamei, J.; Aizawa, N.; Nakagawa, T.; Kaneko, S.; Kume, H.; Homma, Y.; Igawa, Y. Attenuated lipopolysaccharide-induced inflammatory bladder hypersensitivity in mice deficient of transient receptor potential ankilin. *Sci. Rep.* **2018**, *8*, e15622. [CrossRef] [PubMed]
135. Oyama, S.; Dogishi, K.; Kodera, M.; Kakae, M.; Nagayasu, K.; Shirakawa, H.; Nakagawa, T.; Kaneko, S. Pathophysiological role of transient receptor potential ankyrin 1 in a mouse long-lasting cystitis model induced by an intravesical injection of hydrogen peroxide. *Front. Physiol.* **2017**, *8*, e877. [CrossRef] [PubMed]
136. Chanpimol, S.; Seamon, B.; Hernandez, H.; Harris-love, M.; Blackman, M.R. Effects of Estrogen Receptor β Stimulation in a Rat Model of Non-Bacterial Prostatic Inflammation. *Prostate* **2017**, *77*, 803–811.
137. Lim, J.Y.; Park, C.K.; Hwang, S.W. Biological Roles of Resolvins and Related Substances in the Resolution of Pain. *Biomed. Res. Int.* **2015**, *2015*, e830930. [CrossRef] [PubMed]
138. McNamara, C.R.; Mandel-Brehm, J.; Bautista, D.M.; Siemens, J.; Deranian, K.L.; Zhao, M.; Hayward, N.J.; Chong, J.A.; Julius, D.; Moran, M.M.; et al. TRPA1 mediates formalin-induced pain. *Proc. Natl. Acad. Sci. USA* **2007**, *104*, 13525–13530. [CrossRef] [PubMed]
139. Yue, Z.; Xie, J.; Yu, A.; Stock, J.; Du, J.; Yue, L. Role of TRP channels in the cardiovascular system. *Am. J. Physiol. Heart Circ. Physiol.* **2014**, *308*, H157–H182. [CrossRef] [PubMed]
140. Zhao, J.F.; Shyue, S.K.; Kou, Y.R.; Lu, T.M.; Lee, T.S. Transient receptor potential ankyrin 1 channel involved in atherosclerosis and macrophage-foam cell formation. *Int. J. Biol. Sci.* **2016**, *12*, 812–823. [CrossRef]
141. Ogawa, N.; Kurokawa, T.; Mori, Y. Sensing of redox status by TRP channels. *Cell Calcium* **2016**, *60*, 115–122. [CrossRef]
142. Oehler, B.; Kistner, K.; Martin, C.; Schiller, J.; Mayer, R.; Mohammadi, M.; Sauer, R.S.; Filipovic, M.R.; Nieto, F.R.; Kloka, J.; et al. Inflammatory pain control by blocking oxidized phospholipid-mediated TRP channel activation. *Sci. Rep.* **2017**, *7*, e5447. [CrossRef]
143. Wang, Z.; Wang, M.; Liu, J.; Ye, J.; Jiang, H.; Xu, Y.; Ye, D.; Wan, J. Inhibition of TRPA1 attenuates doxorubicin-induced acute cardiotoxicity by suppressing oxidative stress, the inflammatory response, and endoplasmic reticulum stress. *Oxid. Med. Cell. Longev.* **2018**, *2018*, e5179468. [CrossRef]
144. Wang, Z.; Xu, Y.; Wang, M.; Ye, J.; Liu, J.; Jiang, H.; Ye, D.; Wan, J. TRPA1 inhibition ameliorates pressure overload-induced cardiac hypertrophy and fibrosis in mice. *EBioMedicine* **2018**, *36*, 54–62. [CrossRef] [PubMed]

145. Mergler, S.; Valtink, M.; Takayoshi, S.; Okada, Y.; Miyajima, M.; Saika, S.; Reinach, P.S. Temperature-sensitive transient receptor potential channels in corneal tissue layers and cells. *Ophthalmic. Res.* **2014**, *52*, 151–159. [CrossRef] [PubMed]
146. Acosta, C.M.; Luna, C.; Quirce, S.; Belmonte, C.; Gallar, J. Corneal sensory nerve activity in an experimental model of UV keratitis. *Investig. Ophthalmol. Vis. Sci.* **2014**, *55*, 3403–3412. [CrossRef] [PubMed]
147. Okada, Y.; Shirai, K.; Reinach, P.S.; Kitano-Izutani, A.; Miyajima, M.; Flanders, K.C.; Jester, J.V.; Tominaga, M.; Saika, S. TRPA1 is required for TGF-β signaling and its loss blocks inflammatory fibrosis in mouse corneal stroma. *Lab. Investig.* **2014**, *94*, 1030–1041. [CrossRef]
148. Okada, Y.; Reinach, P.; Shirai, K.; Kitano-Izutani, A.; Miyajima, M.; Yamanaka, O.; Sumioka, T.; Saika, S. Transient Receptor Potential Channels and Corneal Stromal Inflammation. *Cornea* **2015**, *34*, S136–S141. [CrossRef]
149. Katagiri, A.; Thompson, R.; Rahman, M.; Okamoto, K.; Bereiter, D.A. Evidence for TRPA1 involvement in central neural mechanisms in a rat model of dry eye. *Neuroscience* **2015**, *290*, 204–213. [CrossRef]
150. Jensen, T.S.; Madsen, C.S.; Finnerup, N.B. Pharmacology and treatment of neuropathic pains. *Curr. Opin. Neurol.* **2009**, *22*, 467–474. [CrossRef] [PubMed]
151. Brix Finnerup, N.; Hein Sindrup, S.; Staehelin Jensen, T. Management of painful neuropathies. *Handb. Clin. Neurol.* **2013**, *115*, 279–290.
152. Andrade, E.L.; Meotti, F.C.; Calixto, J.B. TRPA1 antagonists as potential analgesic drugs. *Pharmacol. Ther.* **2012**, *133*, 189–204. [CrossRef]
153. Story, G.M.; Gereau, R.W. Numbing the senses: role of TRPA1 in mechanical and cold sensation. *Neuron* **2006**, *50*, 177–180. [CrossRef]
154. Demartini, C.; Greco, R.; Zanaboni, A.M.; Francesconi, O.; Nativi, C.; Tassorelli, C.; Deseure, K. Antagonism of Transient Receptor Potential Ankyrin Type-1 Channels as a Potential Target for the Treatment of Trigeminal Neuropathic Pain: Study in an Animal Model. *Int. J. Mol. Sci.* **2018**, *19*, 3320. [CrossRef] [PubMed]
155. Damasceno, M.B.; de Melo Júnior, J.M.; Santos, S.A.; Melo, L.T.; Leite, L.H.; Vieira-Neto, A.E.; Moreira, R.A.; Monteiro-Moreira, A.C.; Campos, A.R. Frutalin reduces acute and neuropathic nociceptive behaviours in rodent models of orofacial pain. *Chem. Biol. Interact.* **2016**, *256*, 9–15. [CrossRef] [PubMed]
156. Nassini, R.; Fusi, C.; Materazzi, S.; Coppi, E.; Tuccinardi, T.; Marone, I.M.; De Logu, F.; Preti, D.; Tonello, R.; Chiarugi, A.; et al. The TRPA1 channel mediates the analgesic action of dipyrone and pyrazolone derivatives. *Br. J. Pharmacol.* **2015**, *172*, 397–411. [CrossRef] [PubMed]
157. Kim, S.H.; Kim, W.; Kim, J.H.; Woo, M.K.; Baek, J.Y.; Kim, S.Y.; Chung, S.H.; Kim, H.J. A Prospective Study of Chronic Oxaliplatin-Induced Neuropathy in Patients with Colon Cancer: Long-Term Outcomes and Predictors of Severe Oxaliplatin-Induced Neuropathy. *J. Clin. Neurol.* **2018**, *14*, 81–89. [CrossRef] [PubMed]
158. Authier, N.; Balayssac, D.; Marchand, F.; Ling, B.; Zangarelli, A.; Descoeur, J.; Coudore, F.; Bourinet, E.; Eschalier, A. Animal models of chemotherapy-evoked painful peripheral neuropathies. *Neurotherapeutics* **2009**, *6*, 620–629. [CrossRef] [PubMed]
159. Zhou, H.H.; Zhang, L.; Zhou, Q.G.; Fang, Y.; Ge, W.H. (+)-Borneol attenuates oxaliplatin-induced neuropathic hyperalgesia in mice. *NeuroReport* **2016**, *27*, 160–165. [CrossRef] [PubMed]
160. Huang, K.; Bian, D.; Jiang, B.; Zhai, Q.; Gao, N.; Wang, R. TRPA1 contributed to the neuropathic pain induced by docetaxel treatment. *Cell. Biochem. Funct.* **2017**, *35*, 141–143. [CrossRef] [PubMed]
161. Zhao, M.; Isami, K.; Nakamura, S.; Shirakawa, H.; Nakagawa, T.; Kaneko, S. Acute cold hypersensitivity characteristically induced by oxaliplatin is caused by the enhanced responsiveness of TRPA1 in mice. *Mol. Pain* **2012**, *28*, 8–55. [CrossRef] [PubMed]
162. Nassini, R.; Gees, M.; Harrison, S.; De Siena, G.; Materazzi, S.; Moretto, N.; Failli, P.; Preti, D.; Marchetti, N.; Cavazzini, A.; et al. Oxaliplatin elicits mechanical and cold allodynia in rodents via TRPA1 receptor stimulation. *Pain* **2011**, *152*, 1621–1631. [CrossRef]
163. Park, J.H.; Chae, J.; Roh, K.; Kil, E.J.; Lee, M.; Auh, C.K.; Lee, M.A.; Yeom, C.H.; Lee, S. Oxaliplatin-induced Peripheral Neuropathy via TRP1 Stimulation in Mice Dorsal Root Ganglion Is Correlated with Aluminium Accumulation. *PLoS ONE* **2015**, *10*, e0124875.
164. Lee, M.; Cho, S.; Roh, K.; Chae, J.; Park, J.H.; Park, J.; Lee, M.A.; Kim, J.; Auh, C.K.; Yeom, C.H.; et al. Glutathione alleviated peripheral neuropathy in oxaliplatin-treated mice by removing aluminum from dorsal root ganglia. *Am. J. Transl. Res.* **2017**, *9*, 926–939. [PubMed]

165. Obata, K.; Yamanaka, H.; Dai, Y.; Mizushima, T.; Fukuoka, T.; Tokunaga, A.; Noguchi, K. Differential activation of MAPK in injured and uninjured DRG neurons following chronic constriction injury of the sciatic nerve in rats. *Eur. J. Neurosci.* **2004**, *20*, 2881–2895. [CrossRef] [PubMed]
166. Wei, H.; Wu, H.Y.; Chen, Z.; Ma, A.N.; Mao, X.F.; Li, T.F.; Li, X.Y.; Wang, Y.X.; Pertovaara, A. Mechanical antihypersensitivity effect induced by repeated spinal administrations of a TRPA1 antagonist or a gap junction decoupler in peripheral neuropathy. *Pharmacol. Biochem. Behav.* **2016**, *150–151*, 57–67. [CrossRef] [PubMed]
167. Chukyo, A.; Chiba, T.; Kambe, T.; Yamamoto, K.; Kawakami, K.; Taguchi, K.; Abe, K. Oxaliplatin-induced changes in expression of transient receptor potential channels in the dorsal root ganglion as a neuropathic mechanism for cold hypersensitivity. *Neuropeptides* **2018**, *67*, 95–101. [CrossRef] [PubMed]
168. Xie, H.T.; Xia, Z.Y.; Pan, X.; Zhao, B.; Liu, Z.G. Puerarin ameliorates allodynia and hyperalgesia in rats with peripheral nerve injury. *Neural. Regen. Res.* **2018**, *13*, 1263–1268. [CrossRef] [PubMed]
169. Lu, S.; Ma, S.; Wang, Y.; Huang, T.; Zhu, Z.; Zhao, G. Mus musculus-microRNA-449a ameliorates neuropathic pain by decreasing the level of KCNMA1 and TRPA1, and increasing the level of TPTE. *Mol. Med. Rep.* **2017**, *16*, 353–360. [CrossRef] [PubMed]
170. Park, J.; Zheng, L.; Acosta, G.; Vega-Alvarez, S.; Chen, Z.; Muratori, B.; Cao, P.; Shi, R. Acrolein contributes to TRPA1 up-regulation in peripheral and central sensory hypersensitivity following spinal cord injury. *J. Neurochem.* **2015**, *135*, 987–997. [CrossRef] [PubMed]
171. Zhuang, Z.Y.; Wen, Y.R.; Zhang, D.R.; Borsello, T.; Bonny, C.; Strichartz, G.R.; Decosterd, I.; Ji, R.R. A peptide c-Jun N-terminal kinase (JNK) inhibitor blocks mechanical allodynia after spinal nerve ligation: respective roles of JNK activation in primary sensory neurons and spinal astrocytes for neuropathic pain development and maintenance. *J. Neurosci.* **2006**, *26*, 3551–3560. [CrossRef] [PubMed]
172. Lin, Y.; Chen, Z.; Tang, J.; Cao, P.; Shi, R. Acrolein Contributes to the Neuropathic Pain and Neuron Damage after Ischemic-Reperfusion Spinal Cord Injury. *Neuroscience* **2017**, *384*, 120–130. [CrossRef]
173. Chen, Y.; Yang, C.; Wang, Z.J. Proteinase-activated receptor 2 sensitizes transient receptor potential vanilloid 1, transient receptor potential vanilloid 4, and transient receptor potential ankyrin 1 in paclitaxel-induced neuropathic pain. *Neuroscience* **2011**, *193*, 440–451. [CrossRef]
174. Butler, B.; Acosta, G.; Shi, R. Exogenous Acrolein intensifies sensory hypersensitivity after spinal cord injury in rat. *J. Neurol. Sci.* **2017**, *379*, 29–35. [CrossRef] [PubMed]
175. Chen, Z.; Park, J.; Butler, B.; Acosta, G.; Vega-Alvarez, S.; Zheng, L.; Tang, J.; McCain, R.; Zhang, W.; Ouyang, Z.; et al. Mitigation of sensory and motor deficits by acrolein scavenger phenelzine in a rat model of spinal cord contusive injury. *J. Neurochem.* **2016**, *138*, 328–338. [CrossRef] [PubMed]
176. Schäfers, M.; Svensson, C.I.; Sommer, C.; Sorkin, L.S. Tumor necrosis factor-alpha induces mechanical allodynia after spinal nerve ligation by activation of p38 MAPK in primary sensory neurons. *J. Neurosci.* **2003**, *23*, 2517–2521. [CrossRef] [PubMed]
177. Obata, K.; Yamanaka, H.; Kobayashi, K.; Dai, Y.; Mizushima, T.; Katsura, H.; Fukuoka, T.; Tokunaga, A.; Noguchi, K. Role of mitogen-activated protein kinase activation in injured and intact primary afferent neurons for mechanical and heat hypersensitivity after spinal nerve ligation. *J. Neurosci.* **2004**, *24*, 10211–10222. [CrossRef] [PubMed]
178. Wang, C.; Gu, L.; Ruan, Y.; Geng, X.; Xu, M.; Yang, N.; Yu, L.; Jiang, Y.; Zhu, C.; Yang, Y.; et al. Facilitation of MrgprD by TRP-A1 promotes neuropathic pain. *FASEB J.* **2019**, *33*, 1360–1373. [CrossRef]
179. Yamamoto, K.; Chiba, N.; Chiba, T.; Kambe, T.; Abe, K.; Kawakami, K.; Utsunomiya, I.; Taguchi, K. Transient receptor potential ankyrin 1 that is induced in dorsal root ganglion neurons contributes to acute cold hypersensitivity after oxaliplatin administration. *Mol. Pain* **2015**, *11*, e69. [CrossRef] [PubMed]
180. Li, C.; Deng, T.; Shang, Z.; Wang, D.; Xiao, Y. Blocking TRPA1 and TNF-α Signal Improves Bortezomib-Induced Neuropathic Pain. *Cell Physiol. Biochem.* **2018**, *51*, 2098–2110. [CrossRef] [PubMed]
181. Tian, L.; Fan, T.; Zhou, N.; Guo, H.; Zhang, W. Role of PAR2 in regulating oxaliplatin-induced neuropathic pain via TRPA. *Transl. Neurosci.* **2015**, *6*, 111–116. [CrossRef]
182. Chen, K.; Zhang, Z.F.; Liao, M.F.; Yao, W.L.; Wang, J.; Wang, X.R. Blocking PAR2 attenuates oxaliplatin-induced neuropathic pain via TRPV1 and releases of substance P and CGRP in superficial dorsal horn of spinal cord. *J. Neurol. Sci.* **2015**, *352*, 62–97. [CrossRef]
183. Wang, Q.; Wang Gao, D.; Li, J. Inhibition of PAR2 and TRPA1 signals alleviates neuropathic pain evoked by chemotherapeutic bortezomib. *J. Biol. Regul. Homeost. Agents* **2017**, *31*, 977–983.

184. Wu, Z.; Wang, S.; Wu, I.; Mata, M.; Fink, D.J. Activation of TLR-4 to produce tumour necrosis factor-α in neuropathic pain caused by paclitaxel. *Eur. J. Pain* **2015**, *19*, 889–898. [CrossRef] [PubMed]
185. Nassini, R.; Materazzi, S.; Benemei, S.; Geppetti, P. The TRPA1 channel in inflammatory and neuropathic pain and migraine. *Rev. Physiol. Biochem. Pharmacol.* **2014**, *167*, 1–43. [PubMed]
186. Trevisan, G.; Benemei, S.; Materazzi, S.; De Logu, F.; De Siena, G.; Fusi, C.; Fortes Rossato, M.; Coppi, E.; Marone, I.M.; Ferreira, J.; et al. TRPA1 mediates trigeminal neuropathic pain in mice downstream of monocytes/macrophages and oxidative stress. *Brain* **2016**, *139*, 1361–1377. [CrossRef] [PubMed]
187. Materazzi, S.; Fusi, C.; Benemei, S.; Pedretti, P.; Patacchini, R.; Nilius, B.; Prenen, J.; Creminon, C.; Geppetti, P.; Nassini, R. TRPA1 and TRPV4 mediate paclitaxel-induced peripheral neuropathy in mice via a glutathione-sensitive mechanism. *Pflugers Arch.* **2012**, *463*, 561–569. [CrossRef]
188. Nakagawa, T.; Kaneko, S. Roles of Transient Receptor Potential Ankyrin 1 in Oxaliplatin-Induced Peripheral Neuropathy. *Biol. Pharm. Bull.* **2017**, *40*, 947–953. [CrossRef] [PubMed]
189. Miyake, T.; Nakamura, S.; Meng, Z.; Hamano, S.; Inoue, K.; Numata, T.; Takahashi, N.; Nagayasu, K.; Shirakawa, H.; Mori, Y.; et al. Distinct Mechanism of Cysteine Oxidation-Dependent Activation and Cold Sensitization of Human Transient Receptor Potential Ankyrin 1 Channel by High and Low Oxaliplatin. *Front. Physiol.* **2017**, *8*, e878. [CrossRef]
190. Trevisan, G.; Materazzi, S.; Fusi, C.; Altomare, A.; Aldini, G.; Lodovici, M.; Patacchini, R.; Geppetti, P.; Nassini, R. Novel therapeutic strategy to prevent chemotherapy-induced persistent sensory neuropathy by TRPA1 blockade. *Cancer Res.* **2013**, *73*, 3120–3131. [CrossRef]
191. Miao, F.; Wang, R.; Cui, G.; Li, X.; Wang, T.; Li, X. Engagement of MicroRNA-155 in Exaggerated Oxidative Stress Signal and TRPA1 in the Dorsal Horn of the Spinal Cord and Neuropathic Pain During Chemotherapeutic Oxaliplatin. *Neurotox. Res.* **2019**. [CrossRef]
192. Sagalajev, B.; Wei, H.; Chen, Z.; Albayrak, I.; Koivisto, A.; Pertovaara, A. Oxidative Stress in the Amygdala Contributes to Neuropathic Pain. *Neuroscience* **2018**, *387*, 92–103. [CrossRef]
193. De Logu, F.; Nassini, R.; Materazzi, S.; Carvalho Gonçalves, M.; Nosi, D.; Rossi Degl'Innocenti, D.; Marone, I.M.; Ferreira, J.; Li Puma, S.; Benemei, S.; et al. Schwann cell TRPA1 mediates neuroinflammation that sustains macrophage-dependent neuropathic pain in mice. *Nat. Commun.* **2017**, *8*, e1887. [CrossRef]
194. Horváth, Á.; Tékus, V.; Bencze, N.; Szentes, N.; Scheich, B.; Bölcskei, K.; Szőke, É.; Mócsai, A.; Tóth-Sarudy, É.; Mátyus, P.; et al. Analgesic effects of the novel semicarbazide-sensitive amine oxidase inhibitor SZV 1287 in mouse pain models with neuropathic mechanisms: Involvement of transient receptor potential vanilloid 1 and ankyrin 1 receptors. *Pharmacol. Res.* **2018**, *131*, 231–243. [CrossRef] [PubMed]
195. Chung, K.F.; Canning, B.; McGarvey, L. Eight International London Cough Symposium 2014: Cough hypersensitivity syndrome as the basis for chronic cough. *Pulm. Pharmacol. Ther.* **2015**, *35*, 76–80. [CrossRef] [PubMed]
196. Kaneko, Y.; Szallasi, A. Transient receptor potential (TRP) channels: A clinical perspective. *Br. J. Pharmacol.* **2014**, *171*, 2474–2507. [CrossRef] [PubMed]
197. ClinicalTrials.gov. Available online: https://clinicaltrials.gov/ct2/show/NCT02432664 (accessed on 6 May 2019).
198. Eberhardt, M.J.; Schillers, F.; Eberhardt, E.M.; Risser, L.; La Roche, J.D.; Herzog, C.; Echtermeyer, F.; Leffler, A. Reactive metabolites of acetaminophen activate and sensitize the capsaicin receptor TRPV. *Sci. Rep.* **2017**, *7*, e12775. [CrossRef] [PubMed]
199. Schwarz, M.G.; Namer, B.; Reeh, P.W.; Fischer, M.J.M. TRPA1 and TRPV1 antagonists do not inhibit human acidosis-induced pain. *J. Pain* **2017**, *18*, 526–534. [CrossRef] [PubMed]

ANNEX II

Compartmentalized primary cultures of dorsal root ganglion neurons to model peripheral pathophysiological conditions

Simona Giorgi[1], Angela Lamberti[1], Laura Butrón[1], Olivia Gross-Amat[1], David Alarcón-Alarcón[1], Enrique Rodríguez-Cañas[1], Asia Fernández-Carvajal[1], Antonio Ferrer-Montiel[1,*]

[1] Instituto de Investigación, Desarrollo e Innovación en Biotecnología Sanitaria de Elche (IDiBE), Avda de la Universidad s/n, Universidad Miguel Hernández, 03202 Elche, Spain.

* Correspondence: aferrer@umh.es

Mol Pain 2023 Aug 14;17448069231197102.

(Q1, impact factor 3.370)

MOLECULAR PAIN

Molecular Pain
Volume 19: 1–11

DOI: 10.1177/17448069231197102
journals.sagepub.com/home/mpx
Sage

Compartmentalized primary cultures of dorsal root ganglion neurons to model peripheral pathophysiological conditions

Simona Giorgi, Angela Lamberti, Laura Butrón, Olivia Gross-Amat, David Alarcón-Alarcón, Enrique Rodríguez-Cañas, Asia Fernández-Carvajal, and Antonio Ferrer-Montiel

Abstract

Neurosensory disorders such as pain and pruritus remain a major health problem greatly impacting the quality of life, and often increasing the risk of mortality. Current pre-clinical models to investigate dysfunction of sensory neurons have shown a limited clinical translation, in part, by failing to mimic the compartmentalized nociceptor anatomy that exhibits a central compartment containing the soma and a peripheral one harboring the axon endings with distinct molecular and cellular environmental composition. Thus, there is a need to validate compartmentalized preclinical neurosensory models for investigating the pathophysiology of peripheral sensory disorders and to test drug candidates. Here, we have addressed this issue and developed a microfluidic-based preclinical nociceptor model and validated it for investigating inflammatory and neuropathic peripheral disorders. We show that this model reproduces the peripheral sensitization and resolution produced by an inflammatory soup and by the chemotherapeutic drug paclitaxel. Furthermore, compartmentalized nociceptor primary cultures were amenable to co-culture with keratinocytes in the axonal compartment. Interaction of axonal endings with keratinocytes modulated neuronal responses, consistent with a crosstalk between both cell types. These findings pave the way towards translational pre-clinical sensory models for skin pathophysiological research and drug development.

Keywords

Chemotherapy-induced peripheral neuropathy, inflammation, keratinocytes, microfluidics, neuropathy, nociceptor, paclitaxel

Date Received: 13 April 2023; Revised 24 July 2023; accepted: 8 August 2023

Introduction

Sensory neurons are pseudo-unipolar cells with their soma located in the dorsal root (DRGs) or trigeminal ganglia (TG) and the axon exhibiting a dual projection, one towards the periphery to innervate the skin or viscera, and the other to the spinal cord to interact with the brain ascending pathway.[1] *In-vivo*, peripheral endings innervating the skin or viscera are the prime targets of pro-algesic and pruritogenic agents and noxious stimuli coming from the external environment, while the soma and the central terminals are transducers of the neuronal excitability to the brain.[2–4] Thus far, nociceptor peripheral endings have been difficult to study due to their small size and peculiar morphology, despite being the main target for painful, inflammatory and pruritogenic mediators. In contrast, because the soma of the primary afferent neurons are readily accessible to experimentation, virtually all *in-vitro* sensory data have been derived from the cell bodies. These studies assumed that exposure of cell bodies to pro-algesic

Instituto de Investigación, Desarrollo e Innovación en Biotecnología Sanitaria de Elche (IDiBE), Universitas Miguel Hernández, Elche, Spain

Corresponding Author:
Antonio Ferrer-Montiel, Instituto de Investigación, Desarrollo e Innovación en Biotecnología Sanitaria de Elche (IDiBE), Universidad Miguel Hernández de Elche, Av. de la Universidad s/n, Elche 03202, Spain.
Email: aferrer@umh.es

and pruritogenic agents provide reliable and predictable models of the peripheral endings pathophysiology,[5,6] although we are learning that this experimental paradigm has limitations because the main communication *in-vivo* is afferent (i.e. peripheral-central) i.e. complemented with an efferent function (i.e. axon-reflex vasodilatation). In addition, these *in-vitro* models have limited the co-culture of sensory neurons with skin cells due to incompatibility of growing conditions.[7] Thus, it is of pivotal importance to correctly study the neural parts in their appropriate environment, and their interactions with and modulation by the innervated peripheral tissue.

In the past 20 years, microfluidic-based compartmentalized neuronal cultures that enable the separation and study the two major parts of a neuron (i.e. soma and axons), have become an emerging technology to investigate neural function and plasticity.[8] The word "microfluidics" refers to devices presenting a series of microchannels connecting two or more chambers. Microchannels range from one to a few hundred micrometers in size, through which microscopic volumes of fluids can be processed and axons can grow.[9] Microfluidic chambers (MFC) facilitate the study of interactions between axonal endings and tissue cells such as keratinocytes and immune cells, under physiological or pathological conditions.[10–15] They permit the investigation of neuronal excitability, including action potential frequency and velocities.[16,17] Therefore, microfluidic-based, compartmentalized nociceptors primary cultures may provide a suitable preclinical model for investigating the contribution of the neurosensory system to skin pathophysiology and to validate drug candidates that contribute to faster resolution of skin disorders by modulating the neuronal input to the disease.

Here, we investigated whether microfluidic-based compartmentalized nociceptor cultures are suitable models for investigating the pro-algesic and neuropathic sensitization and resolution phases upon their exposure to pro-algesic compounds. We also examined the suitability of MFCs to study the interaction between axonal endings and keratinocytes in co-culture. For this task, we exposed axonal ends to an inflammatory soup or to the chemotherapeutic drug paclitaxel, as representative models of two peripheral disorders. Inflammatory mediators (IMs) have a broad effect on sensory neurons excitability by decreasing the activation threshold of ion channels involved in action potential generation and propagation. Examples of IMs include extracellular protons, arachidonic acid, serotonin, nerve growth factor (NGF), prostaglandins (PG), bradykinin (BK), adenosine triphosphate (ATP) and histamine, among others.[18,19] Most IMs increased the activity of Transient Receptor Potential (TRP channels), by promoting their surface expression and/or facilitating their gating.[20,21] Inflammatory potentiation of thermoTRP channels underlies the hypersensitivity of inflamed tissues.[22,23] Mechanistically, the role of thermoTRPs to inflammatory pain has been performed using non-compartmentalized nociceptor cultures where soma and axons have been exposed to IMs, as opposed to the native conditions where only peripherally expressed receptors are affected by pro-algesic compounds. Similarly, chemotherapeutic drugs such as paclitaxel affect peripheral ends provoking a very disturbing and disabling sensory condition referred to as chemotherapy-induced peripheral neuropathy (CIPN), that may lead to dose reduction or even cessation of treatment.[24–26] Rodent models have shown that paclitaxel increases nociceptor excitability by a variety of mechanisms, including increased neuronal electrogenicity, axonal transport, and axonal degeneration.[24,27] We have reported that paclitaxel directly affects nociceptor function by altering the expression and function of Nav, Kv and thermoTRP channels.[28] However, these studies have been performed in non-compartmentalized chambers were soma and endings were exposed to the drug, thus questioning whether this model provide reliable translational information on the peripheral mechanisms underlying paclitaxel neuropathy. Hence, MFC compartmentalization provides a more translational strategy to investigate the pathophysiological sensitization of axonal terminals. We used this approach and report that compartmentalized MFCs are a valuable tool to investigate peripheral nociceptor sensitization along with the crosstalk between peripheral ends and cutaneous cells.

Material and methods

Animals and ethical statement

All procedures were approved by the Institutional Animal and Ethical Committee of the Miguel Hernández University of Elche, in accordance with the guidelines of the Economic European Community, the National Institutes of Health, and the Committee for Research and Ethical Issues of the International Association for the Study of Pain.

Cell cultures

Primary cultures of DRG and TG sensory neurons were carried out as previously described.[20,29,30] Neurons were seeded in the soma compartment of microfluidic chambers (Millipore devices "AXIS™: Axon Investigation System"). The procedure is detailed in supplementary methods.

Scanning electron microscope

At DIV (days *in vitro*) six of co-culture of DRGs and keratinocytes, the cells were fixed with 2.5% glutaraldehyde (EMS) for 45 min maintaining fluidic isolation between soma and keratinocytes. Afterwards, cells were washed with dH_2O and dehydrated with serial washes of ethanol.[31] Liquid was removed, MFCs were carefully detached from the slide and dried at room temperature for at least 24 h. The slides were coated with chromium and analyzed by the SIGMA 300 VP (Zeiss) field emission scanning electron microscope.

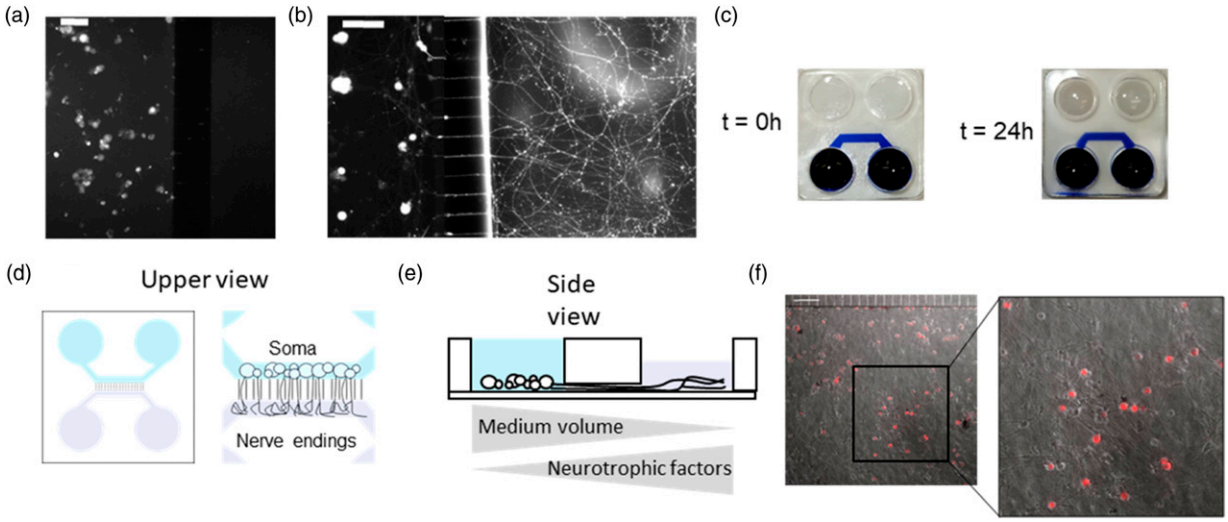

Figure 1. Mouse DRGs cultured in microfluidic chambers (a) DRGs cultured in MFC at DIV 0 loaded with Fluo-4. Scale bar = 100 μm. (b) DRGs cultured in MFC at DIV six loaded with Did'. Scale bar= 100 μm. (c) MFC with 400 μL PBS in the upper compartment and 200 μL blue-coloured PBS in the lower compartment, at time 0 h or 24 h at 37°C (d) Schematic upper view of MFC without cells or with cells and developed axons. (e) Schematic side view of MFC with cells. (f) DRGs cultured in MFC at DIV 6. Merge image of transmitted light and Did' staining (red). Scale bar = 100 μm.

Calcium imaging

Ca^{2+} imaging was used to evaluate the functionality of the sensory neurons and their modulation by the keratinocytes, inflammatory soup and paclitaxel. For these measurements, neuronal activators were added to the axonal chamber, and Ca^{2+} influx monitored in the soma compartment. Methodological details are described in supplementary methods. Analysis of percentage of cells responding to each stimulus was performed considering crossing neurons (Did' and KCl positive) as the total number of cells. The soma KCl response was considered as the maximal Ca^{2+} signal and was used to normalize the size of the responses. An increase in fluorescence was considered a response if it was higher than 10 times the noise of the baseline before adding the stimuli to the axonal compartment or 20 times before the addition of 40 mM KCl in the soma compartment.

Statistical analysis

All data were tested for normal distribution with D'Agostino & Pearson omnibus normality test. Data with normal distribution such as percentage of responses in DRGs or in DRGs co-cultured with keratinocytes were analyzed by two-way ANOVA, Sidak's post-hoc test or with unpaired *t* test (axonal length quantification). All the other data had non-normal distribution and were analyzed by two-tailed Mann-Whitney U or by Kruskal-Wallis test with Dunn's multiple comparisons test in the case of comparing more than two groups at the same time. Statistical analysis was performed using GraphPad Prism 9.4.1 (GraphPad Software Inc.). Throughout the manuscript, data are represented as bars with mean ± SEM while percentage of co-response to two stimuli are expressed as mean values in quantitative Venn diagrams.

Results

In-vitro *compartmentalized axonal sensory endings are functional*

DRGs neurons were seeded in MFCs and a physical and a chemical gradient was established between the compartments to direct axonal growth through microchannels (Figures 1(a)–(e), Table 1). After six DIV, 53 ± 14% neurons (n= 482) extended axons as revealed by Did' labeling (Figure 1(f)), and the axonal endings expressed mRNA of neuronal markers (Figure S1). We observed that 50% of these neurons exhibited Ca^{2+} influx in the soma and triggered electrical activity upon stimulation of axonal endings with 40 mM KCl (ax. KCl) (Figures 2(a) and (b)). Exposure of axonal endings to thermoTRP agonists such as capsaicin, menthol or allyl isothiocyanate (AITC) also evoked action potentials (Figure 3). These chemicals are respectively agonists of the thermoTRP channels TRPV1, TRPM8 and TRPA1.[32–34] Among the Did' labelled neurons, 12.1% responded to 100 nM capsaicin, 9.8% to 100 μM menthol, 7.9% to 100 μM AITC (Figure 2(b)), 1.4% were activated by capsaicin and menthol, 1.6% by capsaicin and AITC, and 3.7% by menthol and AITC (Figure S2). The size of the Ca^{2+} responses was similar for all activating stimuli (Figure 2(c)). As expected, direct stimulation of the neurons cultured on glass coverslips produced higher percentage of response (Figures 2(d) and (e)) and 2-fold larger Ca^{2+} responses (Figure 2(f)). No functional differences were observed between DRG sensory neurons from

Table 1. Media composition for DRGs microfluidic culture.

DIV	Somal compartment 200 µL/well		AXONAL compartment 100 µL/well	
DIV 0	Neurobasal growth medium (Gibco)		Neurobasal growth medium (Gibco)	
	GlutaMAX (gibco)	1%	GlutaMAX (gibco)	1%
	B27 supplement (gibco)	2%	B27 supplement (gibco)	2%
	Penicillin-streptomycin (gibco)	1%	Penicillin-streptomycin (gibco)	1%
	mNGF 25 s (promega)	100 ng/mL	mNGF 25 s (promega)	100 ng/mL
	hGDNF (PeproTech)	100 ng/mL	hGDNF (PeproTech)	100 ng/mL
DIV 1	Neurobasal growth medium (Gibco)		Neurobasal growth medium (Gibco)	
	GlutaMAX (gibco)	1%	GlutaMAX (gibco)	1%
	B27 supplement (gibco)	2%	B27 supplement (gibco)	2%
	Penicillin-streptomycin (gibco)	1%	Penicillin-streptomycin (gibco)	1%
	mNGF 25 s (promega)	50 ng/mL	mNGF 25 s (promega)	100 ng/mL
	hGDNF (PeproTech)	50 ng/mL	hGDNF (PeproTech)	100 ng/mL
	Uridine (sigma)	17.5 µg/mL	Uridine (sigma)	17.5 µg/mL
	5-Fluoro-2'-deoxyuridine (sigma)	7.5 µg/mL	5-Fluoro-2'-deoxyuridine (sigma)	7.5 µg/mL
DIV 3	Neurobasal growth medium (Gibco)		Neurobasal growth medium (Gibco)	
DIV 5	GlutaMAX (gibco)	1%	GlutaMAX (gibco)	1%
	B27 supplement (gibco)	2%	B27 supplement (gibco)	2%
	Penicillin-streptomycin (gibco)	1%	Penicillin-streptomycin (gibco)	1%
	mNGF 25 s (promega)	25 ng/mL	mNGF 25 s (promega)	100 ng/mL
	hGDNF (PeproTech)	25 ng/mL	hGDNF (PeproTech)	100 ng/mL
	Uridine (sigma)	17.5 µg/mL	Uridine (sigma)	17.5 µg/mL
	5-Fluoro-2'-deoxyuridine (sigma)	7.5 µg/mL	5-Fluoro-2'-deoxyuridine (sigma)	7.5 µg/mL

females and males (Figure S2, Tables S4 and S5). Trigeminal sensory neurons were also amenable to culture in MFCs and exhibited a similar functionality than their DRG counterparts (Figure 4).

Keratinocytes interact with axonal sensory endings and modulate their activity

Co-culturing axonal sensory endings with keratinocytes (HaCaT cells), in the presence of 100 ng/mL nerve growth factor (NGF) and 100 ng/mL glial derived neurotrophic factor (GDNF) and the absence of 5-fluoro-2'-deoxyuridine to maintain keratinocyte viability (Table S1, Figure S3), resulted in a strong physical interaction between sensory endings and keratinocytes as revealed by field emission scanning electron microscopy (Figure 2(g)). Electron microscopy images show that peripheral ends form synapse-like contacts with HaCaT cells (Figure 2(h)) or by-pass a particular cell to interact with another as it occurs in the epidermis (Figure 2(i)). Under these conditions up to 70% of neurons extended axons through the microchannels.

Stimulation of the axonal compartment with 40 mM KCl resulted in Ca^{2+} transients in the soma of 70.2% of neurons (Figures 2(j) and (k)). Further analysis revealed that 27.4% of Did′-labelled neurons responded to 100 nM capsaicin, 31.5% to 100 µM menthol, 24.4% to 100 µM AITC (Figure 2(l)), 5% to capsaicin and menthol, 6% to menthol and AITC and 4.4% to capsaicin and AITC (Figure S3). Notably, a higher percentage of neurons responded to capsaicin, menthol and AITC than in the absence of keratinocytes (Figure 2(b), Figure S3, Table S6) and this effect were not due to the medium change in the axonal compartment with respect to the DRGs MFC culture (Table S7). MFC-based DRG cultures and of neurons co-cultured with keratinocytes were exposed to the same NGF and GDNF concentrations to have a comparable neurotrophic effect (Table 1, Table S1). Nonetheless, as human keratinocytes secrete NGF,[35] we cannot exclude that secreted NGF affects neuronal endings length, excitability and thermoTRPs expression.[36,37] The magnitude of the normalized responses was not significantly altered by the presence of the HaCaT cells. These results indicate that keratinocytes increased the number of peripheral ends expressing functional thermoTRPs as well as exhibiting K^+-dependent excitability, suggesting a paracrine increase in axonal growth through microchannels along with a modulation of peripheral endings functionality.

Inflammatory sensitization and resolution of peripheral terminals

Next, we set to validate the microfluidic nociceptor culture as a model to study inflammatory sensitization. We exposed axonal endings to an inflammatory soup or vehicle at DIV five for 24 h (Table S2), and neuronal activity was recorded at DIV six and DIV 8 (0 h and 48 h post insult) to investigate inflammatory sensitization and its resolution. Note that inflammatory mediators reversibly reduced axonal density (Figure S4). Functionally, axonal endings appear to be more active after inflammatory sensitization (Figures. 5(a)–(C)), as reflected by the 2-fold increment in the percentage of neurons

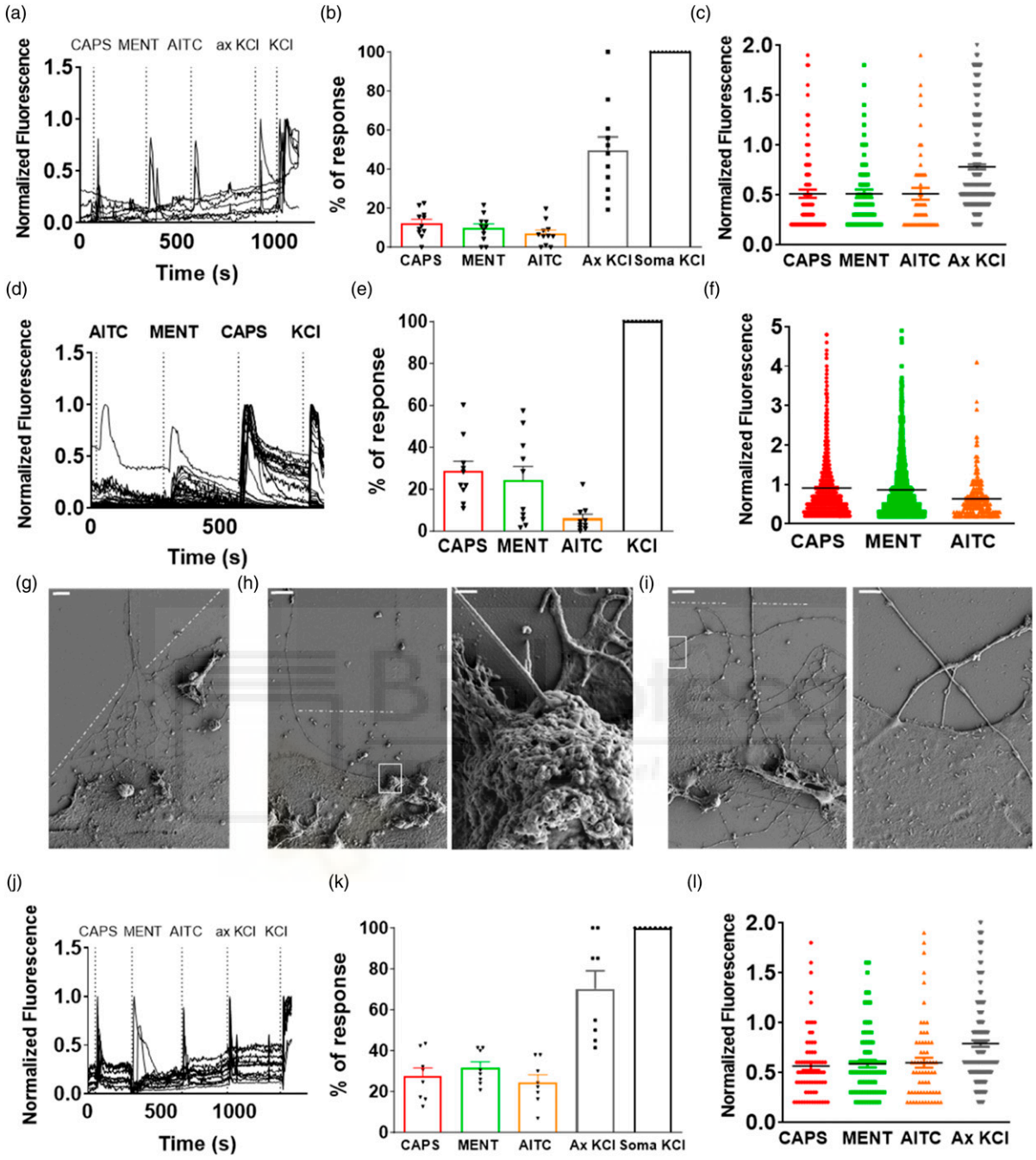

Figure 2. Activity of mouse DRGs cultured in MFCs, non-compartmentalized and co-cultured with human keratinocytes. (a)–(c) Calcium imaging recordings of DRGs cultured in MFC. (a) Representative fluorescent signals recorded in the soma of Did^+ neurons stimulated in the axonal compartment. *Y*-axis represents fluorescence normalized with respect to that evoked by KCl in the soma compartment (KCl). (b) Percentage of response of Did^+ neurons normalized with respect to the response evoked by KCl^+ in the soma. (c) Size of the response normalized with respect to the response evoked by KCl^+ in the soma. Data are as mean ± SEM, every dot is a cell. $N = 4$ animals, two males and two females; $n \geq 2$ coverslips per animal; total number of crossing neurons=747. (d)–(f) Calcium imaging measurements of non-compartmentalized DRGs. (d) Representative fluorescent signals of responsive neurons. *Y*-axis represents fluorescence normalized to that evoked by KCl. (e) Percentage of responses. (f) Size of the response normalized to KCl. Data are mean ± SEM. $N = 4$ mice, two males and two females. $n \geq 2$ coverslips per animal. Total number of neurons= 5498. (g)–(i) Scanning electron microscope pictures of the axonal compartment of co-cultured DRGs with human keratinocytes. The dashed line indicates the end of the microchannels. The white square indicates high magnification views of the selected area. Scale bars: 100 μm (g), 10 μm and 500 nm (h), and 10 and 2 μm (i). (j)–(l) Calcium imaging measurements of co-cultured DRGs with keratinocytes. (j) Representative fluorescent signals of responsive neurons. (k) Percentage of response of Did^+ neurons normalized with respect to the response evoked by KCl^+ in the soma. Mean ± SEM. (l) Size of the response normalized with respect to the response evoked by KCl^+ in the soma. Data are mean ± SEM, every dot is a cell. DRGs-keratinocytes co-culture: $N = 4$ animals, two males and two females; $n = 2$ coverslips per animal; total number of crossing neurons = 298.

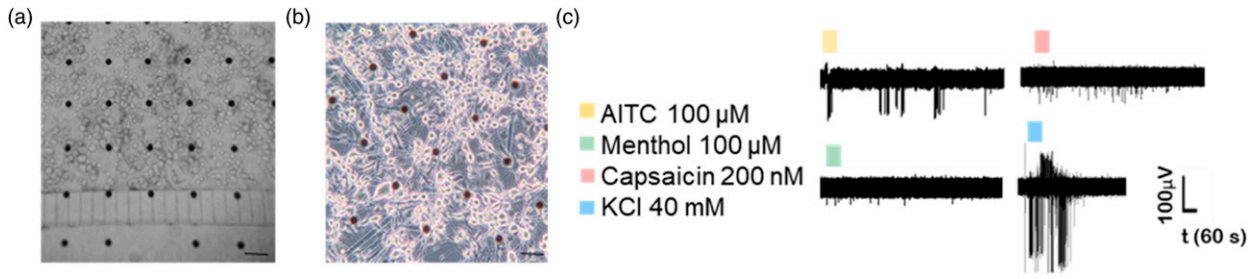

Figure 3. mDRGs cultured in microfluidic chambers coupled to a MEA chip. (a) Picture of cells at DIV 0 (b) Picture of cells at DIV 6 (c) Spikes obtained from mDRGs stimulated with AITC 100 µM, menthol 100 µM, capsaicin 200 nM or KCl 40 mM.

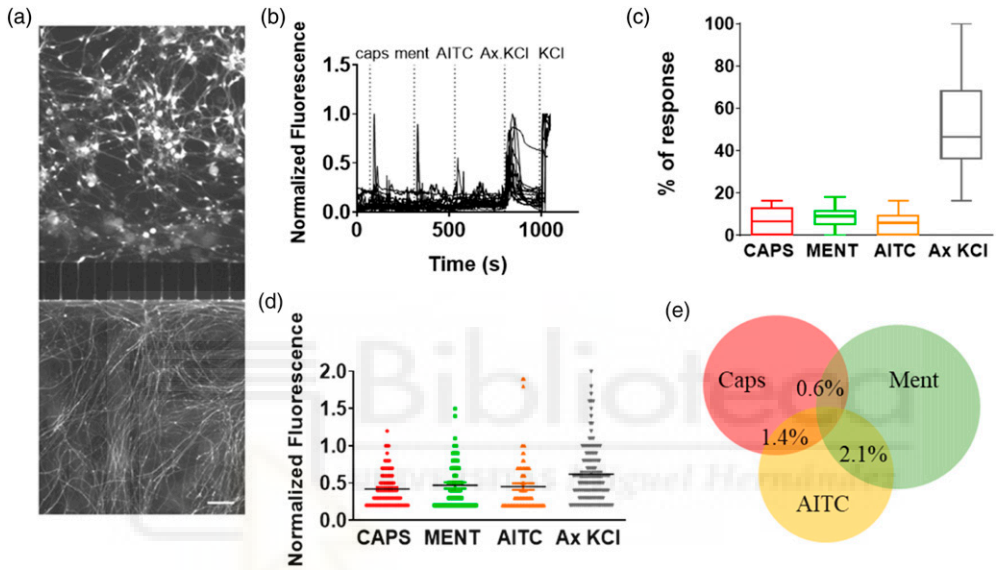

Figure 4. Trigeminal culture in microfluidic chambers (a) TG cultured in microfluidic chambers at DIV six loaded with Fluo-4. Scale bar = 100 µm. (b) Representative traces of neurons responding to capsaicin, menthol, AITC or axonal KCl. *N* = 4 mice, two males and two females. $n \geq 2$ MFC per animal. Total number of crossing neurons= 740. (c) Quantification of the percentage of response to capsaicin, menthol, AITC or axonal KCl normalized to KCl response. (d) Quantification of the size of the response normalized to KCl response. Data are represented as scatter dot plot, mean ± SEM. (e) Quantification of the percentage of response to capsaicin and menthol, menthol and AITC or capsaicin and AITC normalized to KCl response. Data are represented as quantitative Venn Diagram.

responding to 100 nM capsaicin, 100 µM menthol, and 100 µM AITC (Figure 5(d)). This sensitization was reversible, resolving 48 h post-inflammatory insult (DIV 8, Figure 5(d)). Notice that the percentage of neurons exposed to vehicle responding to capsaicin remained constant up to DIV 8, whereas a significant decrease was observed for the responses to menthol, AITC and KCl (Figure 5(d)). This reduction in responses may reflect the neural aging that intriguingly affected less to TRPV1 sensory neurons. The inflammatory soup increased the responses to capsaicin and menthol from 1.8% to 9%, to capsaicin and AITC from 1.6% to 8.7% and to menthol and AITC from 3.7% to 9.8% after 24 h exposure (Figures 5(e) and (f)). This increment in dual responses resolved to basal level 48 h after inflammatory exposure (DIV8) (Figures 5(g) and (h)).

The size of the capsaicin response was significantly augmented by exposure to the inflammatory soup for 24 h, resolving 48 h after removal of the soup (Figure 5(i)). A similar increment was observed for AITC, but not for menthol (Figure 5(i)). KCl responses did not show a significant change after 24 h exposure to the inflammatory soup, but we observed that at DIV eight sensory terminals that were incubated with the inflammatory soup exhibited higher KCl responses than those exposed to the vehicle (Figure 5(i)). Akin to the number of neurons responding to KCl at DIV 8 (Figure 5(d)), we also observed a significant reduction in the magnitude of the KCl-evoked Ca^{2+} transients incubated with vehicle (Figure 5(i)), most likely due to a reduction of responding neurons due to aging of the primary culture.

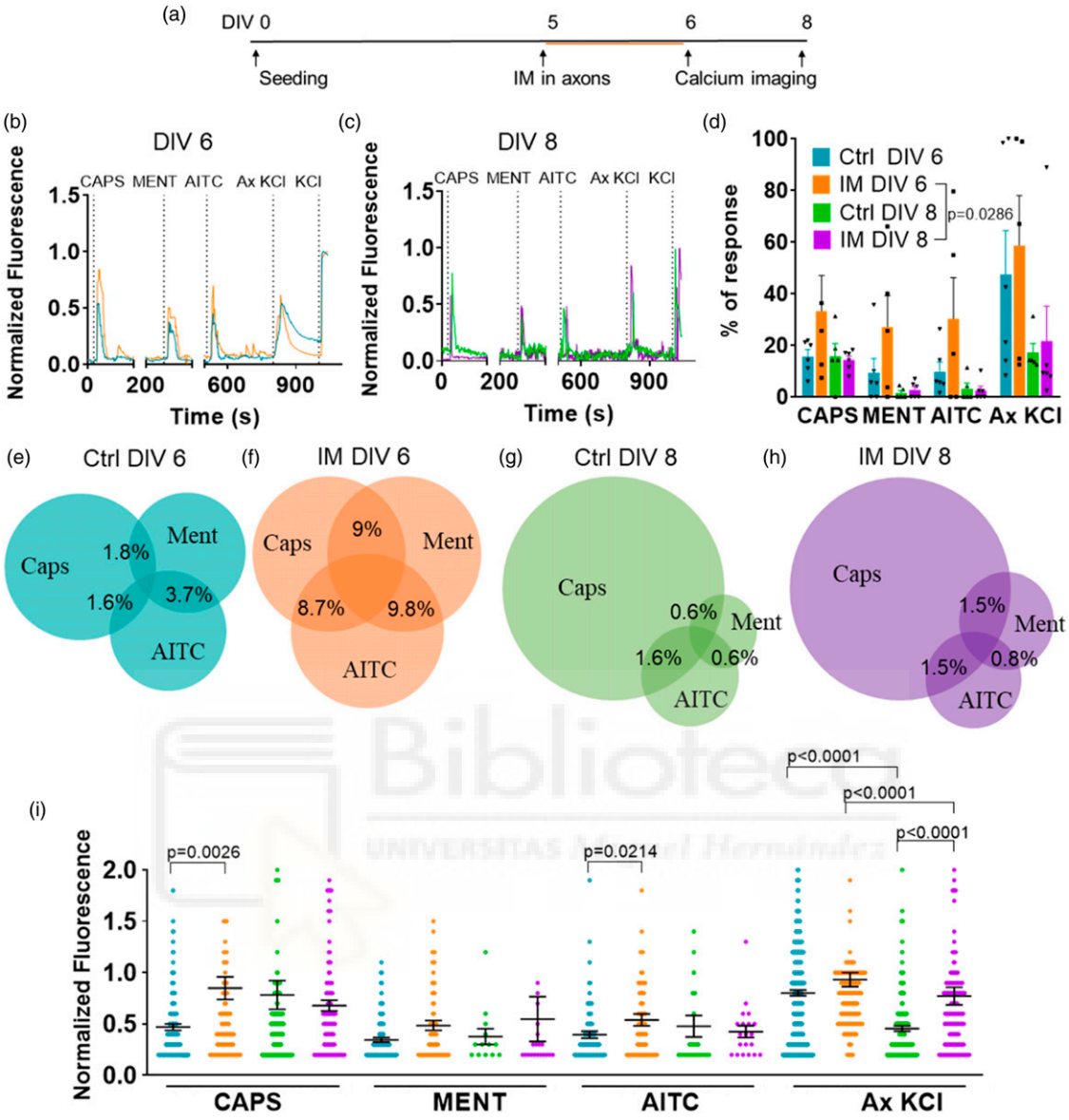

Figure 5. Effect of inflammatory mediators (IM) on DRGs nerve endings. (a) Treatment and assays timeline. Axons were treated with inflammatory mediators or vehicle at DIV five and recorded at DIV six or DIV8. (b)–(c) Representative traces of responsive neurons. *Y* axes represents fluorescence normalized to somal KCl response. (d) Percentage of response normalized to Did+ and somal KCl responsive cells. Mean ± SEM. Statistical analysis two-tailed Mann-Whitney U. (e)–(h) Responses to capsaicin and menthol, menthol and AITC or capsaicin and AITC normalized to KCl response in the soma. (i) Size of the response normalized to somal KCl response. Mean ± SEM, every dot represents a cell. Statistical analysis two-tailed Mann-Whitney U. *N*=6 animals, three males and three females; $n \geq 3$ coverslips per animal; total number of crossing neurons=3018.

Neuropathic sensitization and resolution of peripheral ends

Exposure of nociceptor primary cultures to paclitaxel for 24 h produced a significant increase in neuronal activity that peaked 48 h after removal of the chemotherapeutic drug and mitigated 96 h after exposure.[28] Here, we questioned if a similar sensitization-resolution occurs when the drug is applied onto axonal endings. To investigate the impact of the drug on the peripheral ends, we exposed them to 1 µM paclitaxel (PTX) or vehicle (DMSO 0.04%) for 24 h (DIV6, Table S3). PTX was removed, and neuronal functionality was recorded 48 (DIV8) and 96 h (DIV10) after drug removal (Figure 6(a)). As exhibited in Figure S8, paclitaxel reversibly reduced axonal density, being the strongest effect just after treatment and fully resolving 96 h post-treatment.

Functional analysis revealed that 40 mM KCl in the axonal compartment evoked activity in 20% of neurons at DIV 8 and 10. Paclitaxel did not significantly affect the percentage of

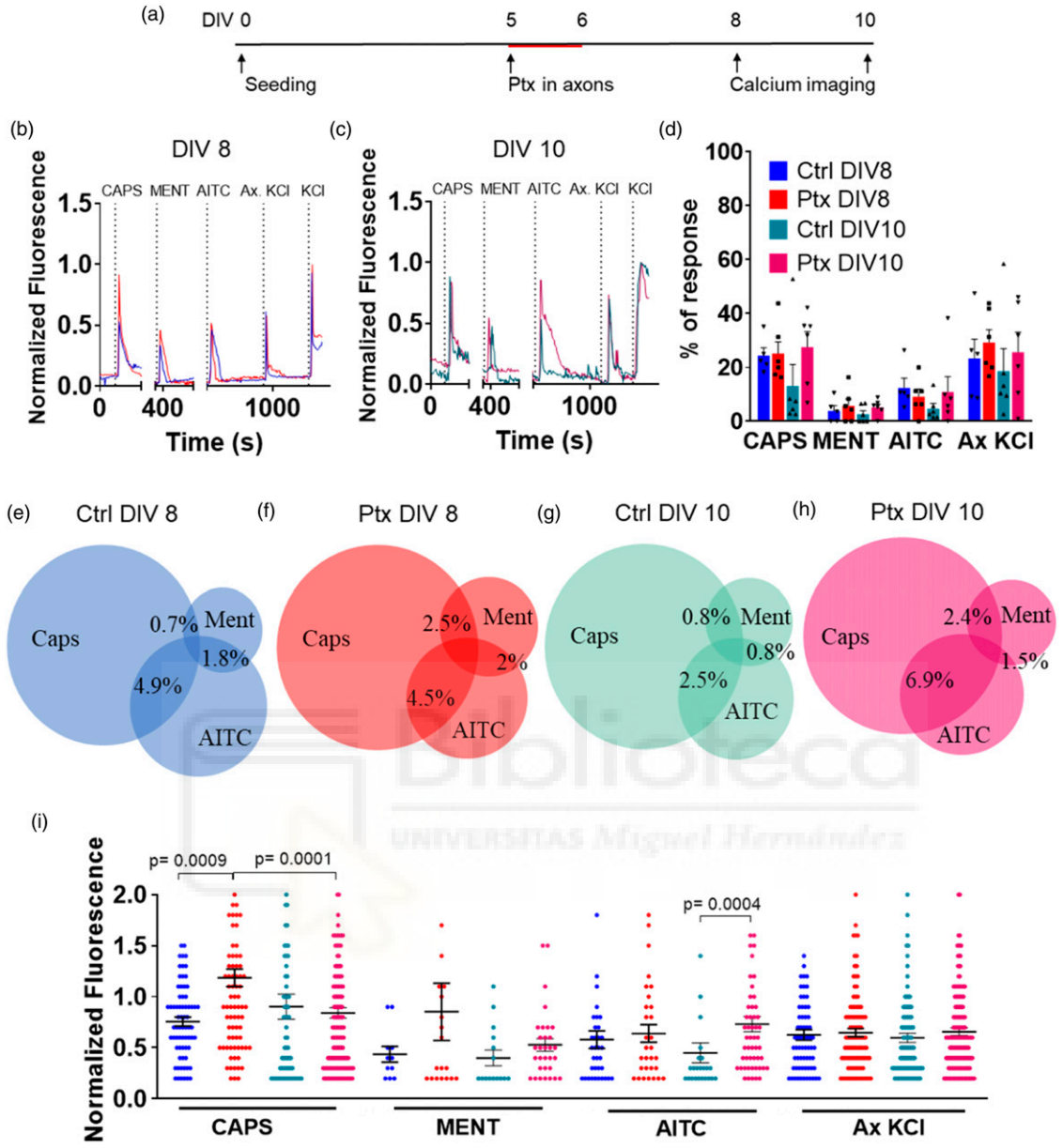

Figure 6. Effect of paclitaxel 1 μM on mDRGs cultured in microfluidic chambers. (a) Treatment and assays timeline (b)–(c) Representative traces of responsive neurons. *Y* axes represents fluorescence normalized to somal KCl response. (d) Percentage of response normalized to Did+ and somal KCl+ responsive cells. Mean ± SEM. (e)–(h) Responses to capsaicin and menthol, menthol and AITC or capsaicin and AITC normalized to somal KCl response. (i) Size of the response normalized to KCl. Mean ± SEM, every dot represents a cell. Statistical analysis two-tailed Mann-Whitney U. $N = 5$ animals, three males and two females; $n \geq 2$ coverslips per animal; total number of crossing neurons = 1638.

functional neurons, activated by capsaicin, menthol, AITC and KCl (Figures 6(b)–(d)). Similarly, terminals responding to two agonists was mildly affected by the chemotherapeutic drug (Figures 6(e)–(H)). In marked contrast, we observed a significant increase in the size of capsaicin responses at DIV eight that resolved at DIV 10 in agreement with previous results (Figure 6(i)).[28] Menthol responses show a tendency to increase 48 h after paclitaxel exposure but did not reach statistical significance. Nonetheless, the cellular distribution suggests the presence of two menthol sensitive subpopulations that deserves further investigation. Higher responses for AITC were observed 96 h (DIV 10) after paclitaxel incubation. Overall, these results substantiate a peripheral action of paclitaxel sensitizing neural endings, consistent with the sensory symptoms provoked by the chemotherapeutic drug.

Conclusions and perspectives

Our findings substantiate that compartmentalized sensory neurons in microfluidic chambers are suitable models to

investigate the interaction of the sensory endings with dermal cells, as well as to study the mechanisms involved in their peripheral sensitization either by pro-inflammatory and neuropathic drugs. A salient contribution of our study is that sensory neurons from DRGs and TGs can be successfully cultured in MFCs for up to 10 DIV, allowing to investigate nociceptor potentiation and its resolution. Furthermore, we established that axonal endings in these cultures serve as models for studying free nociceptive nerve endings and their modulation by trophic and pro-algesic agents. Our findings reinforce and build upon the existing body of knowledge regarding the viability and functionality of sensory neurons in MFCs, highlighting their relevance as a translational model for investigating peripheral nociceptive mechanisms underlying sensitization and desensitization.[14,38,39]

Moreover, co-cultures of nerve endings and keratinocytes represent a proof of concept for investigating the interaction and cross-talk of axonal ends with peripheral cells and tissues. We found that keratinocytes modulate axonal function, most likely by releasing growth factors such as NGF that affect axonal excitability.[35] Thus, compartmentalized cultures provide a strategy to investigate the contribution of nociceptive endings in peripheral neuropathies that lead to cutaneous and visceral pain. In this regard, our inflammation and neuropathic models demonstrate that the axonal compartment can be sensitized by manipulating the environmental composition mimicking an inflammatory soup or the presence of a chemotherapeutic drug. We found that both conditions increase the activity of the peripheral ends by enhancing the functionality of thermoTRP channels leading to a higher excitability. Thus, the effect of IMs and chemotherapeutic drugs on DRG function can be primarily assigned to a peripheral action. MFC-based cultures also permit to investigate the effect of the milieu composition on the integrity/size of the axonal endings, that is if compounds produce axonal retraction. Not least, MCFs allow also to evaluate axonal transport to and from the periphery,[27] and to test the effect of peripherally acting drugs.[40]

Compartmentalized culture methods present numerous advantages, such as being able to expose axons to a different fluid and cellular environment than cell bodies, which is useful for studies of trophic, ionic, and pharmacological regulation. Specifically, in the case of nociceptors, it is of vital importance to separate the soma from the nerve endings because of their peculiar anatomy *in-vivo*. In fact, whereas only the peripheral terminal of the nociceptor will respond to environmental stimuli, both the peripheral and central terminals can be targeted by endogenous molecules.[5,8] Furthermore, distal axons can be removed performing an axotomy, and subsequently regenerated, which permits many useful approaches to the study of axon growth and regeneration after damage.[8,14]

These models hold great promise for the future of sensory neurons and pain investigation and open to the possibility of culturing induced sensory neurons (iSNs) derived from human cells. Using iSNs could reduce the use of animals and avoid problems of unreliability and low translationality of animal experimentation.[41,42] Culturing these cells in microfluidic chambers would increase the representativity of the model making it more similar to the *in-vivo* morphology of sensory neurons.

Author contributions

S.G. conceived the idea, performed all the experiments, wrote and revised the manuscript; A.L. performed DRGs culture and paclitaxel treatment; L.B. performed DRGs culture; O.G. wrote and revised the manuscript; D.A.A. performed DRG and TG culture and calcium imaging; E.R.C contributed to samples preparation and took electron microscope pictures; A.F.C. and A.F.M. supervised the project and data, and revised the manuscript. All authors provided critical feedback and helped improve the research's quality.

Declaration of conflicting interests

The author(s) declared no potential conflicts of interest with respect to the research, authorship, and/or publication of this article.

Funding

The author(s) disclosed receipt of the following financial support for the research, authorship, and/or publication of this article: This work was supported by the S.G. was financed by Generalitat Valenciana [GRISOLIAP/2019/094 44/19]; A.L. received funding from the European Union's Horizon 2020 research and innovation programme under the Marie Skłodowska-Curie Actions [No 956477]; Spanish Ministry of Science, Innovation and Universities financed L.B. [MCI-PID2021-126423OB-C21]; O.G. received funding from Generalitat Valenciana [GVA-PROMETEO/2021/031]; D.A.A. was financed by the Spanish Ministry of Science, Innovation and Universities [AF2015-66275-C2-1-R]; E.R.C. was financed by the Spanish Ministry of Science, Innovation and Universities [PTA2018-015394-I]. The FESEM equipment was funded by Generalitat Valenciana [GVA-IDIFEDER_2018/020]; Financial support of the Spanish Ministry of Science, Innovation and Universities [RTI2018-097189-B-C21] and Miguel Hernández University of Elche [UMH-PAR2019] was granted to to A.F.C. and A.F.M.

ORCID iD

Simona Giorgi https://orcid.org/0000-0001-9431-6759

Supplemental Material

Supplemental material for this article is available online.

References

1. Koop LK, Tadi P. Neuroanatomy, sensory nerves. 2022. In: *StatPearls*. Treasure Island, FL: StatPearls Publishing, 2023 Jan. PMID: 30969668.
2. Debanne D, Campanac E, Bialowas A, Carlier E, Alcaraz G. Axon physiology. *Physiol Rev* 2011; 91(2): 555–602. PMID: 21527732.

3. Kandel ER, Schwartz JH, Jessell TM. *Principles of neural science*. 4th ed.. New York: McGraw-Hill Health Professions Division, 2000.
4. Nascimento AI, Mar FM, Sousa MM. The intriguing nature of dorsal root ganglion neurons: linking structure with polarity and function. *Prog Neurobiol* 2018; 168: 86–103. PMID: 29729299.
5. Basbaum AI, Bautista DM, Scherrer G, Julius D. Cellular and molecular mechanisms of pain. *Cell* 2009; 139(2): 267–284. PMCID: PMC2852643.
6. Dubin AE, Patapoutian A. Nociceptors: the sensors of the pain pathway. *J Clin Invest. American Society for Clinical Investigation* 2010; 120(11): 3760–3772. PMID: 21041958.
7. Malak M, Grantham J, Ericson MB. Monitoring calcium-induced epidermal differentiation in vitro using multiphoton microscopy. *J Biomed Opt* 2020; 25(7): 071205. PMCID: PMC7210787.
8. Campenot RB, Martin G. Construction and use of compartmented cultures for studies of cell biology of neurons. In: Fedoroff S, Richardson A (eds). *Protocols for Neural Cell Culture*. Totowa, NJ: Humana Press, 2001, pp. 49–57.
9. Gross PG, Kartalov EP, Scherer A, Weiner LP. Applications of microfluidics for neuronal studies. *J Neurol Sci* 2007; 252(2): 135–143. PMID: 17207502.
10. Clark AJ, Menendez G, AlQatari M, Patel N, Arstad E, Schiavo G, Koltzenburg M. Functional imaging in microfluidic chambers reveals sensory neuron sensitivity is differentially regulated between neuronal regions. *Pain* 2018; 159(7): 1413–1425. PMID: 29419650.
11. Hosmane S, Yang IH, Ruffin A, Thakor N, Venkatesan A. Circular compartmentalized microfluidic platform: study of axon-glia interactions. *Lab Chip* 2010; 10(6): 741–747. PMID: 20221562.
12. Miny L, Maisonneuve BGC, Quadrio I, Honegger T. Modeling neurodegenerative diseases using in vitro compartmentalized microfluidic devices. *Front Bioeng Biotechnol* 2022; 10: 919646. PMID: 35813998; PMCID: PMC9263267.
13. Saliba J, Daou A, Damiati S, Saliba J, El-Sabban M, Mhanna R. Development of microplatforms to mimic the in vivo architecture of CNS and PNS physiology and their diseases. *Genes. Multidisciplinary Digital Publishing Institute* 2018; 9(6): 285. PMID: 29882823; PMCID: PMC6027402.
14. Tsantoulas C, Farmer C, Machado P, Baba K, McMahon SB, Raouf R. Probing functional properties of nociceptive axons using a microfluidic culture system. *PLoS One* 2013; 8(11): e80722. PMCID: PMC3835735.
15. Varier P, Raju G, Madhusudanan P, Jerard C, Shankarappa SA. A brief review of in vitro models for injury and regeneration in the peripheral nervous system. *Int J Mol Sci* 2022; 23(2): 816. Multidisciplinary Digital Publishing Institute. PMID: 35055003; PMCID: PMC8775373.
16. Levi T, Fujii T. Microfluidic neurons, a new way in neuromorphic engineering? Micromachines. *Multidisciplinary Digital Publishing Institute* 2016; 7(8): 146. PMID: 30404317; PMCID: PMC6189925.
17. Mateus JC, Lopes C, Aroso M, Costa AR, Gerós A, Meneses J, Faria P, Neto E, Lamghari M, Sousa MM, Aguiar P. Bidirectional flow of action potentials in axons drives activity dynamics in neuronal cultures. *J Neural Eng* 2021; 6: 18. PMID: 34891149.
18. Fernández-Carvajal A, González-Muñiz R, Fernández-Ballester G, Ferrer-Montiel A. Investigational drugs in early phase clinical trials targeting thermotransient receptor potential (thermoTRP) channels. *Expert Opin Investig Drugs* 2020; 29(11): 1209–1222. PMID: 32941080.
19. Moore C, Gupta R, Jordt SE, Chen Y, Liedtke WB. Regulation of pain and itch by TRP channels. *Neurosci Bull* 2018; 34(1): 120–142. PMID: 29282613; PMCID: PMC5799130.
20. Devesa I, Ferrándiz-Huertas C, Mathivanan S, Wolf C, Luján R, Changeux JP, Ferrer-Montiel A. αCGRP is essential for algesic exocytotic mobilization of TRPV1 channels in peptidergic nociceptors. *Proc Natl Acad Sci U S A* 2014; 111(51): 18345–18350. PMID: 25489075; PMCID: PMC4280602.
21. Camprubí-Robles M, Planells-Cases R, Ferrer-Montiel A. Differential contribution of SNARE-dependent exocytosis to inflammatory potentiation of TRPV1 in nociceptors. *FASEB J* 2009; 23(11): 3722–3733. PMID: 19584302.
22. Startek JB, Boonen B, Talavera K, Meseguer V. TRP channels as sensors of chemically-induced changes in cell membrane mechanical properties. *Int J Mol Sci* 2019; 20(2): 371. Multidisciplinary Digital Publishing Institute. PMID: 30654572; PMCID: PMC6359677.
23. Ji RR, Nackley A, Huh Y, Terrando N, Maixner W. Neuroinflammation and central sensitization in chronic and widespread pain. *Anesthesiology* 2018; 129(2): 343–366. PMID: 29462012; PMCID: PMC6051899.
24. Zajączkowska R, Kocot-Kępska M, Leppert W, Wrzosek A, Mika J, Wordliczek J. Mechanisms of chemotherapy-induced peripheral neuropathy. *Int J Mol Sci* 2019; 20(6): 1451. PMID: 30909387; PMCID: PMC6471666.
25. Seretny M, Currie GL, Sena ES, Ramnarine S, Grant R, MacLeod MR, Colvin LA, Fallon M. Incidence, prevalence, and predictors of chemotherapy-induced peripheral neuropathy: a systematic review and meta-analysis. *Pain* 2014; 155(12): 2461–2470. PMID: 25261162.
26. Colvin LA. Chemotherapy-induced peripheral neuropathy: where are we now? *Pain*. 2019;160(Suppl 1): S1–S10. PMID: 31008843; PMCID: PMC6499732.
27. Waxman SG, Zamponi GW. Regulating excitability of peripheral afferents: emerging ion channel targets. *Nat Neurosci* 2014; 17(2): 153–163. PMID: 24473263.
28. Villalba-Riquelme E, de la Torre-Martínez R, Fernández-Carvajal A, Ferrer-Montiel A. Paclitaxel in vitro reversibly sensitizes the excitability of IB4(−) and IB4(+) sensory neurons from male and female rats. *Br J Pharmacol* 2022; 179(14): 3693–3710. PMID: 35102580; PMCID: PMC9311666.
29. Alarcón-Alarcón D, Cabañero D, de Andrés-López J, Nikolaeva-Koleva M, Giorgi S, Fernández-Ballester G, Fernández-Carvajal A, Ferrer-Montiel A. TRPM8 contributes to sex dimorphism by promoting recovery of normal sensitivity

in a mouse model of chronic migraine. *Nat Commun* 2022; 13(1): 6304. Nature Publishing Group. PMID: 36272975; PMCID: PMC9588003.
30. Sleigh JN, Weir GA, Schiavo G. A simple, step-by-step dissection protocol for the rapid isolation of mouse dorsal root ganglia. *BMC Res Notes* 2016; 9: 82. PMID: 26864470; PMCID: PMC4750296.
31. Domínguez-Bajo A, Rosa JM, González-Mayorga A, Rodilla BL, Arché-Núñez A, Benayas E, Ocón P, Pérez L, Camarero J, Miranda R, González MT, Aguilar J, López-Dolado E, Serrano MC. Nanostructured gold electrodes promote neural maturation and network connectivity. *Biomaterials* 2021; 279: 121186. PMID: 34700221.
32. Nagata K, Duggan A, Kumar G, García-Añoveros J. Nociceptor and hair cell transducer properties of TRPA1, a channel for pain and hearing. *J Neurosci* 2005; 25(16): 4052–4061. PMID: 15843607; PMCID: PMC6724946.
33. McKemy DD, Neuhausser WM, Julius D. Identification of a cold receptor reveals a general role for TRP channels in thermosensation. *Nature*. 2002;416(6876):52–58. PMID: 11882888
34. Caterina MJ, Rosen TA, Tominaga M, Brake AJ, Julius D. A capsaicin-receptor homologue with a high threshold for noxious heat. *Nature* 1999; 398(6726): 436–441. PMID: 10201375.
35. Yaar M, Grossman K, Eller M, Gilchrest BA. Evidence for nerve growth factor-mediated paracrine effects in human epidermis. *J Cell Biol* 1991; 115(3): 821–828. PMID: 1655813; PMCID: PMC2289176.
36. Barker PA, Mantyh P, Arendt-Nielsen L, Viktrup L, Tive L. Nerve growth factor signaling and its contribution to pain. *J Pain Res* 2020; 13: 1223–1241. PMID: 32547184; PMCID: PMC7266393.
37. Lentz SI, Knudson CM, Korsmeyer SJ, Snider WD. Neurotrophins support the development of diverse sensory axon morphologies. *J Neurosci* 1999; 19(3): 1038–1048. PMID: 9920667; PMCID: PMC6782147.
38. Neto E, Alves CJ, Sousa DM, Alencastre IS, Lourenço AH, Leitão L, Ryu HR, Jeon NL, Fernandes R, Aguiar P, Almeida RD, Lamghari M. Sensory neurons and osteoblasts: close partners in a microfluidic platform. *Integr Biol* 2014; 6(6): 586–595. PMID: 24675920.
39. Baker CA, Tyagi S, Higerd-Rusli GP, Liu S, Zhao P, Dib-Hajj FB, Waxman SG, Dib-Hajj SD. Paclitaxel effects on axonal localization and vesicular trafficking of NaV1.8. *Front Mol Neurosci* 2023; 16: 1130123. PMID: 36860665; PMCID: PMC9970094.
40. Nikolaeva-Koleva M, Butron L, González-Rodríguez S, Devesa I, Valente P, Serafini M, Genazzani AA, Pirali T, Ballester GF, Fernández-Carvajal A, Ferrer-Montiel A. A capsaicinoid-based soft drug, AG1529, for attenuating TRPV1-mediated histaminergic and inflammatory sensory neuron excitability. *Sci Rep* 2021; 11: 246. PMID: 33420359; PMCID: PMC7794549.
41. Akhtar A. The flaws and human harms of animal experimentation. *Camb Q Healthc Ethics* 2015; 24(4): 407–419. PMID: 26364776; PMCID: PMC4594046.
42. Haberberger RV, Barry C, Dominguez N, Matusica D. Human Dorsal Root Ganglia. *Front Cell Neurosci* 2019; 13: 271. PMID: 31293388; PMCID: PMC6598622.
43. Newberry K, Wang S, Hoque N, Kiss L, Ahlijanian MK, Herrington J, Graef JD. Development of a spontaneously active dorsal root ganglia assay using multiwell multielectrode arrays. *J Neurophysiol* 2016; 115(6): 3217–3228. PMID: 27052585; PMCID: PMC4946598.
44. Zhao X, Zhou Y, Weissmiller AM, Pearn ML, Mobley WC, Wu C. Real-time imaging of axonal transport of quantum dot-labeled BDNF in primary neurons. *J Vis Exp* 2014; 91: 51899. PMID: 25286194; PMCID: PMC4828072.